THESIS

FREQUENCY OF PRESSURE FLUCTUATIONS IN THE STILLING BASIN FOR THE SPILLWAY OF RAISED GROSS DAM, COLORADO

Submitted by

Selina Tasdelen

Department of Civil and Environmental Engineering

In partial fulfillment of the requirements

For the Degree of Master of Science

Colorado State University

Fort Collins, Colorado

Summer 2021

Master's Committee:

Advisor: Robert Ettema
Co-Advisor: Christopher Thornton

Ann M. Little

ABSTRACT

FREQUENCY OF PRESSURE FLUCTUATIONS IN THE STILLING BASIN FOR THE SPILLWAY OF RAISED GROSS DAM, COLORADO

Gross Dam, Colorado, was constructed in 1954 to provide potable water to the city of Denver, Colorado. The location of Gross Dam is in Boulder County, Colorado. The dam itself is a high, curved concrete gravity-arch dam that retains Gross Reservoir, a reservoir capacity that of volume 51,573, 109.1 cubic meter. The Gross Reservoir Expansion (GRE) Project will increase the height of the Gross Dam from 39.93 m to an ultimate height of 143.56 m by 2025, thereby creating more storage behind the Gross Dam. The new stepped spillway required for GRE will be the highest stepped spillway in the U.S. Besides the height of the spillway, the steepness, the length, and the curved form of the chute will make the spillway stand out.

This study focused on (1) determining how roller-rotation frequency varied with water discharge for the full range of the discharges expected for the spillway, (2) determining the main frequencies in the pressure fluctuations at selected locations along the stilling basin, and (3) relating frequency fluctuations of measured pressure to frequencies of features evident in the flow field too and through the stilling basin. This effort involved assessing the influence of flow discharge on the rotation frequency of a major roller formed immediately upstream of the row of baffle blocks for each discharge. The experimental investigation carried out at the Hydraulics Laboratory of Colorado State University, Engineering Research Center, for the current Gross Dam.

The frequency of the rotation of the roller formed immediately upstream of the row of the baffle blocks determined approximately from the observation for every flow rate. The mean value of the rotation frequency of the roller formed for the PMF-equivalent discharge down the hydraulic model of the spillway (0.348 m^3/s) was 2.45 Hz or 0.5 Hz at prototype scale. The plot of the roller-rotation frequency versus discharge showed that there was a proportional relationship between the rotation frequency and the discharge.

The dynamic pressures were measured with the use of four pressure sensors which were positioned in front of the floor, behind the floor, at the face of the baffle block, and the behind the baffle block. The sampling rate of these sensors was 2,500 Hz. The maximum pressure (prototype scale) recorded at the front face of the baffle block when the model-scale flowrate was equivalent to the 1.0 PMF was 59.78 kPa.

Low-pass filter applied to the original signal of pressures, and the pressure signal was filtered out at frequencies above 200 Hz (model scale). The cut off frequency of the filtered signal was chosen 200 Hz, as flow oscillations would not occur at this frequency. Then, Fast Fourier Transform (FFT) method was applied to both original and filtered signal. The result showed that filtered FFT gave about the same result as the FFT from the unfiltered data and there was no continuous low frequency or continuous high frequency pattern, indicating that the pressure signals oscillated irregularly, as did the roller formed in the front of the stilling basin. Therefore, FFT could not find the dominant frequency in the signal. The largest peak frequencies at prototype scale for the upstream floor, front face of the baffle block, downstream face of the baffle block, and downstream floor of the stilling basin were 0.496, 1.15, 1.396, and 1.544 Hz, respectively.

ACKNOWLEDGEMENTS

I would like to extend my deepest gratefulness to my advisor and co-advisor, Profs. Robert Ettema and Christopher Thornton, for this opportunity they gave me to take part in the hydraulic model study of the Gross Dam.

Besides my advisor and co-advisor, I would like to thank to Dr. Frank Lan, AECOM, for approving my FFT results. Moreover, I would like to thank to Prof. Ann M. Little who was willing to be in my graduate committee. Additional thanks are given to Fatima Liyari, Alireza Fakhri, Milad Roohi, Ibrahim Bozaid and Blake Biethman.

Finally, I would like to thank my mother and father (Melek and Mahmut Tasdelen) and my brother (Serhat Tasdelen). This achievement could not be possible without their moral support.

TABLE OF CONTENTS

LIST OF TABLES

LIST OF FIGURES

LIST OF SYMBOLS

Symbols

L_r	length scale
Fr	Froude number
L	length
r	a subscript indicating scale ratio (= prototype value/model value)
Re	Reynold number
C_s	skewness
C_e	kurtosis
$C_p{}'$	standard deviation of pressure fluctuation
$C_p{}^+$	the maximum negative deviations
$C_p{}^-$	the maximum positive deviations
y/D_j	pool depth/impact diameter
L_j	length of the jump
f_d	dominant frequency
pV	raw voltage values

Units

cfs	cubic feet per second flow rate
ft	foot or feet
ft/s	foot or feet per second
gpm	gallons per minute

hr, hrs	hour, hours
in	inch(es)
m	meter
m/s	meters per second
m^2/s	square meters per second
m^3/s	cubic meters per second
psi	pressure in pounds per square inch
s	second
^oC	Celsius degree(s)
^oF	Fahrenheit degree(s)

Abbreviations

H:V	ratio of horizontal to vertical step dimensions
psi	pounds per square inch
PMF	probable maximum flood
RSD	STD/Mean, the relative standard deviation
STD	standard deviation
RMS	root mean square
GRE	Gross Dam Expansion

CHAPTER 1- INTRODUCTION

1.1 Introduction

Gross Dam, Colorado, was constructed in 1954 to provide potable water for the city of Denver, Colorado. The dam, located in Boulder County, Colorado, stores water delivered through the Continental Divide by means of the Moffat Tunnel, which draws water from the Fraser River, a tributary of the Colorado River. The dam itself is a high, curved concrete gravity-arch dam that retains Gross Reservoir, a reservoir of volume capacity 51,573, 109 m^3. Figure 1-1 depicts Gross Reservoir and Gross Dam.

Figure 1-1. A view of Gross Reservoir and Dam

The base of the dam's spillway is 2118.4 m above mean sea level. The radius of curvature (prototype) of the reservoir of the dam at the ogee crest of the spillway is 531.9 meter (Stantec, private communication, 2019). As currently built, Gross Dam confines South Boulder Creek to the water surface elevation of 103.6 meter above the stream bed with the water storage capacity of approximately 51.8 million cubic meters (Stantec, private communication, 2019). Figure 1-2 shows the location of Gross Dam and Reservoir.

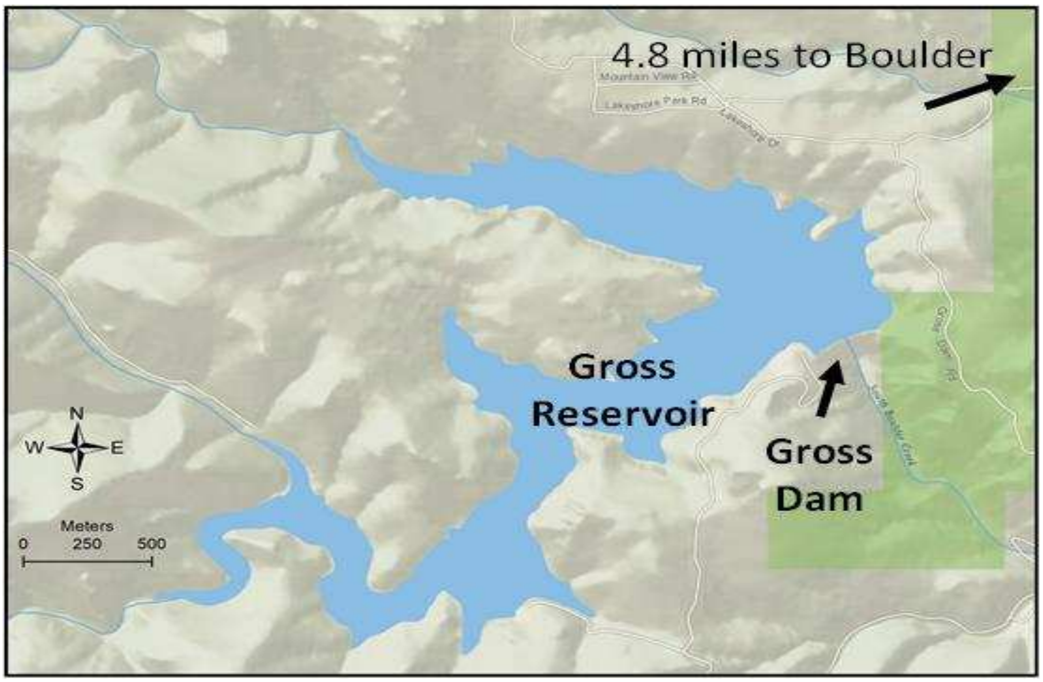

Figure 1-2. Location of Gross Dam and Gross Reservoir near Boulder, Colorado

However, the dam is to be heightened substantially to increase the water-storage capacity of Gross Reservoir to provide more water to the city of Denver, which has grown extensively since 1954. The heightening, termed Gross Reservoir Expansion (GRE) Project, will include a new stepped spillway, fitted to the heightened Gross Dam, which will by 2025 will extend in spillway height from 39.93 m (131 ft) to an ultimate height of 143.56 m (471 ft), thereby creating more storage behind the Gross Dam. The new stepped spillway will be the highest stepped spillway in the U.S. (Stantec, private communication, 2019). Besides the height of the spillway, the steepness, the length, and the curved form of the chute will make the spillway stand out. The extended dam will be a thick-arch type and formed by a roller compacted concrete (RCC). Also, the face of the extended dam will be conventionally vibrated concrete (CVC) (Stantec, private communication, 2019).

Figure 1-3 through Figure 1-5 show the extent of the GRE planned for the Gross Dam and Reservoir, the location of the toe of the extended dam and the stilling basin of the spillway, and the spillway of the current dam, respectively.

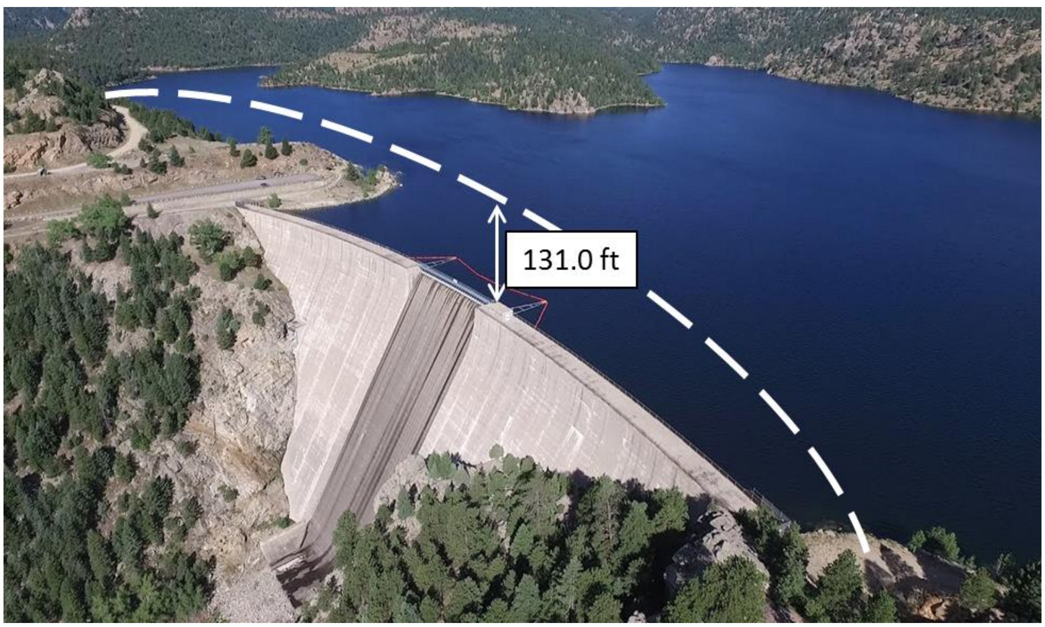

Figure 1-3. The extent of the GRE heightening of the Gross Dam to increase the size of Gross Reservoir

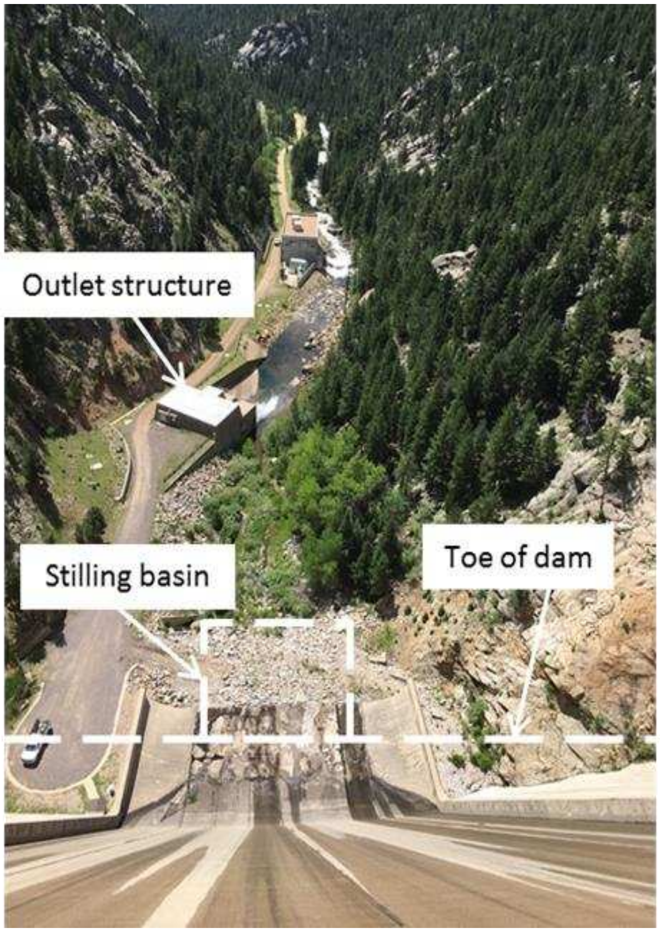

Figure 1-4. The location of the toe of the heightened form of Gross Dam and the location of the proposed stilling basin of the spillway

Figure 1-5. The spillway for the existing Gross Dam

1.2 Objectives

A hydraulic model of the spillway was needed to determine whether the new spillway would perform suitably well. The length scale (prototype/model) of the hydraulic model was 24 and was carried out at the Hydraulics Laboratory of Colorado State University, Engineering Research Center (ERC). Part of the modeling involved designing a novel stilling basin for the steep, stepped spillway. This effort included identifying and evaluating any substantial pressure fluctuations in the stilling basin. A visible feature of flow through the stilling basin was the formation of a flow roller, as flow from the spillway chute entered the basin, struck the basin's invert and rolled back upstream; water in the top of the roller moved upstream.

This thesis study had the ensuing focal objectives:

1. Determine how roller-rotation frequency varied with water discharge for the full range of the discharges expected for the spillway.

2. Determine the main frequencies in the pressure fluctuations at selected locations along the stilling basin. Of interest was the variation of maximum pressure and pressure frequency:

    - on the front floor of the basin (where flow departed the chute and entered the basin)
    - the face of the central baffle block (where flow first encountered the row of baffle block
    - the downstream face of the central block (where flow passed around and over the baffle block)
    - on the downstream floor of the basin at the rear of the central baffle block (where flow departed the basin yet was upstream of the basin's end-sill)

Accomplishing this objective entailed use of the fast-Fourier-transform (FFT) methods and filter analysis to analyze the temporal variations of the measured pressures; and,

3. Relate frequency fluctuations of measured pressure to frequencies of features evident in the flow field too and through the basin. This effort involved assessing the influence of flow discharge of the rotation of a major roller formed immediately upstream of the row of baffle blocks.

1.3 Background

The main prototype values of the dimensions of the stepped spillway were as follow:

- The top of ogee crest to floor of modeling basin was 142.6 m.
- Bottom of head tank to floor of modeling basin was 118.9 m.

- The chute slope was 0.5H:1.0V
- The estimated design head on spillway crest was 4.11 m.
- Net width of crest was 54.8 m converging down-chute to 42.7 m (at the stilling basin), a convergence of 2.2%
- The height of the chute step was 1.22 m, and the step-tread width was 0.610 m.
- The heights of the chute wall were 7.92 m and 3.35 m, respectively.
- The convergence angle of the chute was 63.4°.
- The length and width of the head tank (used in the model) were 4.67 m, and the depth of the head tank (used in the model) was 1.52 m.

1.4 Thesis format

The Table of Contents gives the layout of this thesis. After Chapter 1, Introduction, Chapter 2 reviews pertinent literature related to pressure fluctuations and frequencies in stilling basins. Chapter 3 gives an overview of the hydraulic model and describes the instrumentation used for measuring pressures in the stilling basin and on a central baffle block. Chapter 4 presents the results of the analyses conducted to achieve the goals mentioned above. Chapter 5 summarizes the main conclusions drawn from the study.

CHAPTER 2- LITERATURE REVIEW

2.1 Pressure Fluctuations and Frequencies

This chapter summarizes the frequencies reported in the literature on pressure frequencies measured in stilling basins. Frequencies obtained from prior studies are compared subsequently (Chapter 4) with the frequencies measured for the final design of the stilling basin to be used at the base of the Gross Dam's stepped spillway. A notable novelty of the present analysis is that the analysis characterizes the pressure variations along the basin's centerline and at the locations mentioned above in Section 1.2.

Many prior studies have considered pressure fluctuations in stilling basins because pressure fluctuations are of significant concern for the structural design of most components of a stilling basin. Such fluctuations originate from the flow field in the basin (Wither, 1991, Carlson, 2007, Zhou & Yin, 2011, Chanson et al., 2014). Therefore, to understand the pressure fluctuations, it is necessary to understand the main features of the flow field in a stilling basin (e.g., Nasiri et. al, 2012). If the pressure fluctuations are deemed problematic for a basin's structural integrity, the flow field must be adjusted so that the frequencies of fluctuations are no longer problematic.

The ensuing review summarizes findings from prior leading studies on pressure fluctuations in stilling basins. In this regard, Table 2-1 concisely lists the prototype values of frequencies reported from those studies, which began in the late 1980s, largely because of the advent of pressure-measurement instrumentation and data-storage equipment.

2.1.1 Bowers and Toso (1988)

One of the earliest studies was that by Bowers and Toso (1988) who measured average pressures experienced by the spillway crest, chute, chute blocks, and the floor of the hydraulic jump stilling basin fitted to for Karnafuli Dam, Bangladesh. They used a hydraulic model whose length scale (prototype/model) was 60. Their measurements considered fluctuations in the peak pressure (during the spillway's design flow) and were motivated by design concerns regarding uplift of the spillway's chute concrete slab. For a design discharge of 3,400 m^3/s, the spectral analysis of pressure fluctuations in the hydraulic jump demonstrated that the majority of the energy had prototype values of pressure fluctuation frequencies in the range 0.15-1.0 Hz, with the peak value around 0.2 Hz. Tests of the model drain system with a variable-frequency generator installed at the opening of the chute block drain showed that possible resonance in the prototype was 6.5-7 Hz that was approximately 30 times of the frequency of the peak energy at the openings of the chute block in the hydraulic jump. Figure 2-1 shows the crests and chutes of the spillway for Karnafuli Dam. Figure 2-2 shows a centerline profile of the design hydraulic jump formed in the stilling basin.

Figure 2-1. Crests and chutes of the spillway used for Karnafuli Dam, Bangladesh

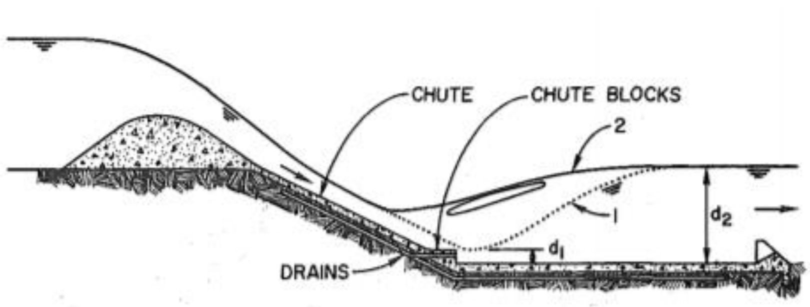

Figure 2-2. Centerline profile of hydraulic jump formed in the stilling basin used for Karnafuli Dam

2.1.2 Ervine et al. (1997)

Ervine et al. (1997) calibrated transducers flush-mounted on the floor of model plunge pool at the downstream end of an overfall (plunging jet) spillway for Morrow Point Dam, Colorado. The value of the sampling rate used for pressure measurements varied in the range of 100-230 Hz. They determined the fluctuations of the root mean square pressure in the plunge pool for a range of spillway discharges, the lengths of the plunge, the depths of water in the plunge pool, and the configurations of the jet nozzle. Additionally, they calculated the maximum positive pressure fluctuation, which they found to be approximately four times higher than the value estimated as the root mean square. Similarly, the authors computed the maximum negative pressure fluctuation, and found that it was approximately three times higher than the value estimated as the root mean square. Two dominant frequencies (model value) introduced in the plunge pool corresponded to the Strouhal numbers of $fL/U = 0.01$ and 0.25; the Strouhal number was the ratio of inertial forces due to flow oscillations relative to the convective movement of an approach flow. The lowest frequencies followed by large scale eddies which have dimensions approximately the depth of the plunge pool. The two probable dominant frequencies at the Morrow Point Dam were found to be: $f = 0.024$ Hz and 0.625 Hz. The coefficient of the maximum pressure head (${C_p}^+$) reached 0.8 when pool depth of y/D_j (pool depth/impact diameter) was close to 10. The coefficient of the minimum pressure (${C_p}^-$) reached 0.6 when pool depth of y/D_j (pool depth/impact diameter) was about 5.

2.1.3 Nakato (2000)

Nakato (2000) investigated pressure fluctuations in the Type III stilling basin for Pit 6 Dam located on the Pit River, California. The dam's overflow spillway was gated, fitted with radial gates used to regulate the flow over ogee crest then flow down into a 33.5-m-wide and 19.5-m-long stilling basin conforming, as Figure 2-3 shows, to a Type III stilling basin. Figure 2-4 shows the plan and section of Pit 6 spillway model, built a length scale of 28. He collected temporal records of pressure data (streamwise and transverse) on every floor block in the Type III stilling basin. Pressure data also were obtained using flush-mounted pressure transducer placed in the left guide wall of the model and was able to obtain data on the pressure fluctuations experienced by the wall. Nakato sampled the output signals at a rate of 200 samples for obtained over 5 seconds. The prototype value of natural frequency of the floor blocks was about 7.5 Hz, which was 39.7 Hz in the model (frequency scale of 5.29 for the model). Spectral analysis of two force components were carried out and, in all cases, no substantial force components with a prototype frequency of more than 0.07 Hz were identified.

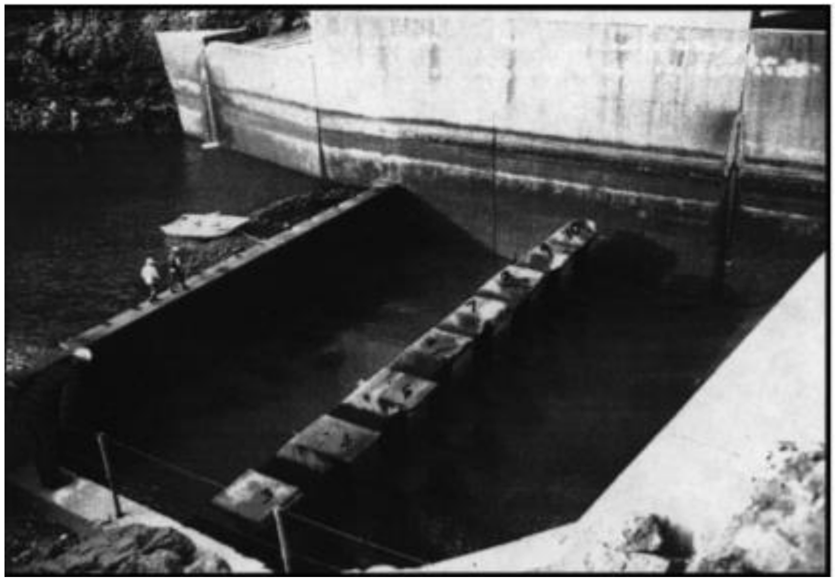

Figure 2-3. A photograph of the prototype Type III stilling basin used for Pit 6 Dam on the Pit River, California

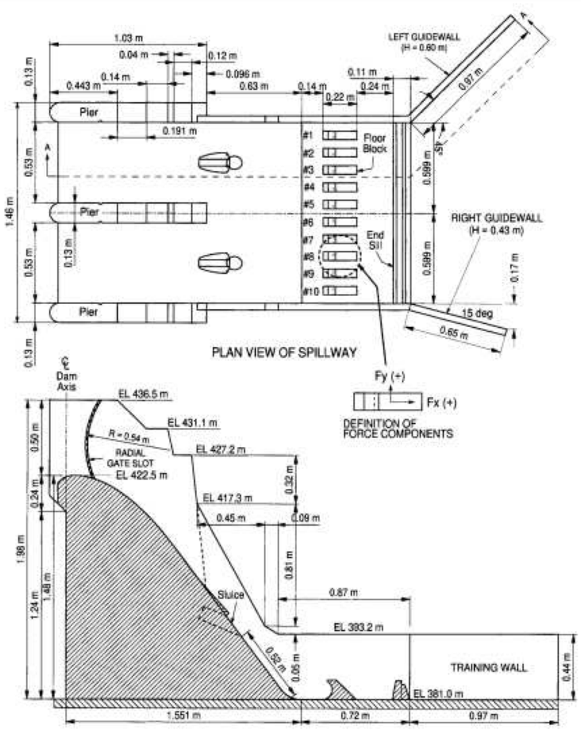

Figure 2-4. Plan and Section of views of the Type III spillway model used by Nakato (2000)

2.1.4 Yan and Zhou (2006)

Yan and Zhou (2006) measured pressures and obtained temporal records of pressure fluctuations produced by flows Froude numbers varying from 3.52 to 6.86 entering a diverging stilling basin. The values of the ratios [$\beta = B/b$] of the channel expansion change from 1.5 to 3.0. The sampling frequency they used was 100 Hz, and they measured pressure fluctuations by means of a stochastic signal processing method. They also obtained the dominant frequency, and the statistical characteristics, of the pressure fluctuations under the hydraulic jump. Their data led them to conclude that, under different hydraulic conditions, the-peak frequency of pressure fluctuations was in the 0.5-1.5 Hz for the basin's upstream floor but increased to the range 3.5-4.5 Hz in the tail-water area of the basins. The peak frequency went up rapidly behind the toe of the jump, and at a position of about 0.2-0.4 of the jump's length (L_j, starting from the toe) it reached the highest point in the hydraulic jump region, and then the frequency decreased gradually toward the rear of the jump. Generally, within the domain of their test setup, the overall peak frequency increased when the expansion ratio and the inflow Froude number increased. The peak frequency of the jump (the highest value they found was 13 Hz) was greater than the classic image of a hydraulic jump, and maximum values were about 2.0-4.5 Hz.

2.1.5 Carlson et al. (2007)

Carlson et al. (2007) installed pressure transducers at the downstream for end of Spillbay 4 and Spillbay 9 of an overflow spillway discharging flow to the Type II stilling basin for Dalles Dam on the Columbia River, Oregon. Figure 2-5 shows the gated spillway and spillbays they studied for Dalles Dam. They also located the transducers on the front faces, the tops, the sides of the baffle blocks, on the front and the top of the end sill, and in the channels between the baffles. Each flow scenario started with a stabilization time of 15 minutes followed by the data taken for a 5-minute period at a sampling frequency of 2500 Hz for Spillbay 4 and 6000 Hz-for Spillbay 9. Carlson et al. (2007) indicated that-some low-frequency spectral peaks existed under 10 Hz, because of the waves or large-scale turbulence in the flow passing through the stilling basin. The corresponding prototype-values of frequencies were 102, 94, and 162 Hz at the baffle blocks, the face of the end sill and the top of the end-sill, respectively.

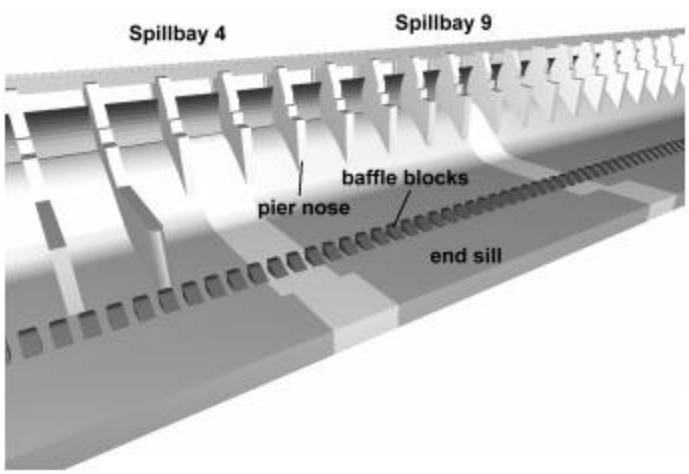

Figure 2-5. The gated spillway and spillbays for Dalles Dam on the Columbia River

2.1.6 Gulliver et al. (2008)

Gulliver et al. (2008) measured pressures and discharges for flow over the gated overflow spillway of Folsom Dam, California. The overall data set was obtained using pressure sensors, a gate elevation sensor, an ultrasonic sensor to measure the water surface, and a device measuring the weir flow rate using the upstream head of the gate and the height of the gate. For water-surface elevation measurements, the sampling frequency for every probe was 10 Hz with 60 seconds used to collect data sets. The authors measured higher flow velocities at the end of the chute and along the stepped spillway. By using Acoustic Doppler Velocimeter, they measured lower flow velocities of the model at the downstream end.

The authors collected the unsteady dynamic pressure measurements for all four sides of the center baffle block and for five locations on the stilling basin floor. Dynamic pressure measurements were taken at the face of the baffle block, the right and left side of the baffle block, and the back of the baffle block and the stilling basin floor. Gulliver et al. could not observe any frequencies at the back of the baffle block and the only frequencies observed were on the baffle block face at 0.4, 0.5 and 1.0 Hz, and these were determined from pressure head fluctuations of 7 ft, 26 ft, and 33 ft, respectively (Gulliver et al., 2008). They also observed the prevalent frequency in the side pressures on the baffle block with a discharge of 135,000 ft^3/s and the value of the frequency was 0.94 Hz and a pressure of nearly 38 feet of water. The stilling basin floor, which is in the vicinity of the separation zone coming off the blocks had a few common frequencies that were lower than 1.5 Hz and the amplitudes of nearly 59 feet of the water (Gulliver et al., 2008). Figure 2-6 shows Folsom Dam spillway. Figure 2-7 illustrates the plan view of the apron stilling basin for Folsom Dam.

Figure 2-6. Folsom Dam spillway, photo taken from
https://www.usbr.gov/tsc/techreferences/hydraulics_lab/pubs/HL/HL-2009-05.pdf

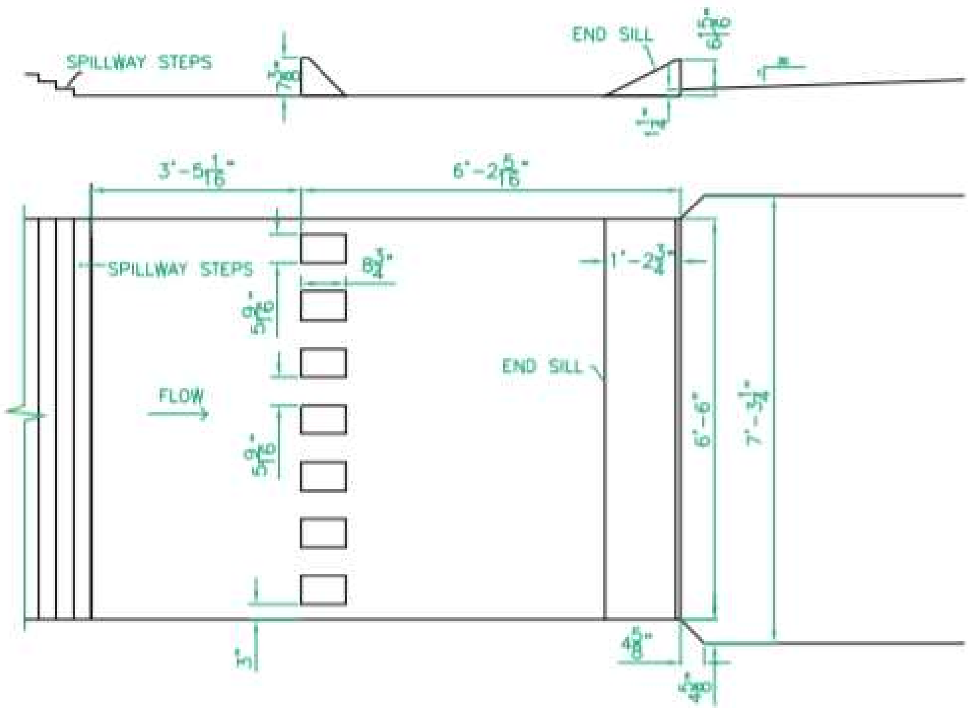

Figure 2-7. The plan view of the stepped approach chute and the apron stilling basin (similar to Type III) for Folsom Dam (U.S. standard units used for dimensions)

2.1.7 Lopardo et al. (2009)

Lopardo et al. (2009) used a gage for measuring the depth of the water (y_2) 6 m downstream from a stilling basin below a gated overflow spillway. They used Acoustic Doppler Velocity Meter to make a record of the time signals of the velocity vectors in the central line of the flume for different locations within the hydraulic jump and further downstream until the flow is the open channel uniform flow. Their article mentions the turbulence intensities in the area near the bed of the hydraulic jump stilling basin. The signal length of the velocity was 8192 at a sampling frequency of 50 Hz. All the values of the recorded velocity signals (Signal to Noise Ratio) were greater than 15db (Lopardo et al., 2009). When applying the Fast Fourier Transform techniques by using Welch method, a resolution bandwidth was found nearly 0.2 Hz and 17 percent of the standard error in the estimation of FFT values is accomplished in the frequency domain (Lopardo et al., 2009). They also used "spectral analysis" to define the effect of Doppler noise on the variance of the velocity signal of the water (2009). Moreover, the authors used bi-directional pressure transducers to compute the components of the random pressure. In addition, they analyzed the data with respect to the value of the discrete sample. The time interval of pressure fluctuations was 0.01 s. Lopardo et al. (2009) defined the intensity of the turbulence as a function of the fluctuations in pressure on a boundary of the flow.

2.1.8 Yin and Zhou (2011)

To study baffle-block effect of the pressure fluctuations, Zhou and Yin (2011) took pressure measurements for model at five points: points #1 and #2 were placed in the front of the baffle block, point #3 was in the center of the baffle block; and points #4 and #5 point were behind the baffle block. Also, the authors tested a system for measuring pressure fluctuations in a model. The system included a pressure sensor, the dynamic strain gauge, an analog-to-digital conversion board, and computer-processing equipment. They found that the presence of baffle blocks did find not to change the power spectrum density and the dominant frequency of the pressure fluctuations on the apron. Strong turbulence and large scale of the vortices played an important role for the pressure fluctuations on the apron and in the region of the low frequency where the hydraulic jump energy with low Froude number usually centered in the range of 0 ~ 10Hz. The sampling frequency of the model $f_c = 50\ Hz$, the interval of sampling was 0.01s and the sample size N = 1024. The dominant frequency (f_d) of the measurement points in the region of the hydraulic jump observed in the 1 ~ 4Hz range. Although there was no apparent dominant frequency downstream of the hydraulic jump, the jump's energy fluctuated at a frequency of about 0~5.8Hz (Yin and Zhou, 2011). Figure 2-8 shows of Type III stilling basin and baffle block configuration used.

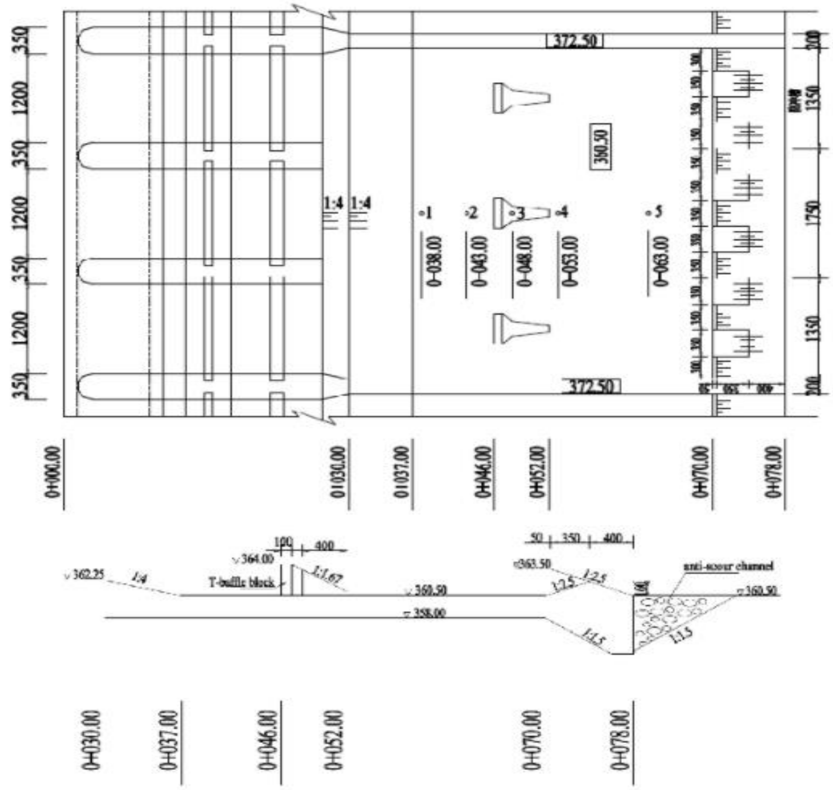

Figure 2-8. Sketch of Type III stilling basin and baffle block studied by Zhou and Yin (2011)

2.1.9 Nasiri et al. (2012)

The variations of the pressure on a basin floor can be attributed to the characteristic, unsteady behavior of a hydraulic jump. Nasiri et al. (2012) investigated the impacts of the baffle blocks on the pressure fluctuations on the basin floor. The authors applied one or two rows of baffle blocks on the basin floor for increasing the efficiency of the Type III stilling basin and enhancing the rate of the dissipation of the energy. The pressure fluctuations of a rotating roller zone of hydraulic jump exert the tension force, compression force, and a forced hydraulic jump. Nasiri et al. (2012) have designed a typical USBR Type III basin to pay attention to the effect of baffle blocks on pressure variations on the floor of the basin. Then, they added a second row of blocks to the basin. The authors mounted a series of pressure tubes in the basin axis to calculate the static and dynamic pressures exerted on the floor of the basin. They expressed the results in dimensionless pressure coefficients: ${C_p}^+, {C_p}', C_p, {C_p}^-$.

Also, the authors computed the power spectra associated with each of the pressure fluctuations. Moreover, they noted that, when the water jet hits the basin, the pressure on the basin floor increased, decreased somewhat under the roller zone of jump's front, and then increased again downstream of the jump's sequent depth. Nasiri et al. (2012) report, from the spectral analysis they conducted, that. In this article, the dominant frequency ranged in from 1.59 Hz to 5.57 Hz.

2.1.10 Tian et al. (2012)

The hydraulic-model study reported by Tian et al. (2012) focused on the time-average pressure, the peak hydrodynamic pressure, and the intensity of the pressure fluctuations on the hydraulic jump stilling basin floor of the stepped spillways for three different chute slopes. Model results demonstrated the peak average pressure, the peak hydrodynamic pressure and the maximum pressure fluctuation occurred at the x / h_k impinging point of the jet nape = 1.2~2.5 (Tian et al., 2012). When the flow rate or the slope of the chute rises, these peak values rise. They measured that the peak of the hydrodynamic pressure was greater 5~8 times than the average value and the intensity of the peak fluctuation. They also computed that the average pressure peak is $\frac{y_p}{h_k}$=5.4; the hydrodynamic peak pressure was 5~8 times greater than the average value, and the intensity of the fluctuating peak was 0.8 of average pressure. The authors observed the lowest pressure when the x/h_k was around 2. 5~5. 1 and the dominant frequencies of fluctuations at impinging zone were around 4Hz~8Hz, in the zone of the hydraulic jump roller around 2Hz~5Hz, and less than 2Hz downstream of the hydraulic jump (Tian et al., 2012).

2.1.11 Chanson et al. (2014)

Chanson et al. (2014) measured the total pressure and the properties of two-phase flow with intrusive total pressure probe and phase-detection probe. The frequency of the sampling was 5 kHz in this study, although a signal amplification device filtered the signal to remove noise was greater than 2 kHz. Chanson et al. (2014) derived the time-averaged total pressure, and they characterized the pressure fluctuation from the standard deviation of the total pressure. Total fluctuations of the pressure and the rate of the bubble count were associated with the intensity of the local turbulence. They observed the maximum mean total pressure and maximum pressure fluctuations at various vertical places. The authors also analyzed the characteristics of the total pressure fluctuation frequencies. The filtered signals of the high-frequency (0–25 Hz) demonstrates the various fluctuation frequencies ${F_p}^H$ ranged in 8 and 12 Hz, but on the contrary the filtered signals of low-frequency (0–5 Hz) pointed out a frequency ${F_p}^L$ around 2.6 Hz (Chanson et al., 2014).

Table 2-1. Summary table for the prototype values of the frequencies reported from the prior studies

Name of the study	**Authors**	**Hydraulic Structures**	**Pressure frequencies reported (prototype values)**
Karnafuli project, model studies of spillway damage	Bowers and Toso (1988)	spillway, chute, and hydraulic jump stilling basin	The spectral analysis of pressure fluctuations in the hydraulic jump demonstrated that the majority of the energy in prototype ranged in 0.15-1.0 Hz, with the peak was around 0.2 Hz
Pressure fluctuations on plunge pool floors	Ervine et al. (1997)	plunge pool floor	The two probable dominant frequencies at the Morrow Point Dam were: (i) f= 0.024 Hz, (ii) f = 0.625 Hz
Model tests of hydraulic performance of Pit 6 dam stilling basin	Nakato (2000)	ogee spillway and Type III stilling basin	The prototype natural frequency of the model floor block was approximately 7.5 Hz, or 39.7 Hz at model scale

Prototype measurements of pressure fluctuations in the Dalles Dam stilling basin	Carlson et al. (2007)	Type II stilling basin, baffle block and end sill	The corresponding frequencies were 102, 94, and 162 Hz at the baffle blocks, the face of the end sill and the top of the end-sill, respectively
The physical model study of the Folsom Dam Auxiliary Spillway	Gulliver et al. (2008)	stepped spillway, apron stilling basin	The only frequencies observed were on the baffle block face, and were 0.4, 0.5 and 1.0 Hz. Also, the prevalent frequency in the side pressures on the baffle block was 0.94 Hz. The stilling basin floor, which is in the vicinity of the separation zone coming off the blocks experienced frequencies that were lower than 1.5 Hz
The baffle block effect of fluctuating pressure in hydraulic jump with low Froude numbers	Yin and Zhou (2011)	low-head spillway, apron stilling basin, baffle block	The dominant frequency (of the measurement points in the region of the hydraulic jump were observed in to be 1 to 4Hz. Although there was no apparent dominant frequency beyond the hydraulic jump, flow turbulence oscillations were 0 to 5.8Hz
Baffle block effects on pressure characteristics on the floor of a USBR III Basin	Nasiri et al. (2012)	baffle block, type III stilling basin	The dominant frequency ranged from 1.59 Hz to 5.57 Hz
Pressure characteristics in stilling basin of stepped spillway	Tian et al. (2012)	stepped spillway, hydraulic jump stilling basin	The dominant frequencies of fluctuations where the approach flow impinged on the basin floor were around 4Hz~8Hz, in the zone of the hydraulic jump roller around 2Hz~5Hz, and less than about 2Hz downstream of the hydraulic jump
Stilling basin performance downstream of stepped spillways	Stojnic (2020)	stepped spillway, Type III stilling basin, and chute	The dominant frequencies were in range of 0.5-12 Hz and 0.4-6 Hz with 30° sloping smooth and stepped chute approach flows, respectively. Typical dominant frequencies for 50° stepped chute approach flows ranged between 1 to 7 Hz for $X_j < 0.5$ and 0.4 to 0.8 Hz for $X_j > 0.5$

2.2 General Conclusion from Prior Studies

Many prior studies have considered the phenomenon of pressure fluctuations occurring in stilling basins, notably because pressure fluctuations were of concern for the structural design of most components of a stilling basin. The stilling basins were used to distribute and dissipate energy in the outlet of the dams by combining water and air and turbulence. This interaction resulted in the development of low-frequency pressure fluctuations not considered in traditional methods for stilling basin design. Also, none of the prior studies yielded data on the temporal variation of pressures along the length of a basin.

Bower and Toso (1988) related that the energy dissipation in a hydraulic jump stilling basin results in the generation of large-scale turbulence and the converting the turbulent energy to heat; therefore, pressure fluctuations should be of concern in the design of hydraulic jump stilling basins. Ervine et al. (1997) explained the pressure fluctuation results from the turbulence. Carlson et al. (2007) stated the high spectral energy in the low frequency pointed out that large-scale motions contributed to the production of turbulent kinetic energy, which was consistent with previous studies by Carlson (2001) that dominant large-scale, unsteady vortices take place in the flows of some regions of hydropower plants. Chanson et al. (2014) correlated the total pressure fluctuations to both velocity fluctuations in the air–water flow and free-surface dynamics above the roller.

CHAPTER 3- LABORATORY EXPERIMENTS

3.1 Introduction

This chapter briefly describes the design and construction of the hydraulic model of the spillway of raised Gross Dam. Further, this chapter describes the instrumentation used to operate the model and record the characteristics of the flows, notable, flow rates, flow depths and velocities, and the pressures in the various designs of stilling basin used for dissipating much of the energy of flow down the spillway.

The design flow for the spillway was the Probable Maximum Flow (PMF), which was set at a model-scale equivalent of 978 m^3/s (prototype value). This value was given by AECOM, the designers of the spillway.

3.2 Model Dimensions

The experiments were carried out at the Hydraulics Laboratory of Colorado State University, Engineering Research Center. Table 3-1 lists the prototype dimension, the model-scale dimension, and the corresponding model scales. The model's length scale, 24, was dictated by the largest length that the laboratory's height could physically accommodate.

The dimensions of the head tank in the prototype (shown in Figure 3-1) were 112.14 m-wide, 112.14 m-long and 36.6 m-deep (Ettema et al., 2019, Biethman, 2019). This head tank centered on the spillway simulates a portion of Gross Reservoir. The tank includes a diffuser (flow-distributor) box. The diffuser has multiple layers of semi-permeable mesh through which forcing the flow to pass on its approach to the spillway's crest. Therefore, the flow inside the head tank stayed uniform when it approached the crest of the spillway (Biethman, 2019). The prototype distance of the bottom of the head tank is 23.16 m below the spillway crest. The design head is 3.66 m on the crest. The head tank was structurally constructed to bear the weight of the water in the head tank safely. The prototype dimensions of the chute heights were 7.92 m and 3.35 m, respectively. Figure 3-2 illustrates the hydraulic model from the side elevation view with the step detail. Figure 3-3 (a) and (b) illustrate the plan view of the model with the stilling basin and side view of the basin with the central baffle block and end sill, respectively.

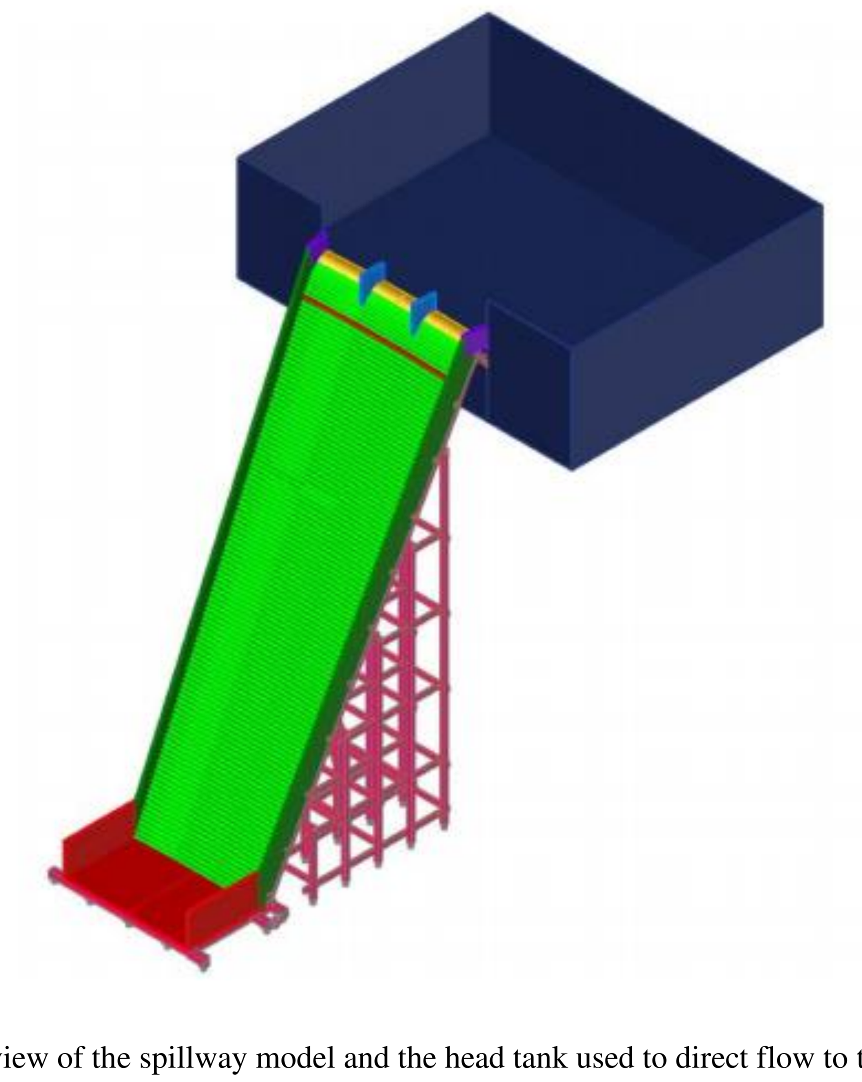

Figure 3-1. A view of the spillway model and the head tank used to direct flow to the spillway

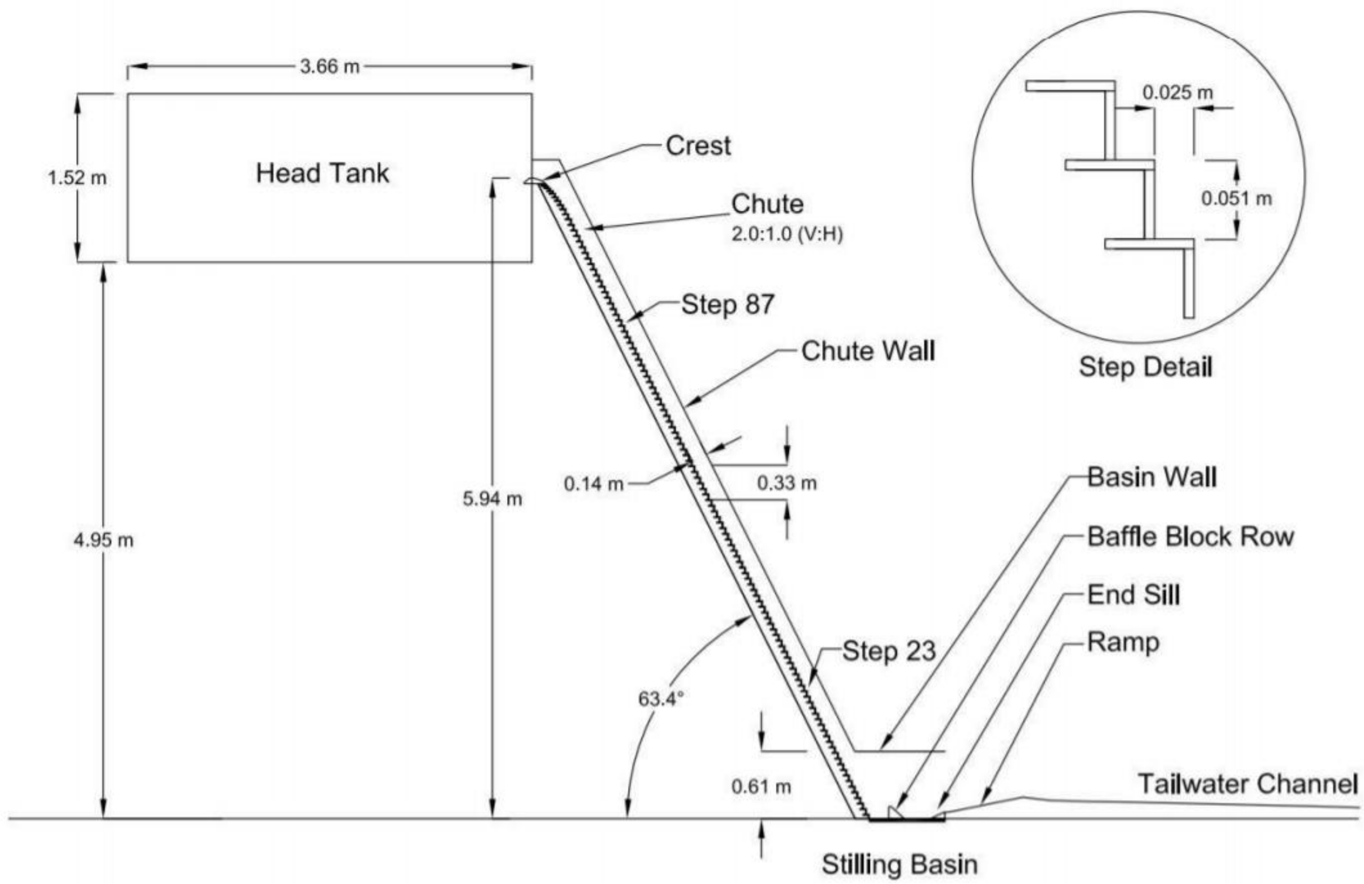

Figure 3-2. Layout of the hydraulic model from side elevation view with the detail of the steps

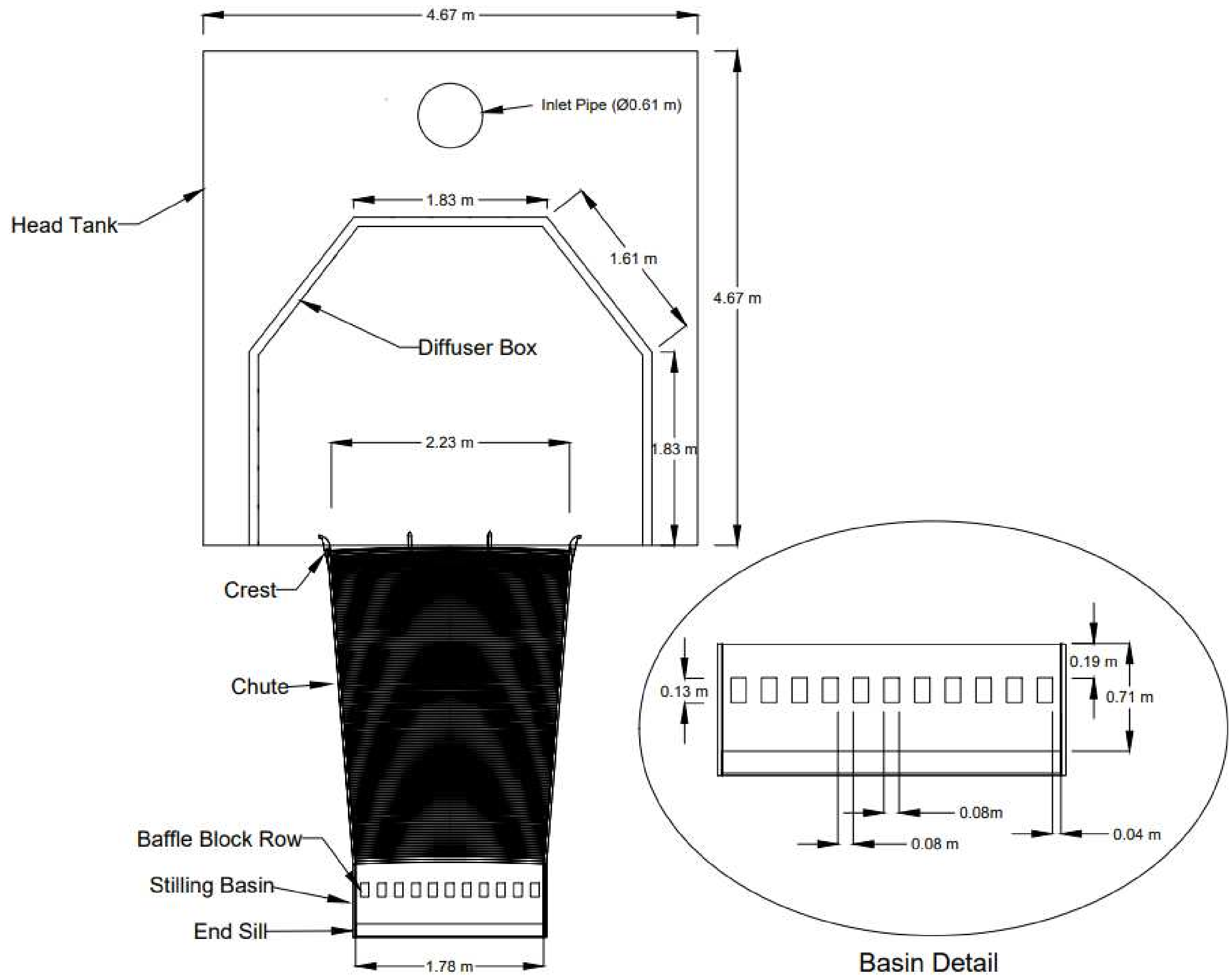
4.67 m
Inlet Pipe (Ø0.61 m)
Head Tank
1.83 m
1.61 m
4.67 m
Diffuser Box
2.23 m
1.83 m
Crest
Chute
Baffle Block Row
Stilling Basin
End Sill
1.78 m
0.19 m
0.13 m
0.71 m
0.08m
0.08 m
0.04 m
Basin Detail

(a)

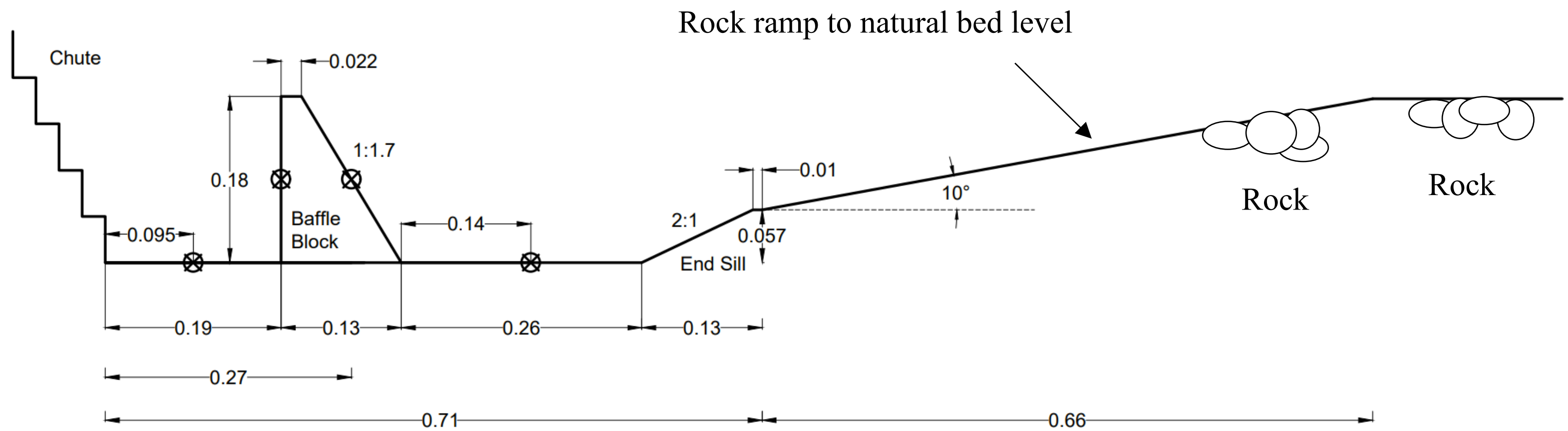

(b)

Figure 3-3. (a) A plan view of the model with the energy dissipation (or stilling) basin (b) Side view of the basin with the central baffle block and end sill (All length dimensions are meters)

Table 3-1. Prototype dimensions, model scale dimensions and corresponding model scales

Prototype Dimension	Model-Scale Dimension	Scale
Top of ogee crest to floor of modeling basin (Prototype elevation at top of crest = 2257.3 m)	5.9 m	24
Bottom of head tank to floor of modeling basin	5.0 m	24
Crest width (Prototype width of crest = 54.1 m, including two piers)	2.3 m	24
Head on spillway for design flow *prototype design head on spillway crest = 4.1 m *(Prototype elevation at spillway = 2261.4 m)	0.17 m	24
Stilling basin width *(Prototype width of basin = 42.7 m)	1.8 m	24
Top of piers to floor of modeling basin	6.1 m	24
Bottom of stilling basin to floor of modeling basin	0.2 m	24
Design discharge of water *978 m^3/s (prototype) (Reservoir level at 7,45.9 m)	0.348 m^3/s	2,821.8
Design discharge of water + 10% increase * 1077.94 m^3/s (prototype) (Reservoir level at 2261.7 m)	0.38 m^3/s	2,821.8

3.3 Similitude

The length scale (prototype/model) of the hydraulic model was 24 and the model was run considering the Froude number similarity, as the dominant forces were flow momentum and gravity. Table 3-2 summarizes the different parameters and their model-scale values for prototype.

Table 3-2. Different parameters and model scale values (prototype/model) for prototype

Variable	Scale	Scale Value
length	L_r	24.0
velocity	${L_r}^{1/2}$	4.9
discharge	${L_r}^{5/2}$	2,821.8

time	${L_r}^{1/2}$	4.9
frequency	${L_r}^{-1/2}$	0.2
force	${L_r}^{3}$	13,824.0
pressure or stress	L_r	24.0
Reynolds no.	${L_r}^{3/2}$	117.6
Weber no. (We)	${L_r}^{2}$	576.0
Froude no. (of flow entering the basin)	1	1

3.4 Measurements in the Stilling Basin

A point-gage was used to measure the water-surface profile along the stilling basin. When the tip of the point-gage was mostly submerged, the flow depths had to be judged approximately. When air was not in the flow, an average value of water depth was more readily determined.

An air-concentration probe was placed near the end of the chute to measure air concentration of the flow and bulked-flow velocity entering the stilling basin. Values of air were calculated over the flow depth into the basin. There were no measurements of air concentration made for the basin itself for the air concentration because the air bubbles rose quickly to the water surface. Also, the air-concentration probe was used to measure the flow velocity and depth of the bulked flow entering the basin.

Dynamic pressures of the flow leaving from the chute and hitting the basin floor near the end of the chute were measured first and approximately at two locations. The measurements were done with electronic pressure transducers (Honeywell PX26PCCFA6D). The following locations were used for the measurements:

- The basin floor placed in halfway between the baffle-block row and the toe of the chute;
- The front face of the central baffle block;
- The rear of the baffle block; and,
- Halfway between the end the baffle-block row and the end of the basin.

Preliminary or initial measurements of pressure were taken using a different pressure transducer (Onset-Hobo U20-001-1, at a slower sampling rate of 1 Hz) to determine the optimum length of the basin and the location of the row of the baffle block.

3.5 Instrumentation

3.5.1 Discharges

Discharges (in Table 3-3) in the model were measured with an Endress + Hauser Promag 53 W, an electromagnetic flow meter set up in the 0.61 m-diameter pipe which provides the water to the head tank and requires a 75 hp, 880 rpm pump. The results from Promag were shown digitally in real-time, and LabView program used to record the results. The discharge measurements for each model recorded as distinct time-series (Biethman, 2019). The maximum error for discharge measurement is ±0.5 percent of the reading. The influence of the ambient temperature of water on discharge is ±0.005%/ºC (Biethman, 2019). The head tank and the spillway act as a weir. As the head tank was filled to the elevation of the crest, the spillway discharge determined by the Promag was taken to be the subsequent volumetric contribution to the already filled head tank, after waiting long enough for the water level inside the head tank to become stable (Biethman, 2019).

Table 3-3- Discharge Summary

Proportion of PMF	Prototype Discharge (cms)	Model-scale Discharge (cms)	Model-scale mean Discharge (cms)
0.09	91.7	0.033	0.033
0.19	185.1	0.066	0.066
0.25	246.5	0.087	0.087
0.50	489.9	0.173	0.174
1.00	979.4 (PMF)	0.347	0.347

Notes:

- 1cfs = 0.0283 m^3/s or 0.0283 cms
- Discharges measured using an Endress+Hauser Promag 53 W electromagnetic flowmeter

3.5.2 Dynamic Pressures in Stilling Basin and Baffle Block

The central baffle block and near locations of the floor of the basin instrumented for pressure measurements. These pressures were measured using four Honeywell PX26PCCFA6D pressure sensors. These sensors were positioned in front of the floor, in the face of the baffle block, and the behind the baffle block, and behind the floor. Figure 3-4 shows the location of the pressure sensors on the floor of the stilling basin and the central baffle block. An NI9237 data-acquisition system was used to sample these sensors at a rate of 2,500 Hz. Also, these pressure transducers were set to compute the pressures in the range of 103.42 kPa (model scale) with a precision of 1.0 percent of the measured value (Ettema et al., 2019).

Preliminary pressures used in evaluating the adjustments in performance of the stilling basin were done using two Onset-Hobo U20-001-1 pressure sensors. These probes evaluated the values of the pressure at two locations on the stilling basin floor. A pressure range of these instruments is from 0 to 89.6 kPa, and measurement accuracy of the reading is 0.1%. Figure 3-5 shows two sensors: one is near the basin wall and the other one is near the center of the basin. The opening of the sensor is aligned with the flow from the chute and placed in 0.025 m above the floor. A data-logging system within the transducer collected the pressure fluctuations at a sampling frequency of 1.0 Hz, and the collected data were transferred to a computer after the test series were completed.

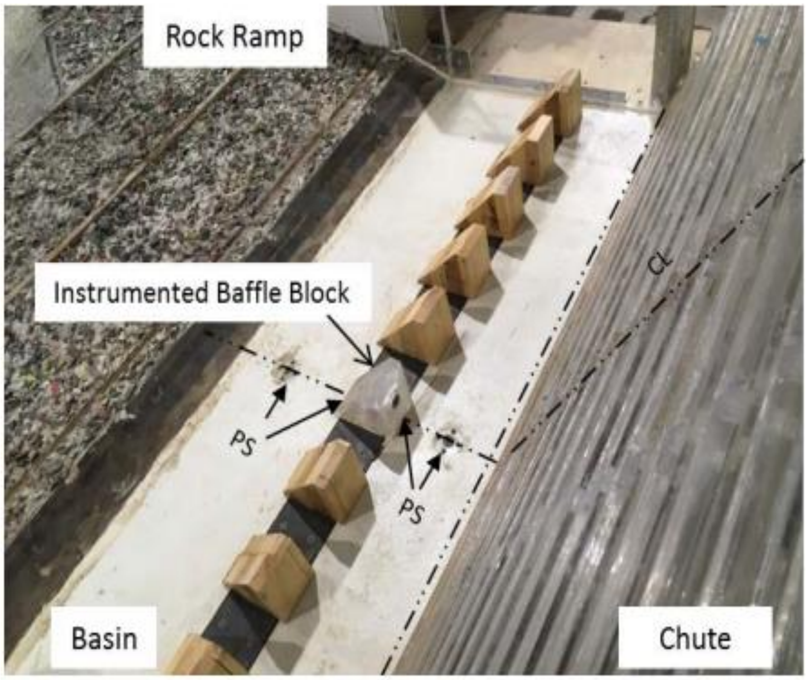

Figure 3-4. Positions of the pressure sensors (Honeywell PX26PCCFA6D) on the floor (front and rear) of the stilling basin and in the central baffle block (front and rear). The sensors measured pressure fluctuations along the centerline (CL) of the basin.

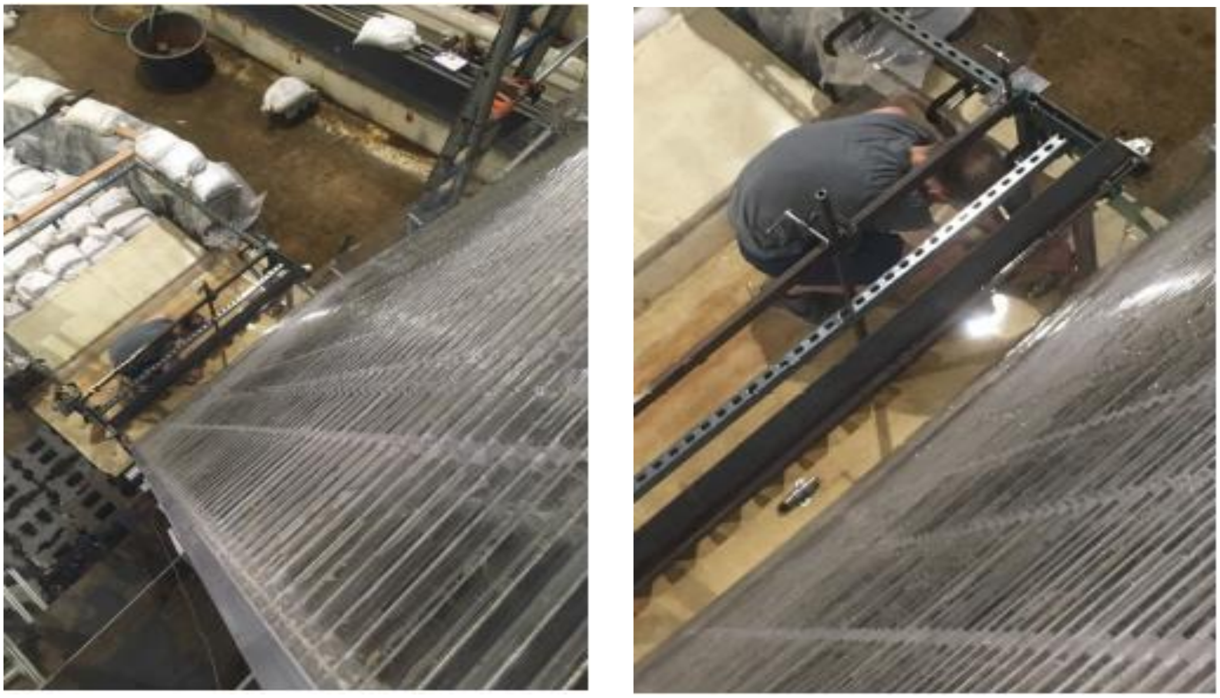

(a) (b)

Figure 3-5. The positions of pressure transducers on the initial floor: (a) view down chute (b)closer view. These pressure transducers (Onset-Hobo U20-001-1) were set to measure the preliminary values of pressure

3.6 Pressure-Data Collection via MATLAB

Each data-input file was named in a format comparable to "pressure2019-10-22-11-10-52.mat", as explained below. The overall handling of data relied heavily on use of the software MATLAB.

The file contained the f-raw matrix and 3 vector files into the workspace (pV2, pV3, and pV4 or pV5), placing them in MATLAB. The f_raw file contained a time stamp in C1 (in numeric format) and a mA signal from the promag meter. The pV# files were raw voltage values for pressure sensors. The label pV2 indicated the raw voltage values at the upstream floor pressure transducer closest to the spillway, and the label pV3 indicated the raw voltage values at the upstream face of the baffle block. Also, the file, pV4 designated the raw voltage values at the downstream face of the baffle block, whereas the label pV5 was the raw voltage values at the channel floor downstream of the baffle block. Once the raw data were loaded, this file and similar file were run in MATLAB. Then, two analyses were performed using in the MATLAB program: estimate and enter pressure file start time from NI metadata as [HH MM SS]; and, estimate and enter the flow rate as decimal PMF for each data set. After these two steps were done, MATLAB estimated and entered pressure sensor number on NI channel #3 (4 or 5), to document the pressure location. This value (or location) was entered as a number. Then, the program loaded values for psi2, psi3, psi4 or psi5, the pressure time, the minimum and maximum pressures, the mean pressure, and the standard deviation of the pressure into the MATLAB workspace. The values psi2, psi3, psi4 or psi5 were the calculated pressures at the four PX26 pressure sensors. The calculated pressures were put in the Excel spreadsheets for every discharge and FFT and low pass filter were applied in MATLAB for the calculated pressures which were put in Excel spreadsheets.

3.7 Fluctuation Frequencies of the Velocity

The velocity of the bulked flow was sampled with the air concentration probe (could also measure velocities of bulked flow) at frequencies of 30 kHz and 60 kHz. The approach used for calculating the bulk-flow velocity entailed time-averaging for each duration of sampling periods (typically 30 or 60 seconds) to determine an average velocity value. The velocity fluctuations were estimated in this process.

CHAPTER 4- RESULTS

4.1 The Frequency of Rotation of Roller

The frequency of the rotation of the roller formed immediately upstream of the row of baffle blocks in the stilling basin was determined approximately by means of visual observation of roller formation for each discharge of water flow departing the spillway chute and entering the basin.

1.0 PMF

From observation of the video record, the rotation speed (frequency) of the roller was determined approximately for 1.0 PMF in slow motion. The number of flow rotations counted as 150 in 60 sec. In accordance with this visual count, the rotation frequency was calculated as 2.50 Hz; as the ensuing example calculation shows:

$$\text{rotation frequency} = \frac{150 \text{ rotation}}{60 \text{ sec}} = 2.50 \, \frac{\text{rotation}}{\text{sec}} = 2.50 \text{ Hz}$$

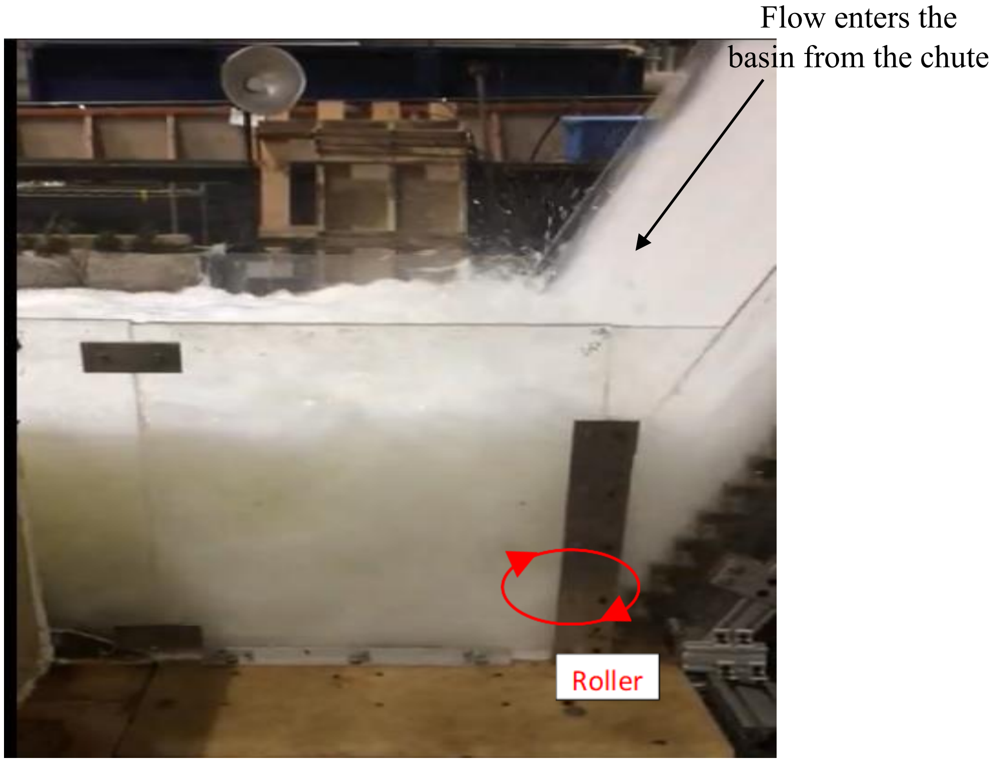

Figure 4-1. Frequency of the rotation of the flow roller in the stilling basin at 1.0 PMF. The flow enters the basin from the chute (on the right of the figure).

0.98 PMF

From observation of the video record, the rotation speed (frequency) of the roller was determined approximately for 0.98 PMF. The mean number of flow rotations were 118 rotations in 54 sec, and the mean rotation frequency thereby was calculated as 2.19 Hz; i.e.,

$$\text{rotation frequency} = \frac{118\ \text{rotation}}{54\ \text{sec}} = 2.19\,\frac{\text{rotation}}{\text{sec}} = 2.19\ \text{Hz}$$

Figure 4-2. Frequency of the rotation of the flow roller in the stilling basin at 0.98 PMF

0.75 PMF

From observation of the video record, the mean rotation speed (frequency) of the roller was determined approximately for 0.75 PMF. The number of flow rotations counted was 93 rotations in 51.5 sec and thereby the mean rotation frequency was calculated as 1.81 Hz; i.e.,

$$\text{rotation frequency} = \frac{93 \text{ rotation}}{51.5 \text{ sec}} = 1.81 \frac{\text{rotation}}{\text{sec}} = 1.81 \text{ Hz}$$

Figure 4-3. Frequency of the rotation of the flow roller in the stilling basin at 0.75 PMF

0.50 PMF

From observation of the video record, the mean rotation speed (frequency) of the roller was determined approximately for 0.50 PMF. The number of flow rotations counted was 107 in 60.5 sec, and thereby the mean rotation frequency was calculated as 1.77 Hz; i.e.,

$$\text{rotation frequency} = \frac{107\ \text{rotation}}{60.5\ \text{sec}} = 1.77\frac{\text{rotation}}{\text{sec}} = 1.77\ \text{Hz}$$

Figure 4-4. Frequency of the rotation of the flow roller in the stilling basin at 0.50 PMF

0.25 PMF

From observation of the video record, the mean rotation speed (frequency) of the roller was determined approximately for 0.25 PMF. The number of flow rotations counted was 123 in 82 sec, and thereby the mean rotation frequency was calculated as 1.50 Hz; i.e.,

$$\text{rotation frequency} = \frac{123 \text{ rotation}}{82 \text{ sec}} = 1.50\,\frac{\text{rotation}}{\text{sec}} = 1.50 \text{ Hz}$$

Figure 4-5. Frequency of the rotation of the flow roller in the stilling basin at 0.25 PMF

0.19 PMF

From observation of the video record, the mean rotation speed (frequency) of the roller was determined approximately for 0.19 PMF. The number of flow rotations counted was 86 rotation in 63.67 sec and, thereby, the mean rotation frequency was calculated as 1.35 Hz; i.e.,

$$\text{rotation frequency} = \frac{86\ \text{rotation}}{63.67\ \text{sec}} = 1.35\,\frac{\text{rotation}}{\text{sec}} = 1.35\ \text{Hz}$$

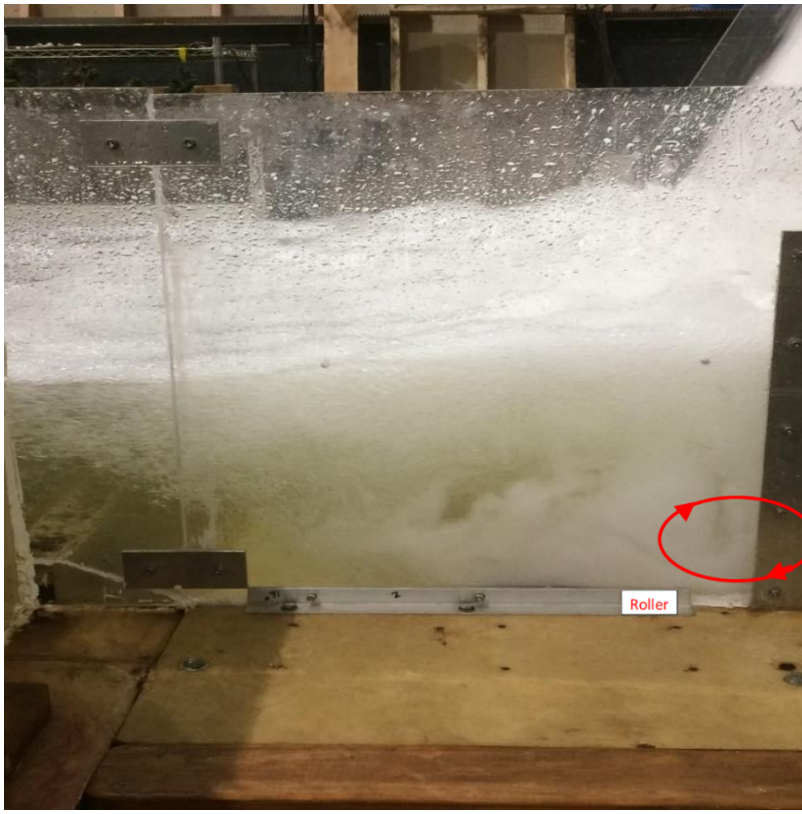

Figure 4-6. Frequency of the rotation of flow roller in the stilling basin at 0.19 PMF

0.09 PMF

From observation of the video record, the mean rotation speed (frequency) of the roller is determined approximately for 0.09 PMF. The number of flow rotations counted was 83 rotation in 72 sec and, thereby, the mean rotation frequency was calculated as 1.15 Hz; i.e.,

$$\text{rotation frequency} = \frac{83 \text{ rotation}}{72 \text{ sec}} = 1.15 \frac{\text{rotation}}{\text{sec}} = 1.15 \text{ Hz}$$

Figure 4-7. Frequency of the rotation of the flow roller in the stilling basin at 0.09 PMF

4.2 Pressure Measurements

Six measurements were collected for sensor locations 2 and 3 at the discharge of 1.0 PMF, and three measurements for locations 4 and 5 (again at 1.0 PMF) for this discharge. In addition, four measurements collected at each discharge from 0.98 PMF to 0.09 PMF for locations 2 and 3, and two measurements were obtained for locations 4 and 5 (again at each discharge from 0.98 PMF to 0.09 PMF). Table 4-1 summarizes the position of each pressure sensor, the sensor number, discharge, mean pressure, standard deviation of the pressure, minimum and maximum pressure in the stilling basin. As this table lists, the discharge was varied from 1.0 PMF to 0.09 PMF.

Table 4-1. Summary of pressure measurements in the stilling basin (model scale)

Sensor Position	**Sensor #**	**Ratio of PMF**	**Discharge** (m^3/s)	**Pressure mean** (kPa)	**Pressure STD** (kPa)	**Pressure min.** (kPa)	**Pressure max.** (kPa)
upstream floor	2	1	0.348	10.07	4.07	-7.24	49.50
upstream floor	2	1	0.347	10.07	4.00	-8.55	47.02
upstream floor	2	1	0.348	10.27	4.14	-9.17	49.50
upstream floor	2	1	0.347	10.07	4.07	-9.45	42.82
upstream floor	2	1	0.347	10.07	4.07	-9.79	49.57
upstream floor	2	1	0.348	10.14	4.14	-8.83	51.78
upstream baffle face	3	1	0.348	12.82	5.03	-5.45	54.47
upstream baffle face	3	1	0.347	12.82	5.03	-6.76	54.05
upstream baffle face	3	1	0.348	12.62	5.03	-7.79	43.78
upstream baffle face	3	1	0.347	12.76	5.03	-4.69	59.78
upstream baffle face	3	1	0.347	12.76	4.96	-5.72	50.19
upstream baffle face	3	1	0.348	12.82	5.03	-5.58	54.12
downstream baffle slope	4	1	0.348	-0.07	0.48	-2.34	3.31
downstream baffle slope	4	1	0.347	-0.07	0.48	-3.24	4.34
downstream baffle slope	4	1	0.348	3.45	1.10	-5.10	11.72
downstream floor	5	1	0.348	2.90	0.76	-2.83	8.69
downstream floor	5	1	0.347	2.90	0.76	-3.72	9.10

downstream floor	5	1	0.347	2.90	0.76	-3.03	10.14
upstream floor	2	0.98	0.340	10.20	4.21	-8.76	66.9
upstream floor	2	0.98	0.340	10.14	4.07	-6.41	46.88
upstream floor	2	0.98	0.341	10.20	4.07	-6.69	51.16
upstream floor	2	0.98	0.340	10.20	4.14	-8.14	44.47
upstream baffle face	3	0.98	0.340	11.93	4.96	-19.31	56.67
upstream baffle face	3	0.981	0.340	12.00	4.90	-14.55	52.26
upstream baffle face	3	0.98	0.341	12.13	4.96	-16.48	54.74
upstream baffle face	3	0.98	0.340	12.13	4.90	-17.17	63.85
downstream baffle slope	4	0.98	0.340	0.00	0.48	-2.07	4.07
downstream baffle slope	4	0.98	0.340	0.00	0.48	-11.31	5.86
downstream floor	5	0.98	0.341	2.90	0.76	-2.55	11.03
downstream floor	5	0.98	0.340	2.90	0.76	-2.55	10.41
upstream floor	2	0.75	0.260	8.48	3.31	-6.00	41.02
upstream floor	2	0.75	0.261	8.55	3.38	-5.79	44.82
upstream floor	2	0.75	0.260	8.48	3.31	-8.07	38.89
upstream floor	2	0.75	0.259	8.55	3.31	-5.86	40.54
upstream baffle face	3	0.75	0.260	7.45	2.90	-17.24	38.89
upstream baffle face	3	0.75	0.261	7.45	2.90	-12.82	36.82
upstream baffle face	3	0.75	0.260	7.38	2.90	-12.07	39.02
upstream baffle face	3	0.75	0.259	7.45	2.90	-13.79	39.51
downstream baffle slope	4	0.75	0.260	1.10	0.55	-1.38	4.48
downstream baffle slope	4	0.75	0.259	0.97	0.48	-1.52	4.14
downstream floor	5	0.75	0.260	3.24	0.55	-1.17	7.24
downstream floor	5	0.75	0.261	3.24	0.55	-2.07	8.76
upstream floor	2	0.5	0.173	5.65	2.00	-7.93	32.75
upstream floor	2	0.5	0.173	5.65	2.07	-4.55	30.61
upstream floor	2	0.5	0.173	5.65	2.07	-6.41	27.44
upstream floor	2	0.5	0.174	5.72	2.07	-6.55	30.47
upstream baffle face	3	0.5	0.173	4.34	1.38	-9.10	16.55
upstream baffle face	3	0.5	0.173	4.41	1.38	-9.45	24.96
upstream baffle face	3	0.5	0.173	4.41	1.38	-11.72	27.79
upstream baffle face	3	0.5	0.174	4.41	1.45	-7.65	16.41
downstream baffle slope	4	0.5	0.173	2.14	0.21	0.97	3.10

downstream baffle slope	4	0.5	0.173	2.14	0.21	0.90	3.31
downstream floor	5	0.5	0.173	3.10	0.28	0.97	4.76
downstream floor	5	0.5	0.174	3.10	0.28	0.34	5.52
upstream floor	2	0.25	0.087	2.96	0.76	-2.34	13.65
upstream floor	2	0.25	0.087	2.96	0.76	-1.38	14.62
upstream floor	2	0.25	0.087	2.96	0.69	-2.28	12.00
upstream floor	2	0.25	0.089	2.96	0.76	-3.59	13.65
upstream baffle face	3	0.25	0.087	2.48	0.48	-1.59	8.96
upstream baffle face	3	0.25	0.087	2.48	0.48	-0.90	6.76
upstream baffle face	3	0.25	0.087	2.48	0.48	-0.69	7.38
upstream baffle face	3	0.25	0.089	2.48	0.48	-0.90	8.00
downstream baffle slope	4	0.25	0.087	1.79	0.07	1.31	2.21
downstream baffle slope	4	0.25	0.089	1.59	0.21	0.62	2.28
downstream floor	5	0.25	0.087	2.83	0.07	2.34	3.17
downstream floor	5	0.25	0.087	2.83	0.07	2.34	3.24
upstream floor	2	0.19	0.065	2.55	0.41	-0.97	9.93
upstream floor	2	0.19	0.065	2.48	0.41	-0.83	8.62
upstream floor	2	0.19	0.065	2.55	0.41	-1.59	11.03
upstream floor	2	0.19	0.065	2.55	0.41	-2.14	10.55
upstream baffle face	3	0.19	0.065	2.14	0.28	0.48	5.03
upstream baffle face	3	0.19	0.065	2.14	0.28	0.07	4.83
upstream baffle face	3	0.19	0.065	2.14	0.28	0.07	4.76
upstream baffle face	3	0.19	0.065	2.14	0.28	0.07	5.31
downstream baffle slope	4	0.19	0.065	1.65	0.07	1.17	1.93
downstream baffle slope	4	0.19	0.065	1.59	0.07	0.97	1.93
downstream floor	5	0.19	0.065	2.69	0.07	2.34	2.96
downstream floor	5	0.19	0.065	2.69	0.07	2.34	2.96
upstream floor	2	0.09	0.032	2.34	0.14	0.34	5.38
upstream floor	2	0.09	0.032	2.34	0.14	0.90	4.21
upstream floor	2	0.09	0.032	2.34	0.14	0.34	6.27
upstream floor	2	0.09	0.032	2.34	0.14	1.03	4.76
upstream baffle face	3	0.09	0.032	1.65	0.07	1.17	2.55
upstream baffle face	3	0.09	0.032	1.65	0.07	0.83	2.21
upstream baffle face	3	0.09	0.032	1.65	0.07	1.10	2.41

upstream baffle face	3	0.09	0.032	1.65	0.07	0.97	2.28
downstream baffle slope	4	0.09	0.032	1.38	0.07	1.24	1.59
downstream baffle slope	4	0.09	0.032	1.38	0.07	1.24	1.59
downstream floor	5	0.09	0.032	2.41	0.07	2.28	2.62
downstream floor	5	0.09	0.032	2.41	0.07	2.28	2.62

Based on Table 4-1, the values of the mean pressures at the upstream face of the central baffle block face were higher than at the upstream floor of the stilling basin at 1.0 PMF and 0.98 PMF. At the discharges from 0.75 PMF to 0.09 PMF, the values of the mean pressures at the upstream floor of the stilling basin were higher than at the upstream face of the baffle block. At the discharges of 0.19 PMF and 0.09 PMF, the values of the mean pressures at the downstream floor of the stilling basin were higher than at the upstream floor of the stilling basin. The maximum pressure recorded at the front face of the baffle block when the model-scale flow rate was equivalent to the 1.00 PMF flowrate was 59.78 kPa at model scale. There were also some negative pressure values observed at upstream floor, upstream baffle face, downstream baffle slope and downstream floor.

The pressures in the stilling basin measured when the design discharge of the spillway was 1.0 PMF were as follow:

- Upstream floor: mean pressure was 10.1 kPa, standard deviation of pressure was 4.14 kPa, maximum pressure measured in data series was 51.8 kPa, minimum pressure measured in the data series was –9.79 kPa. At prototype scale, the mean pressure + STD (standard deviation) pressure was 341.8 kPa.
- Upstream baffle face: mean pressure was 12.8 kPa, standard deviation of pressure was 4.83 kPa, maximum pressure measured in data series was 59.8 kPa, minimum pressure

measured in the data series was –7.79 kPa. At prototype scale, the mean pressure + STD (standard deviation) pressure was 423.1 kPa.

- Downstream baffle slope: mean pressure was 1.1 kPa, standard deviation of pressure was 0.69 kPa, maximum pressure measured in data series was 11.7 kPa, minimum pressure measured in the data series was –5.1 kPa. At prototype scale, the mean pressure + STD (standard deviation) pressure was 42.96 kPa.
- Downstream floor***:*** mean pressure was 2.90 kPa, standard deviation of pressure was 0.76 kPa, maximum pressure measured in data series was 10.14 kPa, minimum pressure measured in the data series was –3.72 kPa. At prototype scale, the mean pressure + STD (standard deviation) pressure was 87.8 kPa.

4.3 FFT Results for 1 PMF Flow

This section demonstrates the Fast-Fourier Transform (FFT) results of the 1.0 PMF flow (model scale) obtained from the original and filtered signals produced by the pressure transducers. Six data sets were obtained. Each data set had a different sampling time, however.

DATA SET 1

This data set was taken when the pressure start time from NI metadata was 11:07:45.367. Pressure data collected over 168.87 seconds. After the time and pressure sensor number were entered on NI channel in MATLAB, another figure window was entered and pressures for sensor 2, sensor 3, and either sensor 4 or 5 were plotted. For this data set, the calculated pressures were at the upstream floor of the stilling basin, upstream baffle face and downstream baffle slope.

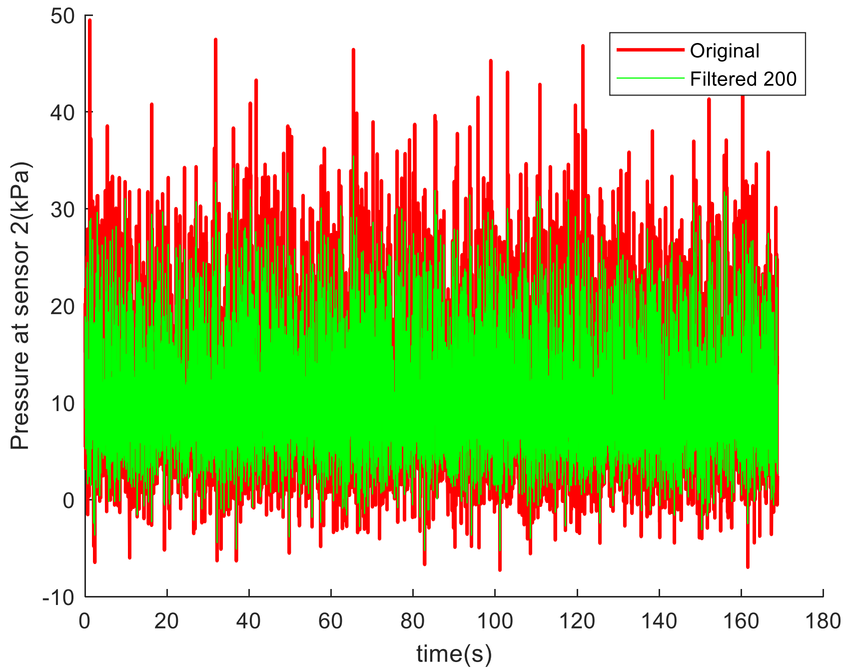

Original
Filtered 200
Pressure at sensor 2(kPa)
time(s)

(a)

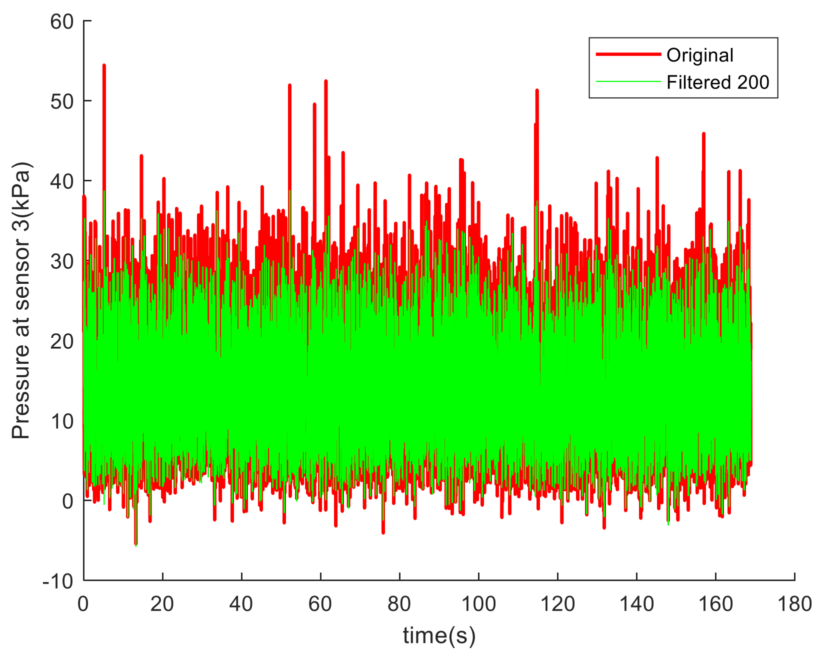

Original
Filtered 200
Pressure at sensor 3(kPa)
time(s)

(b)

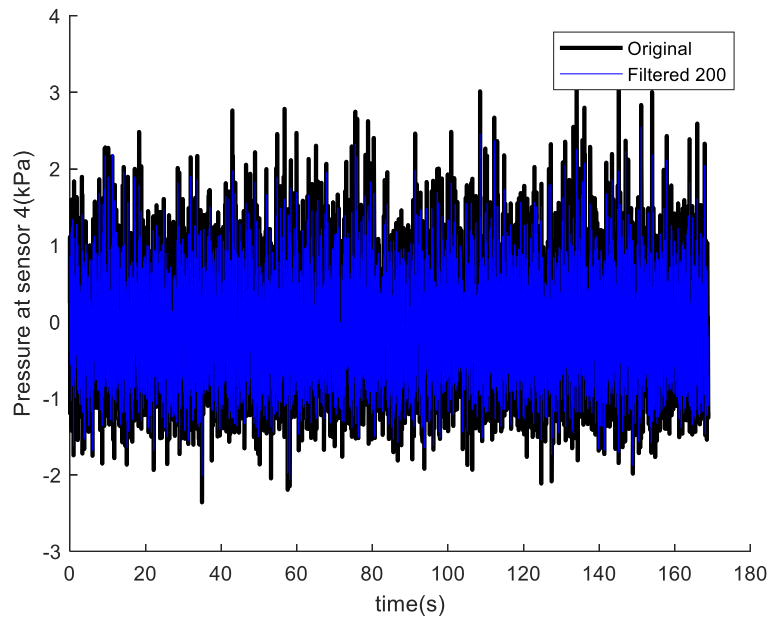

Original
Filtered 200
Pressure at sensor 4(kPa)
time(s)

(c)

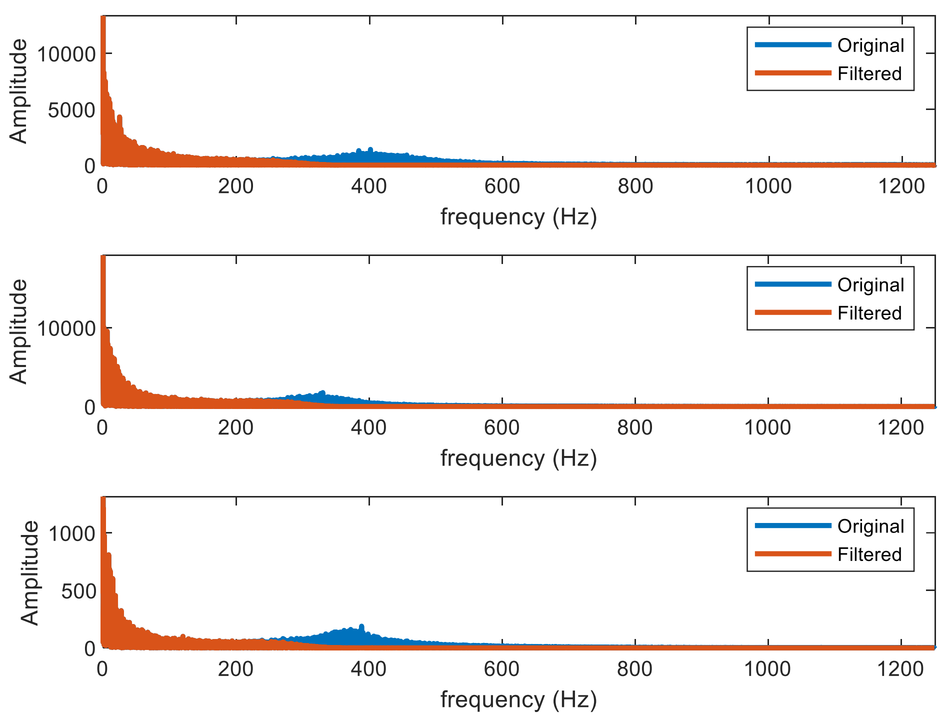

Original
Filtered
Amplitude
frequency (Hz)

(d)

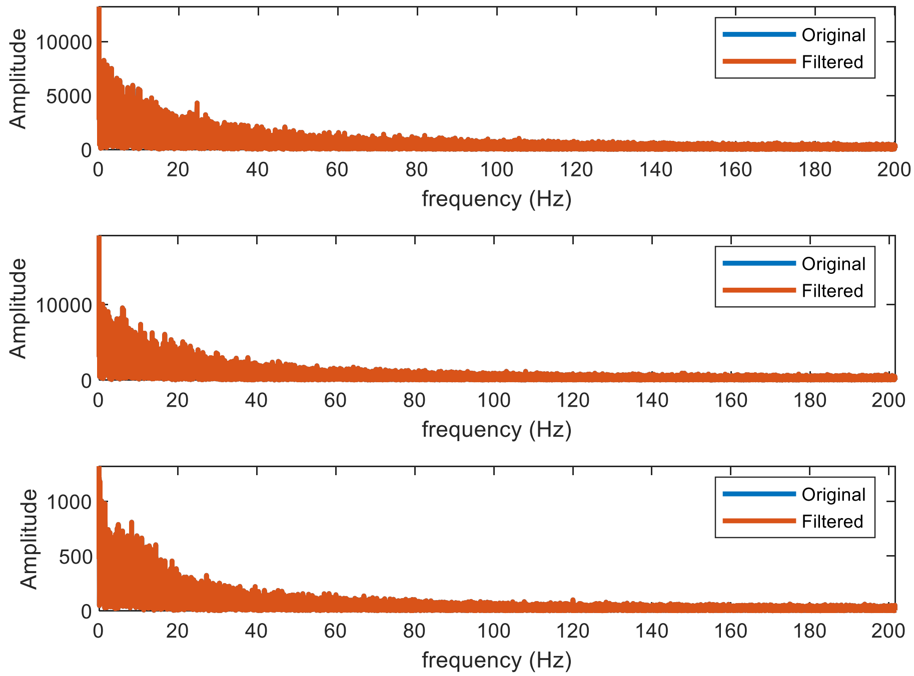

(e)

Figure 4-8. Pressure data-set 1: (a) Time versus pressure at sensor 2 (upstream floor); (b) at sensor 3 (upstream baffle face); (c) at sensor 4 (downstream baffle slope) for the original and filtered signal at the discharge of 1 PMF; (d) FFT plots for both the original and filtered signal at upstream floor (sensor 2), upstream baffle face (sensor 3) and downstream baffle slope (sensor 4) at the discharge of 1 PMF; and, (e) closer views of the FFT plots for frequencies below 200 Hz, for both the original and filtered signals.

A low-pass filter was applied to the original signal in MATLAB, and the signal filtered out at frequencies above 200 Hz for data set 1. The cut-off frequency of the signal was chosen to be 200 Hz to outline the fluctuating pressure patterns in a variety of scales. Figures 4-8(a) through (c) show the original signal and low pass filtered signal at 200 Hz at the upstream floor of the stilling basin, upstream baffle face and downstream baffle slope, respectively. Then, the FFT method was applied to both original and filtered signal. Figure 4-8 (d) illustrates the FFT plots for both the filtered and original signal. The difference between the filtered signal and original signal can be seen readily. The filter did not (strictly speaking) cut the signal after the cut-off frequency had been set, so it still had some of content from high frequency content of the original signal. Figure 4-8 (e) gives a closer view of the FFT plots for both the filtered and original signals, for frequencies to 200 Hz. The result, given in Figure 4-8 (e), shows that filtered FFT gives about the same result as the FFT from the unfiltered data and there is no continuous low frequency or continuous high frequency pattern in the signal because the signal is so randomly distributed. Therefore, the FFT did not reveal the dominant frequency in the signal. Average values of frequency for each location were 100 Hz. The low-frequency peaks existed (in Figure 4-8(e)) which might have arisen from the waves or large-scale turbulent taking place in the flow, as Carlson et al., (2007) suggest. The corresponding frequencies were 1.214, 0.9179, 0.02961 Hz at the upstream floor of the stilling basin, upstream baffle face and downstream baffle slope, respectively.

DATA SET 2

This data set was taken when the pressure start time from NI metadata was 11:11:14.096. Pressure data were collected over 181.11 seconds. For this data set, the calculated pressures were at the upstream floor of the stilling basin, upstream baffle face and downstream baffle slope, respectively.

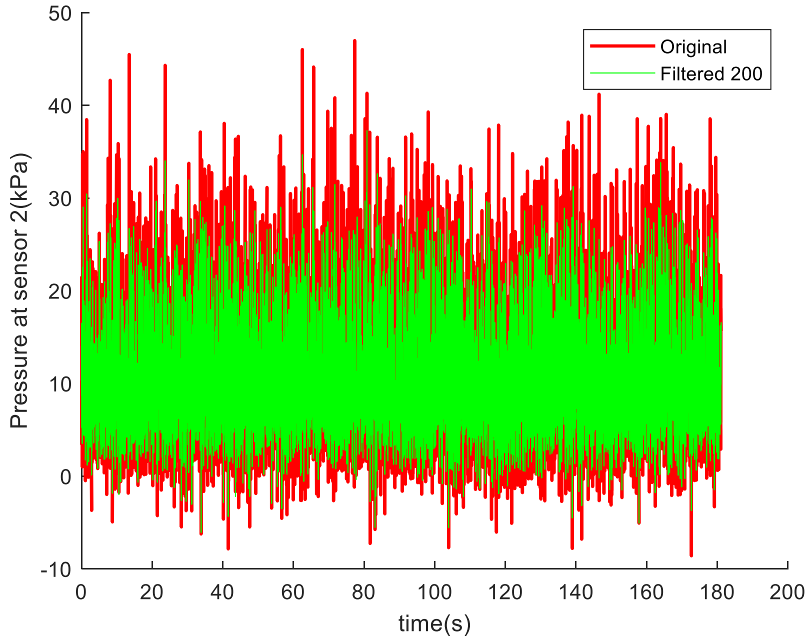

Original
Filtered 200
Pressure at sensor 2(kPa)
time(s)
50
40
30
20
10
0
-10
0
20
40
60
80
100
120
140
160
180
200

(a)

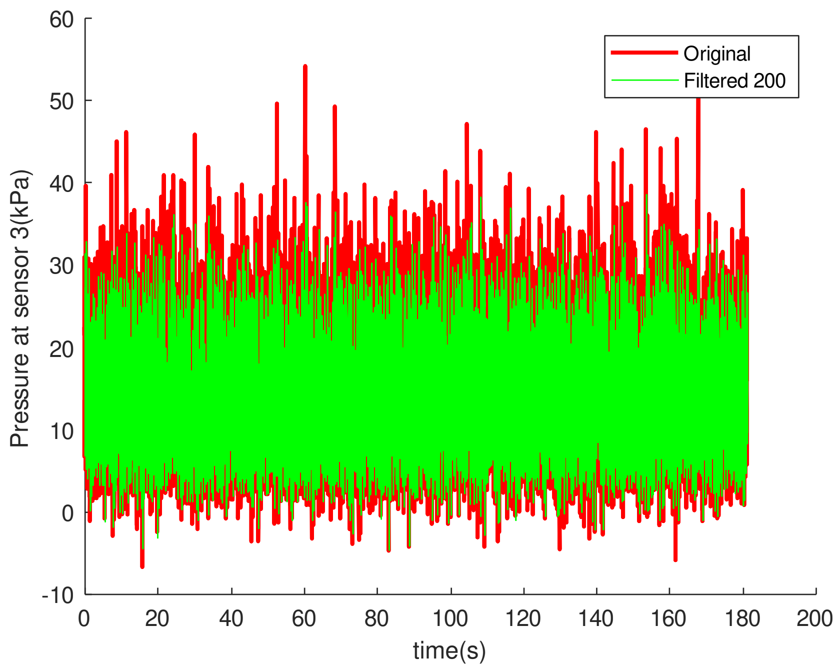

Original
Filtered 200
Pressure at sensor 3(kPa)
time(s)
60
50
40
30
20
10
0
-10
0
20
40
60
80
100
120
140
160
180
200

(b)

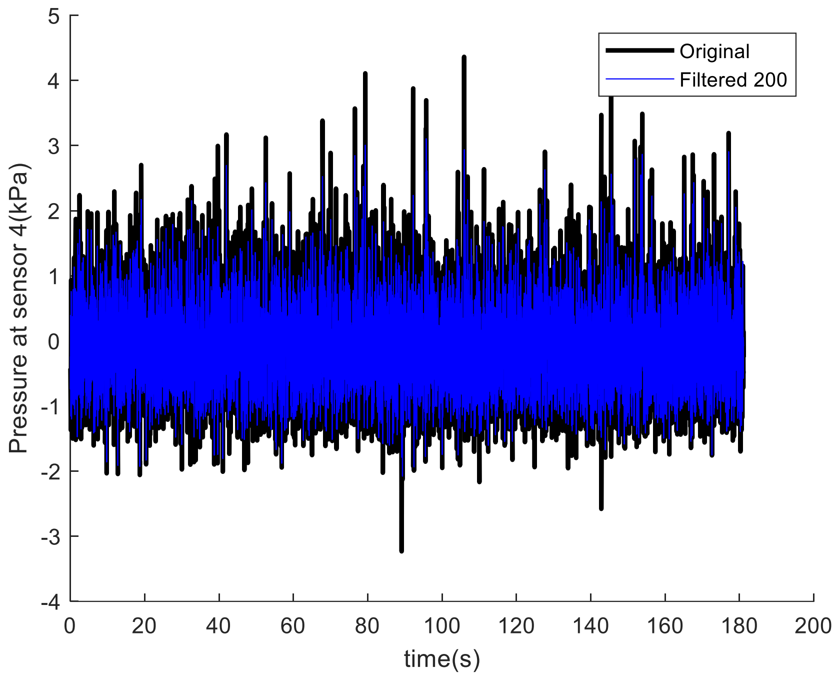

Original
Filtered 200
Pressure at sensor 4(kPa)
time(s)

(c)

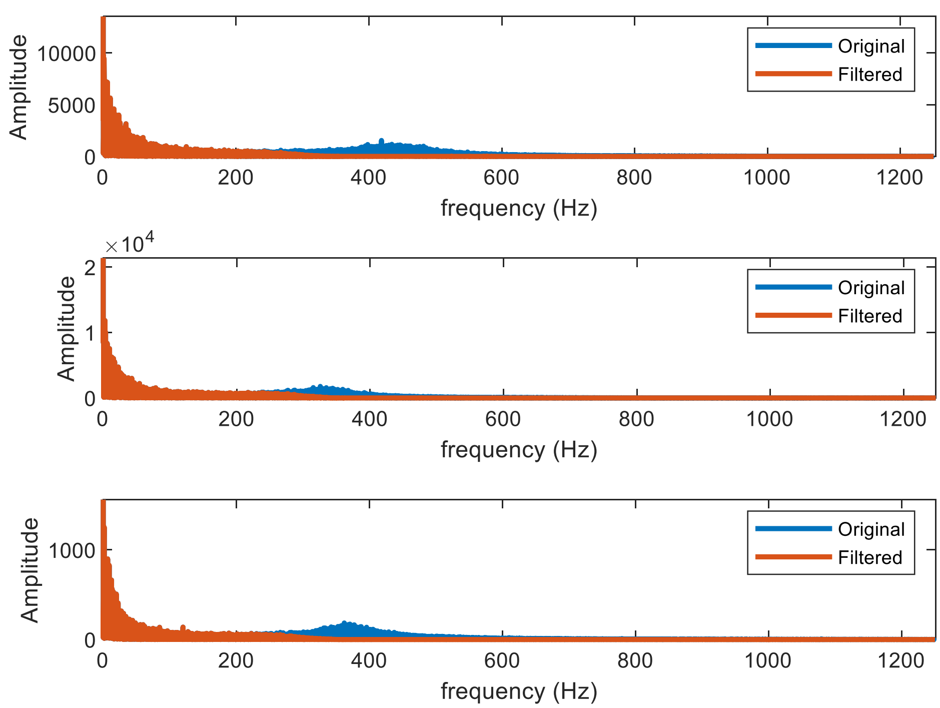

Original
Filtered
Amplitude
frequency (Hz)
$\times 10^4$

(d)

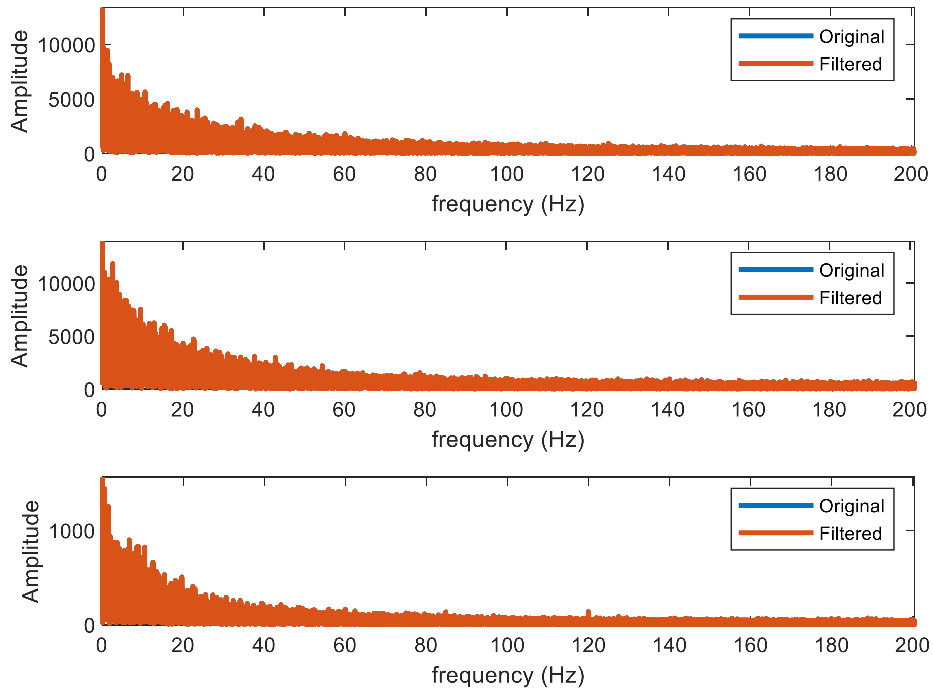

(e)

Figure 4-9. Pressure data-set 2: (a)Time versus pressure at sensor 2 (upstream floor) (b) at sensor 3 (upstream baffle face) and (c) at sensor 4 (downstream baffle slope) for the original and filtered signal at the discharge of 1 PMF (d) FFT plots for both the original and filtered signal at upstream floor (sensor 2), upstream baffle face (sensor 3) and downstream baffle slope (sensor 4) at the discharge of 1 PMF (e) closer views of the FFT plots for frequencies below 200 Hz, for both the original and filtered signals

Figures 4-9 (a) through (c) show the original signal and low pass filtered signal at 200 Hz at the upstream floor of the stilling basin, upstream baffle face and downstream baffle slope, respectively. Figure 4-9 (d) illustrates the FFT plots for both the filtered and original signal. Figure 4-9 (e) demonstrates the closer view of the FFT plots for both the filtered and original signal to 200 Hz. Average values of frequency for each location were 100 Hz. The low-frequency peaks were 0.2374, 2.573, 0.519 Hz at the upstream floor of the stilling basin, upstream baffle face and downstream baffle slope, respectively.

DATA SET 3

This data set was taken when the pressure start time from NI metadata was 11:17:07.153. Pressure data collected over 61.96 seconds. For this data set, the calculated pressures were at the upstream floor of the stilling basin, upstream baffle face and downstream floor of the stilling basin.

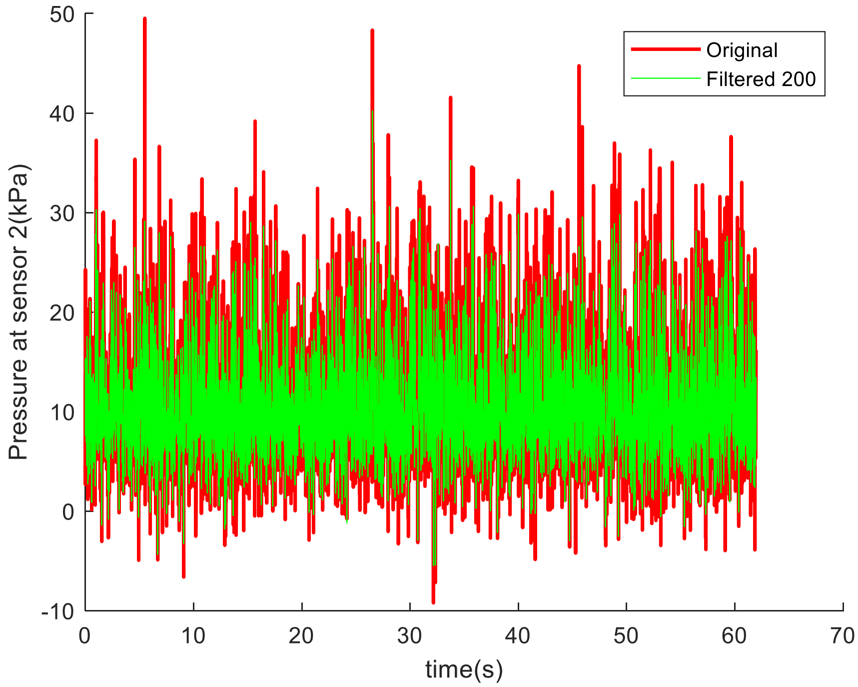

(a)

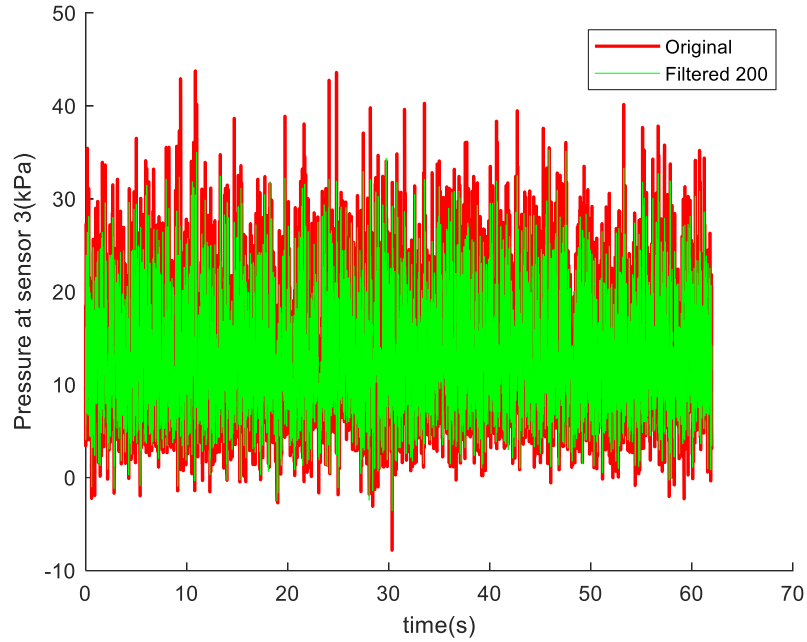

Original
Filtered 200
Pressure at sensor 3(kPa)
time(s)

(b)

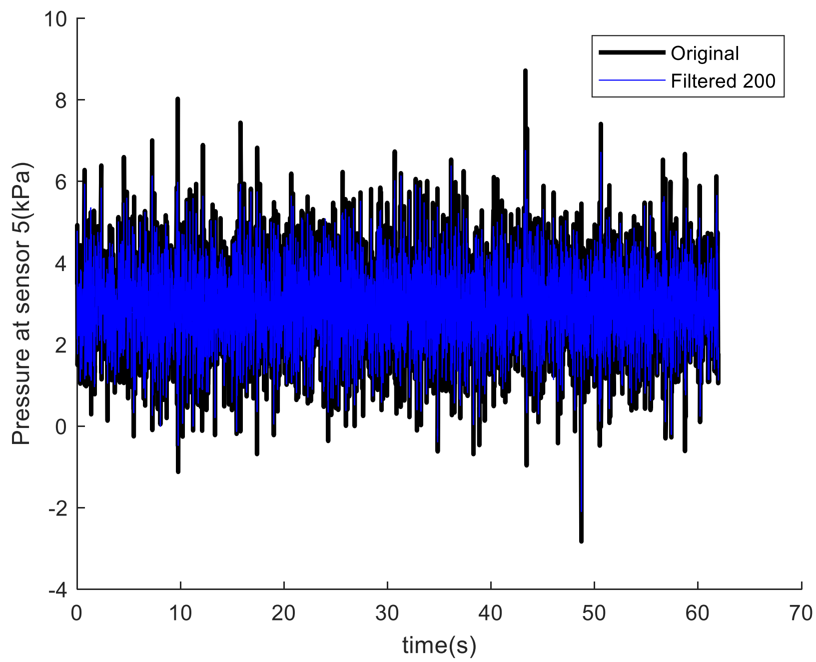

Original
Filtered 200
Pressure at sensor 5(kPa)
time(s)

(c)

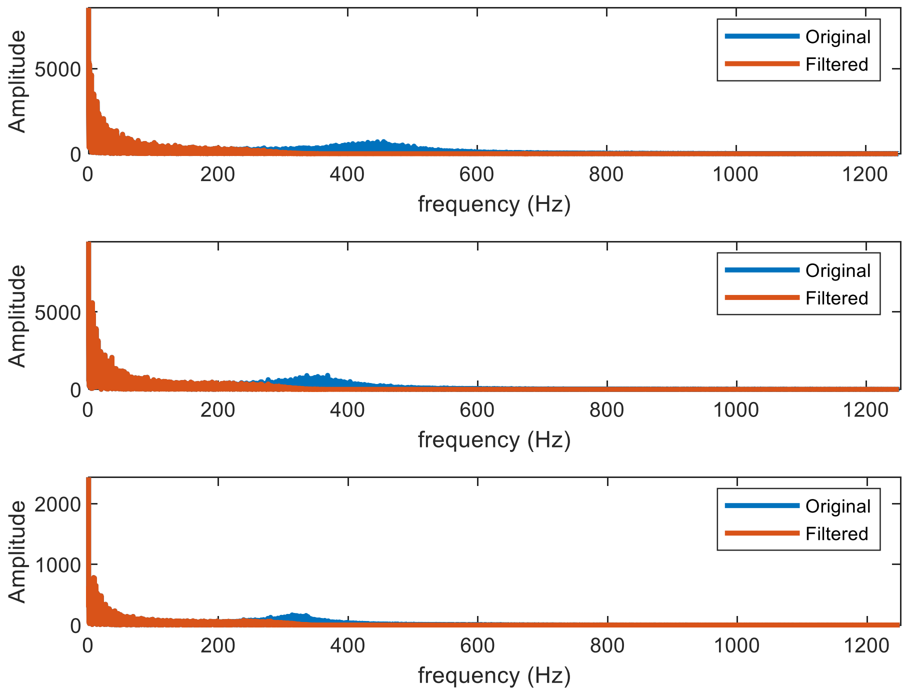
Amplitude
frequency (Hz)
Original
Filtered

(d)

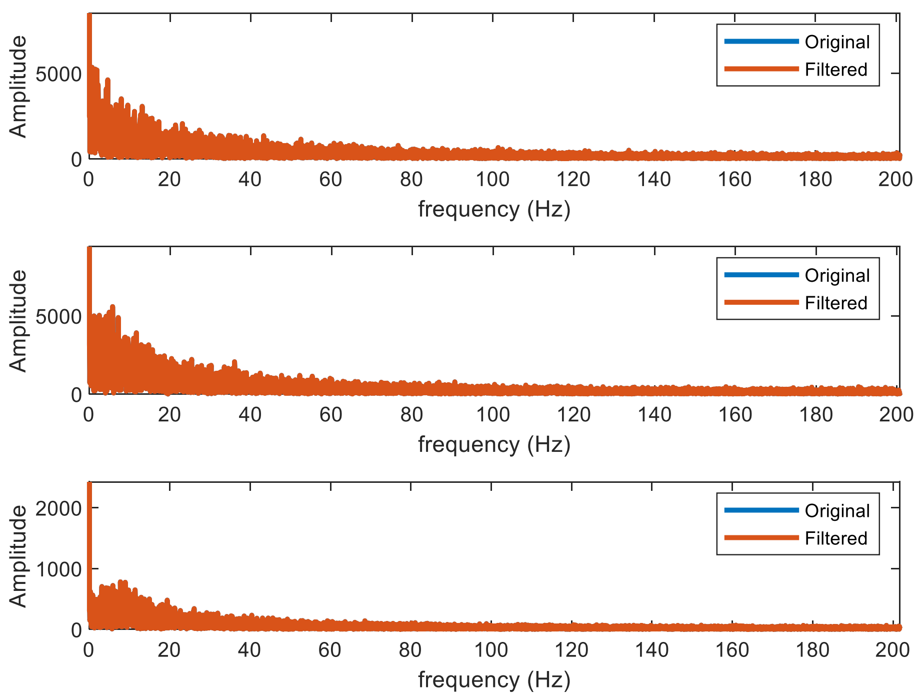
Amplitude
frequency (Hz)
Original
Filtered

(e)

Figure 4-10. Pressure data-set 3: (a) Time versus pressure at sensor 2 (upstream floor) (b) at sensor 3 (upstream baffle face) and (c) at sensor 5 (downstream floor) for the original and filtered signal at the discharge of 1 PMF (d) FFT plots for both the original and filtered signal at upstream floor (sensor 2), upstream baffle face (sensor 3) and downstream floor (sensor 5) at the discharge of 1 PMF (e) closer views of the FFT plots for frequencies below 200 Hz, for both the original and filtered signals

Figures 4-10 (a) through (c) show the original signal and low pass filtered signal at 200 Hz at upstream floor of the stilling basin, upstream baffle face and downstream floor of the stilling basin, respectively. Figure 4-10 (d) illustrates the FFT plots for both the filtered and original signal. Figure 4-10(e) demonstrates the closer view of the FFT plots for both the filtered and original signal to 200 Hz. Average values of frequency for each location were 100 Hz. The low-frequency peaks were 0.6617, 5.746, and 7.715 Hz at upstream floor of the stilling basin, upstream baffle face and downstream floor of the stilling basin, respectively.

DATA SET 4

This data set was taken when the pressure start time from NI metadata was 11:21:23.477. Pressure data collected over 180.03 seconds. For this data set, the calculated pressures were at upstream floor of the stilling basin, upstream baffle face and downstream floor of the stilling basin, respectively.

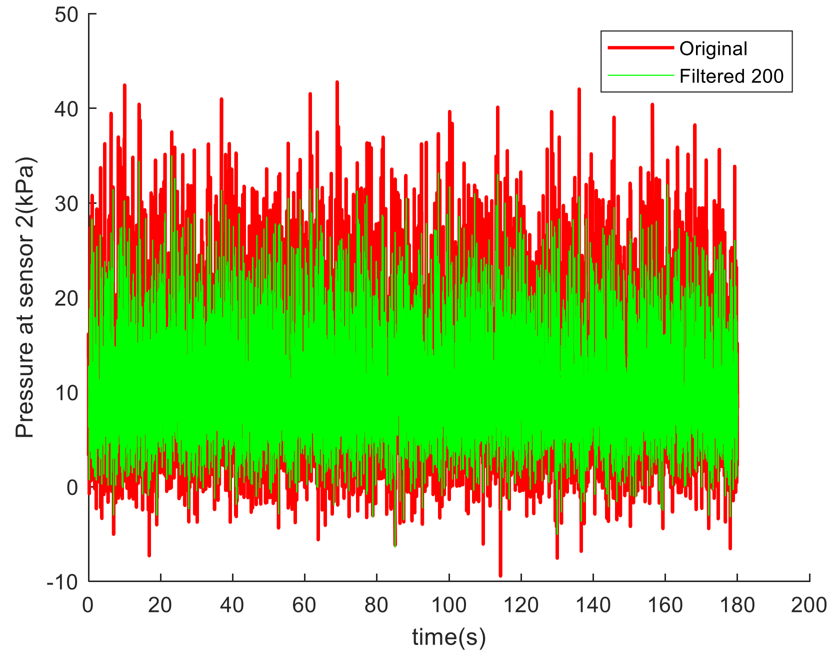
Original
Filtered 200
Pressure at sensor 2(kPa)
time(s)
50
40
30
20
10
0
-10
0
20
40
60
80
100
120
140
160
180
200

(a)

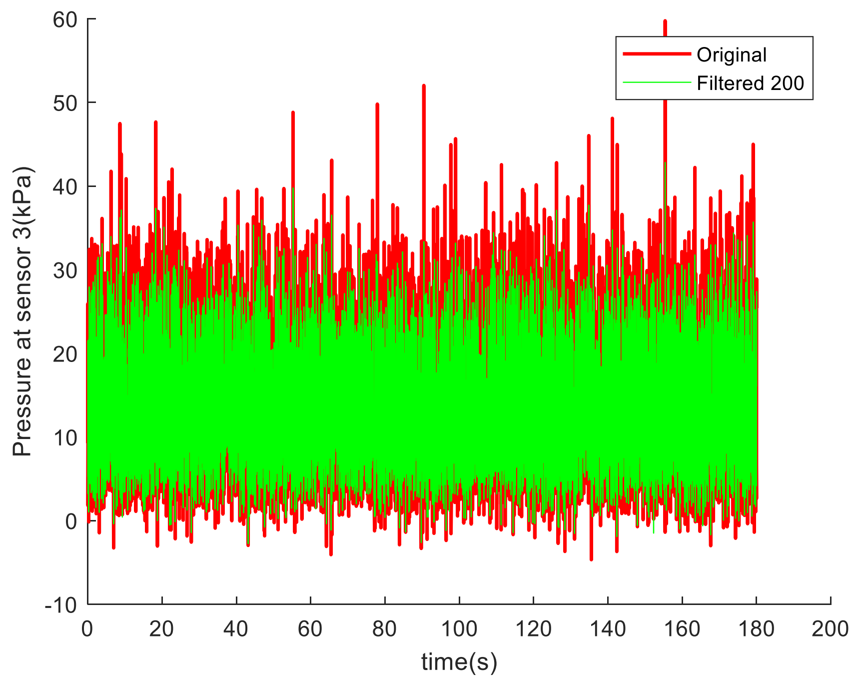
Original
Filtered 200
Pressure at sensor 3(kPa)
time(s)
60
50
40
30
20
10
0
-10
0
20
40
60
80
100
120
140
160
180
200

(b)

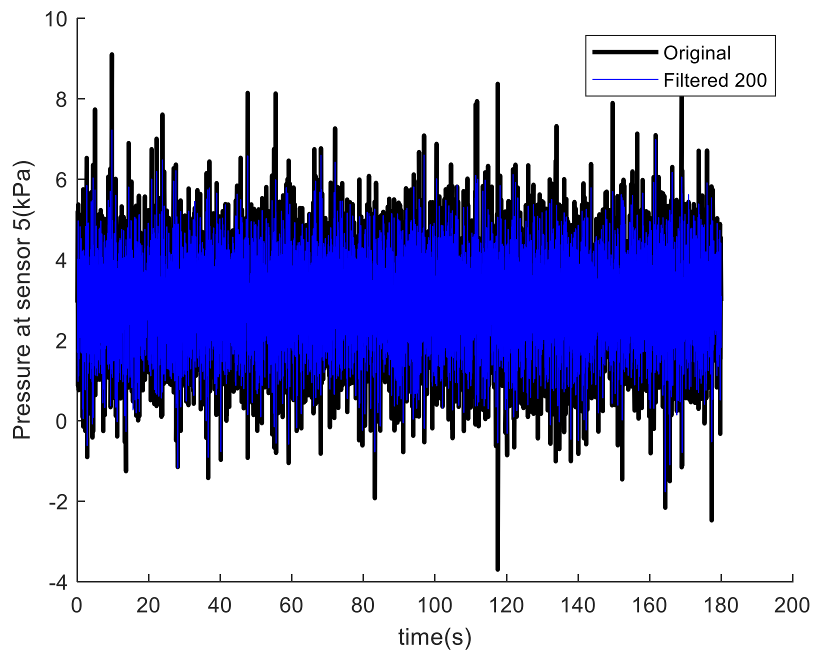

Original
Filtered 200
Pressure at sensor 5(kPa)
time(s)

(c)

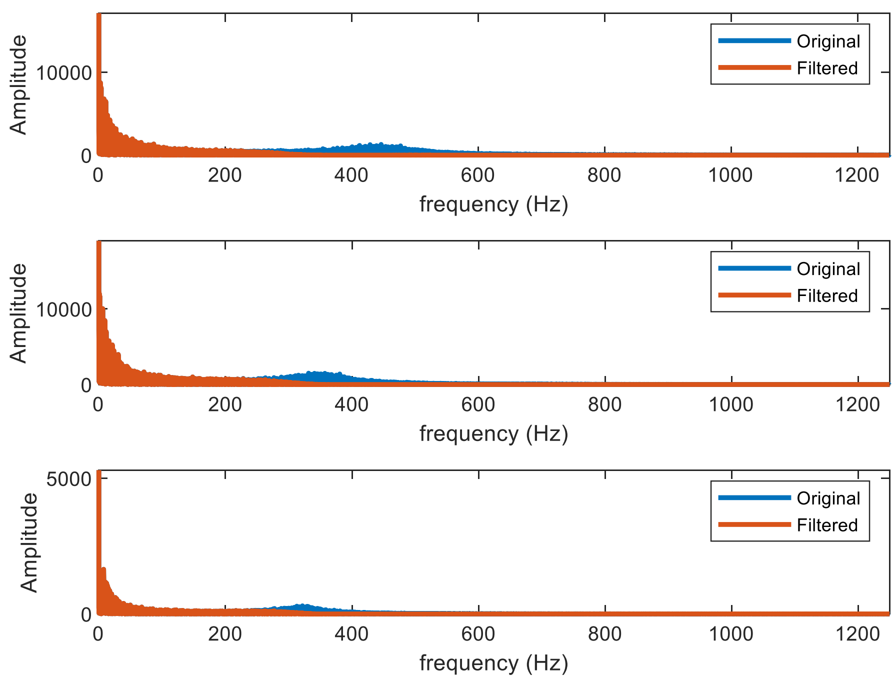

Original
Filtered
Amplitude
frequency (Hz)
Original
Filtered
Amplitude
frequency (Hz)
Original
Filtered
Amplitude
frequency (Hz)

(d)

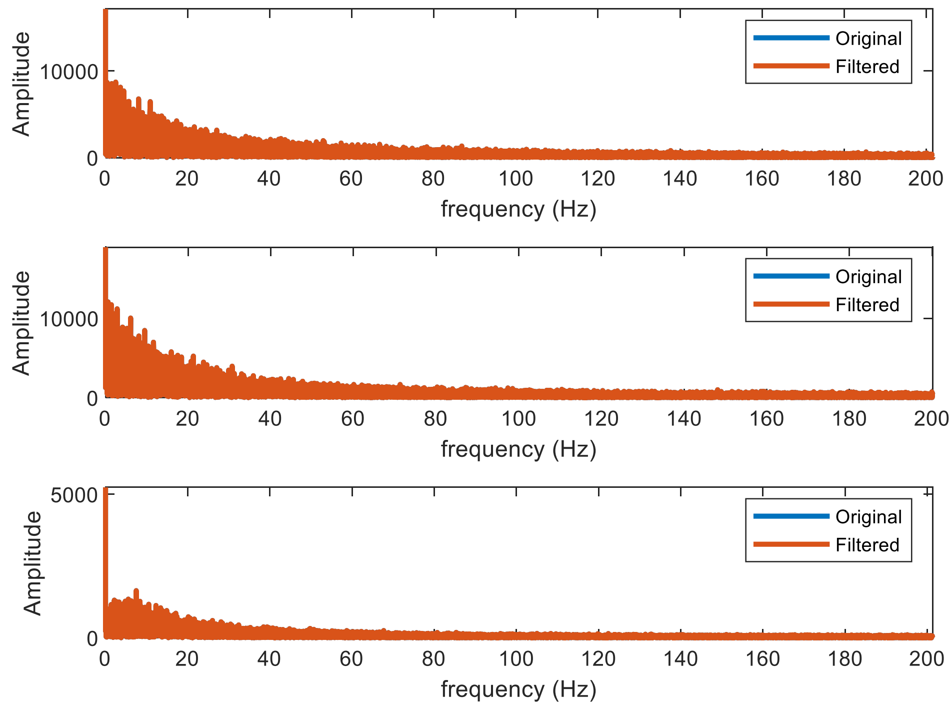

(e)

Figure 4-11. Pressure data-set 4: (a) Time versus pressure at sensor 2 (upstream floor) (b) at sensor 3 (upstream baffle face) and (c) at sensor 5 (downstream floor) for the original and filtered signal at the discharge of 1 PMF (d) FFT plots for both the original and filtered signal at upstream floor (sensor 2), upstream baffle face (sensor 3) and downstream floor (sensor 5) at the discharge of 1 PMF (e) closer views of the FFT plots for frequencies below 200 Hz, for both the original and filtered signals

Figures 4-11 (a) through (c) show the original signal and low pass filtered signal at 200 Hz at the upstream floor of the stilling basin, upstream baffle face and downstream floor of the stilling basin, respectively. Figure 4-11 (d) illustrates the FFT plots for both the filtered and original signal. Figure 4-11 (e) demonstrates the closer view of the FFT plots for both the filtered and original signal to 200 Hz. Average values of frequency for each location were 100 Hz. The low-frequency peaks were 2.483, 0.611, and 7.476 Hz at the upstream floor of the stilling basin, upstream baffle face and downstream floor of the stilling basin, respectively.

DATA SET 5

This data set was taken when the pressure start time from NI metadata was 11:26:58.457. Pressure data were collected over 195.90 seconds. For this data set, the calculated pressures were at the upstream floor of the stilling basin, upstream baffle face and downstream floor of the stilling basin.

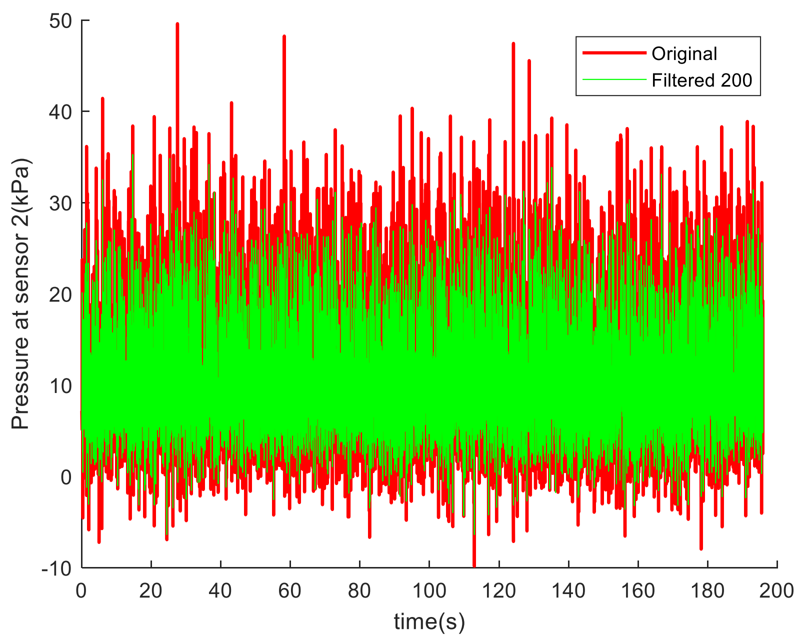

(a)

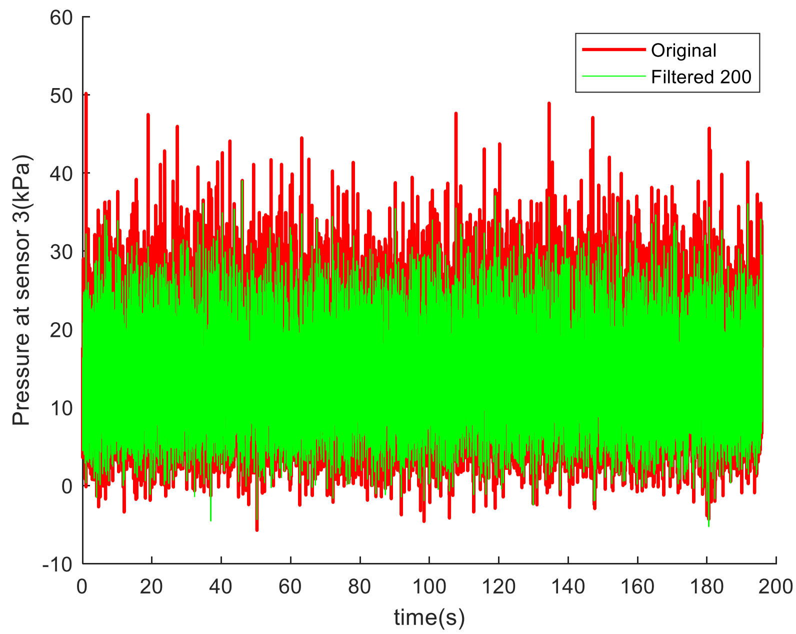
Original
Filtered 200
Pressure at sensor 3(kPa)
time(s)
60
50
40
30
20
10
0
-10
0
20
40
60
80
100
120
140
160
180
200

(b)

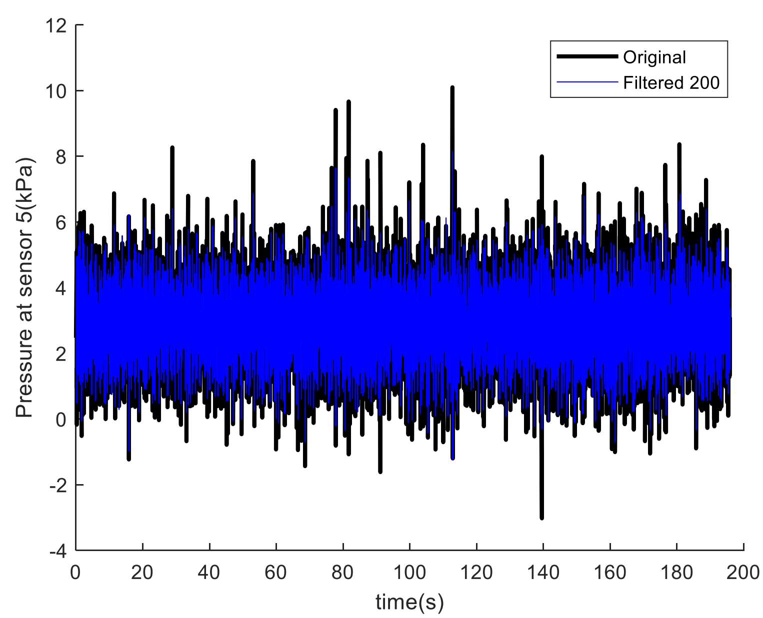
Original
Filtered 200
Pressure at sensor 5(kPa)
time(s)
12
10
8
6
4
2
0
-2
-4
0
20
40
60
80
100
120
140
160
180
200

(c)

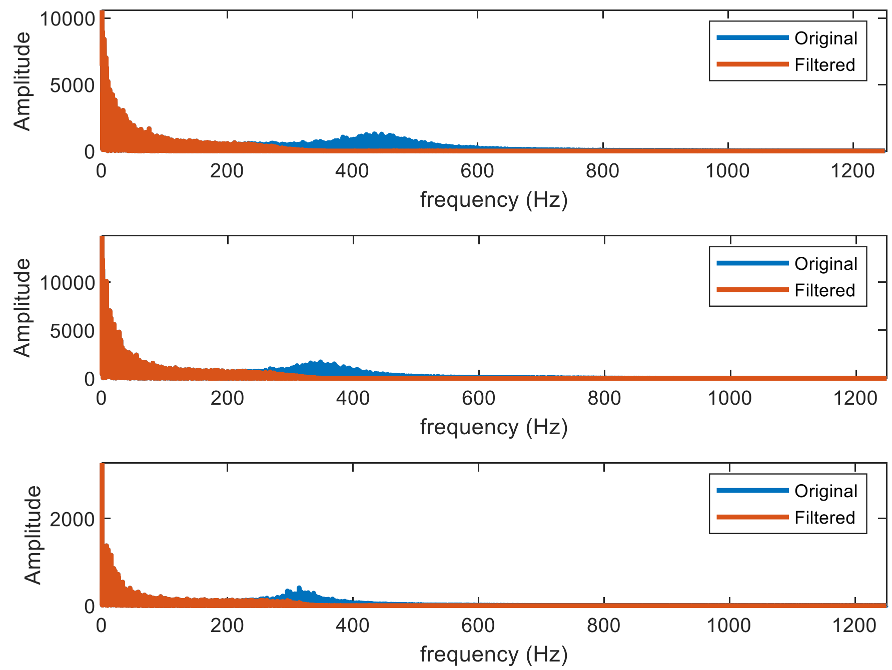
Amplitude
frequency (Hz)
Original
Filtered

(d)

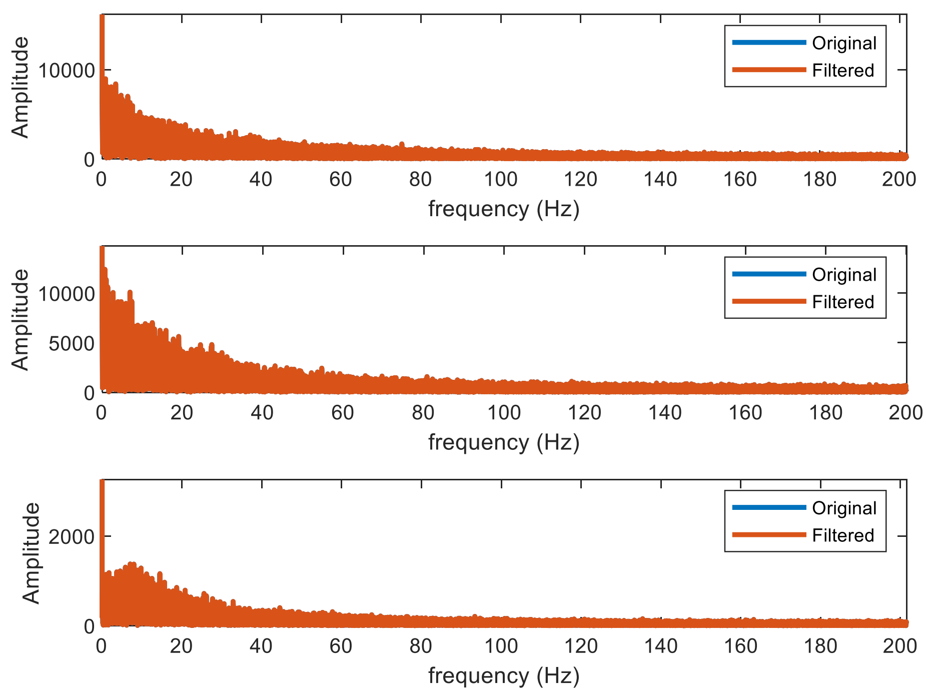
Amplitude
frequency (Hz)
Original
Filtered

(e)

Figure 4-12. Pressure data-set 5: (a) Time versus pressure at sensor 2 (upstream floor) (b) at sensor 3 (upstream baffle face) and (c) at sensor 5 (downstream floor) for the original and filtered signal at the discharge of 1 PMF (d) FFT plots for both the original and filtered signal at upstream floor (sensor 2), upstream baffle face (sensor 3) and downstream floor (sensor 5) at the discharge of 1 PMF (e) closer views of the FFT plots for frequencies below 200 Hz, for both the original and filtered signals

Figures 4-12 (a) through (c) show the original signal and low pass filtered signal at 200 Hz at the upstream floor of the stilling basin, upstream baffle face and downstream floor of the stilling basin, respectively. Figure 4-12 (d) illustrates the FFT plots for both the filtered and original signal. Figure 4-12 (e) demonstrates the closer view of the FFT plots for both the filtered and original signal to 200 Hz. Average values of frequency for each location were 100 Hz. The low-frequency peaks were 0.8576, 0.6942, and 7.034 Hz at the upstream floor of the stilling basin, upstream baffle face and downstream floor of the stilling basin, respectively.

DATA SET 6

This data set was taken when the pressure start time from NI metadata was 11:35:46.244. Pressure data collected over 220.47 seconds. For this data set, the calculated pressures were at the upstream floor of the stilling basin, upstream baffle face and downstream baffle slope.

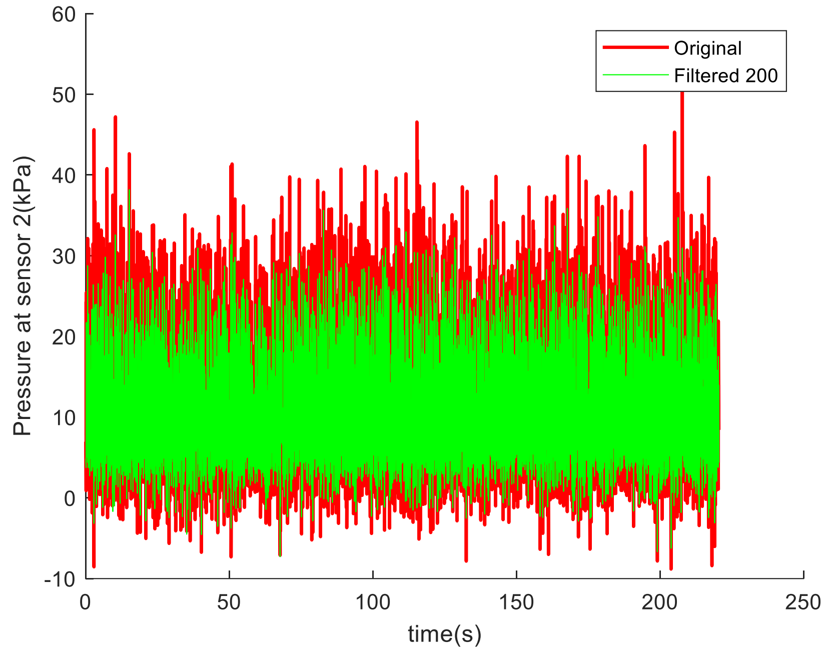
60
50
40
30
20
10
0
-10
0
50
100
150
200
250
time(s)
Pressure at sensor 2(kPa)
Original
Filtered 200

(a)

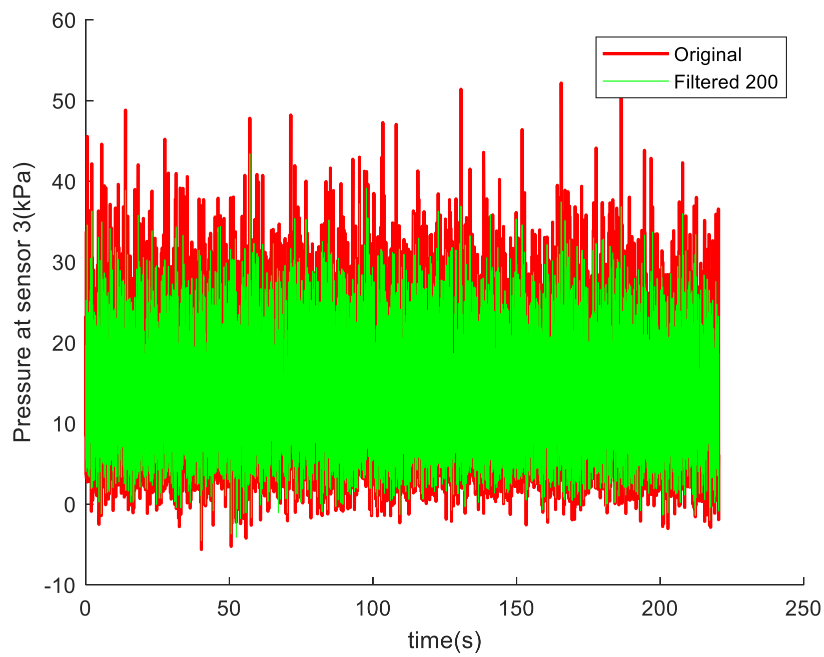
60
50
40
30
20
10
0
-10
0
50
100
150
200
250
time(s)
Pressure at sensor 3(kPa)
Original
Filtered 200

(b)

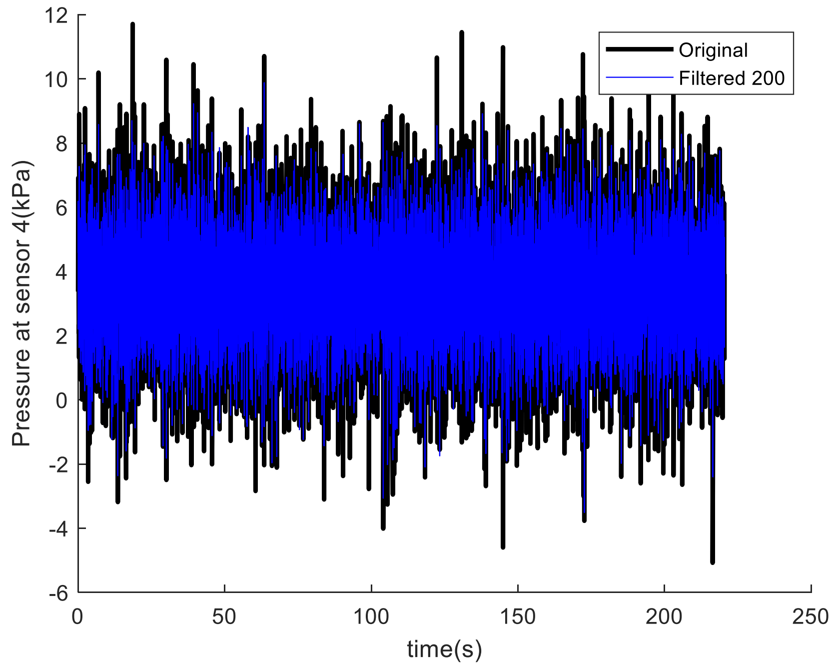
Original
Filtered 200
Pressure at sensor 4(kPa)
time(s)

(c)

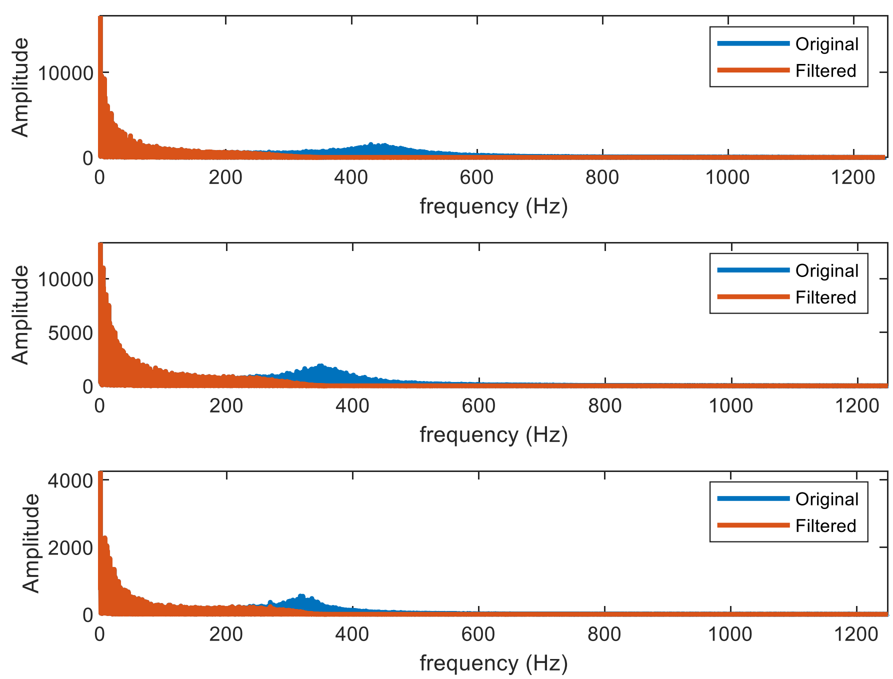
Original
Filtered
Amplitude
frequency (Hz)

(d)

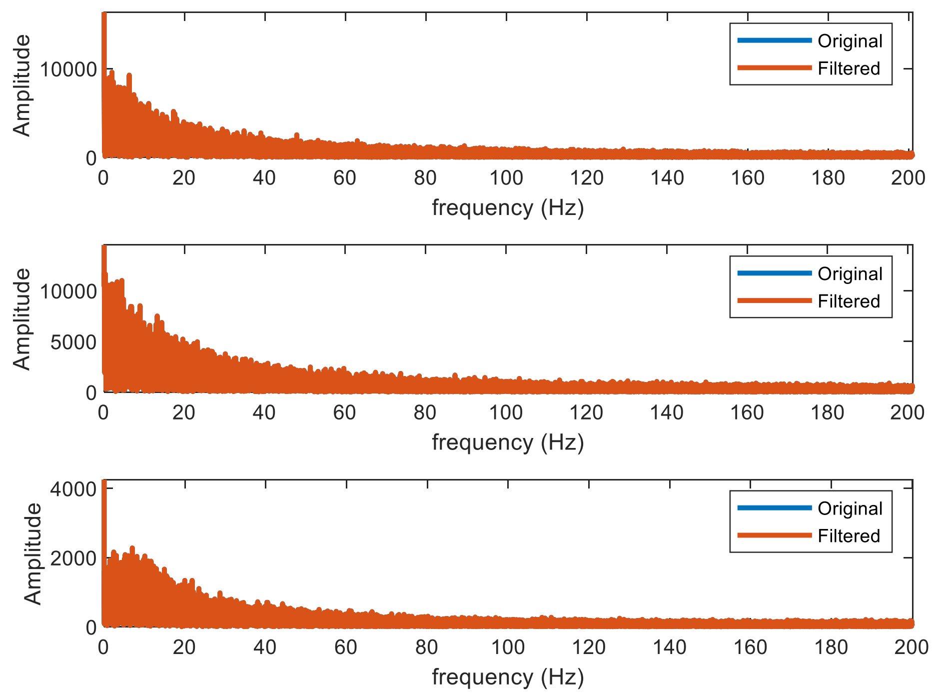

(e)

Figure 4-13. Pressure data-set 6: (a) Time versus pressure at sensor 2 (upstream floor) (b) at sensor 3 (upstream baffle face) and (c) at sensor 4 (downstream baffle slope) for the original and filtered signal at the discharge of 1 PMF (d) FFT plots for both the original and filtered signal at upstream floor (sensor 2), upstream baffle face (sensor 3) and downstream baffle slope (sensor 4) at the discharge of 1 PMF (e) closer views of the FFT plots for frequencies below 200 Hz, for both the original and filtered signals

Figures 4-13 (a) through (c) show the original signal and low pass filtered signal at 200 Hz at the upstream floor of the stilling basin, upstream baffle face and downstream baffle slope, respectively. Figure 4-13 (d) illustrates the FFT plots for both the filtered and original signal. Figure 4-13 (e) demonstrates the closer view of the FFT plots for both the filtered and original signal to 200 Hz. Average values of frequency for each location were 100 Hz. The low-frequency peaks were 1.946, 0.04536, and 6.976 Hz at the upstream floor of the stilling basin, upstream baffle face and downstream baffle slope, respectively.

4.4 Rotation Frequency versus Discharge

As can be seen from Figure 4-14, there is a proportional relationship between the rotation frequency of the roller in the stilling basin and the discharge entering the basin from the chute. When the discharge increases, the rotation frequency also increases. For the 1.0 PMF discharge, the maximum value of the frequency was 2.50 Hz, and the minimum value was 2.39 Hz. This variation is shown in Figure 4-14. The relationship indicates that flow on the chute powers the roller and sets the roller's rotational speed. It is useful to observe that the roller persisted for the full range of flows tested.

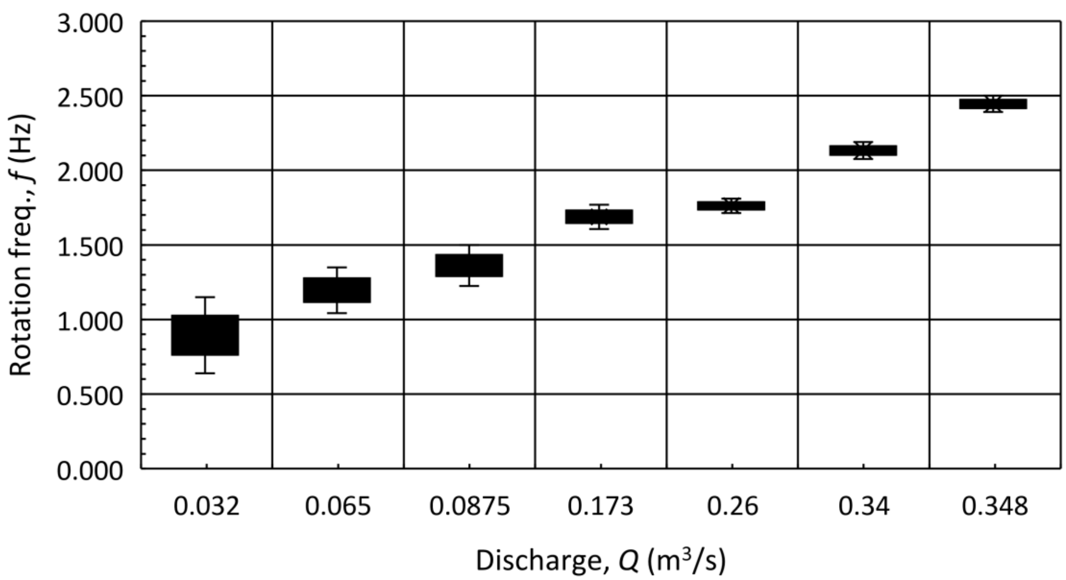

Figure 4-14. Discharge, Q (model scale), versus roller rotation frequency, f (model scale). The variation in rotation frequencies is indicated by the length of the data band

Table 4-2. Mean values of discharge, Q, and rotation frequency, f (all model scale values)

PMF	Mean Q (m^3/s)	Mean f (Hz)
0	0	0
0.09	0.0317	0.89
0.19	0.0650	1.20

0.25	0.0882	1.36
0.5	0.173	1.69
0.75	0.259	1.76
0.98	0.340	2.13
1.0	0.348	2.45

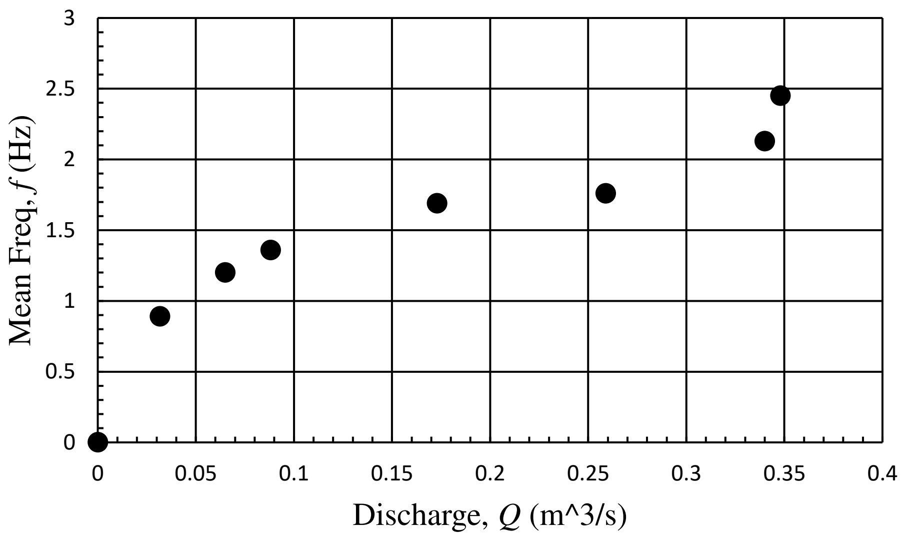

Figure 4-15. Plot of the mean discharge, *Q,* of water through the model basin versus mean frequency *f*, of roller rotation (model-scale values)

Table 4-2 presents the mean value of the discharge and the rotation frequency. The trend in Figure 4-15 shows the variation with the mean rotation frequency of the mean discharge. As it can be seen in Figure 4-15 and Table 4-2, the maximum value of the mean frequency was 2.45 Hz when the mean discharge was 0.348 m^3/s, i.e., at 1.0 PMF, the basin's design discharge.

4.5 Prototype Values of Pressure Frequencies

There was no dominant frequency observed in the signal for the final design of the stilling basin considered for the heightened Gross Dam with 63.4 convergence angle of the chute. But the low-frequency peaks which were below 10 Hz existed in the signal for each varying discharge.

The peak frequency values obtained the prototype scale discharge equivalent to the 1.0 PMF discharge were for six data sets:

- **Data set 1 (168.87 seconds)** -The frequency peaks were 0.242, 0.184, 0.006 Hz on the upstream floor, upstream baffle face, and downstream baffle slope, respectively.
- **Data set 2 (181.11 seconds)** -The frequency peaks were 0.048, 0.52, and 0.104 Hz on the upstream floor, upstream baffle face, and downstream baffle slope, respectively.
- **Data set 3 (61.96 seconds)** -The frequency peaks were 0.132, 1.15, and 1.544 Hz on the upstream floor, upstream baffle face, and downstream floor, respectively.
- **Data set 4 (180.03 seconds)** -The frequency peaks were 0.496, 0.122, and 1.496 Hz on the upstream floor, upstream baffle face, and downstream floor, respectively.
- **Data set 5 (195.90 seconds)** -The frequency peaks were 0.172, 0.138, and 1.406 Hz on the upstream floor, upstream baffle face, and downstream floor, respectively.
- **Data set 6 (220.47 seconds) -** The frequency peaks were 0.39, 0.009, and 1.396 Hz on the upstream floor, upstream baffle face, and downstream baffle slope, respectively.

The pressure frequencies for the heightened Gross Dam were recorded at upstream floor, front face of the baffle block and downstream face of the baffle block and downstream floor of the stilling basin.

The pressure frequencies at the upstream floor were between 0.048 - 0.496 Hz. The pressure frequencies at the downstream floor were between 1.406 – 1.544 Hz. The pressure frequencies at the front face of the baffle block were between 0 – 1.15 Hz and the pressure frequencies at the downstream face of the baffle block were between 0 – 1.396 Hz. The largest peak frequencies for the upstream floor, front face of the baffle block, downstream face of the baffle block, and downstream floor of the stilling basin were 0.496, 1.15, 1.396, and 1.544 Hz, respectively. The frequencies on the back of the baffle block and on the downstream floor were the greatest because these pressure frequencies related to the rotation of flow in the roller formed in the stilling basin and significant shedding of flow as flow passed between the baffle blocks. The frequency of the rotation of the roller formed immediately upstream of the row of the baffle blocks determined approximately from the observation for every flow rate. The roller's axis extended across the basin's width, though the roller's diameter varied across the basin, as therefore did the pressure frequencies. There was a direct relationship existed between the roller's rotation frequency and the discharge, as Figure 4-14 shows. When the discharge increased, the rotation frequency of the roller also increased. The frequencies of the rotation roller (model scale) at 1.00 PMF, 0.98PMF, 0.75 PMF, 0.50 PMF, 0.25 PMF, 0.19 PMF and 0.09 PMF were 2.50, 2.19,1.81, 1.77, 1.50, 1.35, 1.15 Hz, respectively.

Table 4-3 summarizes the mean and maximum values (prototype scale) of pressure at the four measurement locations used when the basin was passing its design discharge (1.00 PMF = 982 m3/s). Also listed in this table are the peak-frequency ranges measured for these fluctuating pressures. As this table shows, the pressures on the upstream floor and the front face of the central baffle block are comparable, though the front face experienced slightly larger mean and maximum values of pressure than did the upstream floor. The pressure values decreased at the two measurement locations downstream of the front face of the block.

Also, Table 4.3 shows that the maximum frequencies of pressure fluctuations increased with distance along the basin. This trend is because the presence of the row of baffle blocks introduced additional and higher frequencies of velocity oscillation in the basin flow field. These oscillations (not measured) can be attributed to flow shedding from the baffle block. The frequency of flow shedding was difficult to estimate accurately (let alone measure) because of the highly three-dimensional and unsteady nature of the flow around the central baffle. A very approximate estimate of shedding (based on a circular cylinder in a uniform flow field) was about 15; this value is mentioned here to indicate the much higher frequencies associated with flow shedding than with roller rotation. Also, observations of the water surface over and immediately downstream of the baffle block row indicated the presence of large-scale turbulence (from flow shedding) jostling unsteadily in the body of flow through the basin.

Figures 4-16a&b show, at model scale and prototype scale, the maximum and mean pressures for the measured pressures at selected sensor locations and their distance from the chute end. Also, Figures 4-17a&b show, at model scale and prototype scale, the pressure frequency ranges for measured pressures at selected sensor locations and their distance from the chute end. For the pressures and lengths, the model and prototype values scale with length scale. For frequencies, the model and prototype values scale with (length scale)$^{-0.5}$.

Table 4-3. Summary table for the mean and maximum values (prototype scale) of pressure and the frequency range of fluctuating pressures at the four measurement locations when the design discharge is 1.0 PMF

<table>
<tr><th>Sensor Position</th><th>Discharge
(m^3/s)</th><th>Pressure mean
(10^4 kPa)</th><th>Pressure max.
(10^4 kPa)</th><th>Pressure Frequency Range
(Hz)</th></tr>
<tr><td>upstream floor</td><td>981.9864</td><td>24.168</td><td>118.8</td><td rowspan="3">0.048 - 0.496</td></tr>
<tr><td>upstream floor</td><td>979.1646</td><td>24.168</td><td>112.848</td></tr>
<tr><td>upstream floor</td><td>981.9864</td><td>24.648</td><td>118.8</td></tr>
</table>

upstream floor	979.1646	24.168	102.768	
upstream floor	979.1646	24.168	118.968	
upstream floor	981.9864	24.336	124.272	
upstream baffle face	981.9864	30.768	130.728	0.009 - 1.15
upstream baffle face	979.1646	30.768	129.72	
upstream baffle face	981.9864	30.288	105.072	
upstream baffle face	979.1646	30.624	143.472	
upstream baffle face	979.1646	30.624	120.456	
upstream baffle face	981.9864	30.768	129.888	
downstream baffle slope	981.9864	-0.168	7.944	0.006 - 1.396
downstream baffle slope	979.1646	-0.168	10.416	
downstream baffle slope	981.9864	8.28	28.128	
downstream floor	981.9864	6.96	20.856	1.406 - 1.544
downstream floor	979.1646	6.96	21.84	
downstream floor	979.1646	6.96	24.336	

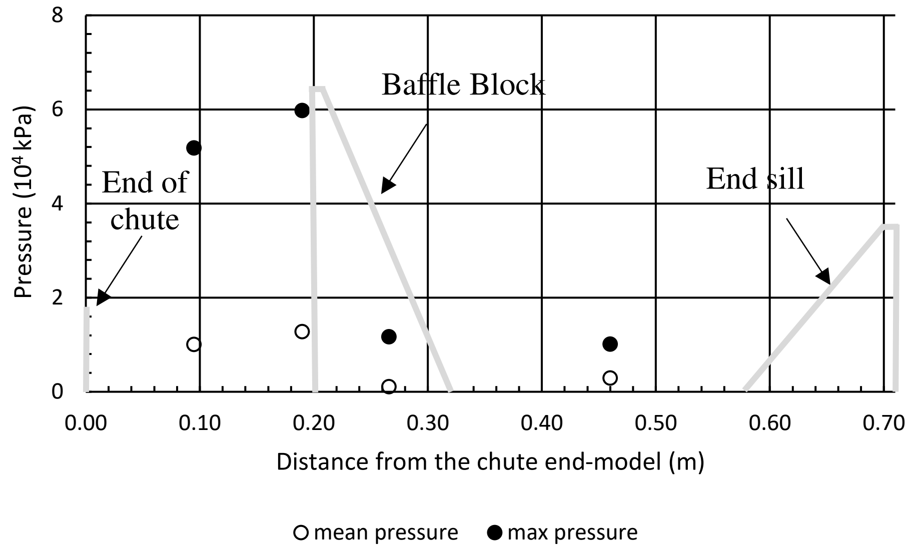

(a)

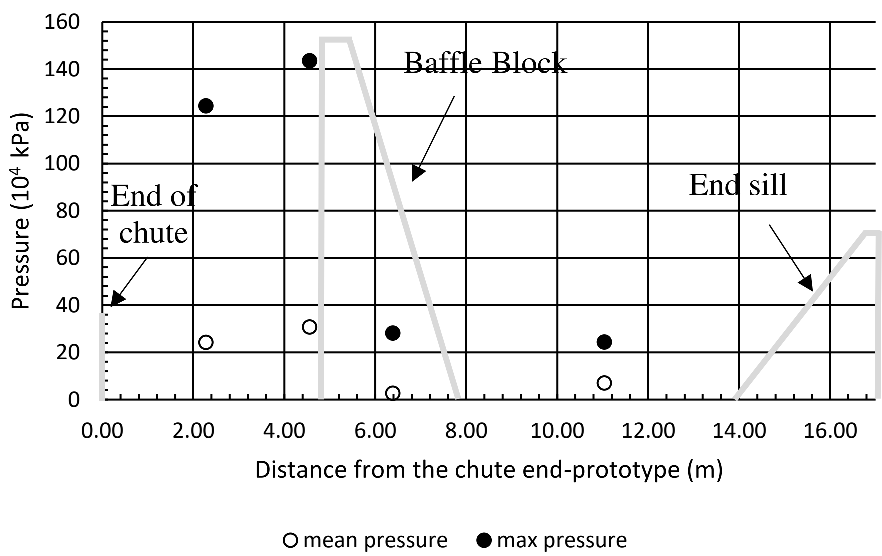

(b)

Figure 4-16. (a) Plot of the distance from end of the chute versus mean and max pressure (model scale) (b) Plot of the distance from end of the chute versus mean and max pressure (prototype scale)

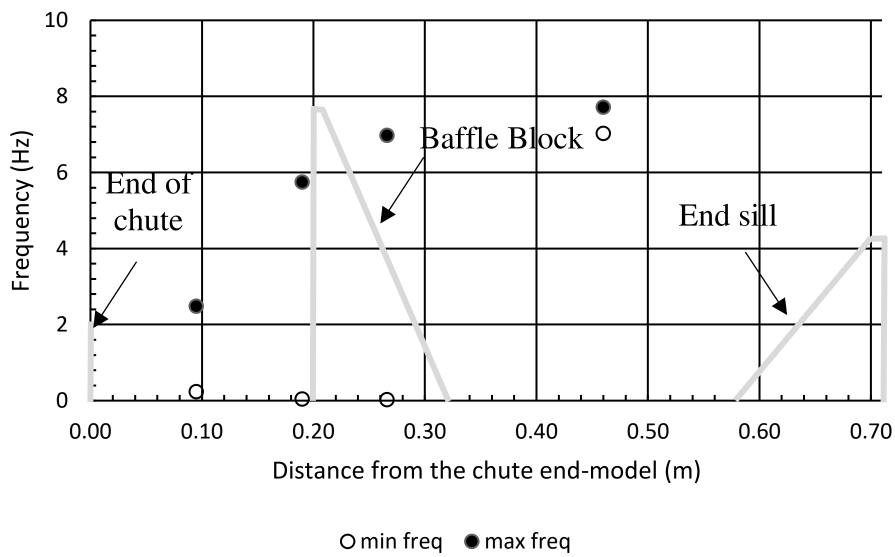

(a)

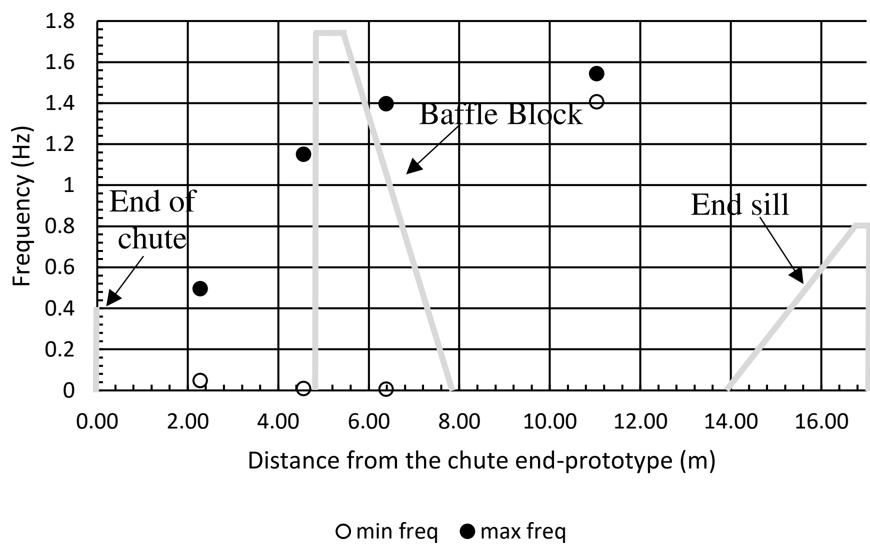

(b)

Figure 4-17. (a) Plot of the distance from end of the chute versus peak frequency (model scale)
(b) Plot of the distance from end of the chute versus peak frequency (prototype scale)

4.6 Comparison of Pressure Frequencies with Literature

Bower and Toso (1988) demonstrated most of the energy in prototype ranged in 0.15-1.0 Hz in the hydraulic jump, with the peak of the pressure fluctuations was around 0.2 Hz. They also observed that pressure fluctuations occurred on the face of the chute and the bottom of the stilling basin. Ervine et al. (1997) observed pressure fluctuations on a floor of the plunge pool and two probable dominant pressure fluctuation frequencies (model scale) at the Morrow Point Dam were 0.024 Hz and 0.625 Hz. Yan and Zhou (2006) observed the peak frequency occurred in the hydraulic jump area and its value (model scale) was about 2.0 Hz-4.5 Hz. Carlson et al. (2007) indicated that the pressure frequencies (prototype) were taken at the baffle block top, end sill face and end sill top and there were some low-frequency spectral peaks existed under 10 Hz and the high frequency peaks were 102, 94, and 162 Hz at the baffle blocks, the face of the end sill and the top of the end-sill, respectively. The dynamic pressure measurements taken by Gulliver et al. (2008) occurred at face of the baffle block, the right and left side of the baffle block, and the back of the baffle block and the stilling basin floor. The only frequencies observed (prototype) by Gulliver et al. (2008) were on the baffle block face at 0.4, 0.5 and 1.0 Hz and the stilling basin floor had a few common frequencies that were lower than 1.5 Hz. In the study of Yin and Zhou (2011), the fluctuating pressures were taken in the front of baffle block and behind the baffle block, and the dominant frequency in the region of the hydraulic jump (prototype) observed in the 1 ~ 4Hz. Although there was no apparent dominant frequency beyond the hydraulic jump, its energy was in 0~5.8Hz.

Moreover, the research by Tian et al. (2012) pointed out the dominant frequencies of fluctuations occurred at impinging zone, in the zone of the hydraulic jump roller, at downstream of the hydraulic jump. The values were (model) around 4Hz~8Hz, 2Hz~5Hz, and less than 2Hz, respectively. In the study of Chanson et al. (2014), the pressure fluctuations were measured at the hydraulic jump roller and the filtered signals of the high-frequency (0–25 Hz) ranged in 8 and 12 Hz, but on the contrary the filtered signals of low-frequency (0–5 Hz) pointed out a frequency ${F_p}^L$ around 2.6 Hz (model scale).

According to Stojnic (2020), a 50° stepped chute approach flows had an increase of spectral content the across all range of frequencies and larger spectral content was observed with 50° stepped chute approach flows. He observed that the dominant frequencies for 50° stepped chute approach flows were in the range of 1 and 7 Hz (model scale). Figure 4-18 shows the comparison of pressure frequency values cited in the literature and at the selected sensor locations for Gross Dam (at the prototype).

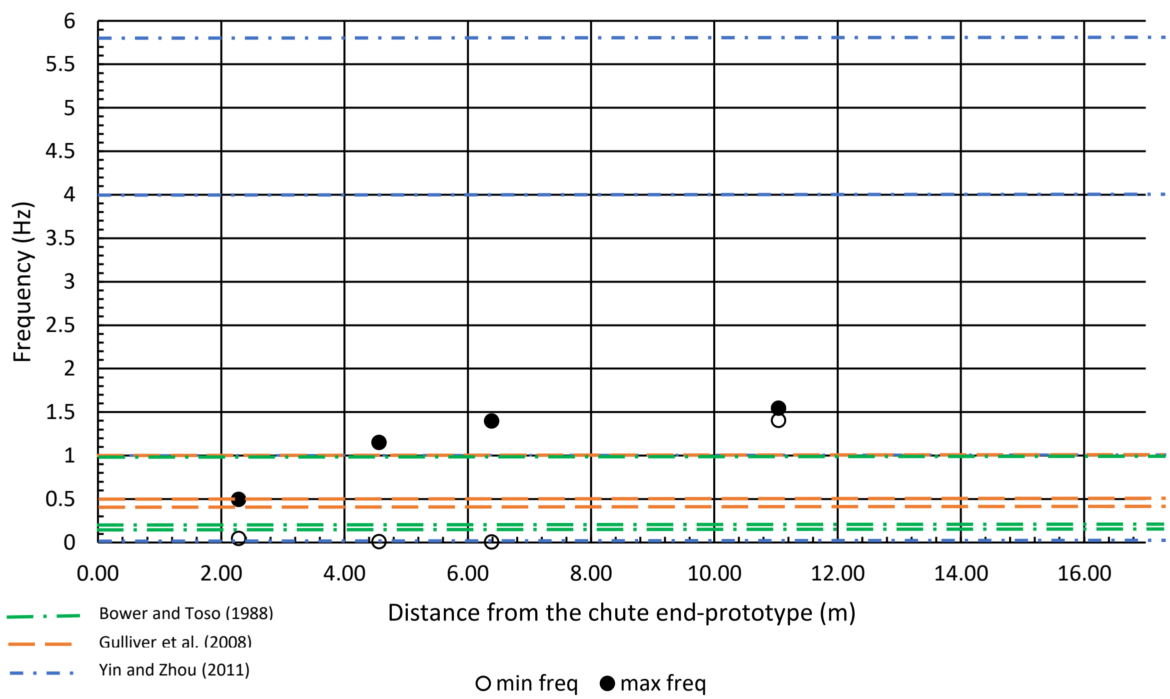

Figure 4-18. Comparison of pressure frequencies cited in the literature and at the selected sensor locations for Gross Dam (prototype scales)

CHAPTER 5- CONCLUSIONS

The Gross Reservoir Expansion (GRE) project will increase the height of the Gross Dam from 39.93 m (131 ft) to an ultimate height of 143.56 m (471 ft) by 2025, thereby creating more storage behind the Gross Dam. The new stepped spillway required for GRE will be the highest stepped spillway in the U.S. The spillway's design required an extensive redesign of the spillway's stilling basin. Included in the redesign were measurements of pressures exerted on components of the stilling basin by flow exiting the spillway's stepped chute.

The following main conclusions were drawn from the 24-scale hydraulic model (operated in accordance with the precepts of Froude number similitude) this study used for investigating the stilling basin at the base of stepped spillway:

- A transverse roller formed immediately upstream of the row of baffle blocks in the basin. The roller's axis extended across the basin's width, though the roller's diameter varied across the basin. There was a direct relationship existed between the roller's rotation frequency and the discharge. When the discharge increased, the rotation frequency of the roller also increased. The frequency was determined approximately by means of visual observation made for every flow rate. The average frequencies of the rotation roller formed for the varying discharges were shown in Figure 4-15. The mean value of the rotation frequency of the roller formed for the PMF-equivalent discharge down the hydraulic model of the spillway (0.348 m^3/s) was 2.45 Hz or 0.5 Hz at prototype scale.
- At the model-scale values of the water discharges equivalent to the 1.0 PMF flowrate on the spillway, the values of the mean pressures exerted at the upstream face of the central

baffle block were 20.8 % higher than on the upstream floor of the stilling basin and at the model-scale values of the water discharges equivalent to the 0.98 PMF flowrate on the spillway, the values of the mean pressures exerted at the upstream face of the central baffle block were 16 % higher than on the upstream floor of the stilling basin. Table 4-3 summarizes the pressures for the four positions along the basin conveying 1.00 PMF.

- The maximum pressure recorded at the front face of the baffle block when the model-scale flow rate was equivalent to the 1.00 PMF flowrate was 59.78 kPa at model scale (the prototype value of 1434.7 kPa).
- There were slight negative pressures (gauge) recorded at the upstream floor of the stilling basin, the front face of the baffle block and the behind the baffle block. (-9.79 kPa, -19.3 kPa and -11.3 kPa, respectively)
- The values of the mean pressures exerted on the upstream floor of the stilling basin were 13, 22.5, 16, 15, and 29.5 % higher than at the upstream face of the central baffle block at the model-scale discharges equivalent to 0.75, 0.50, 0.25, 0.19, and 0.09 PMF flowrates, respectively.
- At the model-scale discharges equivalent to the 0.19 PMF flow rate, the values of the mean pressures on the downstream floor of the stilling basin were 6 % higher than at the upstream floor of the stilling basin and at the model-scale discharges equivalent to the 0.09 PMF flowrate, the values of the mean pressures on the downstream floor of the stilling basin were 3 % higher than at the upstream floor of the stilling basin.
- The Fast-Fourier Transform (FFT) results obtained from the original and filtered signals produced by the pressure transducers showed no continuous low frequency or continuous high frequency spikes, indicating that the pressure signals oscillated irregularly, as did the

roller formed in the front of the stilling basin. There were 6 datasets for 1 PMF because each dataset was taken at different start time and consequently reflected different moments in the oscillation of the roller. Therefore, large variations for the frequencies were obtained for the six data sets. The peak frequency values obtained the prototype-scale discharge equivalent to the 1.0 PMF were:

  - Upstream floor: 0.496 Hz
  - Front face of the baffle block: 1.15 Hz
  - Downstream face of the baffle block: 1.396 Hz
  - Downstream floor: 1.544 Hz

Note that the pressure magnitudes on the downstream face of the baffle block and the downstream floor were much less than on the upstream floor and the upstream face of the baffle block.

- The value of maximum frequency increased with pressure-measurement point location along the basin. The least value occurred on the upstream floor and coincided approximately with the rotation frequency of the roller, as the measurement location was beneath the roller. As the measurement location moved to the front face of the baffle block, other flow-field factors led to higher frequencies of pressure fluctuation. Notably, flow shedding from the sides and top of the blocks affected the frequencies. The pressure measurements on the block's downstream face and on the downstream floor were extensively affected by flow around the block. For instance, the shedding frequency for an isolated block in a flow equivalent to the chute flow was estimated to be of approximate magnitude 15 Hz. This frequency magnitude together with the frequency of roller rotation (and its fluctuations) would produce the higher frequencies downstream of the baffle block.

REFERENCES

Biethman, B. (2019). "Air Concentration and Bulked Flow Along a curved, converging stepped chute." Hydraulic Laboratory. Colorado State University.

Bowers, C.E., Toso, J. (1988). "Extreme Pressures in Hydraulic Jump Stilling Basins." *Journal of Hydraulic Engineering*, ASCE 114(8):829-843.

Bowers, C.E., Toso, J. (1988). "Karnafuli project, model studies of spillway damage." *Journal of Hydraulic Engineering*, ASCE 114(5):469-483.

Carlson, T., Richmond, M.C. and Weiland, M.A. (2007). "Prototype measurements of pressure fluctuations in the Dalles Dam stilling basin." *Journal of Hydraulic Research*. Vol. 45, No. 5., (2007), pp. 674–678.

Chanson, H., Murzyn, F., and Wang, H. (2014). "Total pressure fluctuations and two-phase flow turbulence in hydraulic jumps". *Exp Fluids.* DOI 10.1007/s00348-014-1847-9.

Ervine, D.A., Falvey, H.T., & Withers, W. (1997). "Pressure fluctuations on plunge pool floors." *Journal of Hydraulic Research*, 35:2, 257-279, DOI: 10.1080/00221689709498430.

Ettema, R., Thornton, C.I., Hogan, T., and Biethman, B. (2019). "Gross Dam Reservoir Expansion: Hydraulic Model Study of Stepped Spillway Design." Hydraulic Laboratory. Colorado State University.

Gulliver, John S., Mohseni, O., Schulz, Harry E. (2008). "The Physical Model Study of the Folsom Dam Auxiliary Spillway System". DOI: 10.13140/2.1.1009.4887.

Karimi, M., Musavi Jahromi, S.H., and Shafai-Bajestan, M. "Pressure Fluctuations in Hydraulic Jump Investigation of Stilling Basin at Sudden Expansion." *Amirkabir J. Civil Engineering*. 49(2) (2017) 79-81. DOI:10.22060/ceej.2016.678.

Lopardo, R., Tang, H., and Romagnoli, M. (2009). "Pressure and Velocity Fluctuations in Stilling Basins". DOI: 10.1007/978-3-540-89465-0_359.

Nakato, T. (2000). "Model Tests of Hydraulic Performance of Pit 6 Dam Stilling Basin." *Journal of Hydraulic Eng*., 126(9): 638-652.

Nasiri, K., Kavianpour, M.R., and Haghighi, S. (2012). The Baffle Blocks Effects of Pressure Characteristics on USBR III Basin Floor. *Applied Mechanics and Materials*, 212–213, 821–825. https://doi.org/10.4028/www.scientific.net/amm.212-213.821

Stojnic, Ivan. "Stilling Basin Performance Downstream of Stepped Spillways." (2020). *Lausanne, EPFL.* DOI: 10.5075/epfl-thesis-7481.

Tian, J, Zhao, Q., Fan, L. (2012). "Pressure Characteristics in Stilling basin of stepped spillway." *Journal of Hydroelectric Engineering.*

Withers, W.J. (1991). "Pressure fluctuations in the plunge pool of an impinging jet spillway." Ph. D thesis. http://theses.gla.ac.uk/8246/

Yan, Z., Zhou, C., "Pressure fluctuations beneath spatial hydraulic jumps." *Journal of Hydrodynamics*, *Series B*, 2006, 18(6):723-726

Yin, C., Zhou, Q. (2011). "The Baffle block Effect of Fluctuating pressure in hydraulic Jump with Low Froude Number." *IEEE*

"Gross Reservoir Expansion Project". https://www.denverwater.org/project-updates/gross-reservoir-expansion-project. Accessed by 16 October 2020.

https://www.usbr.gov/tsc/techreferences/hydraulics_lab/pubs/HL/HL-2009-05.pdf. Accessed by 10 December 2020

APPENDIX A: THE FREQUENCY OF ROTATION OF THE ROLLER FOR EACH DISCHARGE

1 PMF

Figure A.1. Frequency of the rotation of the roller at 1 PMF

0.98 PMF

Figure A.2. Frequency of the rotation of the roller at 0.98 PMF

0.75 PMF

Figure A.3. Frequency of the rotation of the roller at 0.75 PMF

0.50 PMF

Figure A.4. Frequency of the rotation of the roller at 0.50 PMF

0.25 PMF

Figure A.5. Frequency of the rotation of the roller at 0.25 PMF

0.19 PMF

Figure A.6. Frequency of the rotation of the roller at 0.19 PMF

0.09 PMF

Figure A.7. Frequency of the rotation of the roller at 0.09 PMF

APPENDIX B: FFT RESULTS AT MODEL SCALE (in English units)

0.98 PMF

DATA SET1

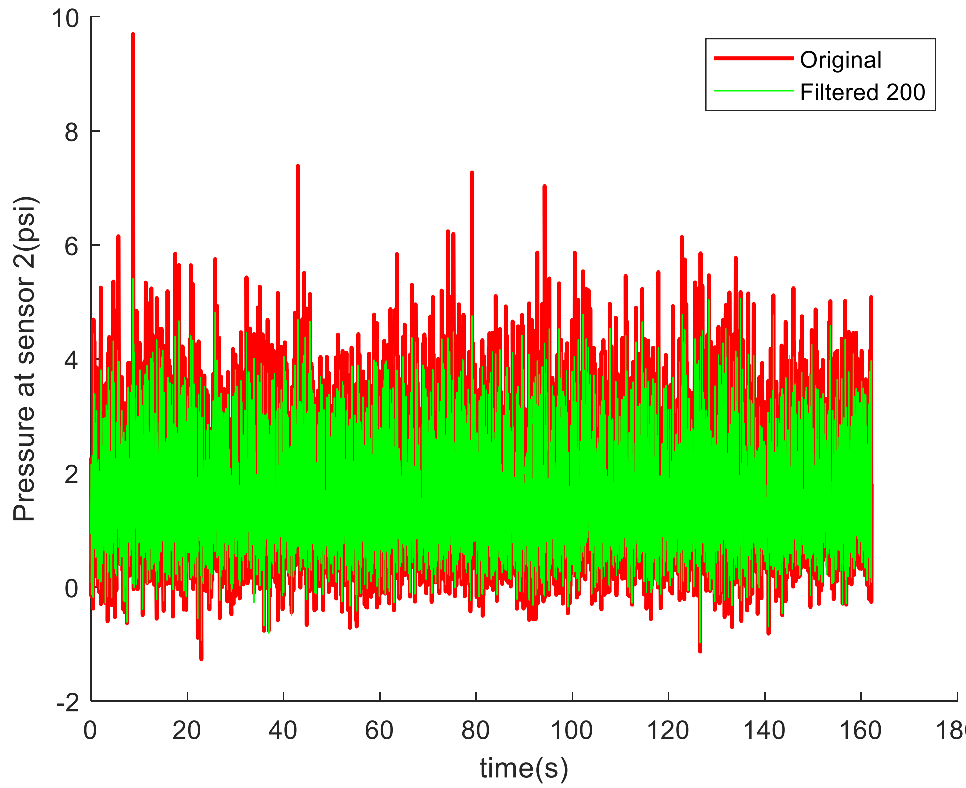

Figure B.1. Time versus pressure at sensor 2 (upstream floor) for the original and filtered signal at the discharge of 0.98 PMF- data set 1

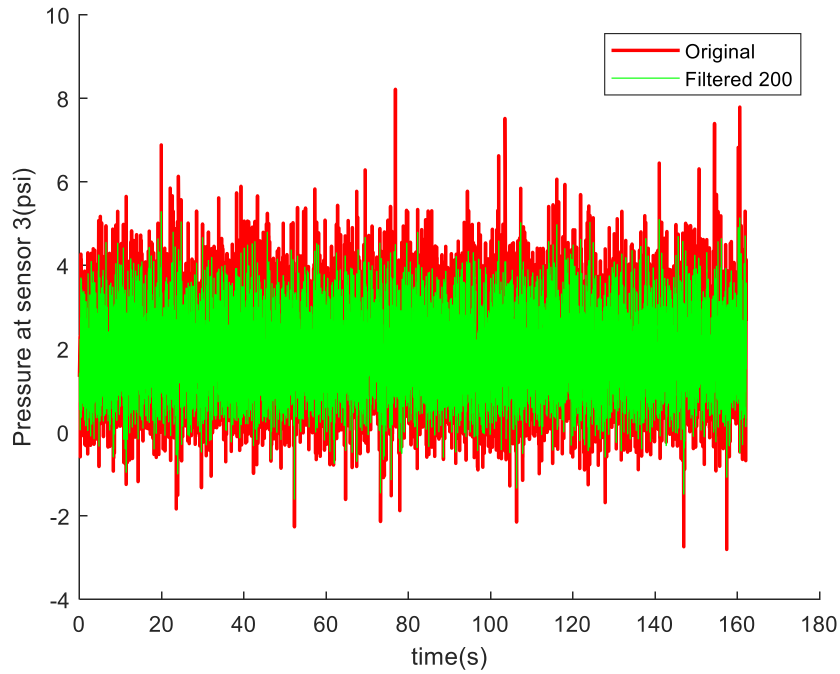

Figure B.2. Time versus pressure at sensor 3 (upstream baffle face) for the original and filtered signal at the discharge of 0.98 PMF- data set 1

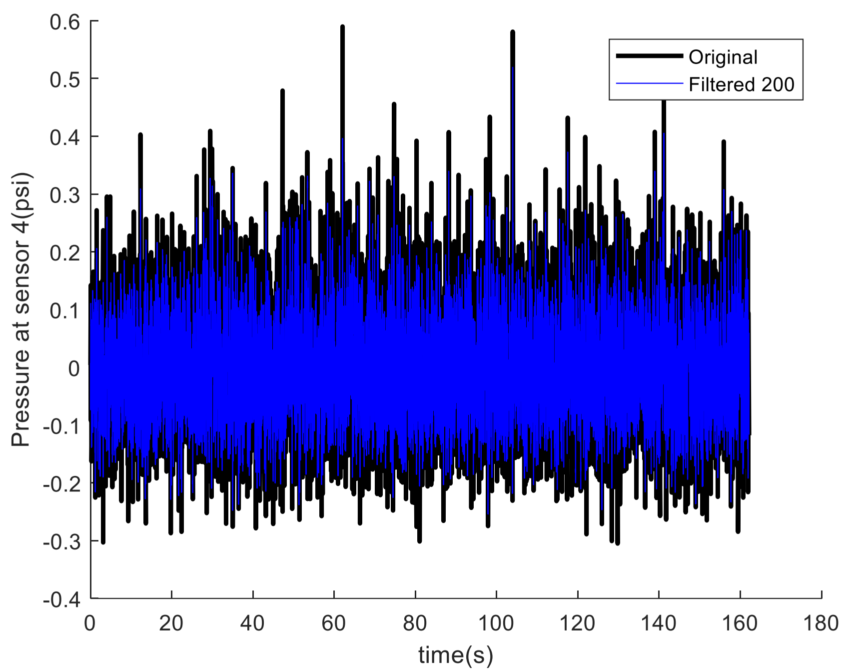

Figure B.3. Time versus pressure at sensor 4 (upstream baffle face) for the original and filtered signal at the discharge of 0.98 PMF- data set 1

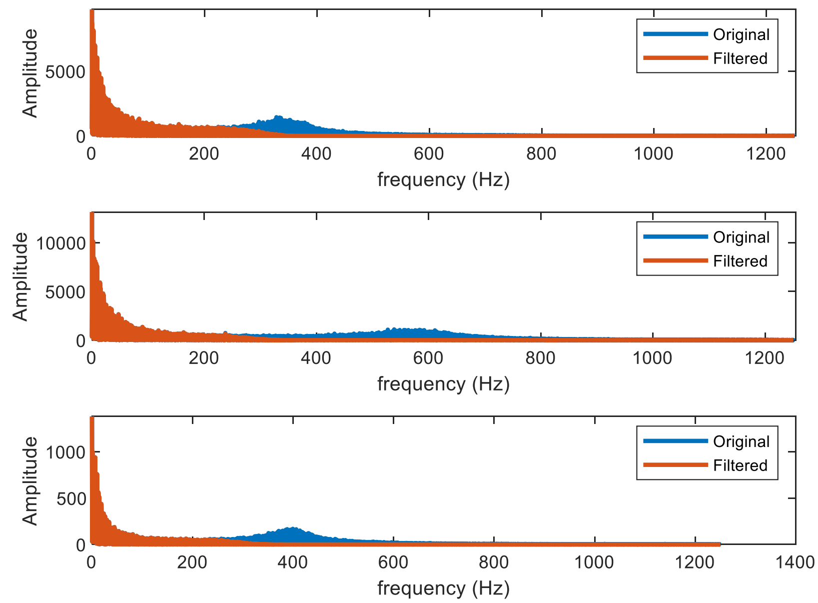

Figure B.4. FFT plots for both the original and filtered signal at upstream floor (sensor 2), upstream baffle face (sensor 3) and downstream baffle slope (sensor 4) at the discharge of 0.98 PMF- data set 1

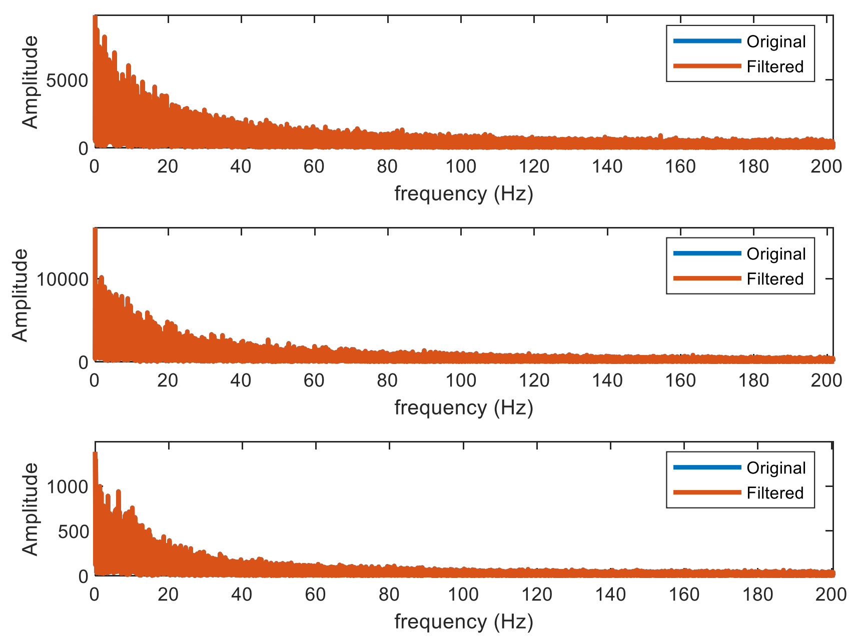

Figure B.5. Closer view to 200 Hz-FFT plots for both the original and filtered signal at upstream floor (sensor 2), upstream baffle face (sensor 3) and downstream baffle slope (sensor 4) at the discharge of 0.98 PMF- data set 1

The low-frequency peaks are 0.5118, 1.745, 0.1665 Hz at the upstream floor, upstream baffle face, and downstream baffle slope, respectively.

DATA SET2

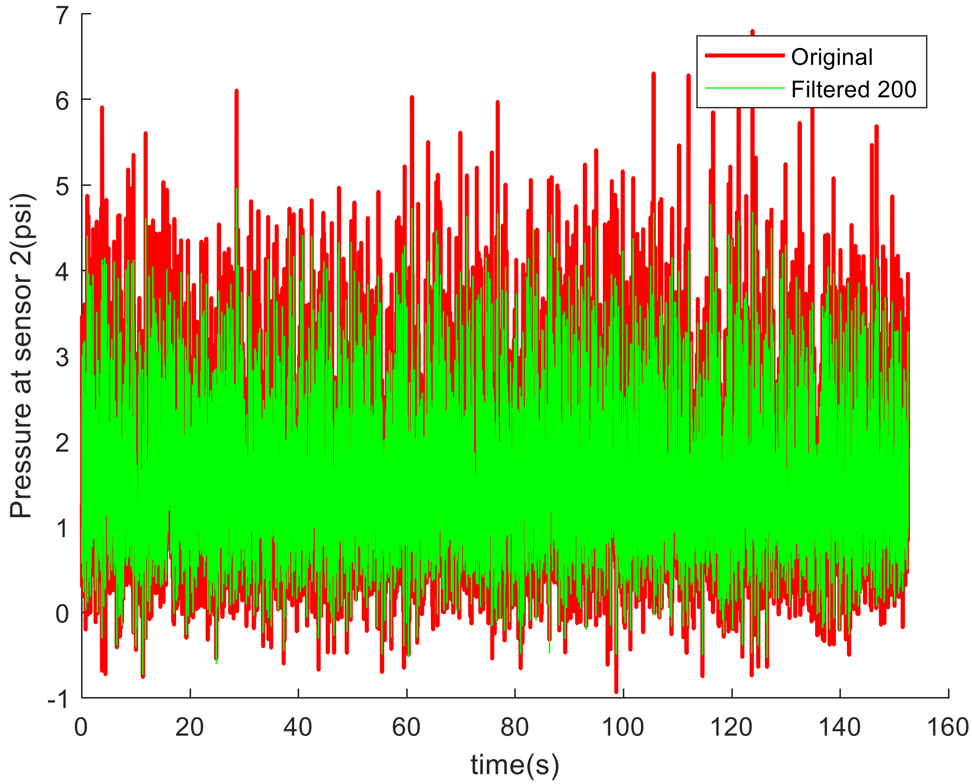

Figure B.6. Time versus pressure at sensor 2 (upstream floor) for the original and filtered signal at the discharge of 0.98 PMF- data set 2

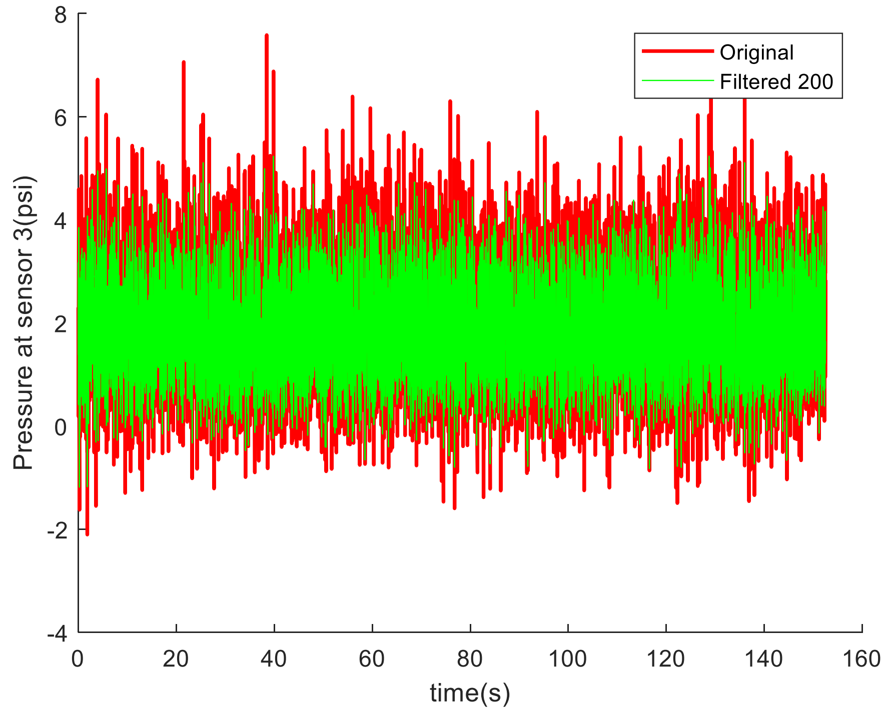

Figure B.7. Time versus pressure at sensor 3 (upstream baffle face) for the original and filtered signal at the discharge of 0.98 PMF- data set 2

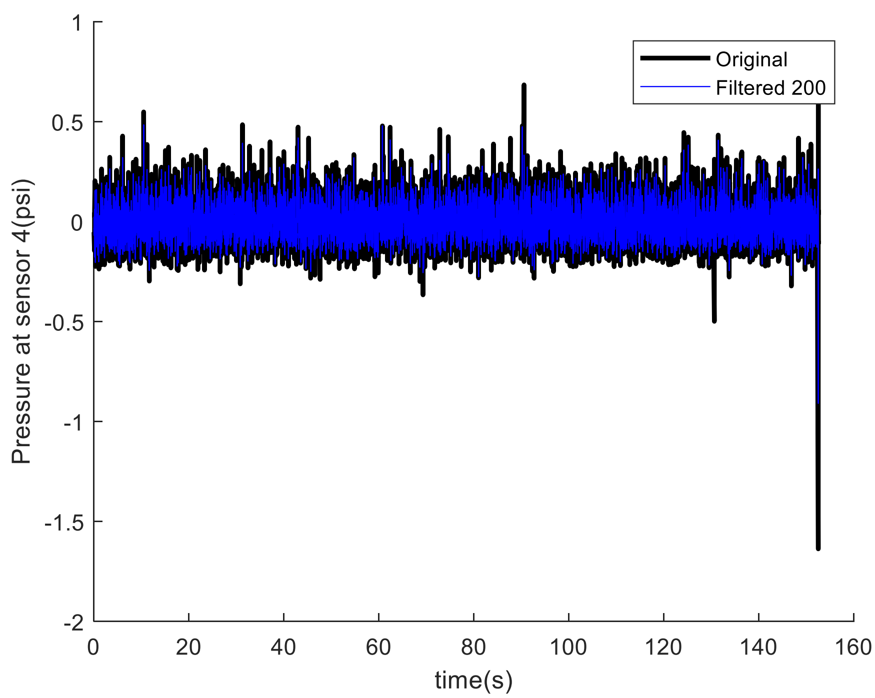

Figure B.8. Time versus pressure at sensor 4 (downstream baffle slope) for the original and filtered signal at the discharge of 0.98 PMF- data set 2

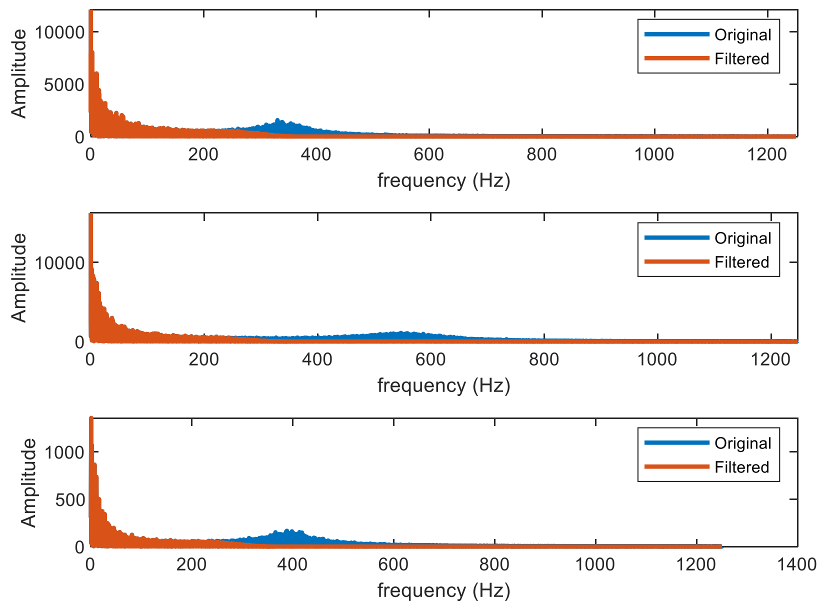

Figure B.9. FFT plots for both the original and filtered signal at upstream floor (sensor 2), upstream baffle face (sensor 3) and downstream baffle slope (sensor 4) at the discharge of 0.98 PMF- data set 2

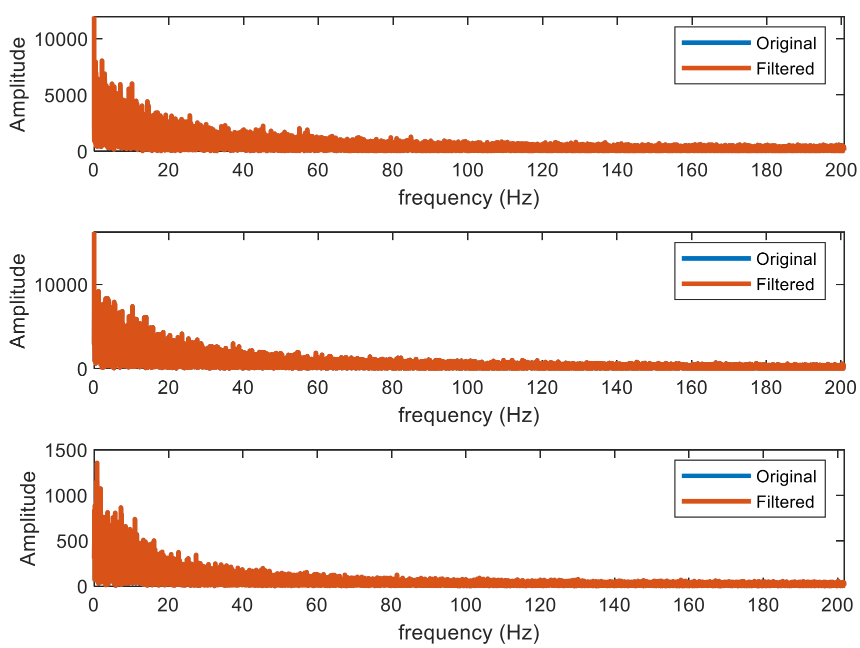

Figure B.10. Closer view to 200 Hz-FFT plots for both the original and filtered signal at upstream floor (sensor 2), upstream baffle face (sensor 3) and downstream baffle slope (sensor 4) at the discharge of 0.98 PMF- data set 2

The low-frequency peaks are 2.085, 1.167, 0.7802 Hz at the upstream floor, upstream baffle face, and downstream baffle slope, respectively.

DATA SET3

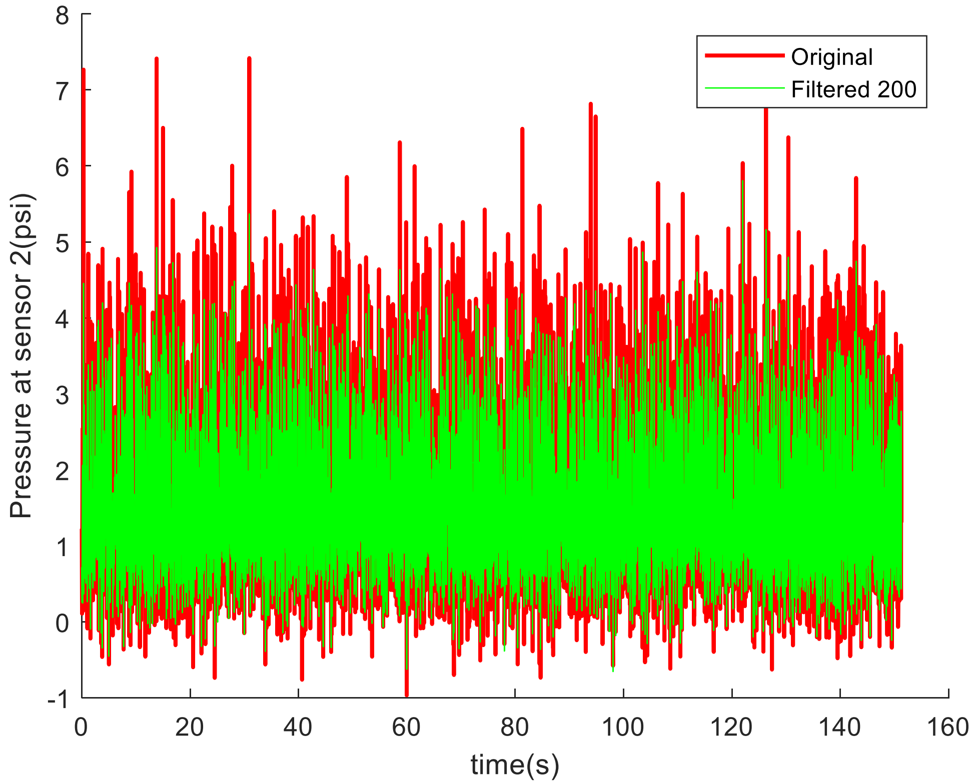

Figure B.11. Time versus pressure at sensor 2 (upstream floor) for the original and filtered signal at the discharge of 0.98 PMF- data set 3

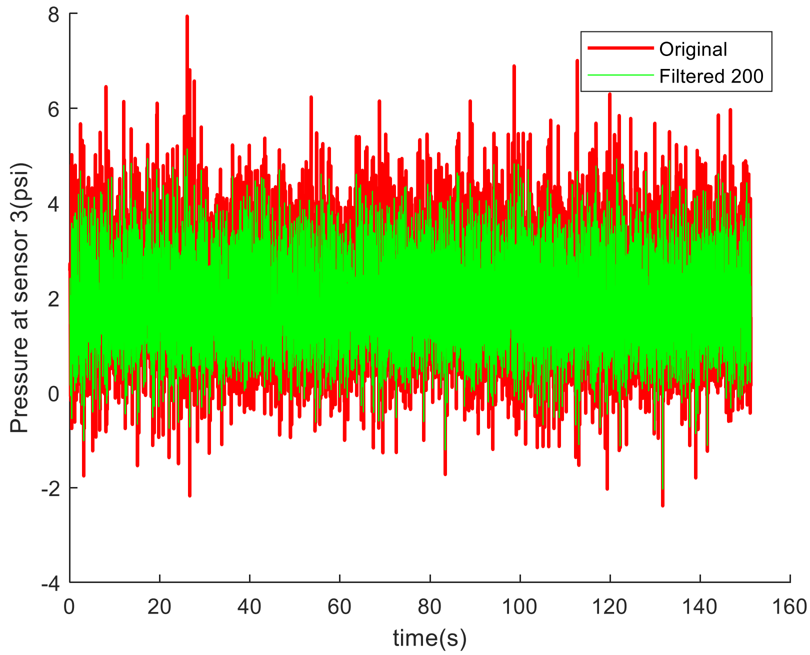

Figure B.12. Time versus pressure at sensor 3 (upstream baffle face) for the original and filtered signal at the discharge of 0.98 PMF- data set 3

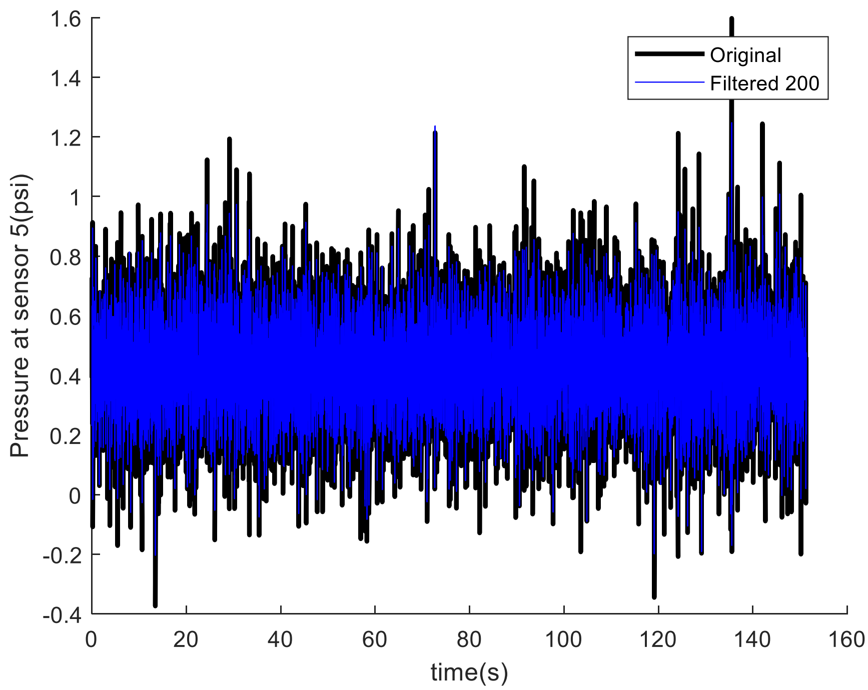

Figure B.13. Time versus pressure at sensor 5 (downstream floor) for the original and filtered signal at the discharge of 0.98 PMF- data set 3

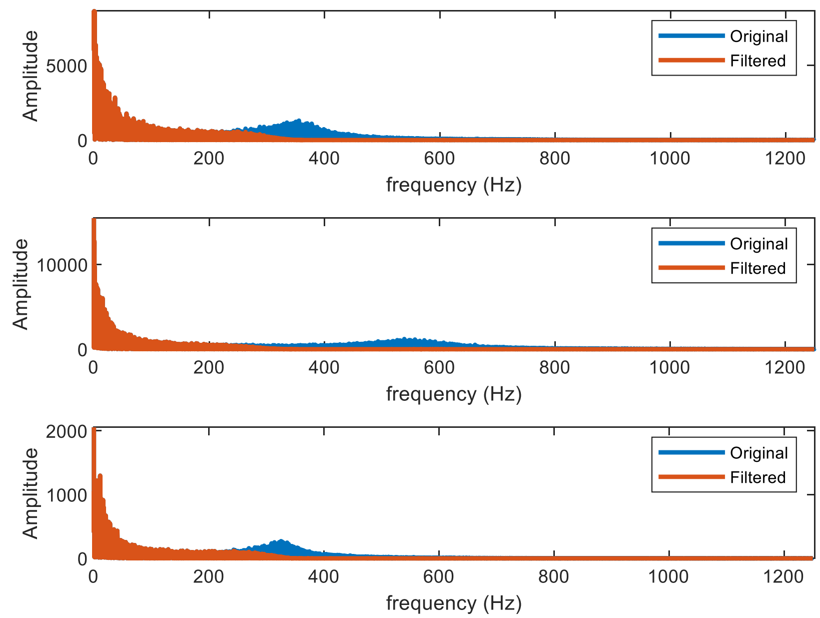

Figure B.14. FFT plots for both the original and filtered signal at upstream floor (sensor 2), upstream baffle face (sensor 3) and downstream floor (sensor 5) at the discharge of 0.98 PMF- data set 3

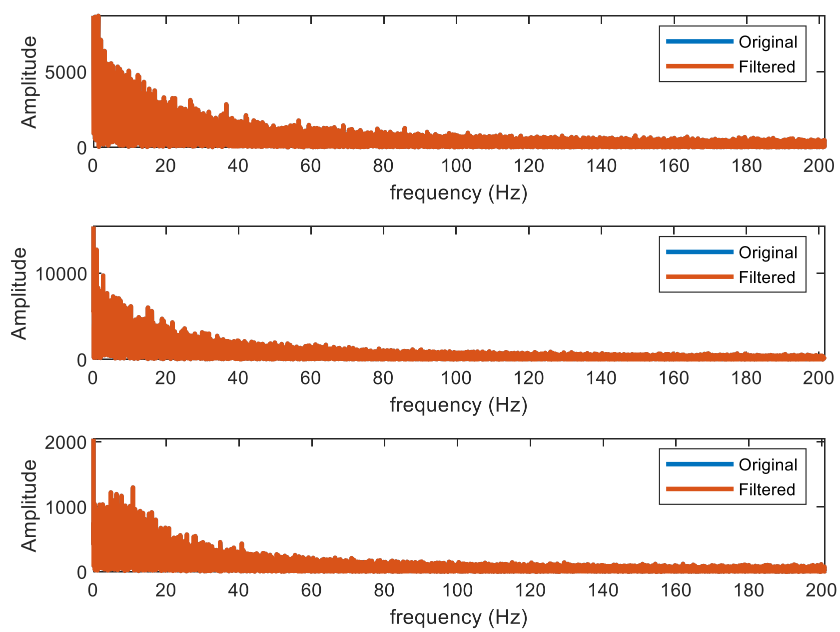

Figure B.15. Closer view to 200 Hz-FFT plots for both the original and filtered signal at upstream floor (sensor 2), upstream baffle face (sensor 3) and downstream floor (sensor 5) at the discharge of 0.98 PMF- data set 3

The low-frequency peaks are 1.349, 0.8395, 10.85 Hz at the upstream floor, upstream baffle face, and downstream floor, respectively.

DATA SET4

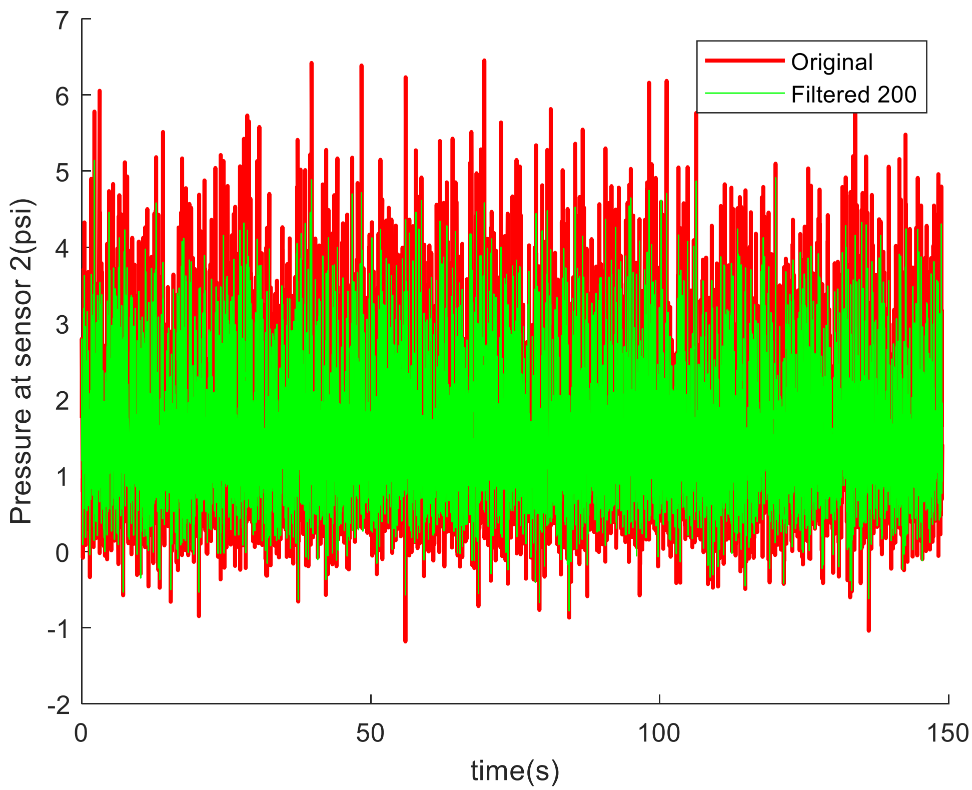

Figure B.16. Time versus pressure at sensor 2 (upstream floor) for the original and filtered signal at the discharge of 0.98 PMF- data set 4

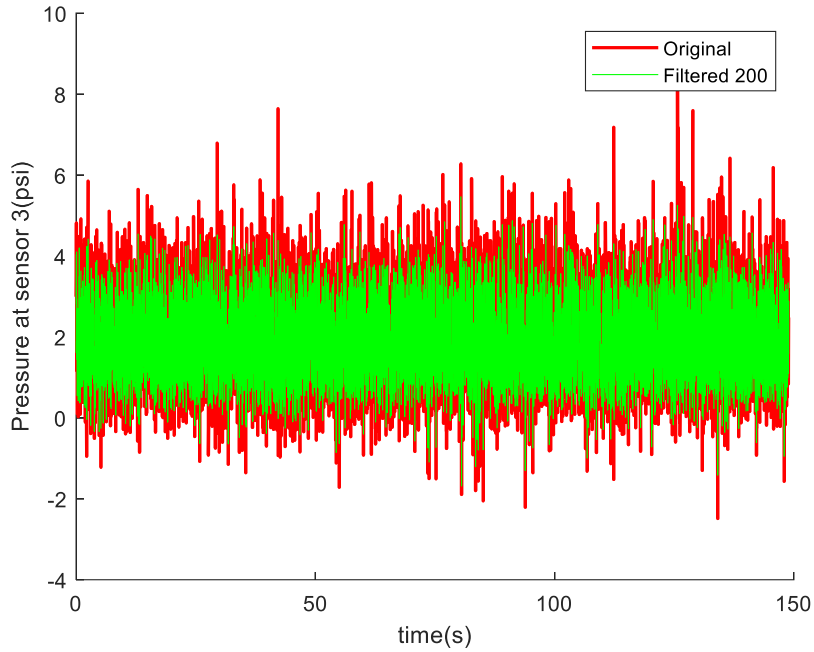

Figure B.17. Time versus pressure at sensor 3 (upstream baffle face) for the original and filtered signal at the discharge of 0.98 PMF- data set 4

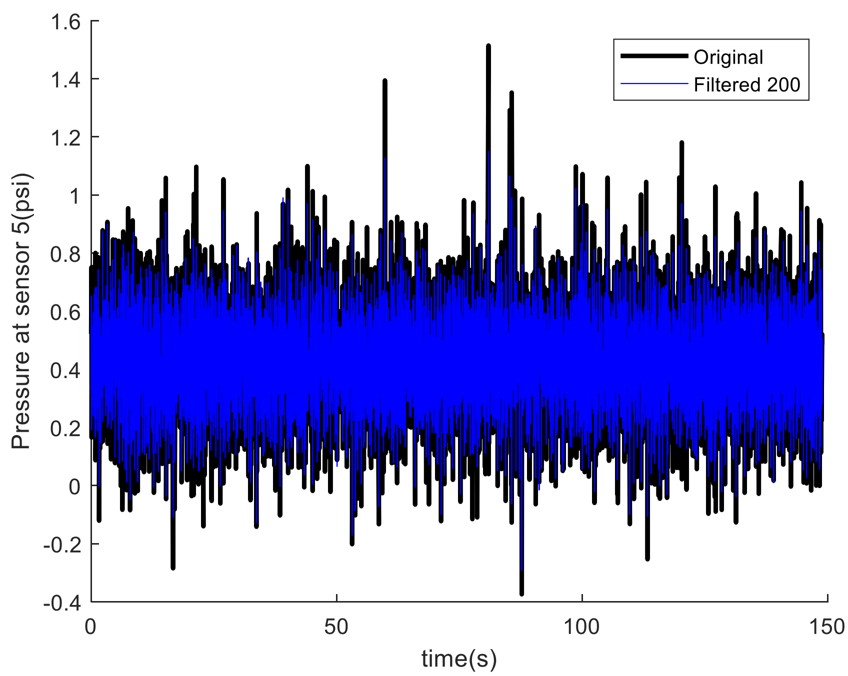

Figure B.18. Time versus pressure at sensor 5 (downstream floor) for the original and filtered signal at the discharge of 0.98 PMF- data set 4

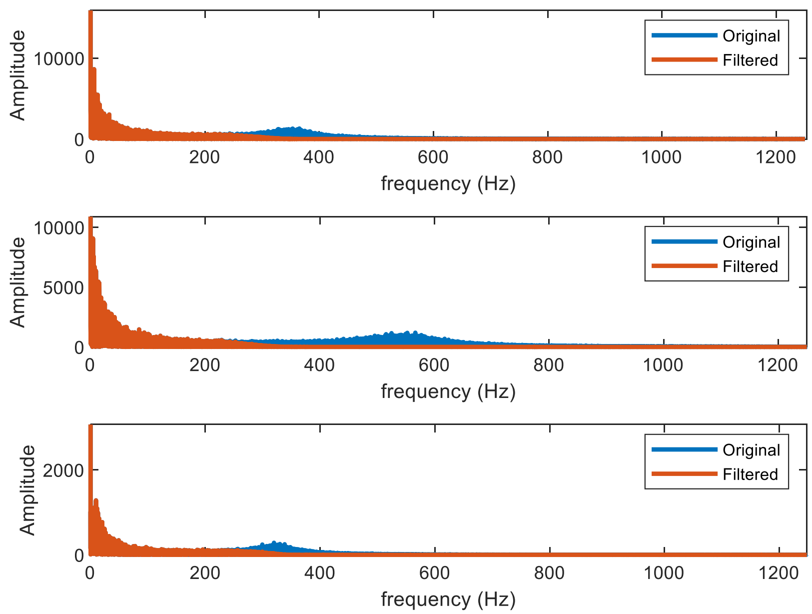

Figure B.19. FFT plots for both the original and filtered signal at upstream floor (sensor 2), upstream baffle face (sensor 3) and downstream floor (sensor 5) at the discharge of 0.98 PMF- data set 4

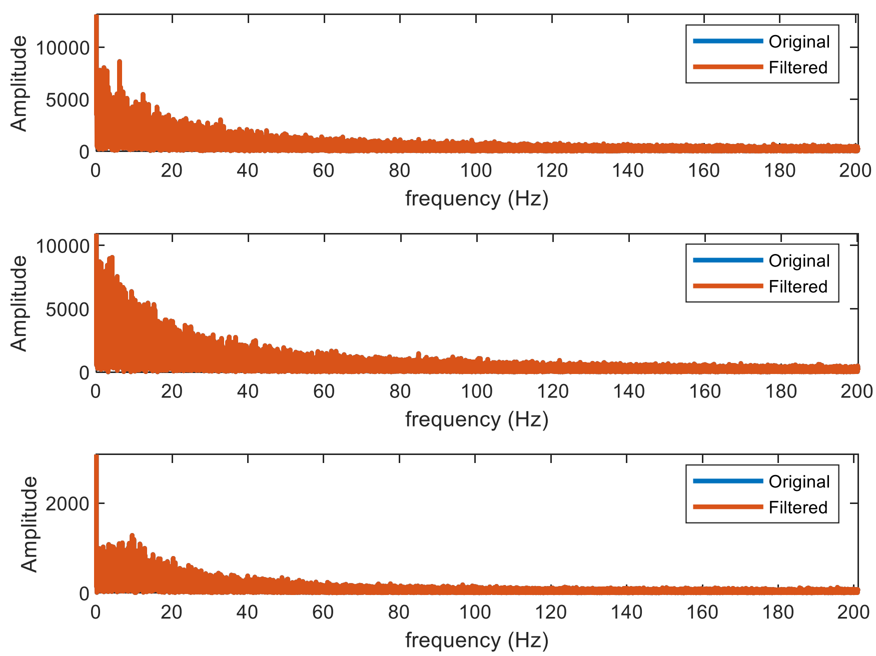

Figure B.20. Closer view to 200 Hz-FFT plots for both the original and filtered signal at upstream floor (sensor 2), upstream baffle face (sensor 3) and downstream floor (sensor 5) at the discharge of 0.98 PMF- data set 4

The low-frequency peaks are 6.112, 4.151, 9.45 Hz at the upstream floor, upstream baffle face, and downstream floor, respectively.

0.75 PMF

DATA SET1

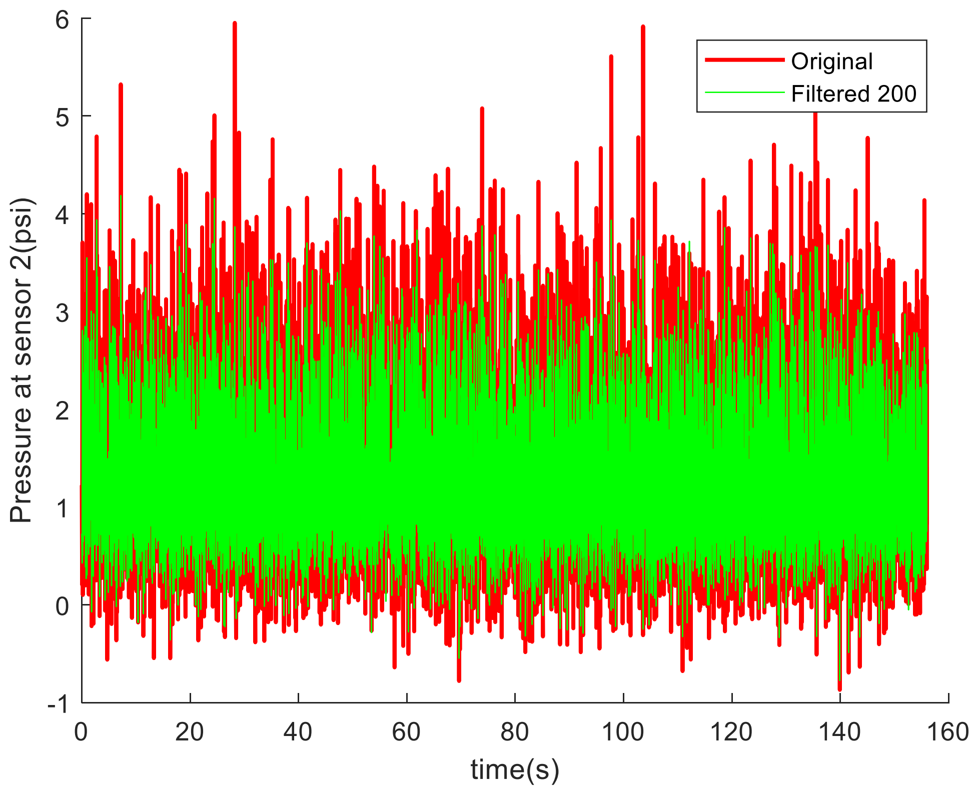

Figure B.21. Time versus pressure at sensor 2 (upstream floor) for the original and filtered signal at the discharge of 0.75 PMF- data set 1

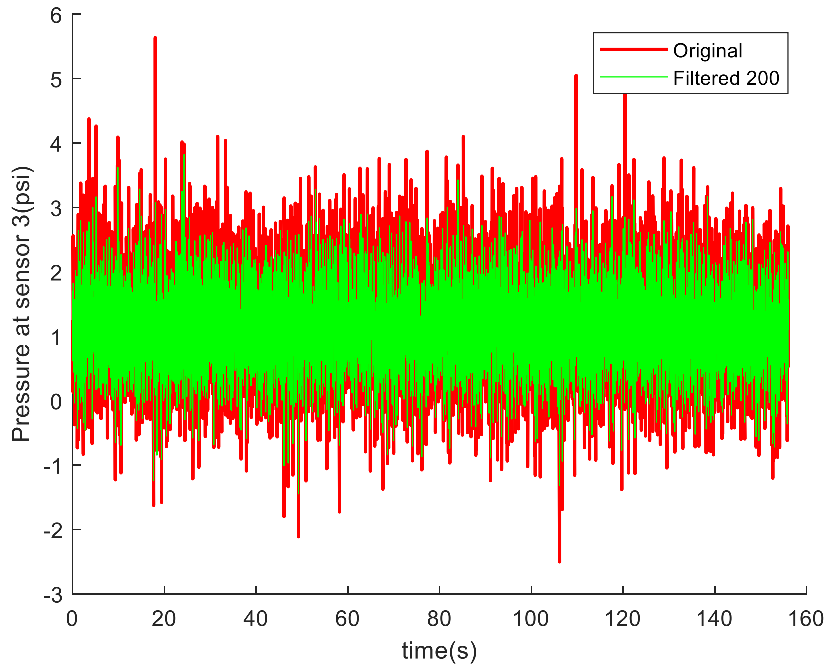

Figure B.22. Time versus pressure at sensor 3 (upstream baffle face) for the original and filtered signal at the discharge of 0.75 PMF- data set 1

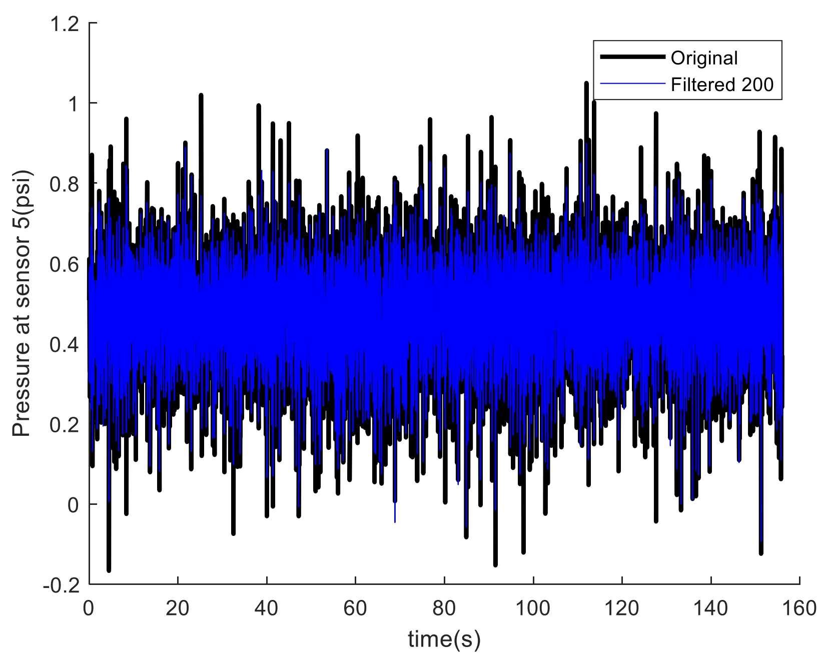

Figure B.23. Time versus pressure at sensor 5 (downstream floor) for the original and filtered signal at the discharge of 0.75 PMF- data set 1

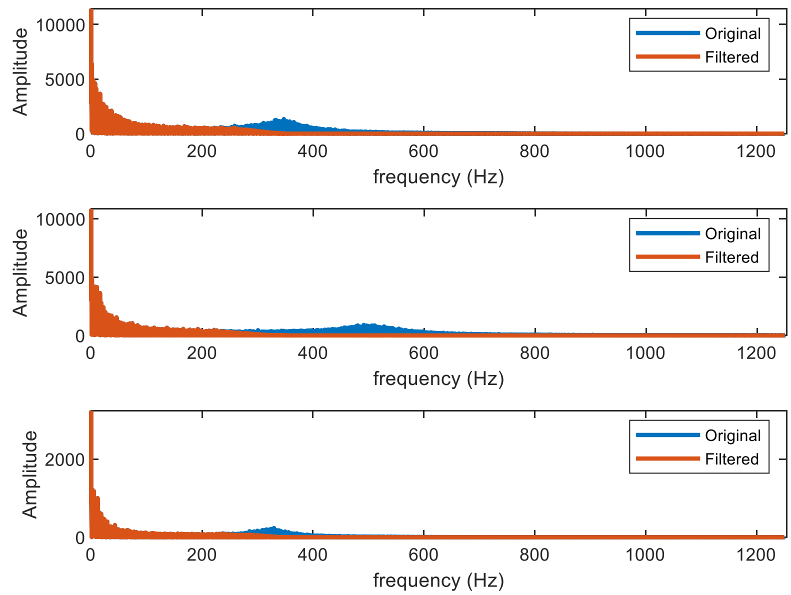

Figure B.24. FFT plots for both the original and filtered signal at upstream floor (sensor 2), upstream baffle face (sensor 3) and downstream floor (sensor 5) at the discharge of 0.75 PMF- data set 1

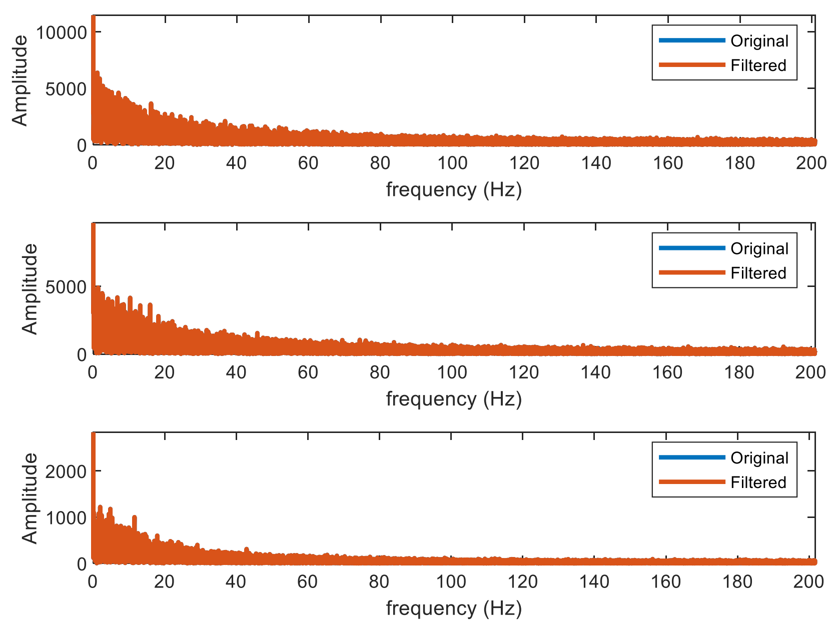

Figure B.25. Closer view to 200 Hz-FFT plots for both the original and filtered signal at upstream floor (sensor 2), upstream baffle face (sensor 3) and downstream floor (sensor 5) at the discharge of 0.75 PMF- data set 1

The low-frequency peaks are 1.128, 1.321, 1.923 Hz at the upstream floor, upstream baffle face, and downstream floor, respectively.

DATA SET2

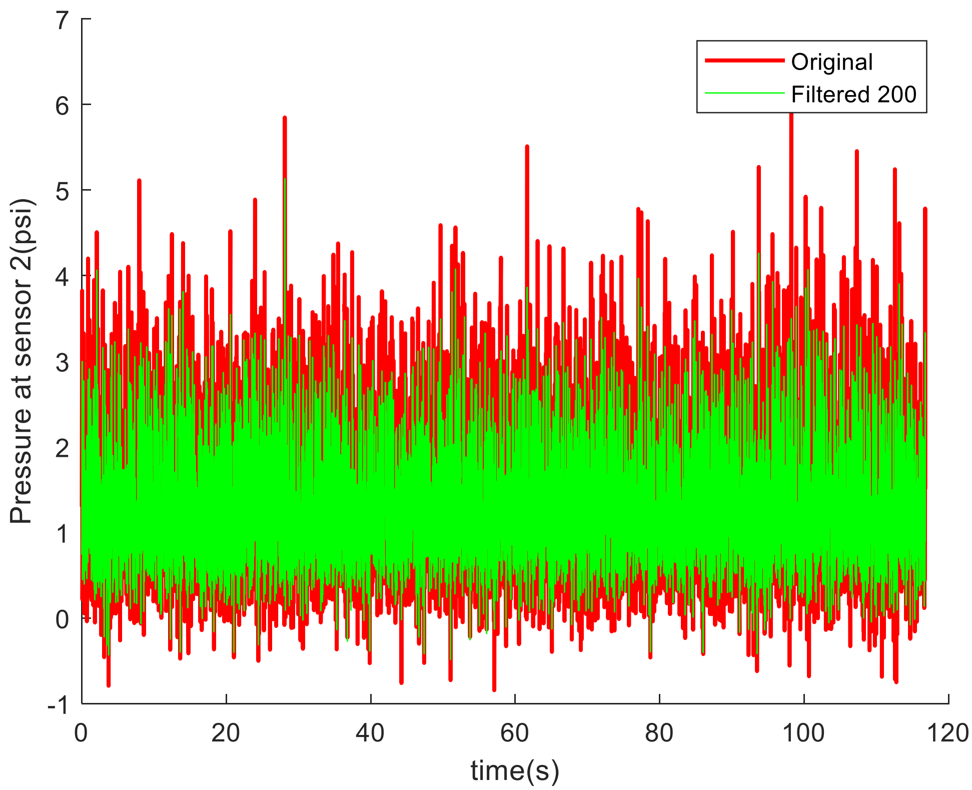

Figure B.26. Time versus pressure at sensor 2 (upstream floor) for the original and filtered signal at the discharge of 0.75 PMF- data set 2

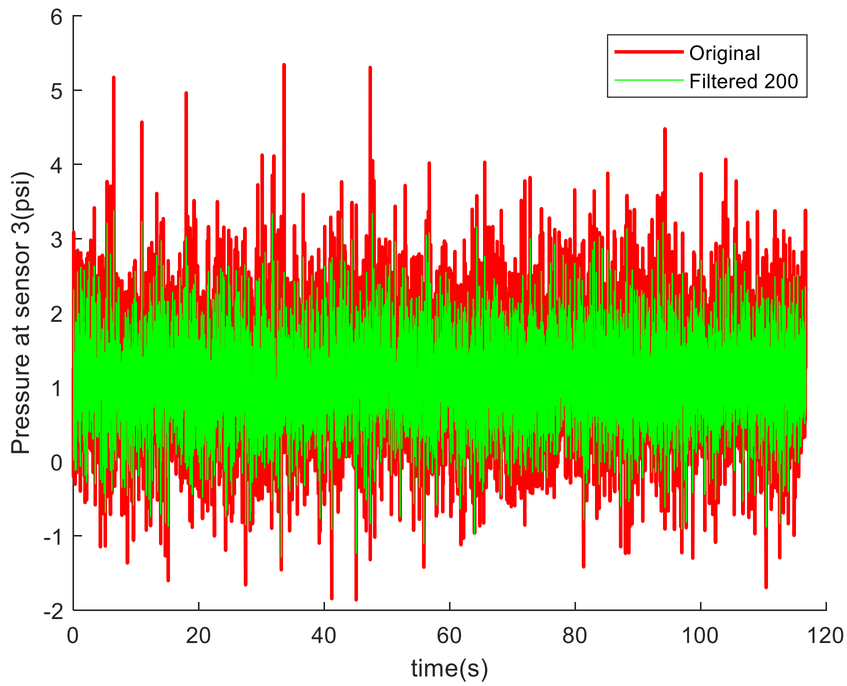

Figure B.27. Time versus pressure at sensor 3 (upstream baffle face) for the original and filtered signal at the discharge of 0.75 PMF- data set 2

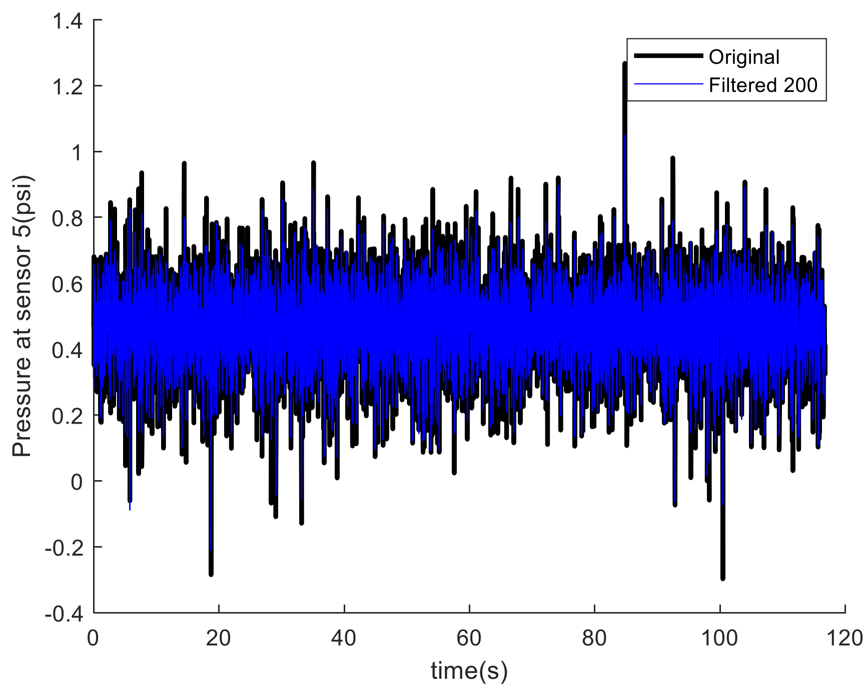

Figure B.28. Time versus pressure at sensor 5 (downstream floor) for the original and filtered signal at the discharge of 0.75 PMF- data set 2

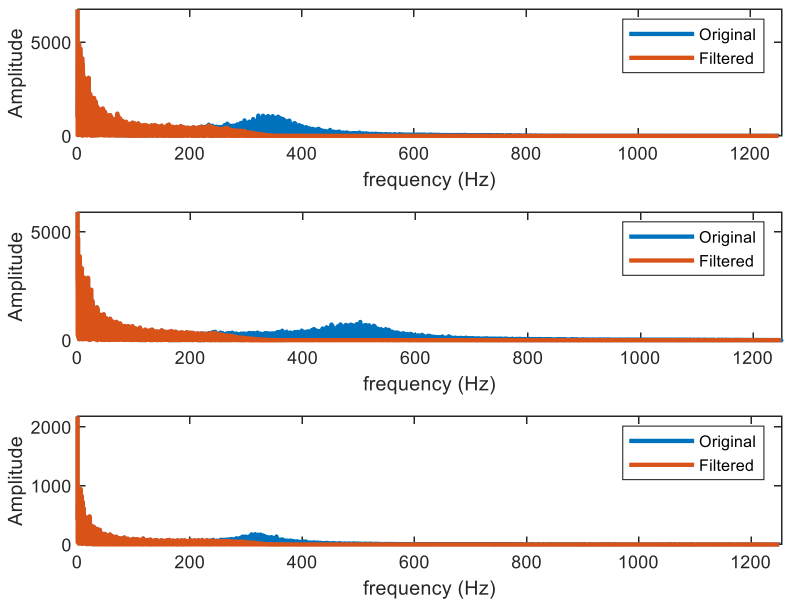

Figure B.29. FFT plots for both the original and filtered signal at upstream floor (sensor 2), upstream baffle face (sensor 3) and downstream floor (sensor 5) at the discharge of 0.75 PMF- data set 2

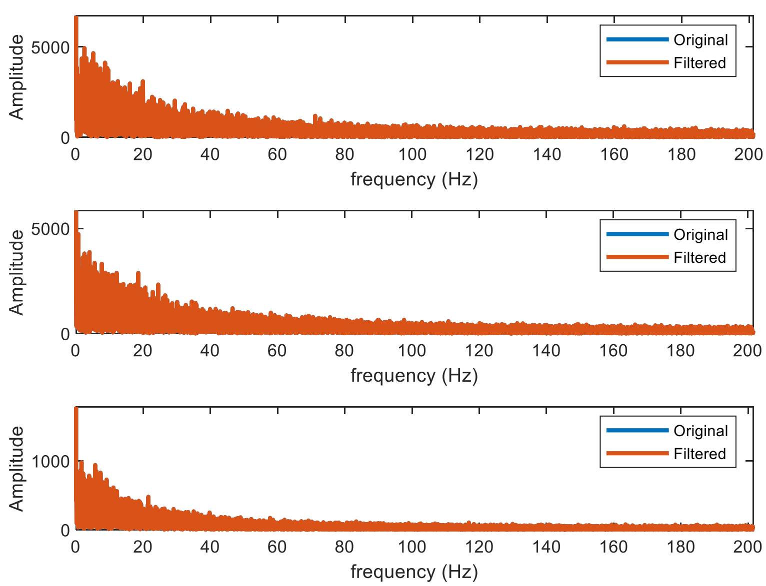

Figure B.30. Closer view to 200 Hz-FFT plots for both the original and filtered signal at upstream floor (sensor 2), upstream baffle face (sensor 3) and downstream floor (sensor 5) at the discharge of 0.75 PMF- data set 2

The low-frequency peaks are 2.501, 0.6766, 1.619 Hz at the upstream floor, upstream baffle face, and downstream floor, respectively.

DATA SET3

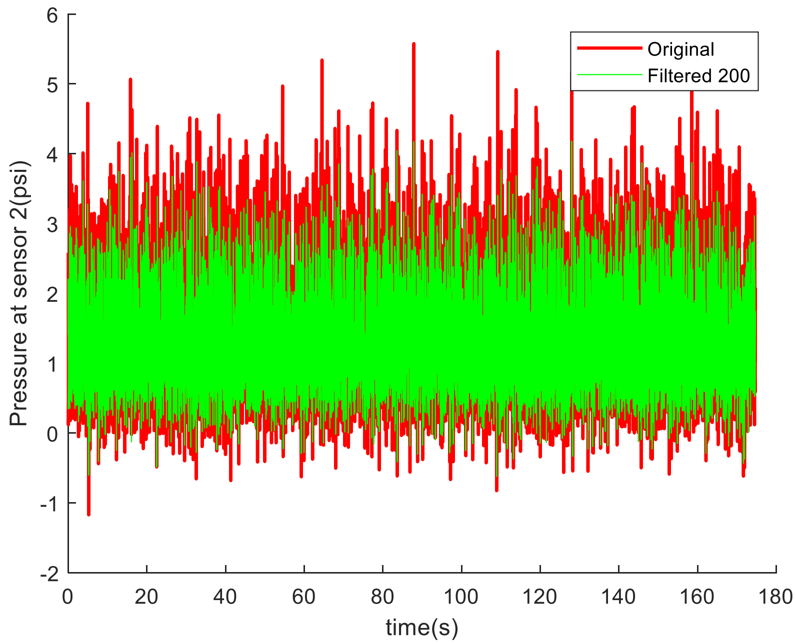

Figure B.31. Time versus pressure at sensor 2 (upstream floor) for the original and filtered signal at the discharge of 0.75 PMF- data set 3

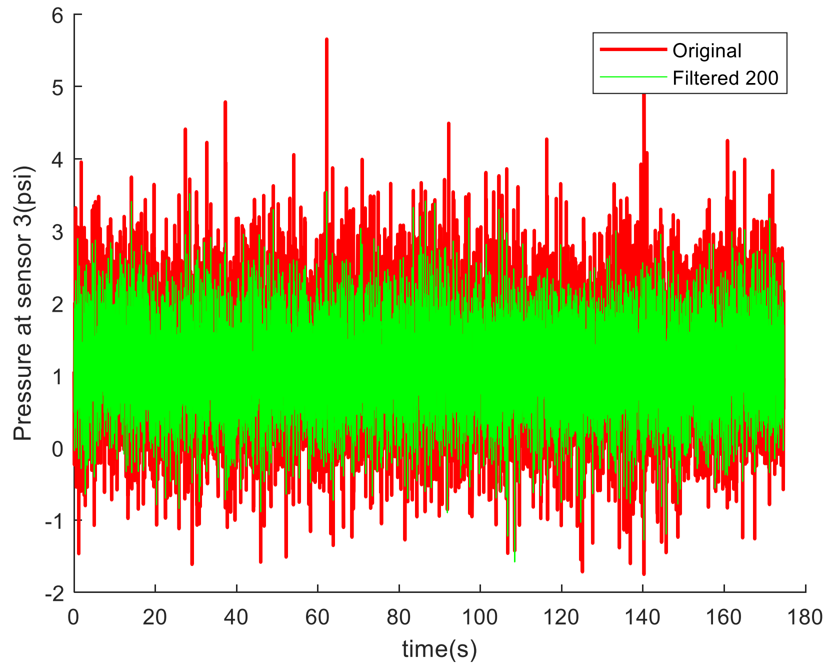

Figure B.32. Time versus pressure at sensor 3 (upstream baffle face) for the original and filtered signal at the discharge of 0.75 PMF- data set 3

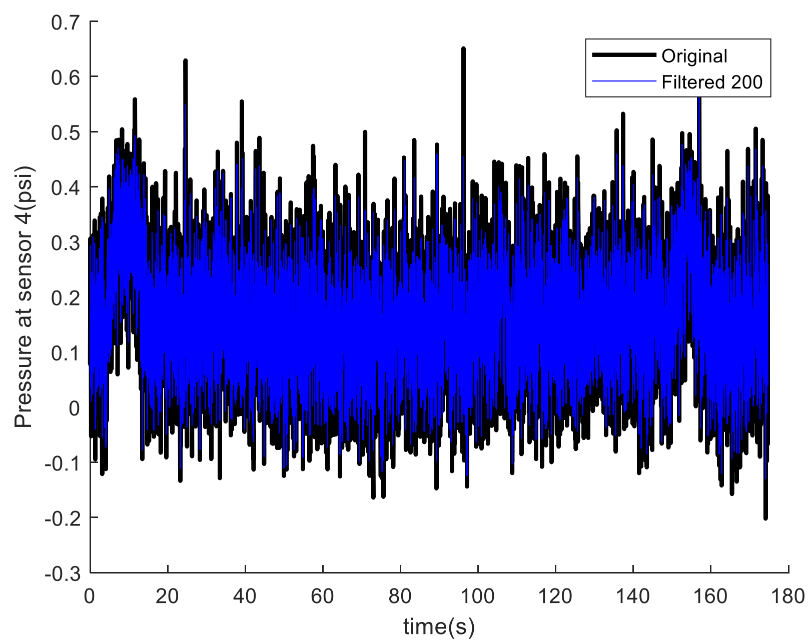

Figure B.33. Time versus pressure at sensor 4 (downstream baffle slope) for the original and filtered signal at the discharge of 0.75 PMF- data set 3

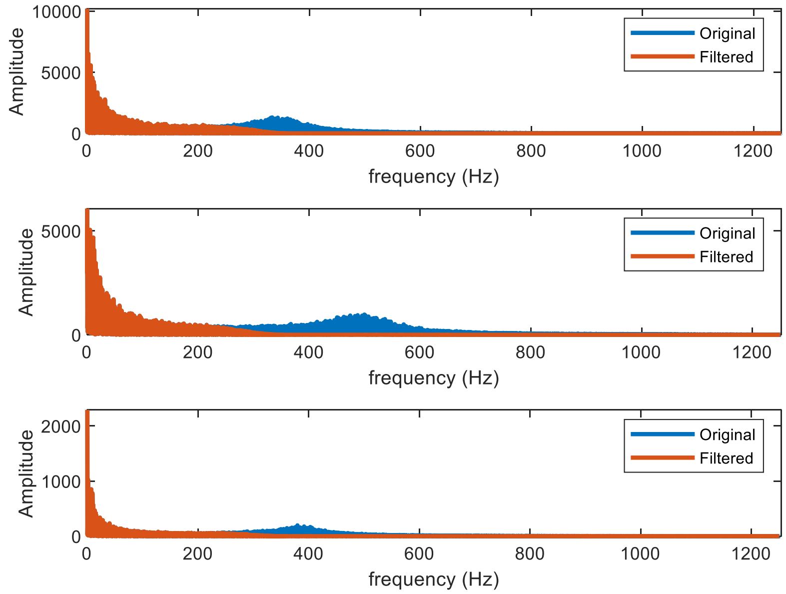

Figure B.34. FFT plots for both the original and filtered signal at upstream floor (sensor 2), upstream baffle face (sensor 3) and downstream baffle slope (sensor 4) at the discharge of 0.75 PMF- data set 3

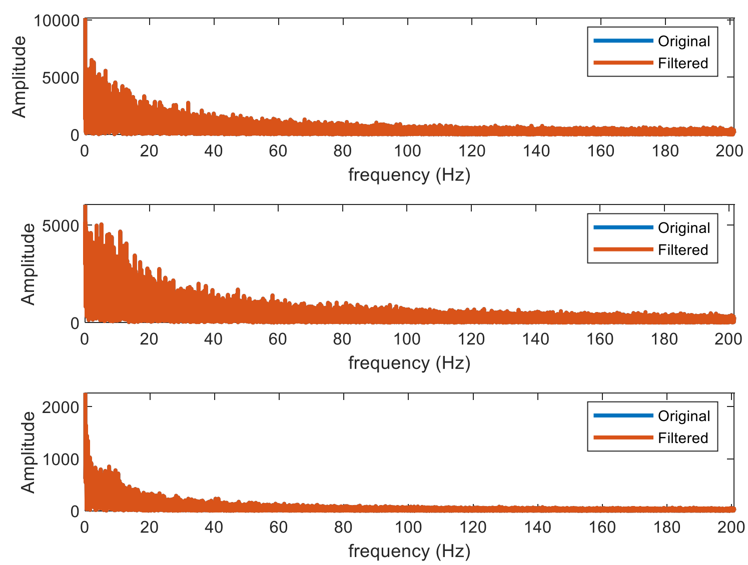

Figure B.35.Closer view to 200 Hz- FFT plots for both the original and filtered signal at upstream floor (sensor 2), upstream baffle face (sensor 3) and downstream baffle slope (sensor 4) at the discharge of 0.75 PMF-data set 3

The low-frequency peaks are 1.964, 0.05152, 0.04007 Hz at the upstream floor, upstream baffle face, and downstream baffle slope, respectively.

DATA SET4

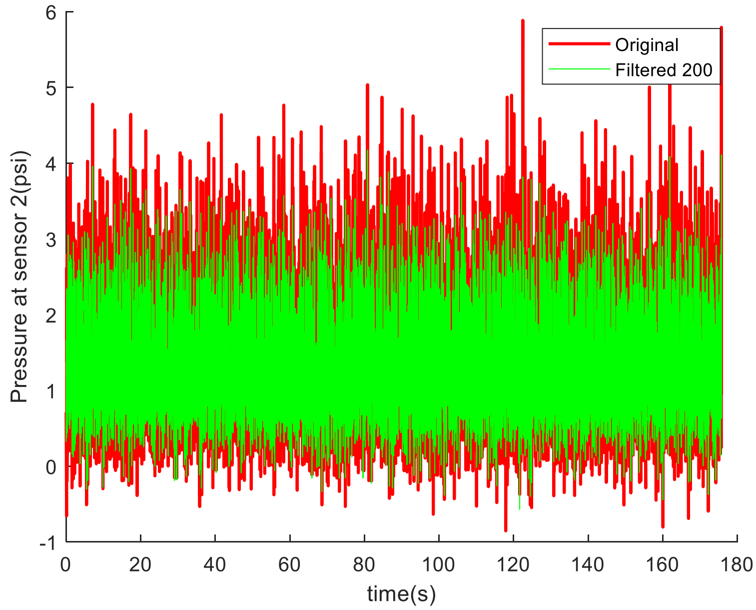

Figure B.36. Time versus pressure at sensor 2 (upstream floor) for the original and filtered signal at the discharge of 0.75 PMF- data set 4

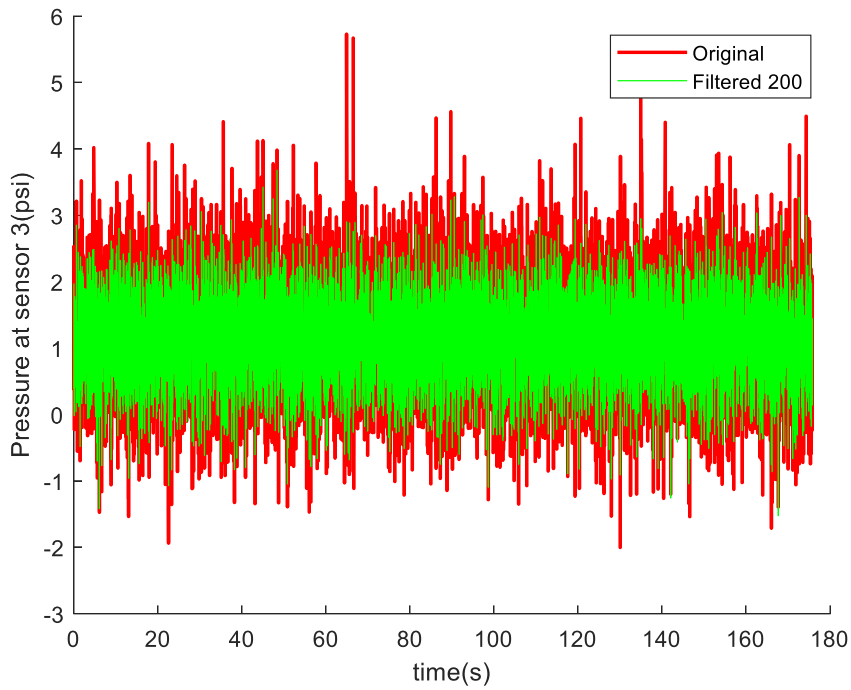

Figure B.37. Time versus pressure at sensor 3 (upstream baffle face) for the original and filtered signal at the discharge of 0.75 PMF- data set 4

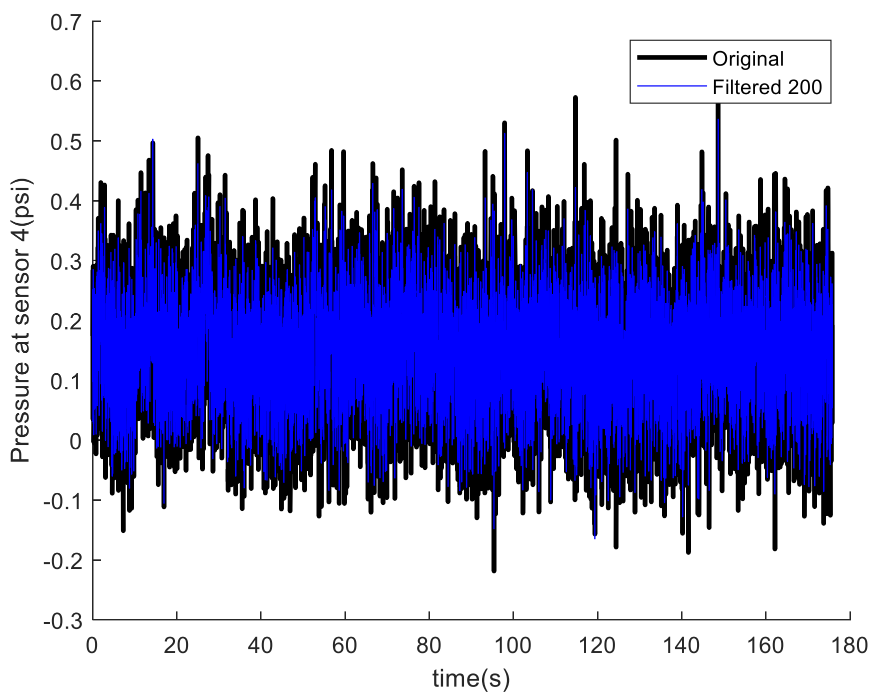

Figure B.38. Time versus pressure at sensor 4 (downstream baffle slope) for the original and filtered signal at the discharge of 0.75 PMF- data set 4

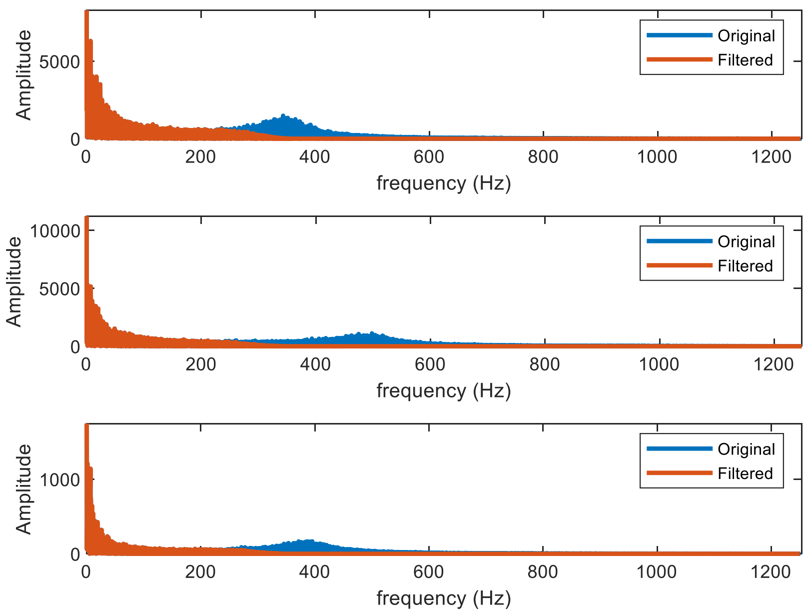

Figure B.39. FFT plots for both the original and filtered signal at upstream floor (sensor 2), upstream baffle face (sensor 3) and downstream baffle slope (sensor 4) at the discharge of 0.75 PMF- data set 4

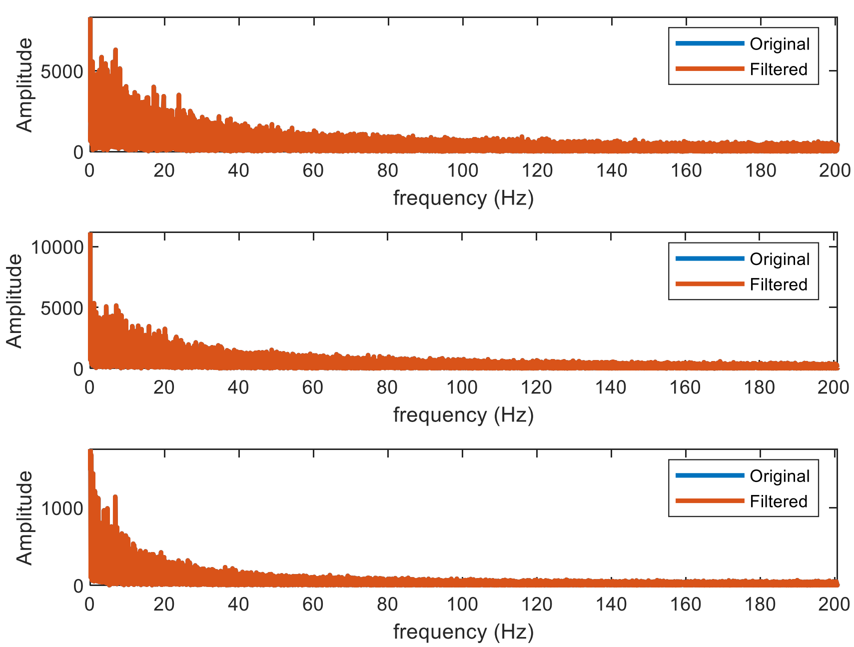

Figure B.40.Closer view to 200 Hz- FFT plots for both the original and filtered signal at upstream floor (sensor 2), upstream baffle face (sensor 3) and downstream baffle slope (sensor 4) at the discharge of 0.75 PMF- data set 4

The low-frequency peaks are 6.799, 0.9956, 0.02276 Hz at the upstream floor, upstream baffle face, and downstream baffle slope, respectively.

0.50 PMF

DATA SET1

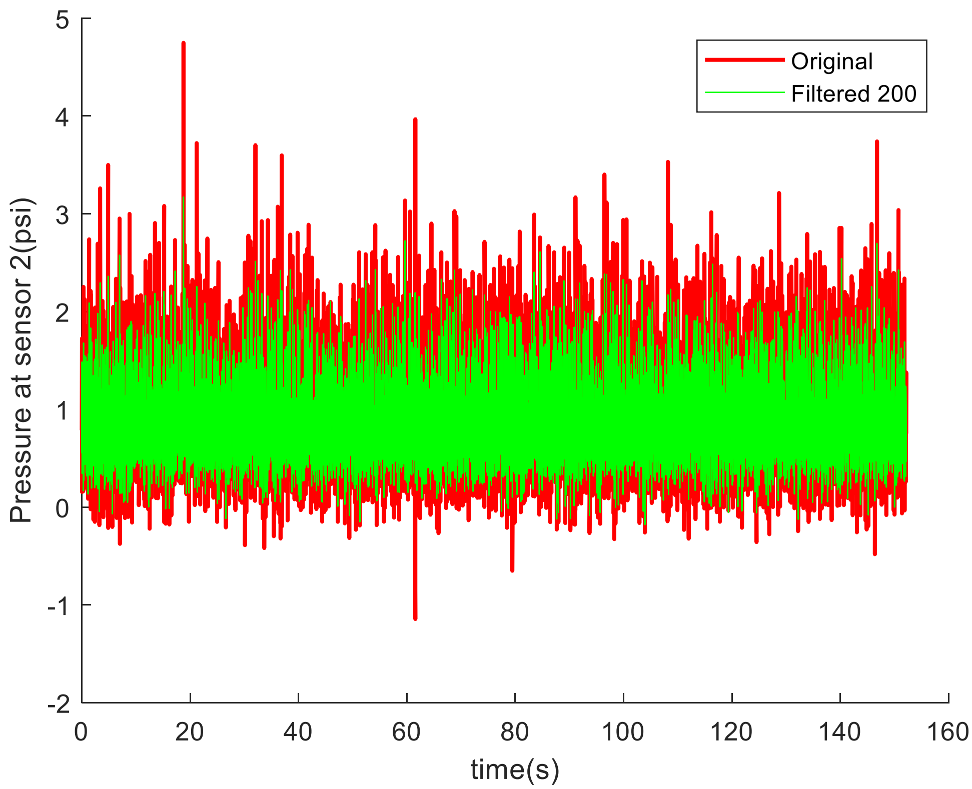

Figure B.41. Time versus pressure at sensor 2 (upstream floor) for the original and filtered signal at the discharge of 0.50 PMF- data set 1

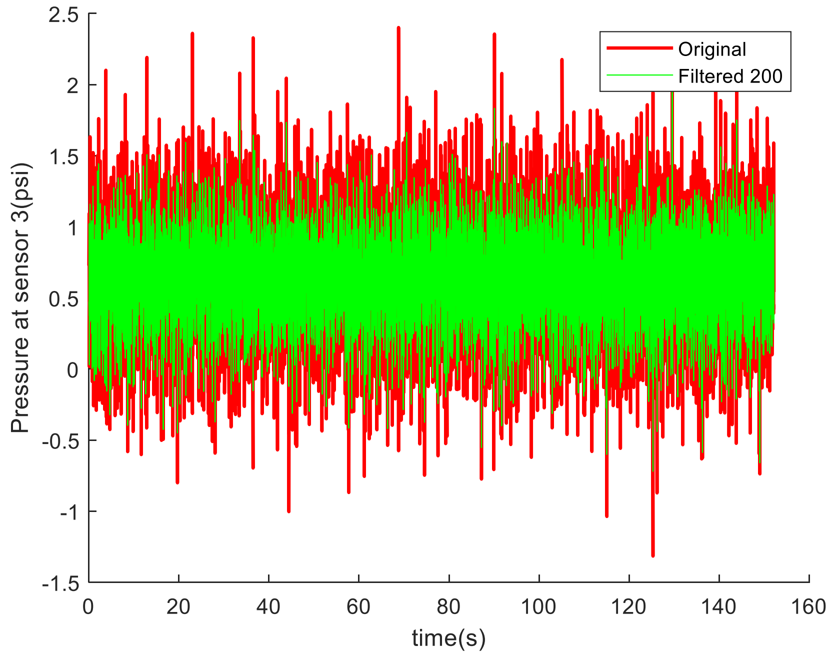

Figure B.42. Time versus pressure at sensor 3 (upstream baffle face) for the original and filtered signal at the discharge of 0.50 PMF- data set 1

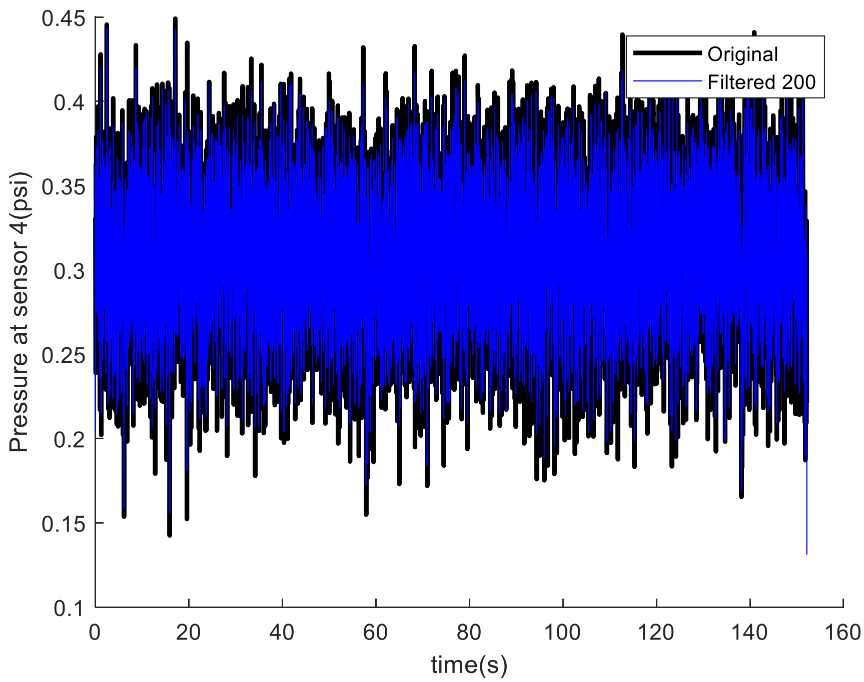

Figure B.43. Time versus pressure at sensor 4 (downstream baffle slope) for the original and filtered signal at the discharge of 0.50 PMF- data set 1

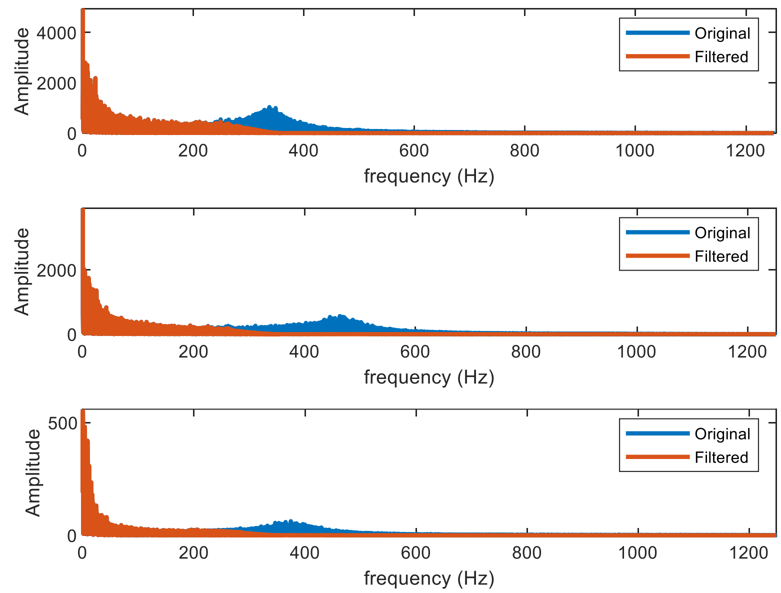

Figure B.44. FFT plots for both the original and filtered signal at upstream floor (sensor 2), upstream baffle face (sensor 3) and downstream baffle slope (sensor 4) at the discharge of 0.50 PMF- data set 1

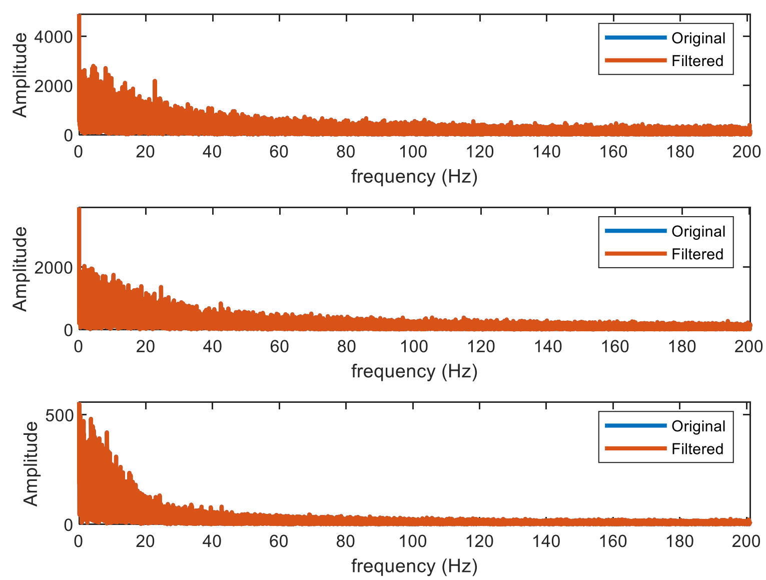

Figure B.45. Closer view to 200 Hz- FFT plots for both the original and filtered signal at upstream floor (sensor 2), upstream baffle face (sensor 3) and downstream baffle slope (sensor 4) at the discharge of 0.50 PMF- data set 1

The low-frequency peaks are 4.265, 1.59, 0.01971 Hz at the upstream floor, upstream baffle face, and downstream baffle slope, respectively.

DATA SET2

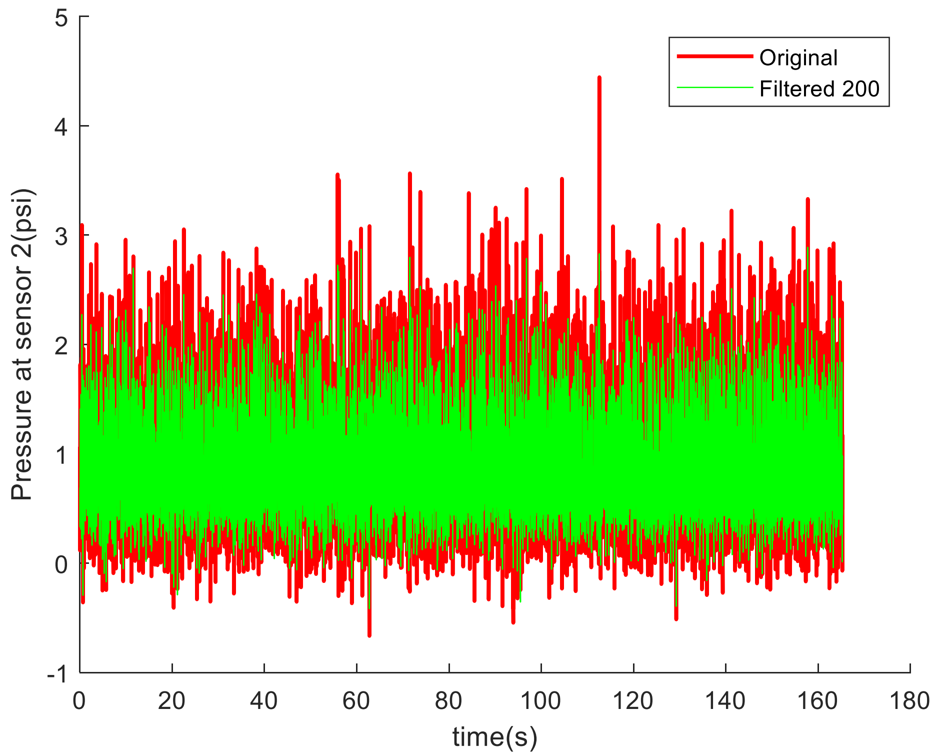

Figure B.46. Time versus pressure at sensor 2 (upstream floor) for the original and filtered signal at the discharge of 0.50 PMF- data set 2

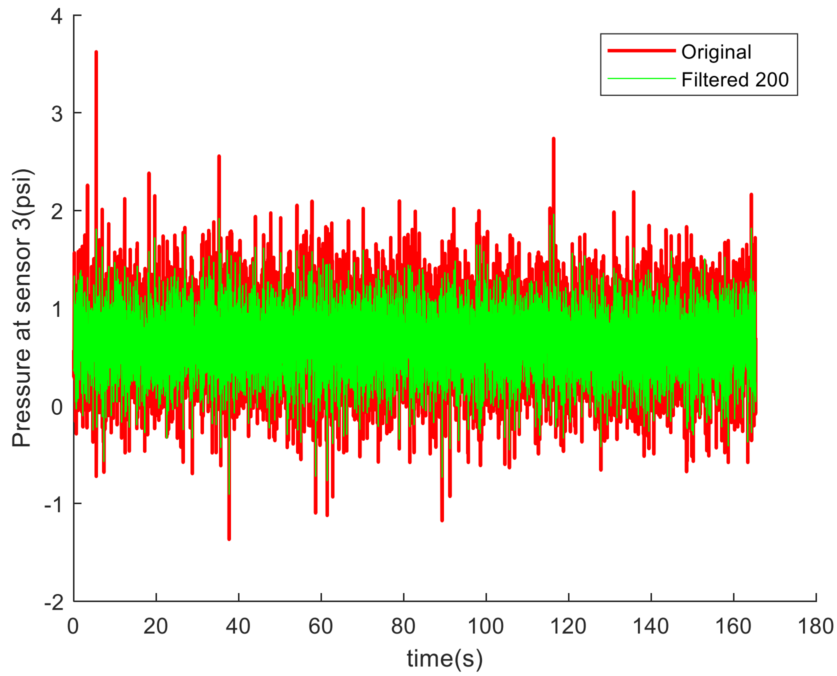

Figure B.47. Time versus pressure at sensor 3 (upstream baffle face) for the original and filtered signal at the discharge of 0.50 PMF- data set 2

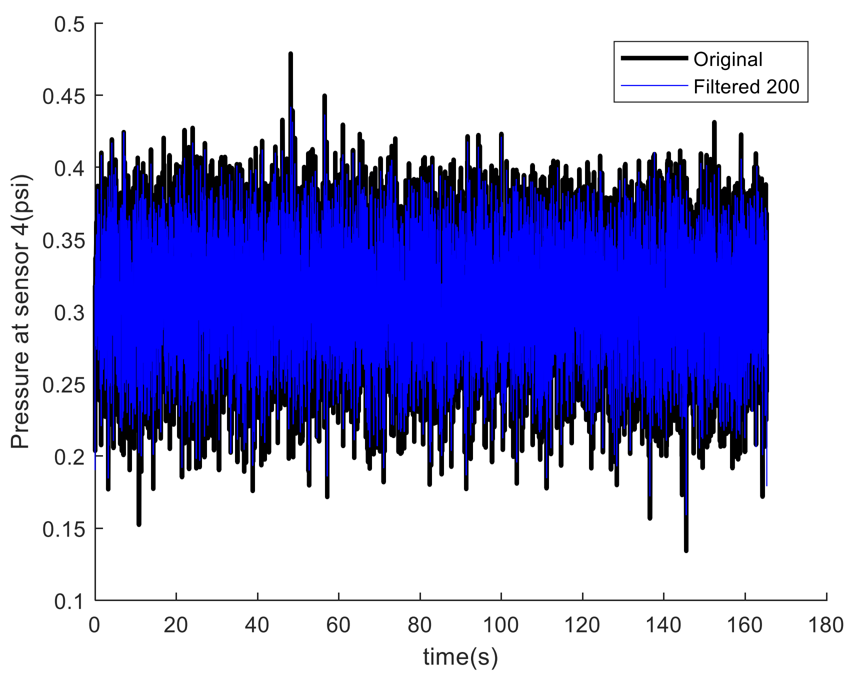

Figure B.48. Time versus pressure at sensor 4 (downstream baffle slope) for the original and filtered signal at the discharge of 0.50 PMF- data set 2

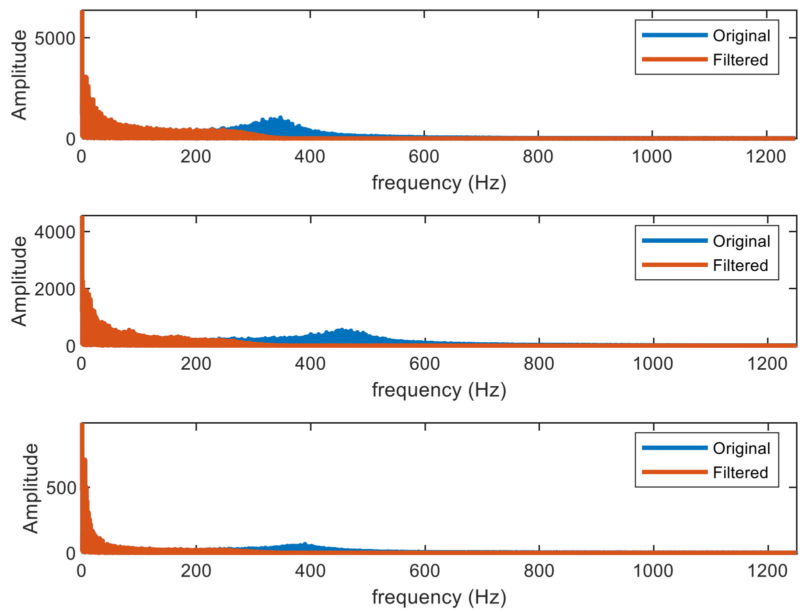

Figure B.49. FFT plots for both the original and filtered signal at upstream floor (sensor 2), upstream baffle face (sensor 3) and downstream baffle slope (sensor 4) at the discharge of 0.50 PMF-data set 2

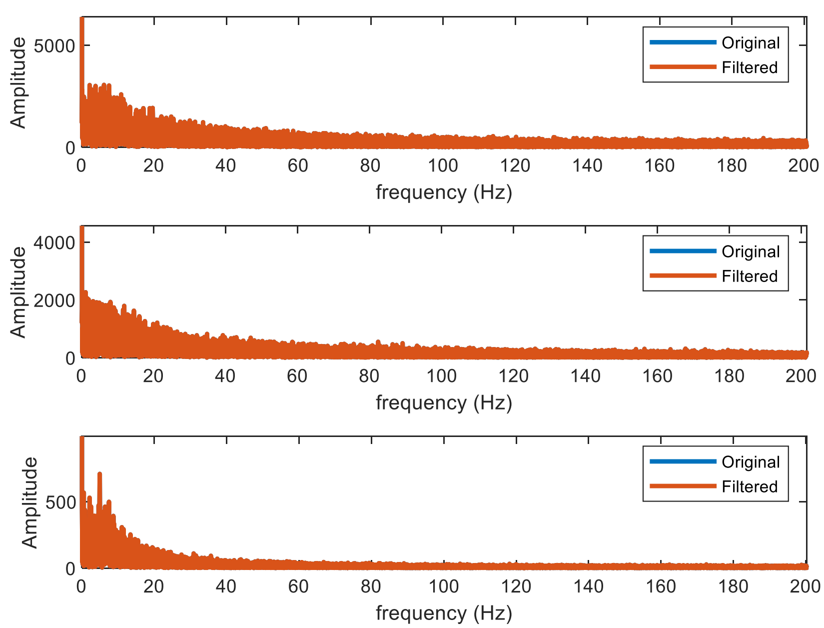

Figure B.50. Closer view to 200 Hz- FFT plots for both the original and filtered signal at upstream floor (sensor 2), upstream baffle face (sensor 3) and downstream baffle slope (sensor 4) at the discharge of 0.50 PMF - data set 2

The low-frequency peaks are 6.11, 1.022, 4.918 Hz at the upstream floor, upstream baffle face, and downstream baffle slope, respectively.

DATA SET3

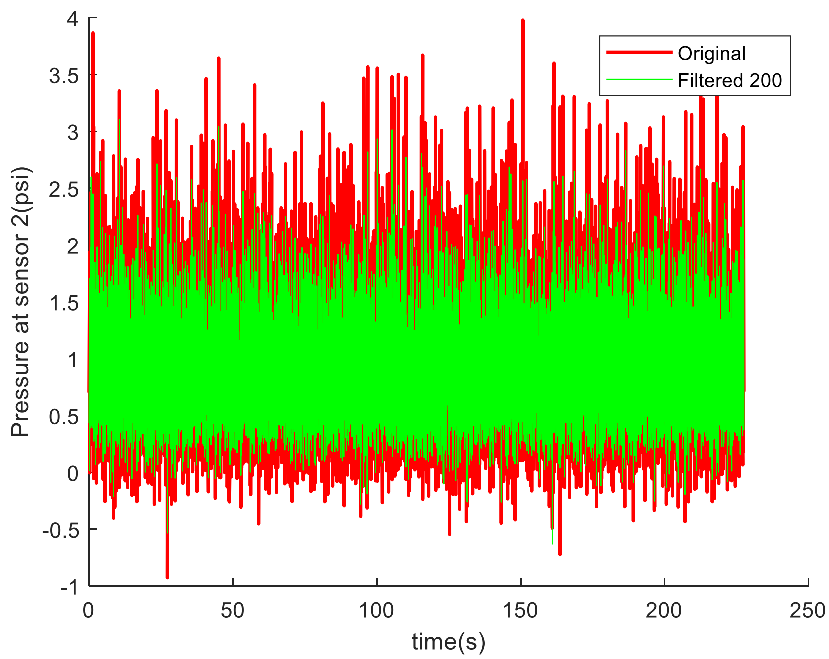

Figure B.51. Time versus pressure at sensor 2 (upstream floor) for the original and filtered signal at the discharge of 0.50 PMF- data set 3

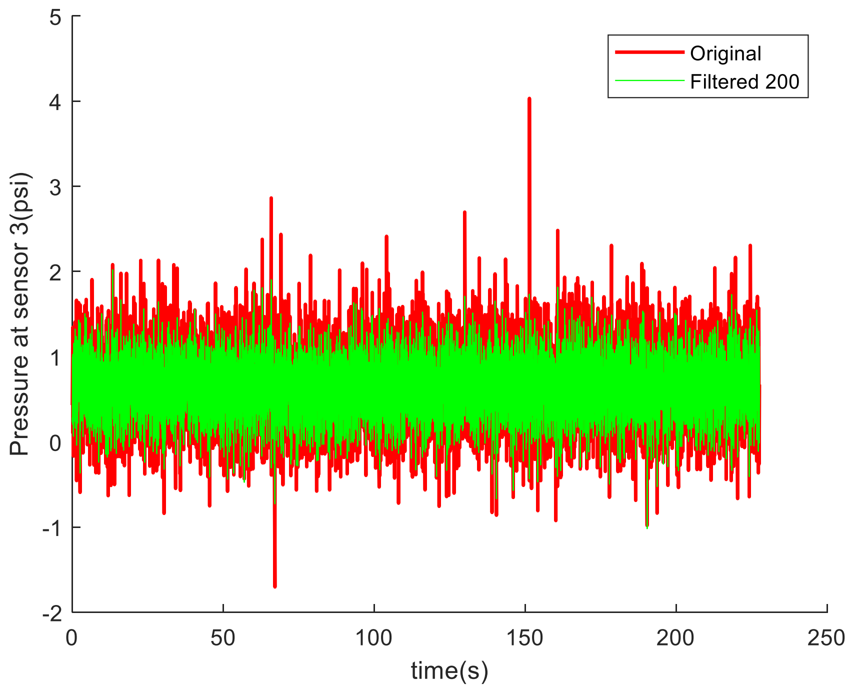

Figure B.52. Time versus pressure at sensor 3 (upstream baffle face) for the original and filtered signal at the discharge of 0.50 PMF- data set 3

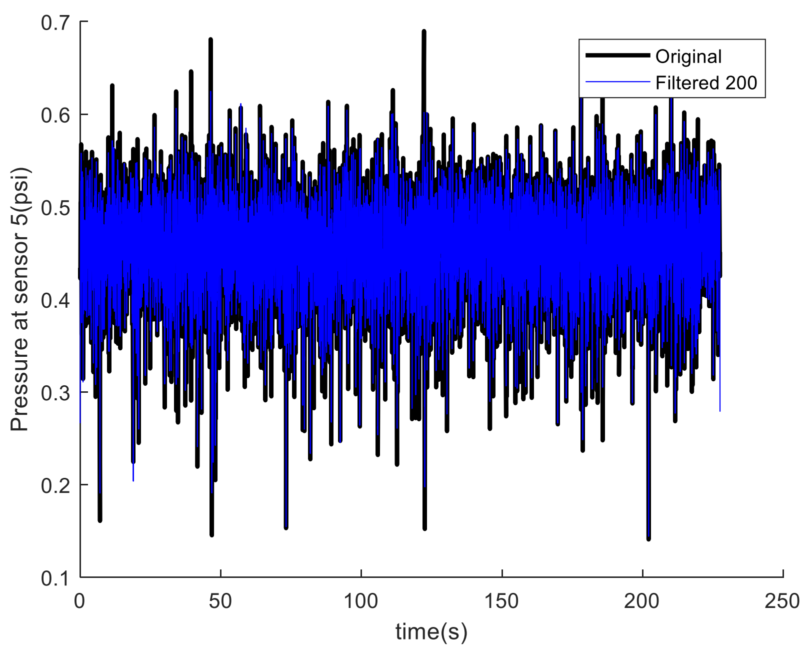

Figure B.53. Time versus pressure at sensor 5 (downstream floor) for the original and filtered signal at the discharge of 0.50 PMF- data set 3

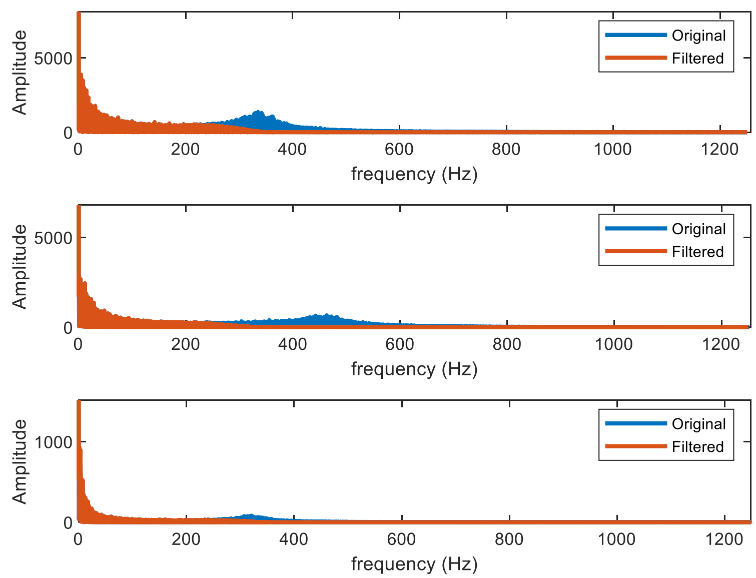

Figure B.54. FFT plots for both the original and filtered signal at upstream floor (sensor 2), upstream baffle face (sensor 3) and downstream floor (sensor 5) at the discharge of 0.50 PMF- data set 3

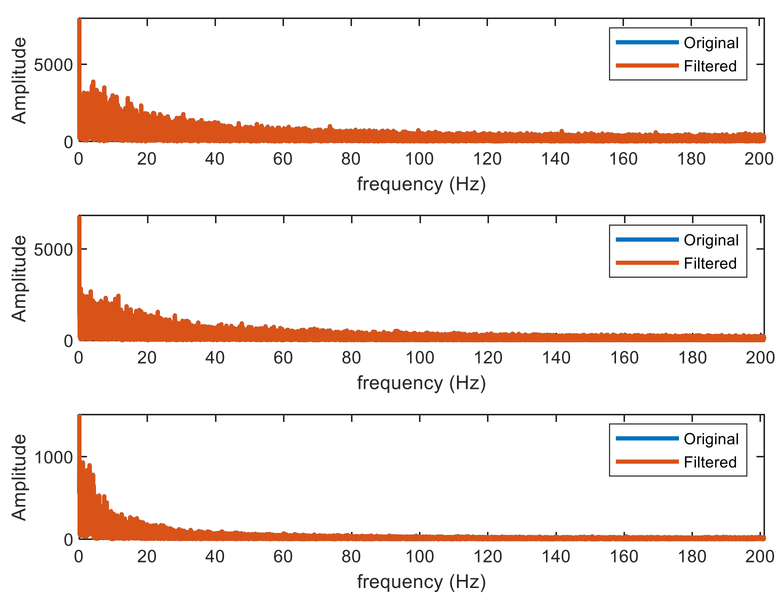

Figure B.55. Closer view to 200 Hz- FFT plots for both the original and filtered signal at upstream floor (sensor 2), upstream baffle face (sensor 3) and downstream floor (sensor 5) at the discharge of 0.50 PMF- data set 3

The low-frequency peaks are 4.088, 0.4351, 0.07032 Hz at the upstream floor, upstream baffle face, and downstream floor, respectively.

DATA SET4

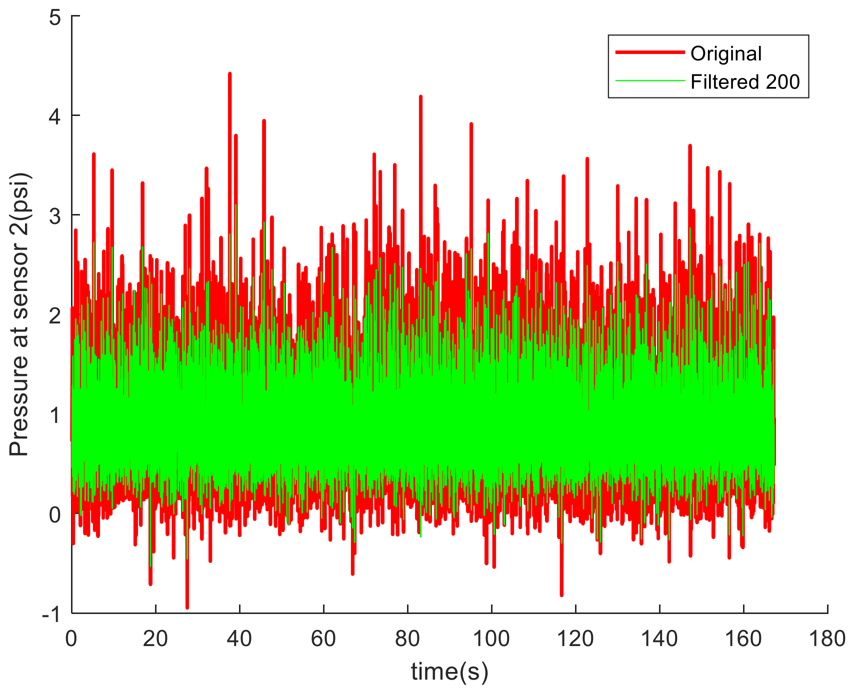

Figure B.56. Time versus pressure at sensor 2 (upstream floor) for the original and filtered signal at the discharge of 0.50 PMF- data set 4

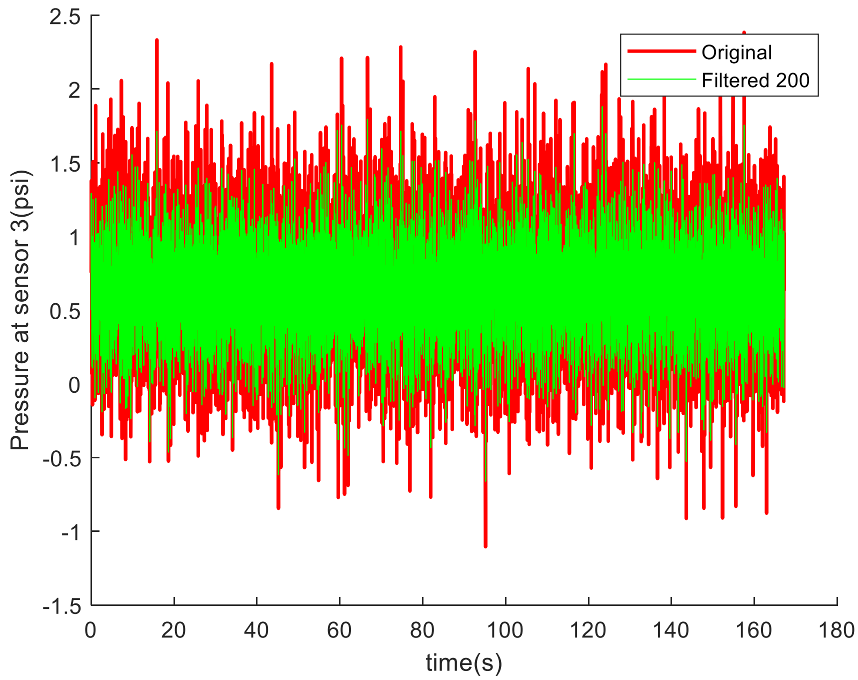

Figure B.57. Time versus pressure at sensor 3 (upstream baffle face) for the original and filtered signal at the discharge of 0.50 PMF- data set 4

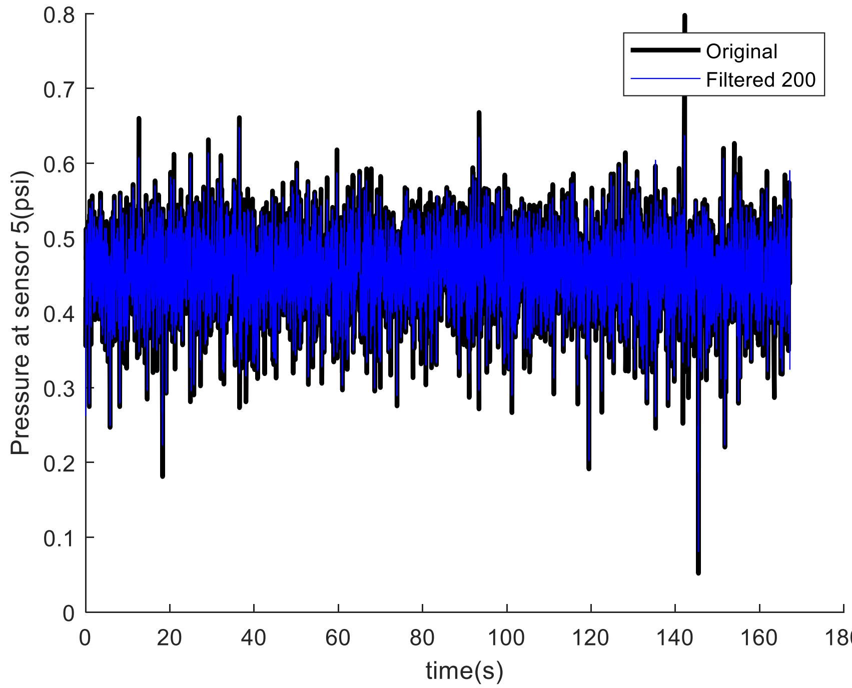

Figure B.58. Time versus pressure at sensor 5 (downstream floor) for the original and filtered signal at the discharge of 0.50 PMF- data set 4

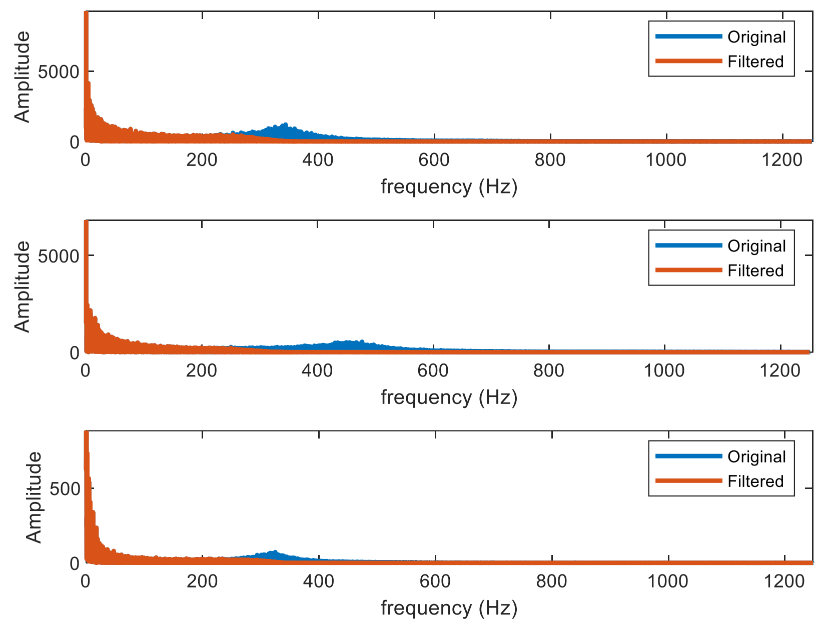

Figure B.59. FFT plots for both the original and filtered signal at upstream floor (sensor 2), upstream baffle face (sensor 3) and downstream floor (sensor 5) at the discharge of 0.50 PMF- data set 4

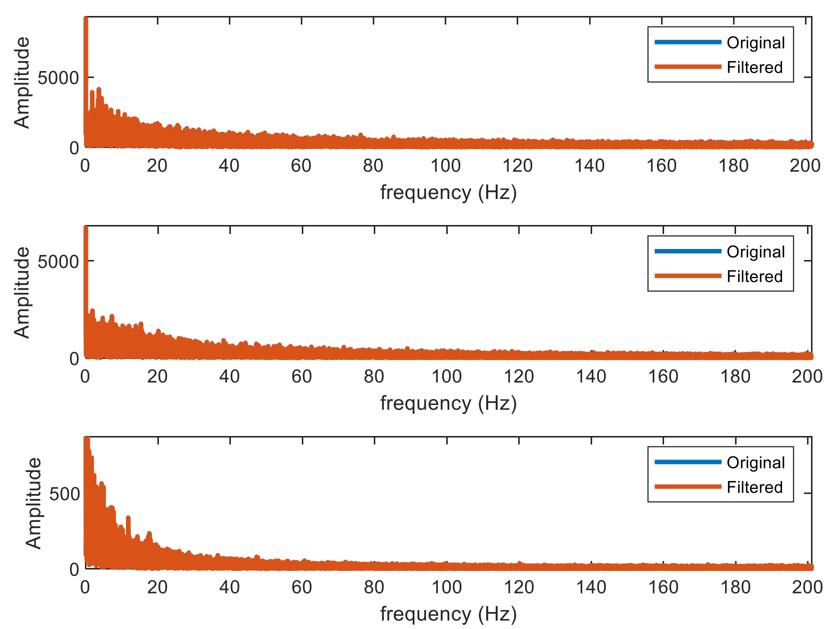

Figure B.60. Closer view to 200 Hz- FFT plots for both the original and filtered signal at upstream floor (sensor 2), upstream baffle face (sensor 3) and downstream floor (sensor 5) at the discharge of 0.50 PMF- data set 4

The low-frequency peaks are 3.612, 1.836, 0.5144 Hz at the upstream floor, upstream baffle face, and downstream floor, respectively.

0.25 PMF

DATA SET1

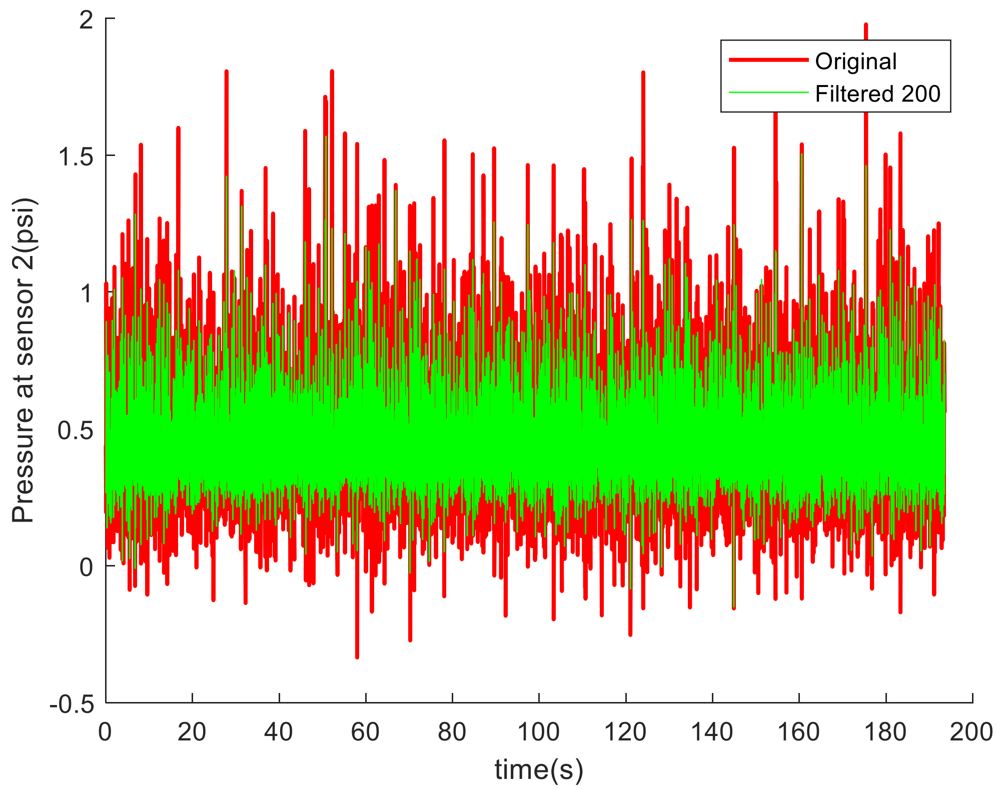

Figure B.61. Time versus pressure at sensor 2 (upstream floor) for the original and filtered signal at the discharge of 0.25 PMF- data set 1

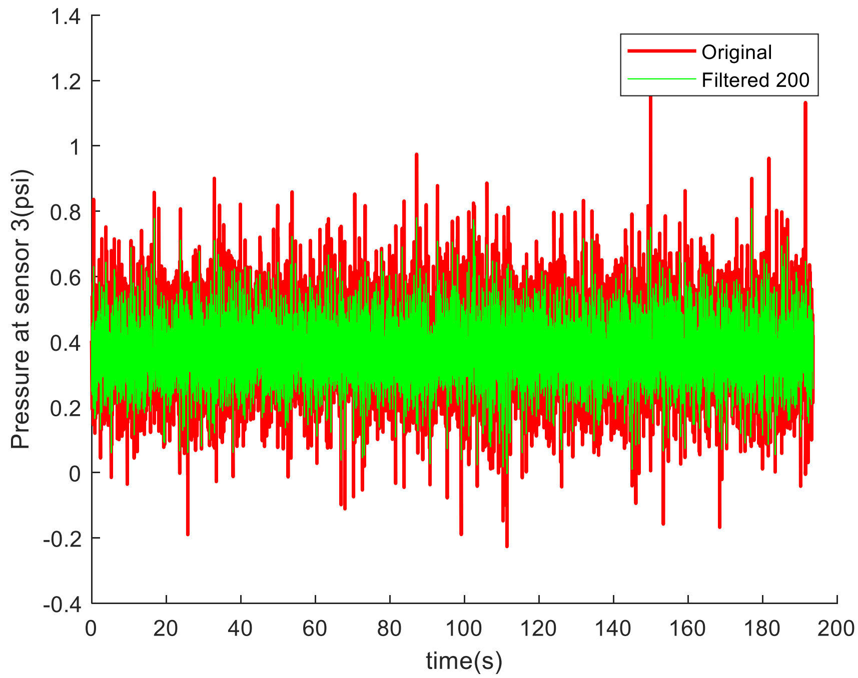

Figure B.62. Time versus pressure at sensor 3 (upstream baffle face) for the original and filtered signal at the discharge of 0.25 PMF- data set 1

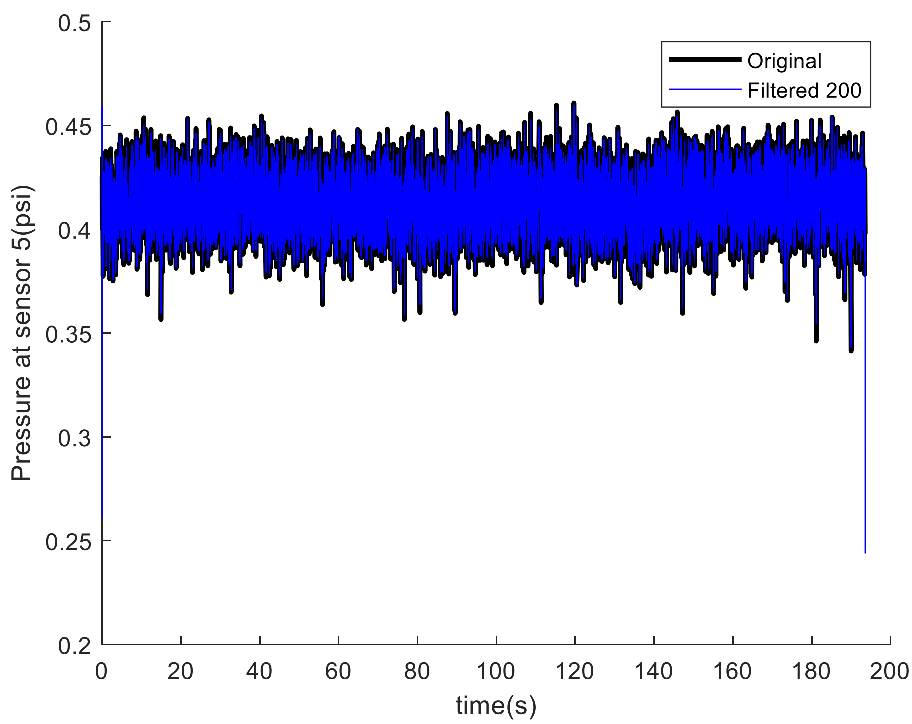

Figure B.63. Time versus pressure at sensor 5 (downstream floor) for the original and filtered signal at the discharge of 0.25 PMF- data set 1

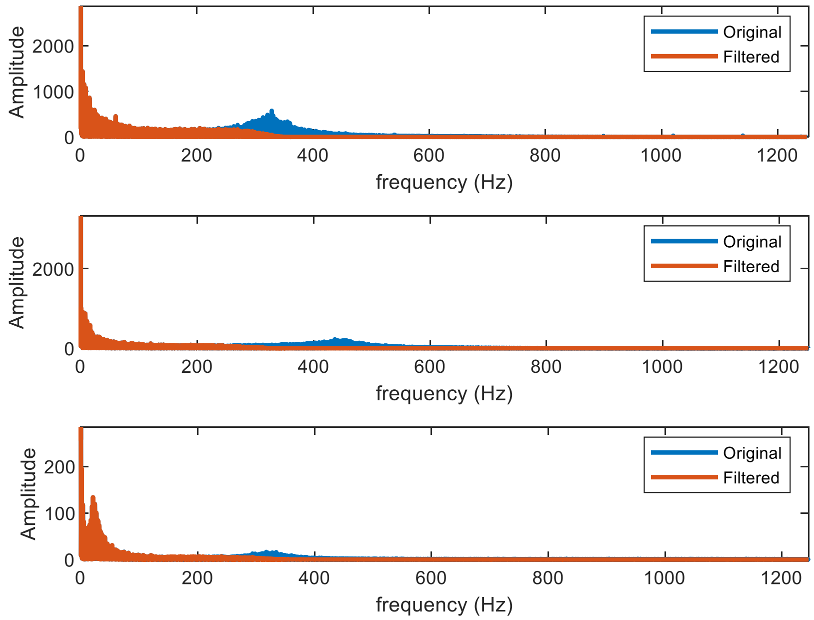

Figure B.64. FFT plots for both the original and filtered signal at upstream floor (sensor 2), upstream baffle face (sensor 3) and downstream floor (sensor 5) at the discharge of 0.25 PMF- data set 1

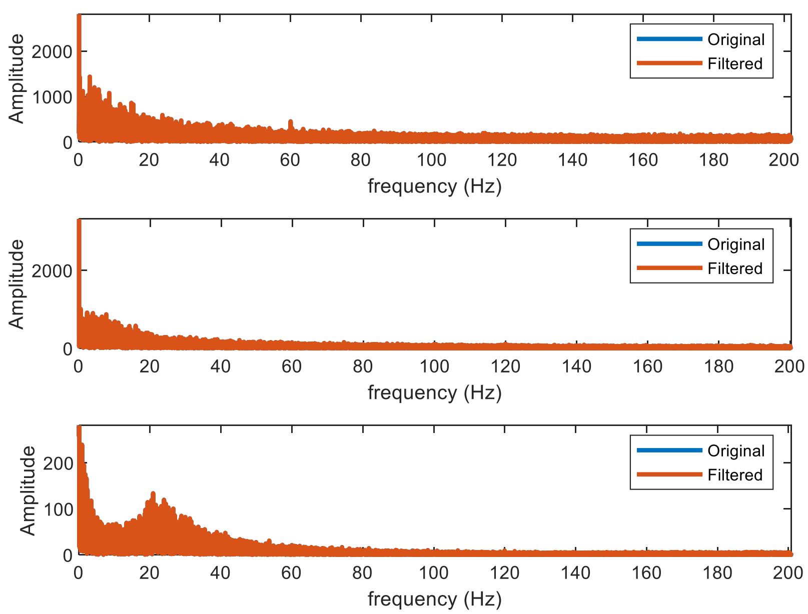

Figure B.65. Closer view to 200 Hz- FFT plots for both the original and filtered signal at upstream floor (sensor 2), upstream baffle face (sensor 3) and downstream floor (sensor 5) at the discharge of 0.25 PMF- data set 1

The low-frequency peaks are 3.043, 0.444, 0.0155 Hz at the upstream floor, upstream baffle face, and downstream floor, respectively.

DATA SET2

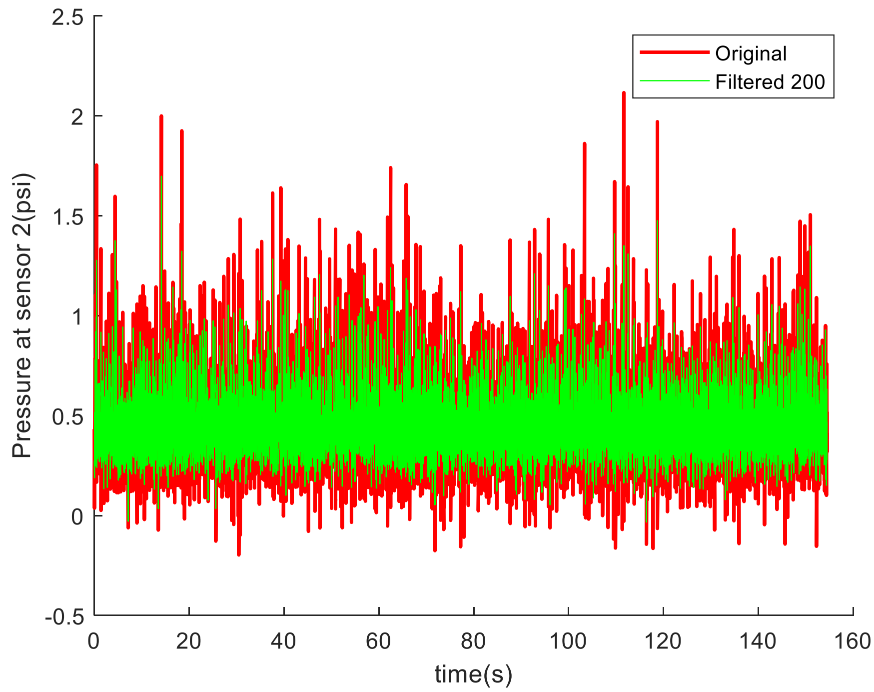

Figure B.66. Time versus pressure at sensor 2 (upstream floor) for the original and filtered signal at the discharge of 0.25 PMF- data set 2

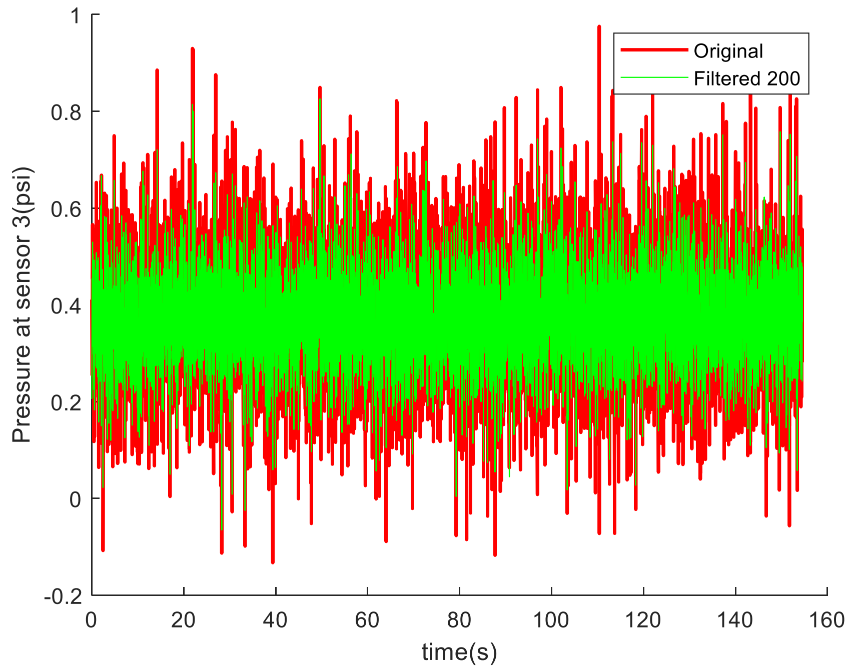

Figure B.67. Time versus pressure at sensor 3 (upstream baffle face) for the original and filtered signal at the discharge of 0.25 PMF- data set 2

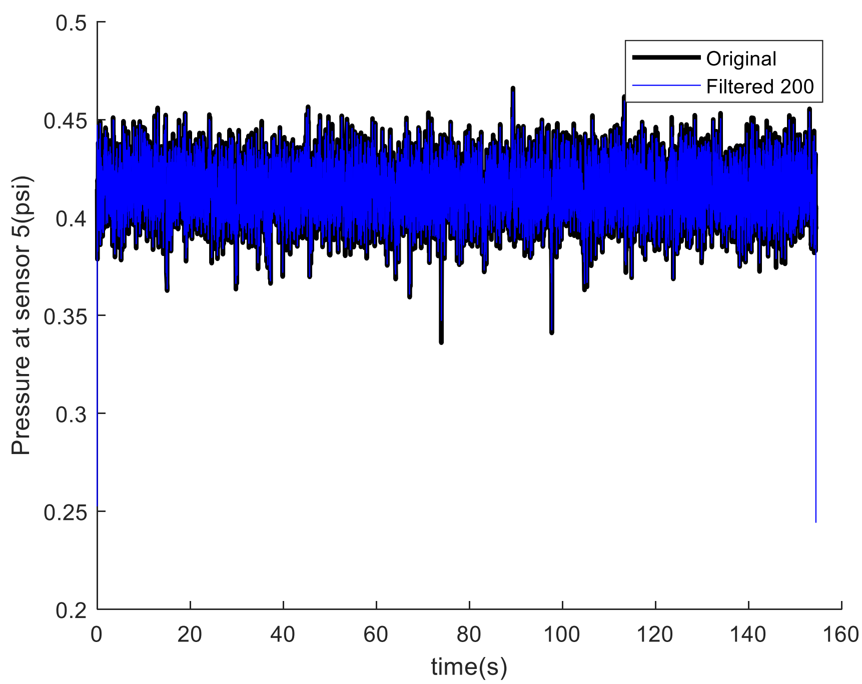

Figure B.68. Time versus pressure at sensor 5 (downstream floor) for the original and filtered signal at the discharge of 0.25 PMF- data set 2

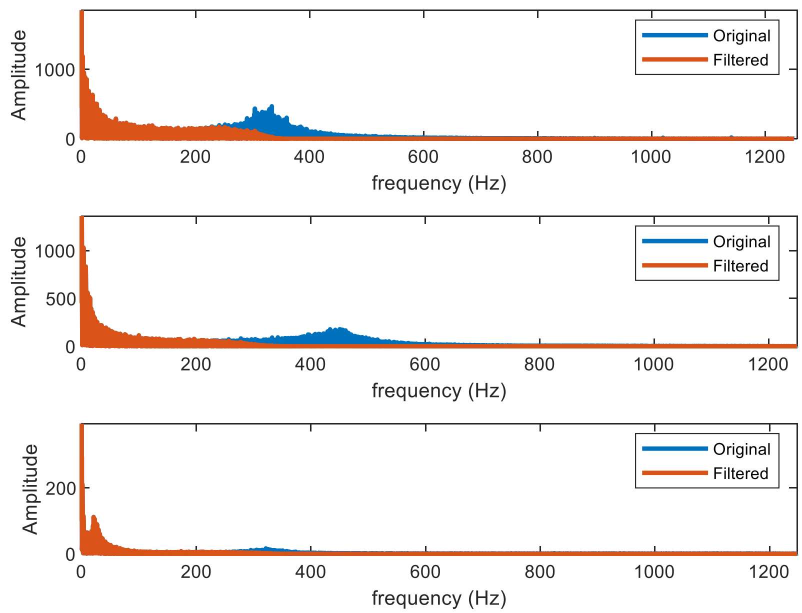

Figure B.69. FFT plots for both the original and filtered signal at upstream floor (sensor 2), upstream baffle face (sensor 3) and downstream floor (sensor 5) at the discharge of 0.25 PMF- data set 2

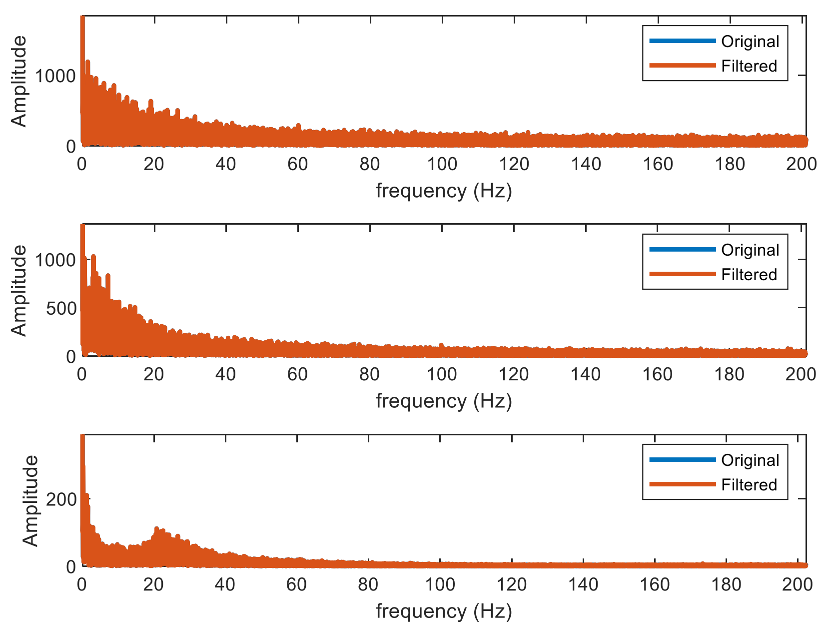

Figure B.70. Closer view to 200 Hz- FFT plots for both the original and filtered signal at upstream floor (sensor 2), upstream baffle face (sensor 3) and downstream floor (sensor 5) at the discharge of 0.25 PMF- data set 2

The low-frequency peaks are 1.456, 0.03884, 0.1942 Hz at the upstream floor, upstream baffle face, and downstream floor, respectively.

DATA SET3

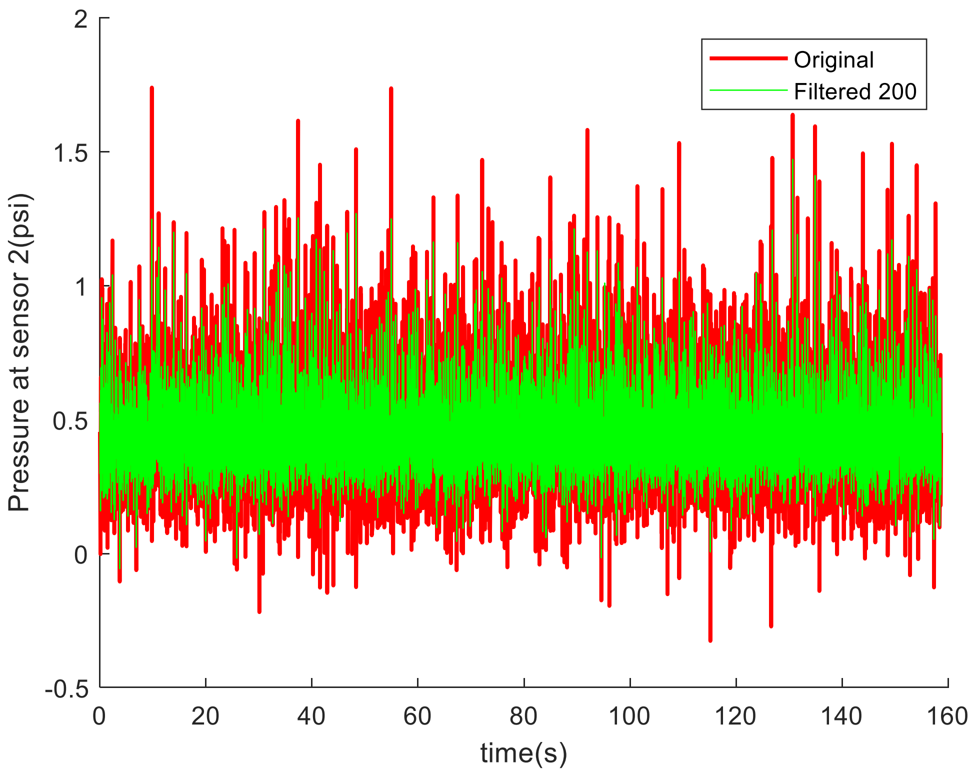

Figure B.71. Time versus pressure at sensor 2 (upstream floor) for the original and filtered signal at the discharge of 0.25 PMF- data set 3

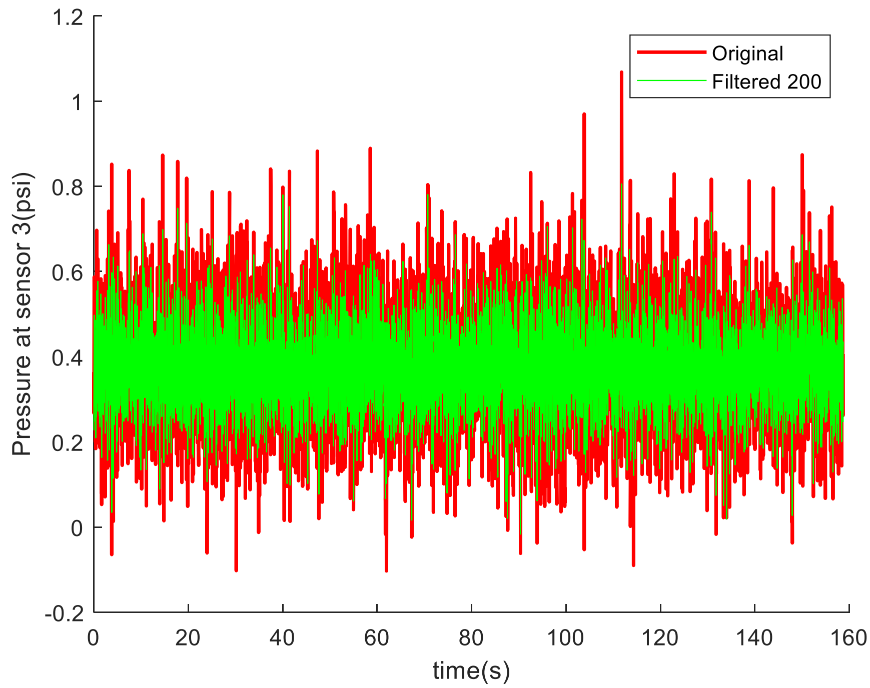

Figure B.72. Time versus pressure at sensor 3 (upstream baffle face) for the original and filtered signal at the discharge of 0.25 PMF- data set 3

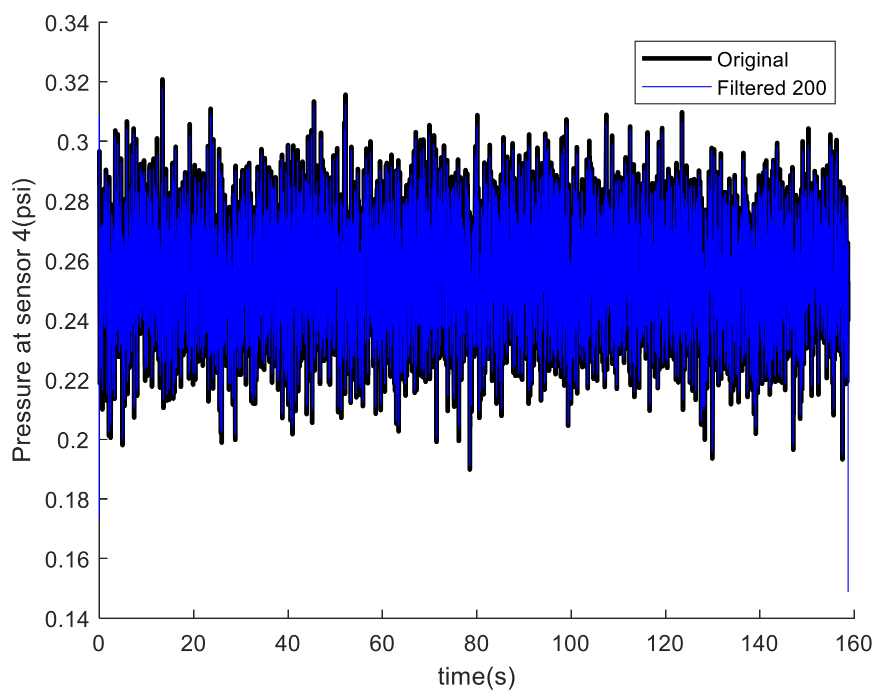

Figure B.73. Time versus pressure at sensor 4 (downstream baffle slope) for the original and filtered signal at the discharge of 0.25 PMF- data set 3

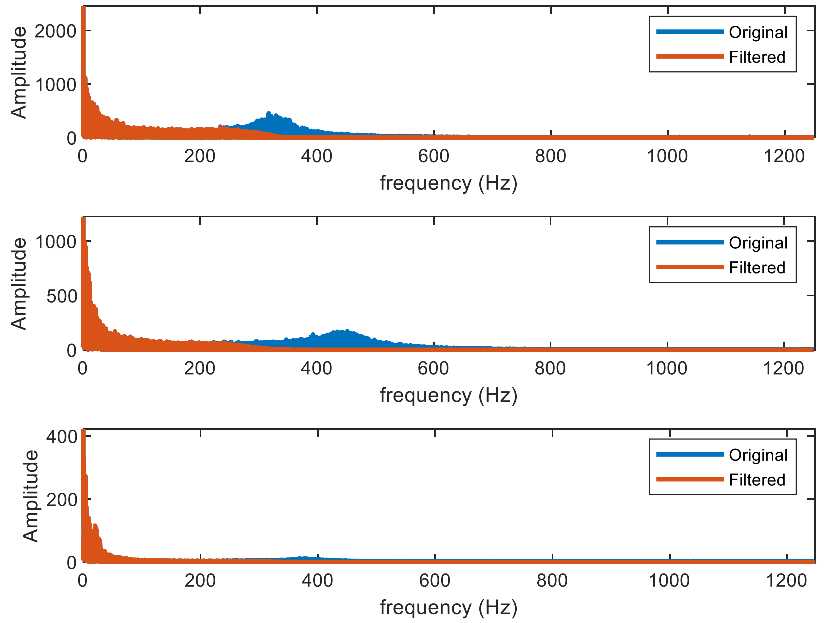

Figure B.74. FFT plots for both the original and filtered signal at upstream floor (sensor 2), upstream baffle face (sensor 3) and downstream baffle slope (sensor 4) at the discharge of 0.25 PMF- data set 3

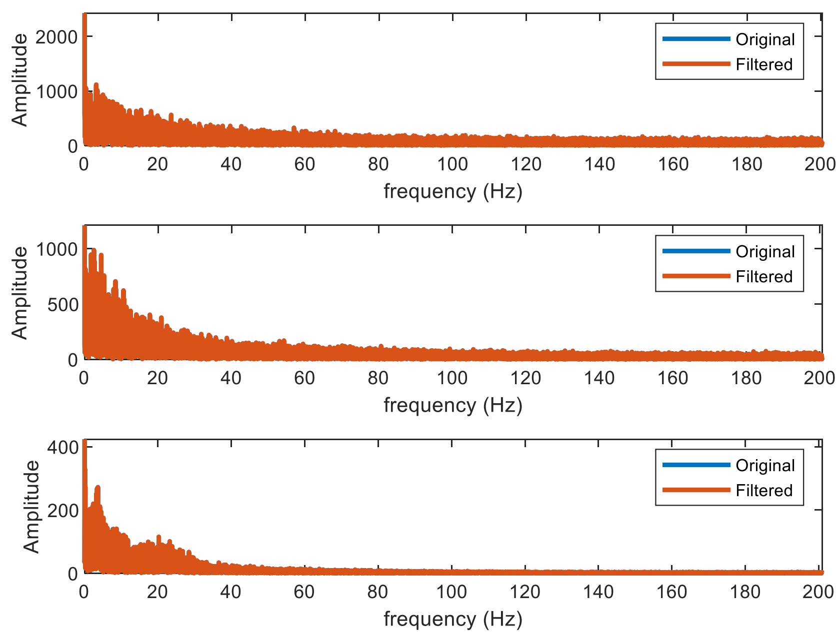

Figure B.75. Closer view to 200 Hz- FFT plots for both the original and filtered signal at upstream floor (sensor 2), upstream baffle face (sensor 3) and downstream baffle slope (sensor 4) at the discharge of 0.25 PMF- data set 3

The low-frequency peaks are 3.157, 2.540, 0.08193 Hz at the upstream floor, upstream baffle face, and downstream baffle slope, respectively.

DATA SET4

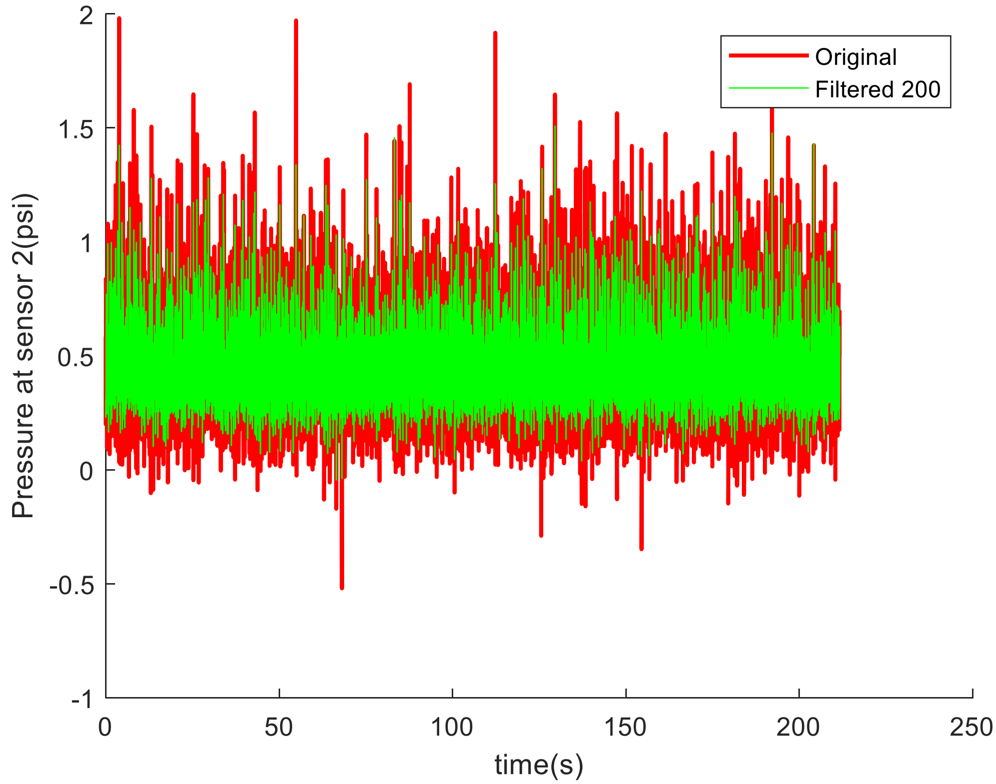

Figure B.76. Time versus pressure at sensor 2 (upstream floor) for the original and filtered signal at the discharge of 0.25 PMF- data set 4

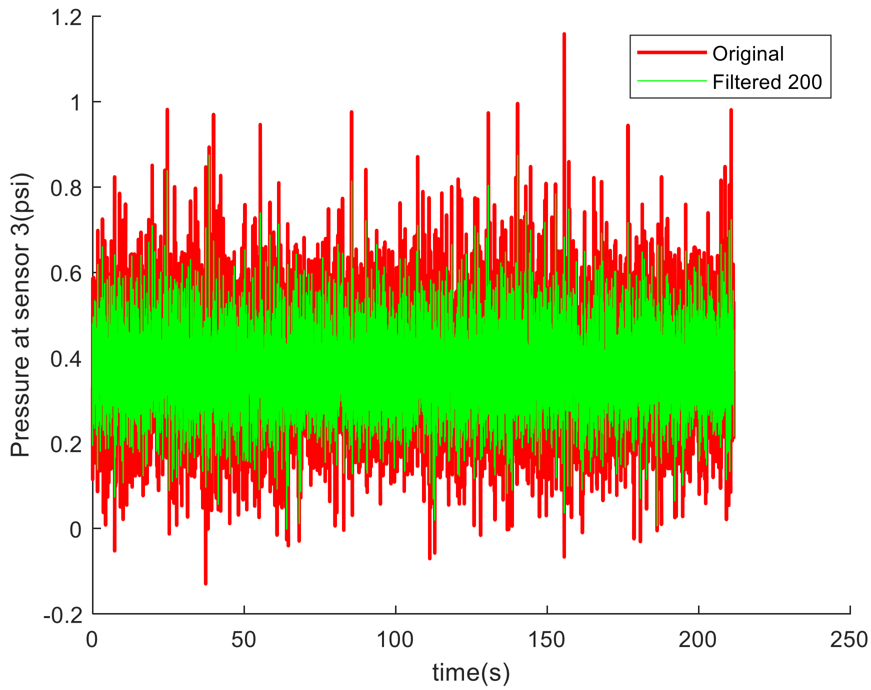

Figure B.77. Time versus pressure at sensor 3 (upstream baffle face) for the original and filtered signal at the discharge of 0.25 PMF- data set 4

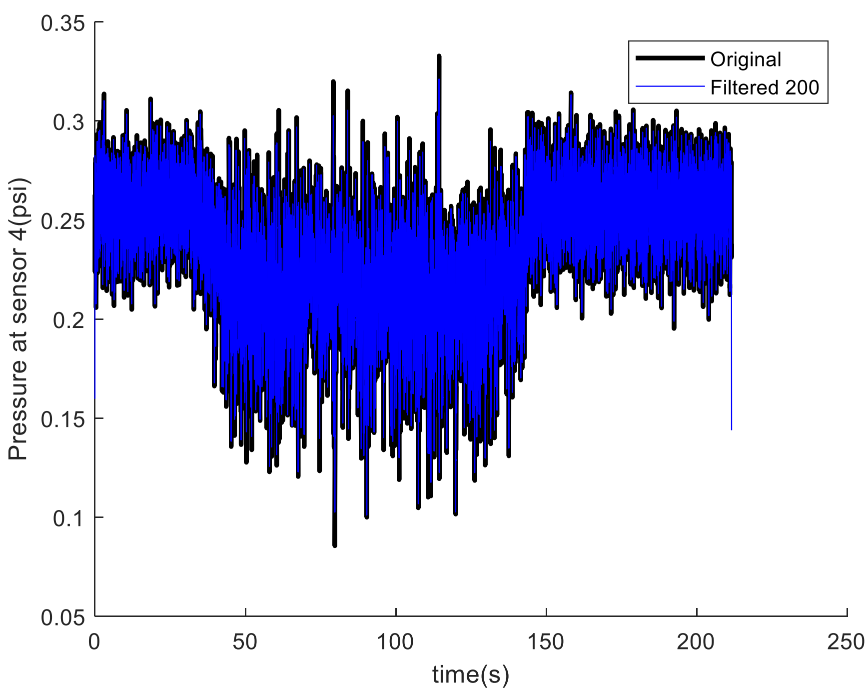

Figure B.78. Time versus pressure at sensor 4 (downstream baffle slope) for the original and filtered signal at the discharge of 0.25 PMF- data set 4

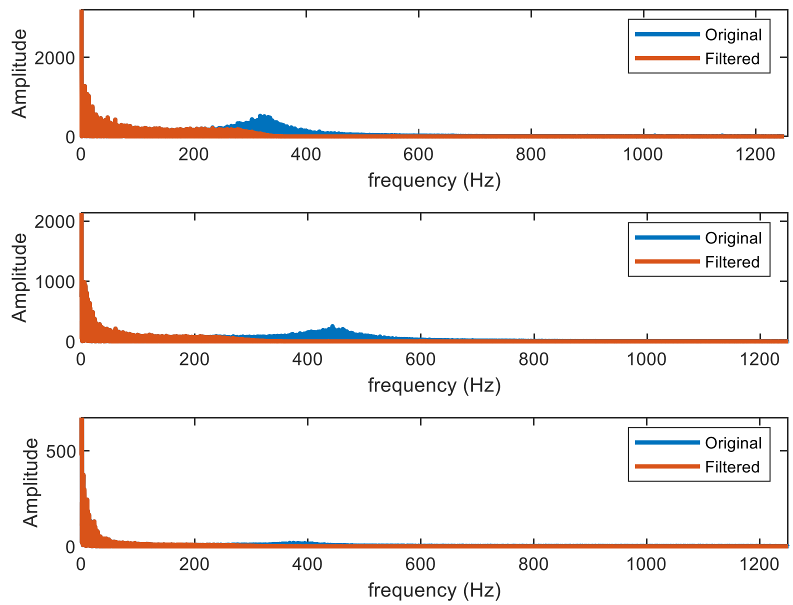

Figure B.79. FFT plots for both the original and filtered signal at upstream floor (sensor 2), upstream baffle face (sensor 3) and downstream baffle slope (sensor 4) at the discharge of 0.25 PMF- data set 4

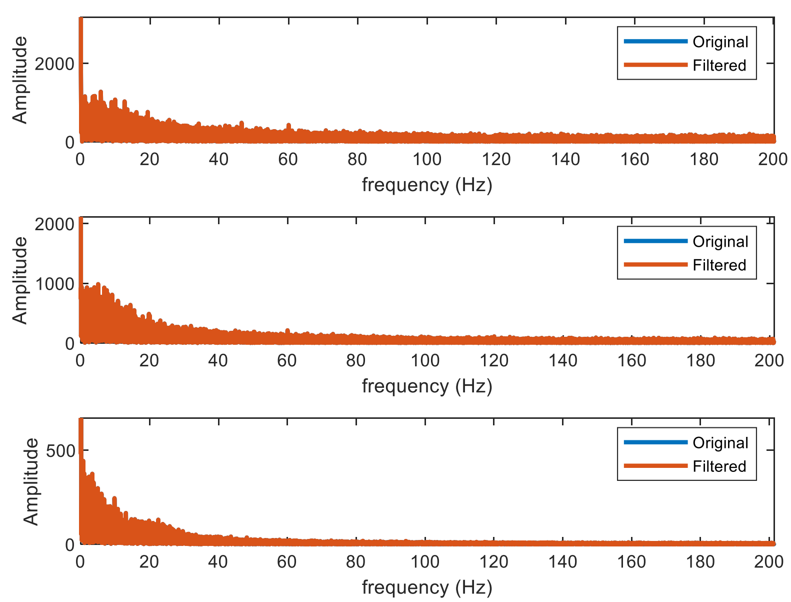

Figure B.80. Closer view to 200 Hz- FFT plots for both the original and filtered signal at upstream floor (sensor 2), upstream baffle face (sensor 3) and downstream baffle slope (sensor 4) at the discharge of 0.25 PMF- data set 4

The low-frequency peaks are 0.08979, 5.014, 0.01418 Hz at the upstream floor, upstream baffle face, and downstream baffle slope, respectively.

0.19 PMF

DATA SET1

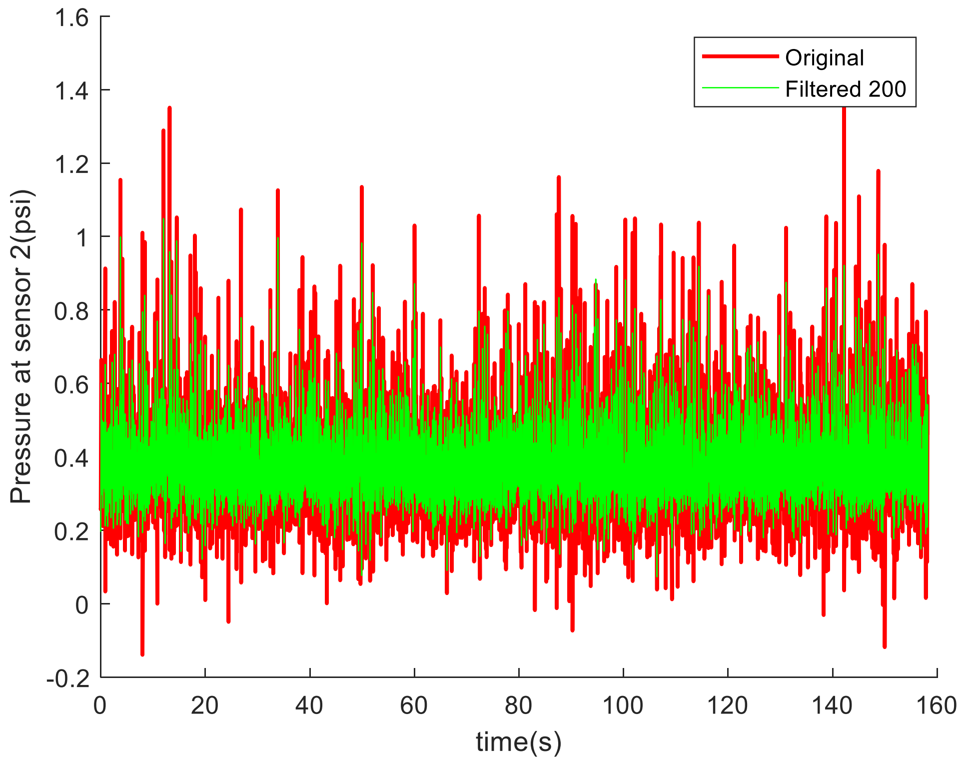

Figure B.81. Time versus pressure at sensor 2 (upstream floor) for the original and filtered signal at the discharge of 0.19 PMF- data set 1

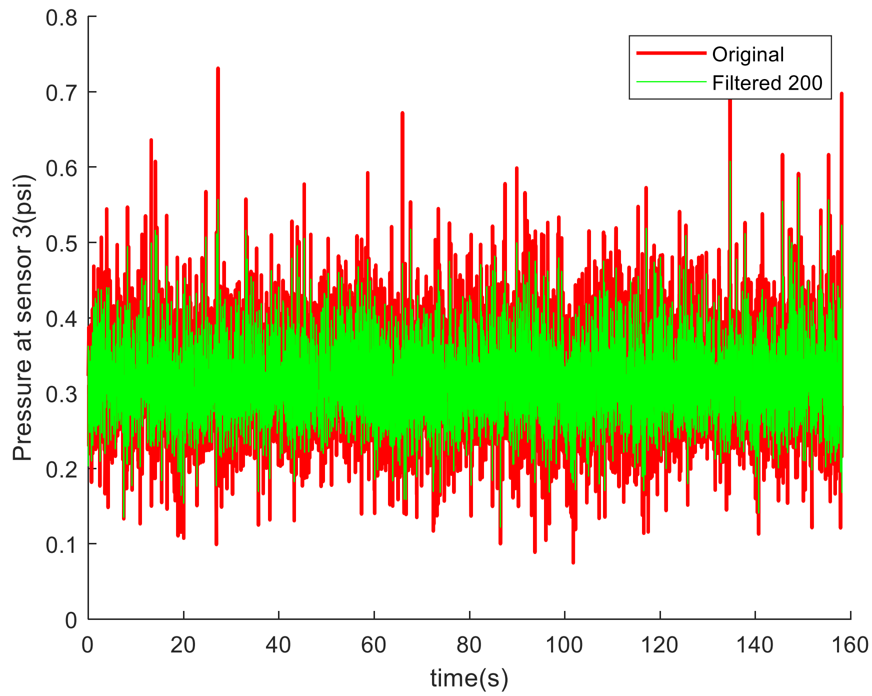

Figure B.82. Time versus pressure at sensor 3 (upstream baffle face) for the original and filtered signal at the discharge of 0.19 PMF- data set 1

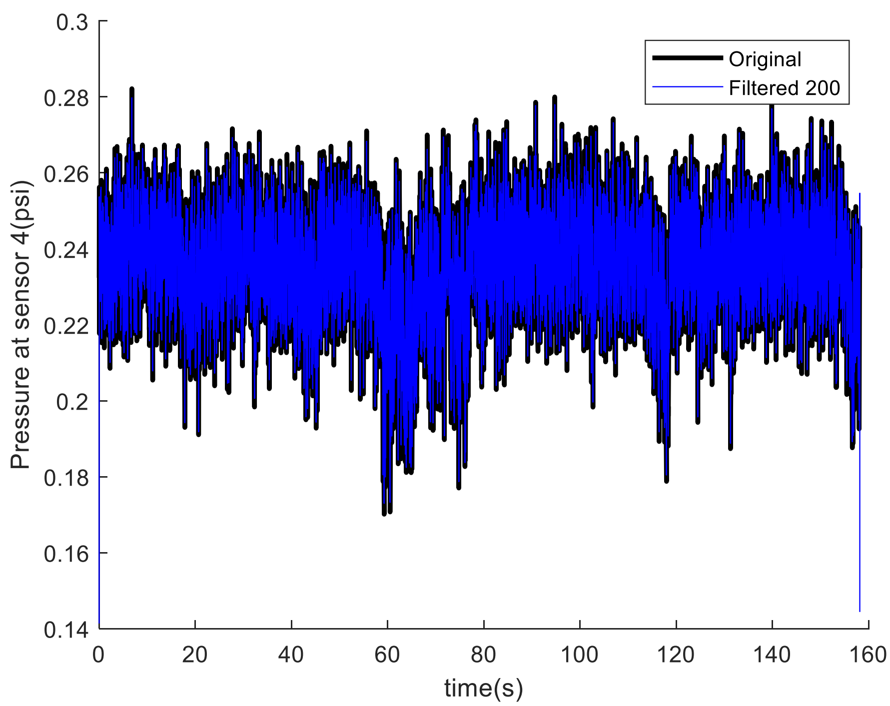

Figure B.83. Time versus pressure at sensor 4 (downstream baffle slope) for the original and filtered signal at the discharge of 0.19 PMF- data set 1

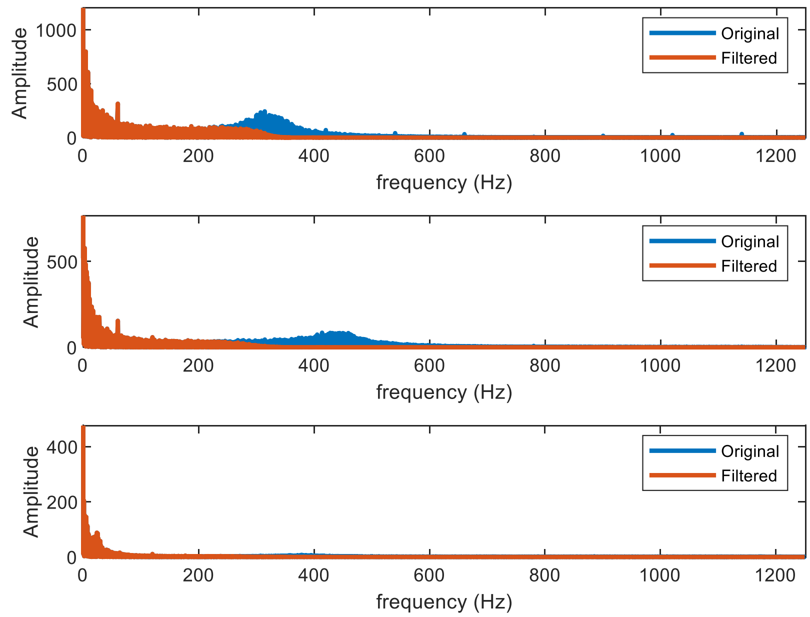

Figure B.84.FFT plots for both the original and filtered signal at upstream floor (sensor 2), upstream baffle face (sensor 3) and downstream baffle slope (sensor 4) at the discharge of 0.19 PMF- data set 1

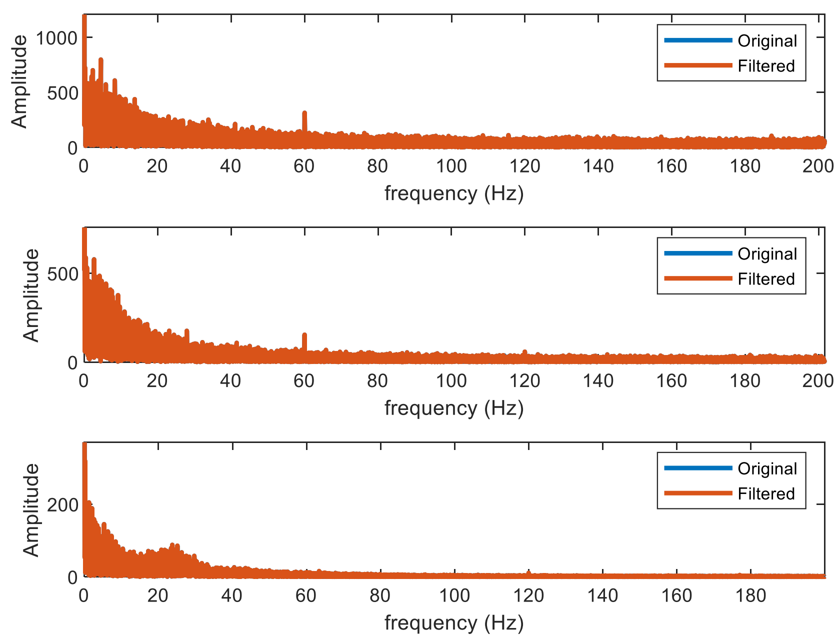

Figure B.85. Closer view to 200 Hz- FFT plots for both the original and filtered signal at upstream floor (sensor 2), upstream baffle face (sensor 3) and downstream baffle slope (sensor 4) at the discharge of 0.19 PMF- data set 1

The low-frequency peaks are 4.483, 0.05058, 0.01897 Hz at the upstream floor, upstream baffle face, and downstream baffle slope, respectively.

DATA SET2

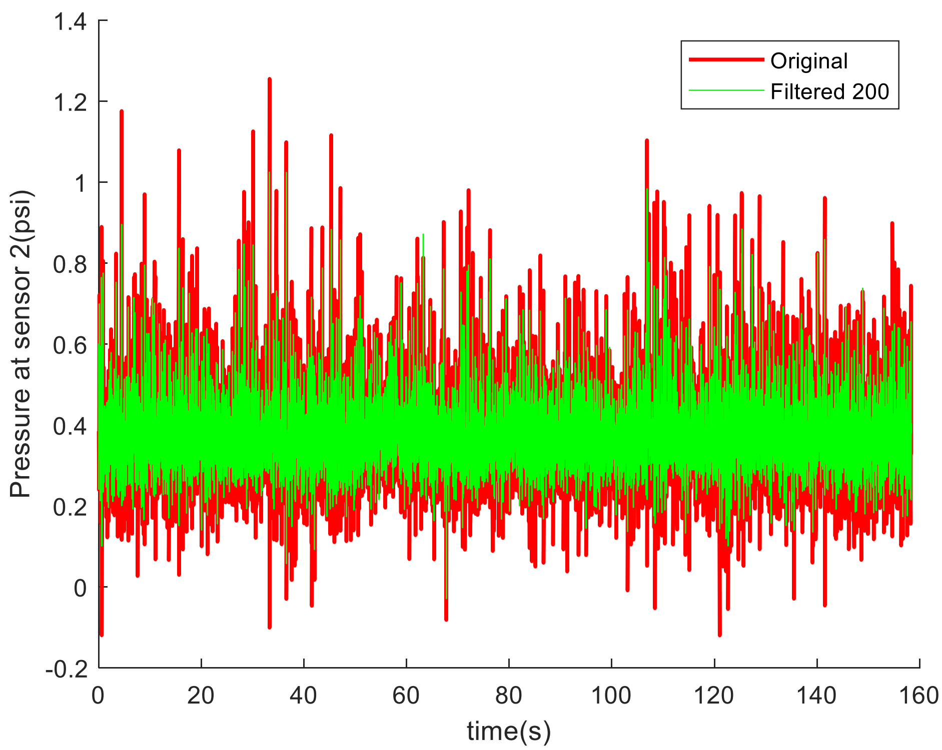

Figure B.86. Time versus pressure at sensor 2 (upstream floor) for the original and filtered signal at the discharge of 0.19 PMF- data set 2

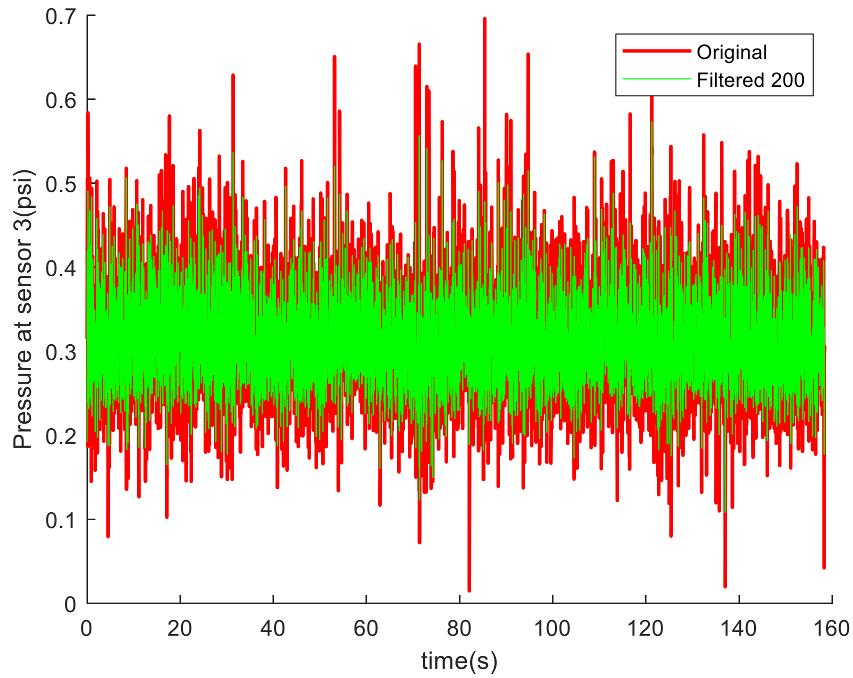

Figure B.87. Time versus pressure at sensor 3 (upstream baffle face) for the original and filtered signal at the discharge of 0.19 PMF- data set 2

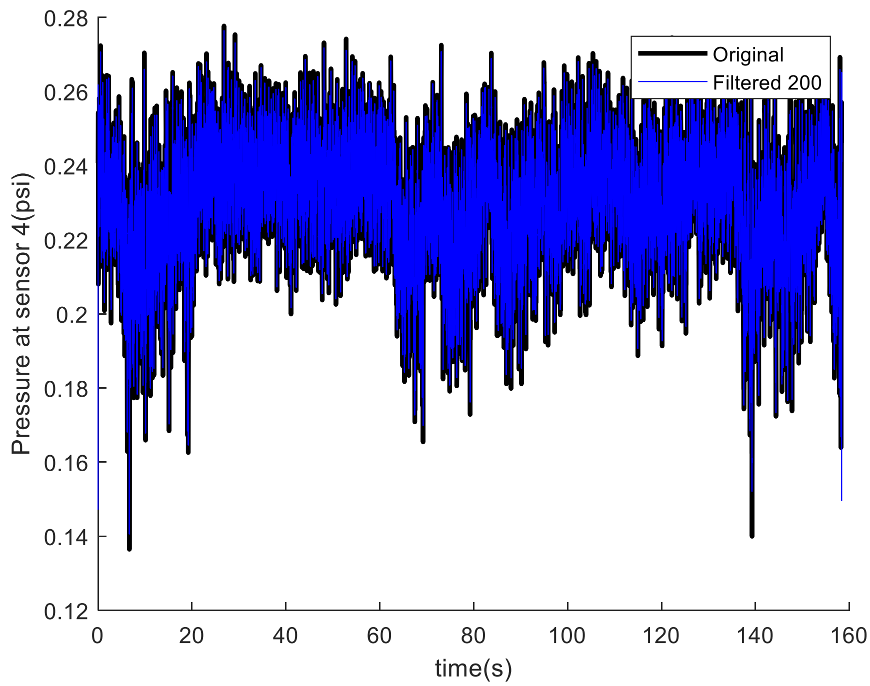

Figure B.88. Time versus pressure at sensor 4 (downstream baffle slope) for the original and filtered signal at the discharge of 0.19 PMF- data set 2

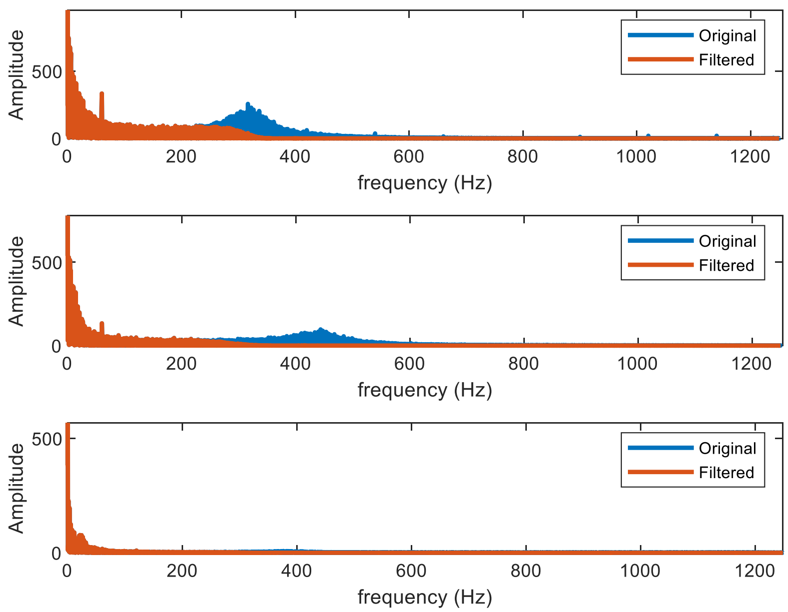

Figure B.89. FFT plots for both the original and filtered signal at upstream floor (sensor 2), upstream baffle face (sensor 3) and downstream baffle slope (sensor 4) at the discharge of 0.19 PMF- data set 2

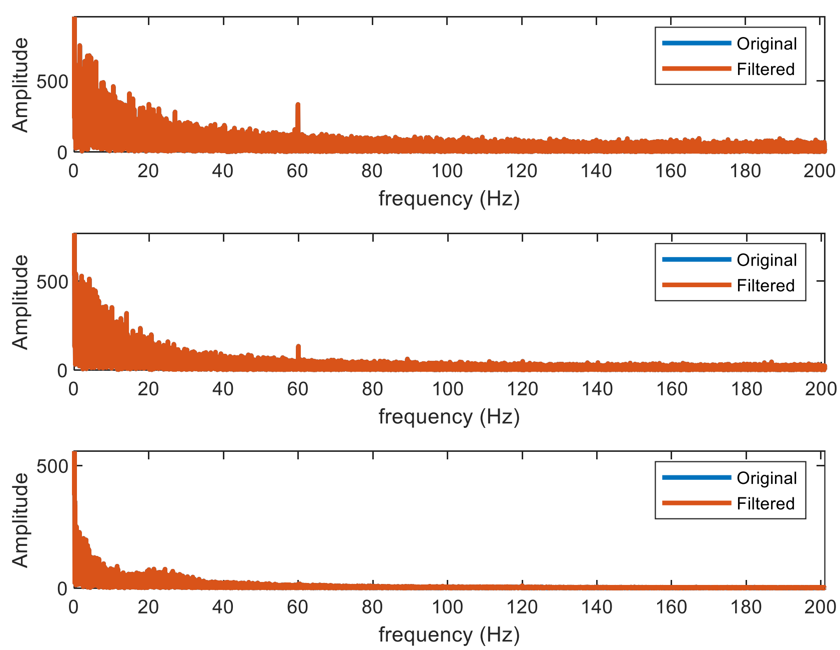

Figure B.90. Closer view to 200 Hz- FFT plots for both the original and filtered signal at upstream floor (sensor 2), upstream baffle face (sensor 3) and downstream baffle slope (sensor 4) at the discharge of 0.19 PMF- data set 2

The low-frequency peaks are 0.03789, 0.03789, 0.01263 Hz at the upstream floor, upstream baffle face, and downstream baffle slope, respectively.

DATA SET3

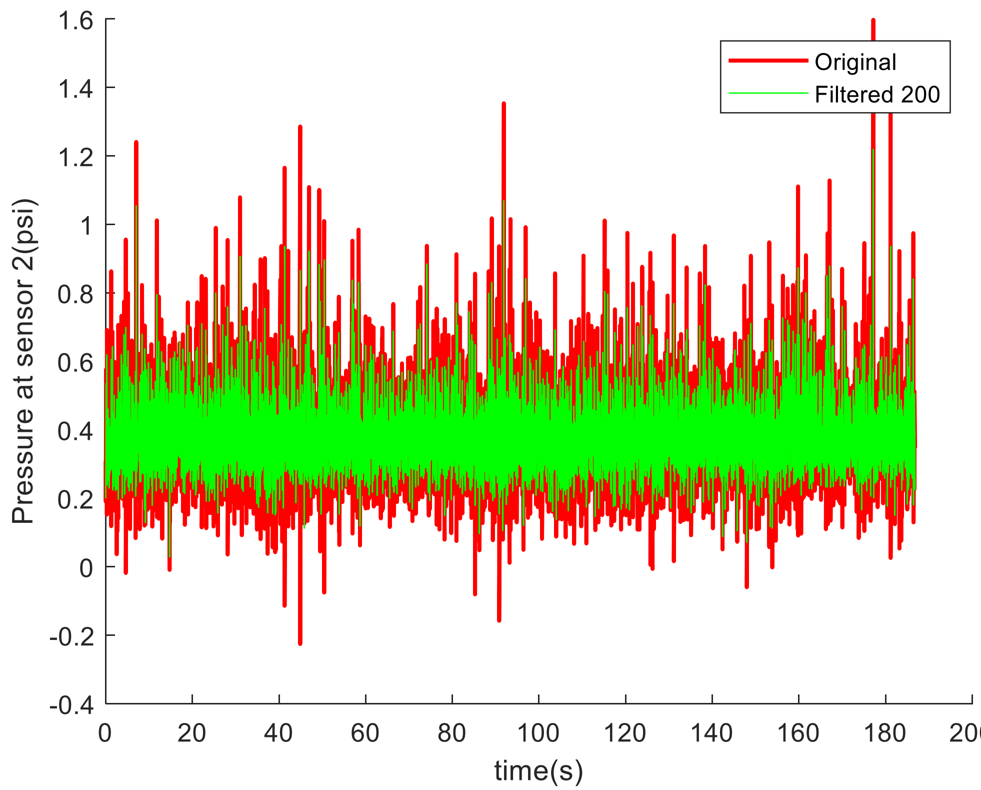

Figure B.91. Time versus pressure at sensor 2 (upstream floor) for the original and filtered signal at the discharge of 0.19 PMF- data set 3

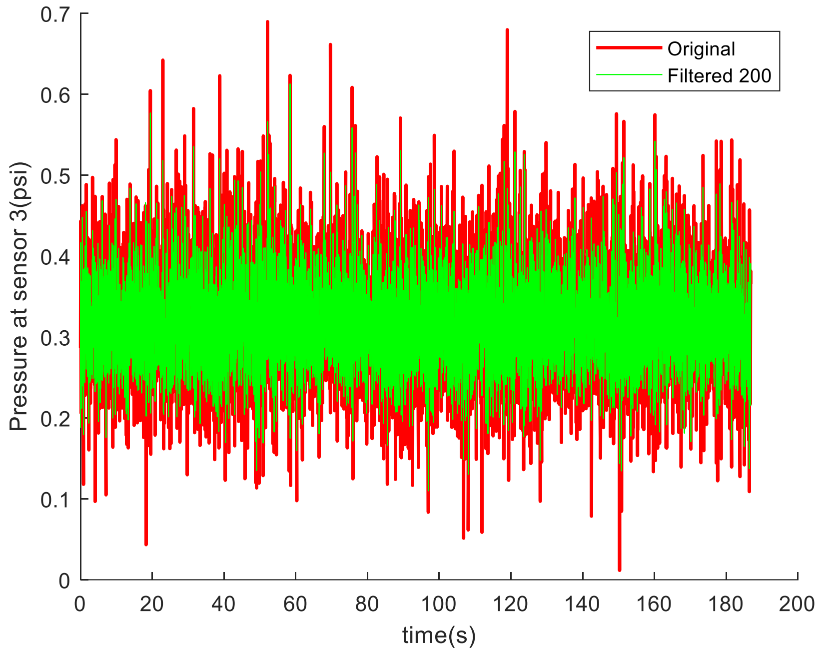

Figure B.92. Time versus pressure at sensor 3 (upstream baffle face) for the original and filtered signal at the discharge of 0.19 PMF- data set 3

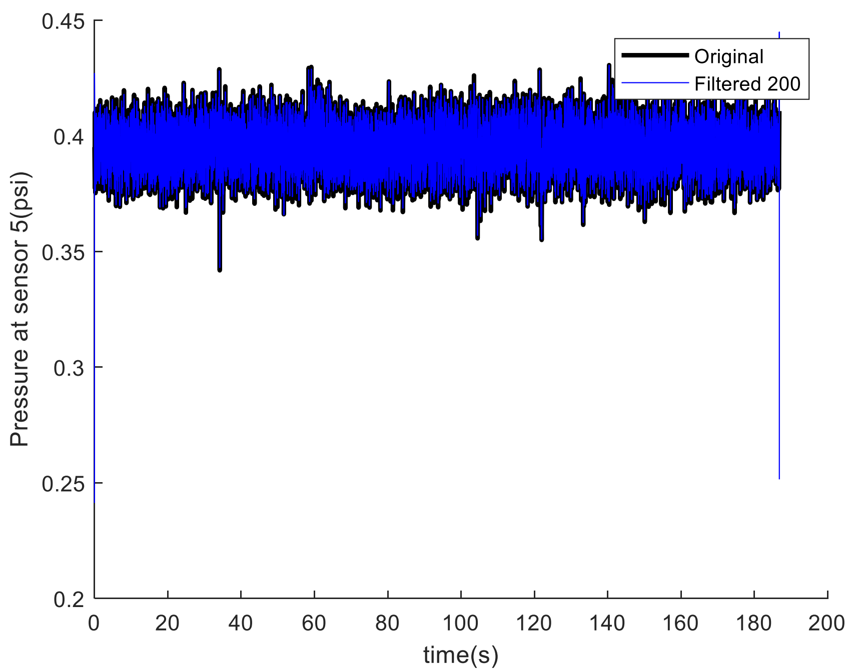

Figure B.93. Time versus pressure at sensor 5 (downstream floor) for the original and filtered signal at the discharge of 0.19 PMF- data set 3

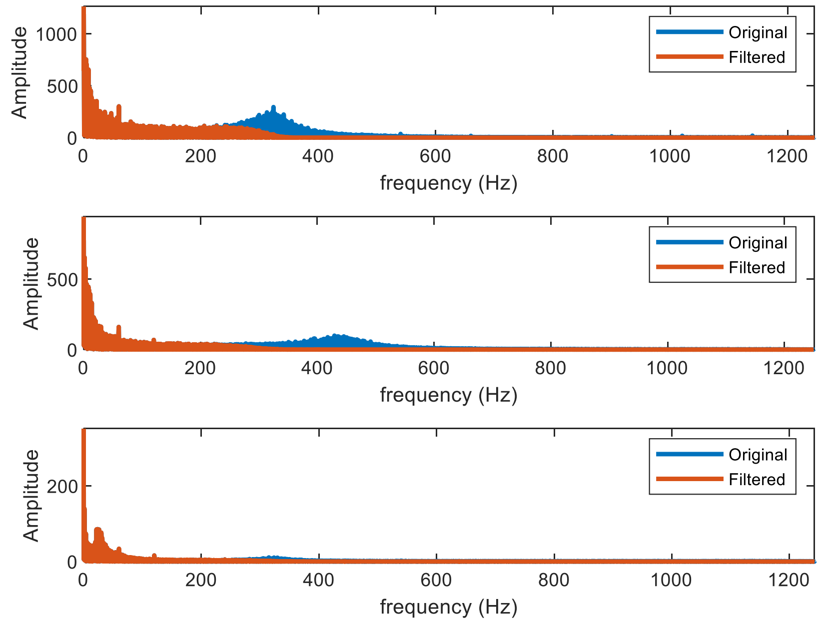

Figure B.94. FFT plots for both the original and filtered signal at upstream floor (sensor 2), upstream baffle face (sensor 3) and downstream floor (sensor 5) at the discharge of 0.19 PMF- data set 3

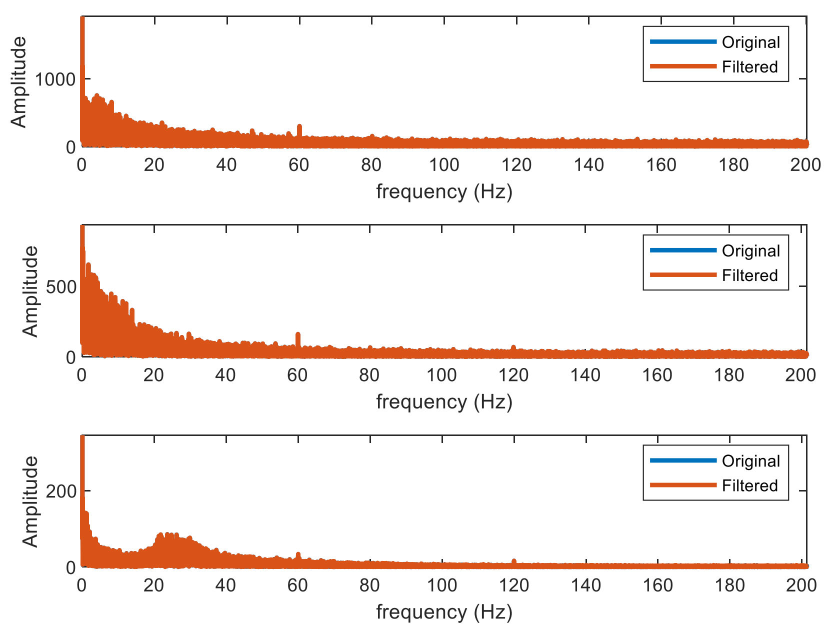

Figure B.95. Closer view to 200 Hz- FFT plots for both the original and filtered signal at upstream floor (sensor 2), upstream baffle face (sensor 3) and downstream floor (sensor 5) at the discharge of 0.19 PMF- data set 3

The low-frequency peaks are 0.02676, 0.02676, 0.01606 Hz at the upstream floor, upstream baffle face, and downstream floor, respectively.

DATA SET4

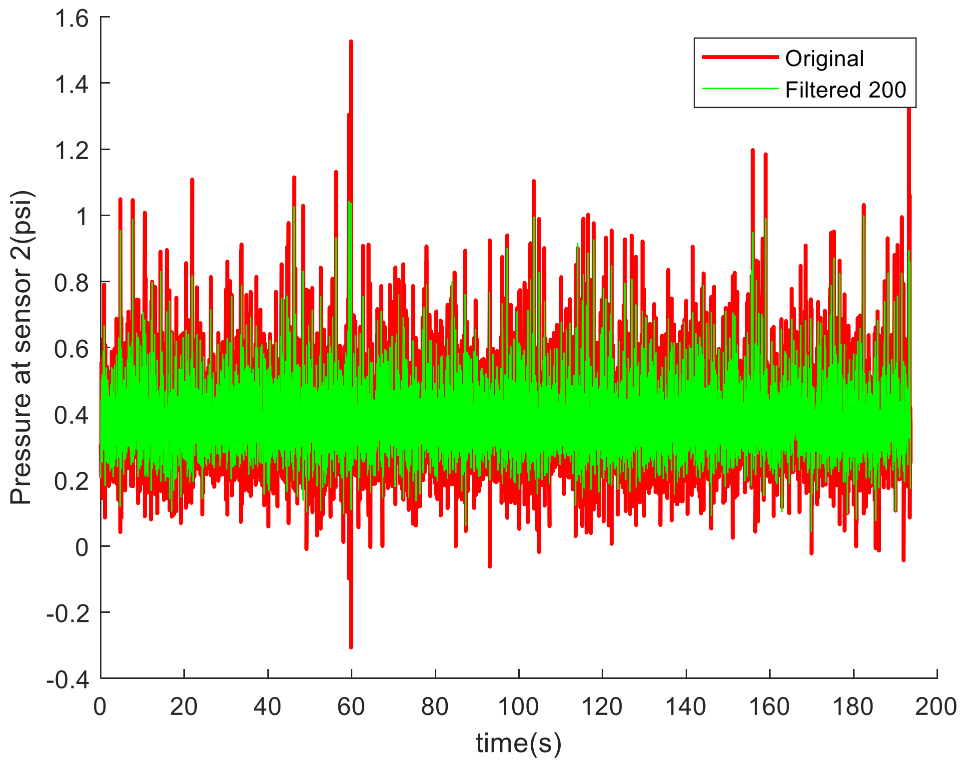

Figure B.96. Time versus pressure at sensor 2 (upstream floor) for the original and filtered signal at the discharge of 0.19 PMF- data set 4

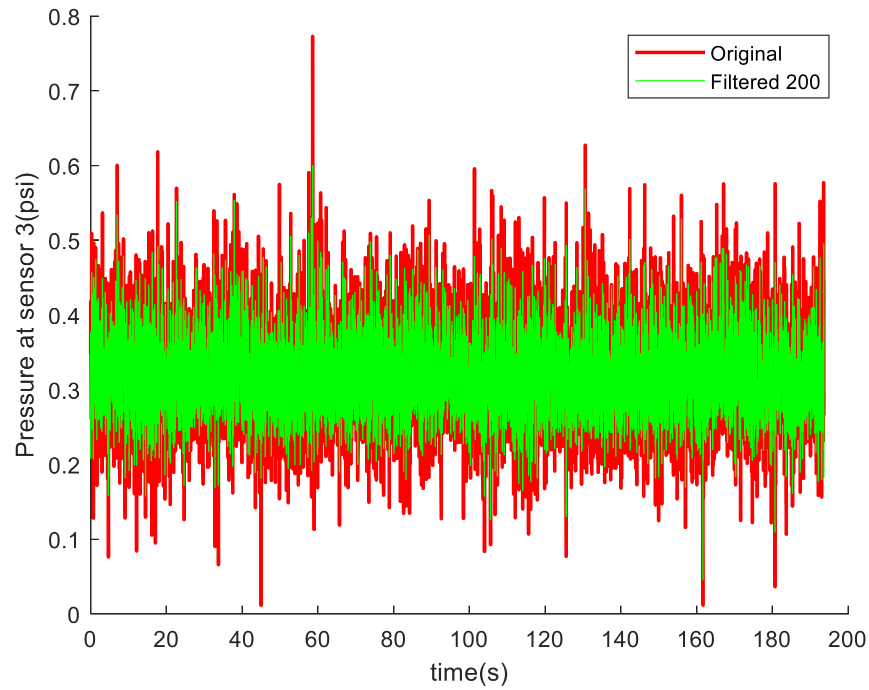

Figure B.97. Time versus pressure at sensor 3 (upstream baffle face) for the original and filtered signal at the discharge of 0.19 PMF- data set 4

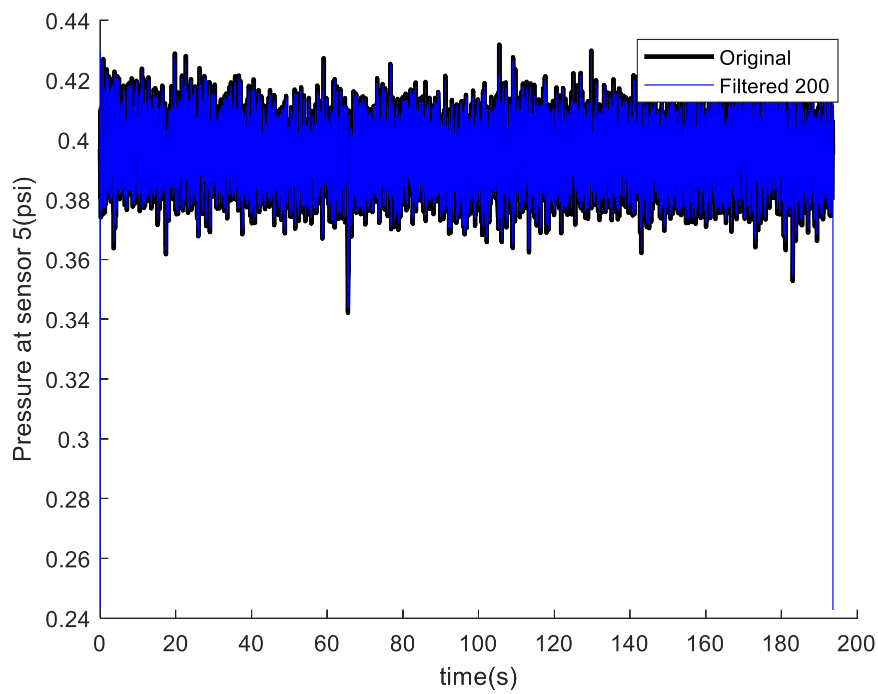

Figure B.98. Time versus pressure at sensor 5 (downstream floor) for the original and filtered signal at the discharge of 0.19 PMF- data set 4

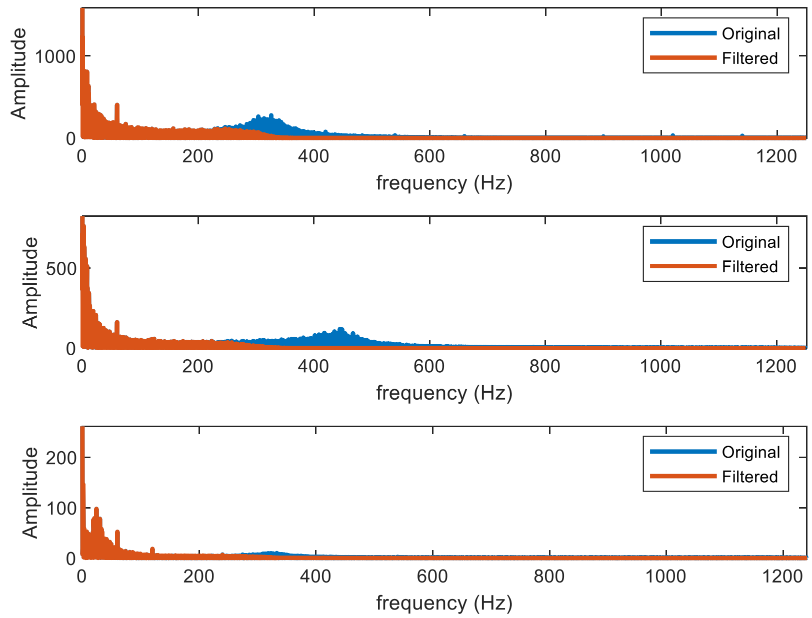

Figure B.99. FFT plots for both the original and filtered signal at upstream floor (sensor 2), upstream baffle face (sensor 3) and downstream floor (sensor 5) at the discharge of 0.19 PMF- data set 4

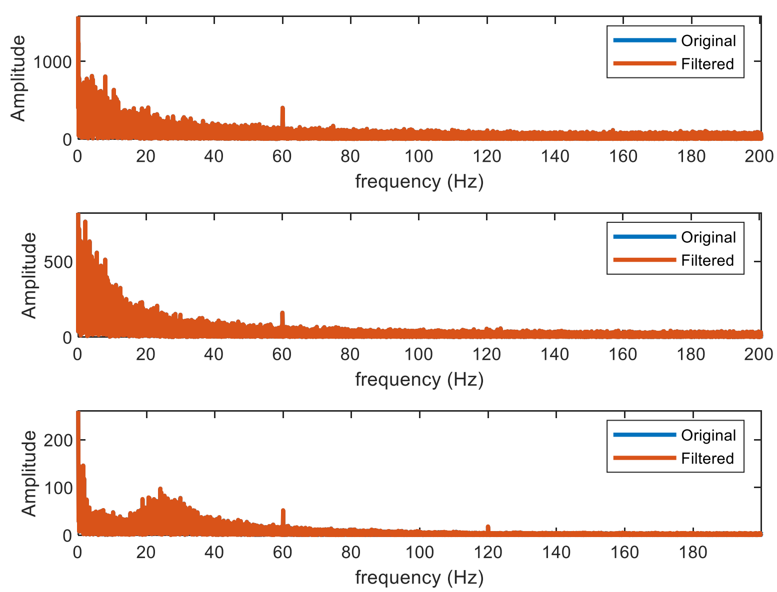

Figure B.100. Closer view to 200 Hz-FFT plots for both the original and filtered signal at upstream floor (sensor 2), upstream baffle face (sensor 3) and downstream floor (sensor 5) at the discharge of 0.19 PMF- data set 4

The low-frequency peaks are 0.08265, 2.082, 0.02066 Hz at the upstream floor, upstream baffle face, and downstream floor, respectively.

0.09 PMF

DATA SET1

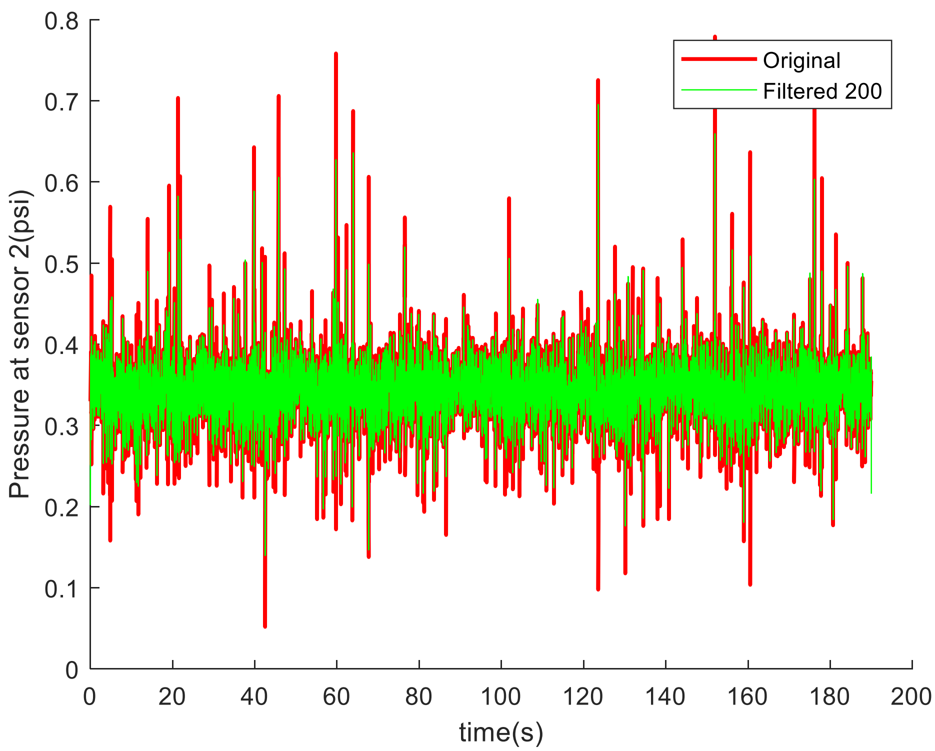

Figure B.101. Time versus pressure at sensor 2 (upstream floor) for the original and filtered signal at the discharge of 0.09 PMF- data set 1

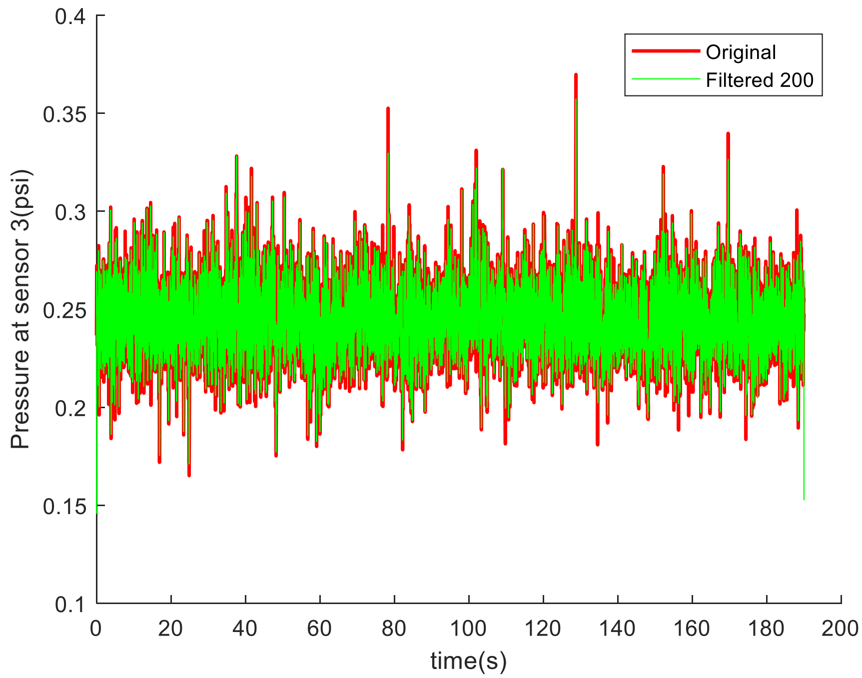

Figure B.102. Time versus pressure at sensor 3 (upstream baffle face) for the original and filtered signal at the discharge of 0.09 PMF- data set 1

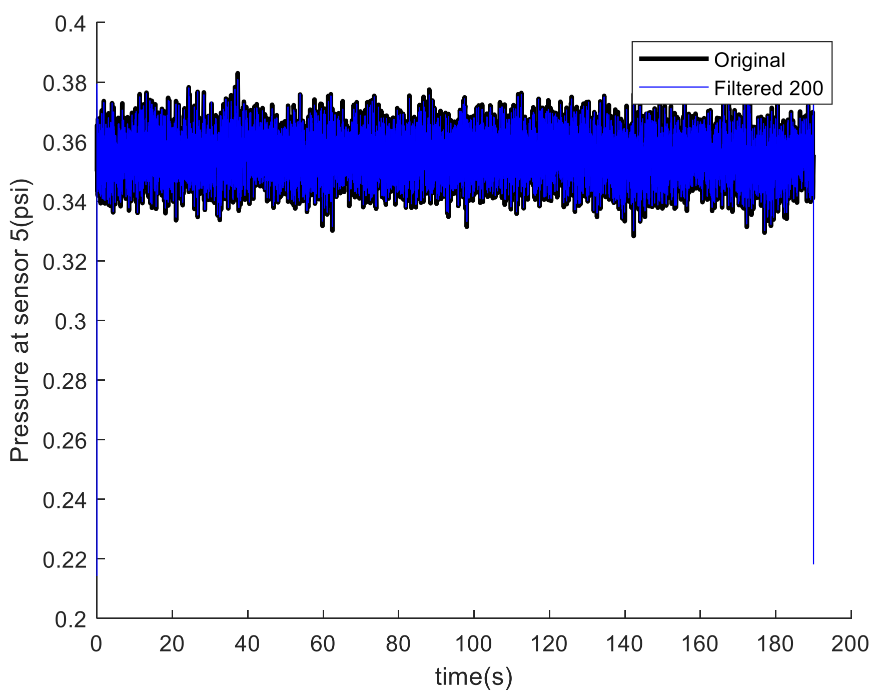

Figure B.103. Time versus pressure at sensor 5 (downstream floor) for the original and filtered signal at the discharge of 0.09 PMF- data set 1

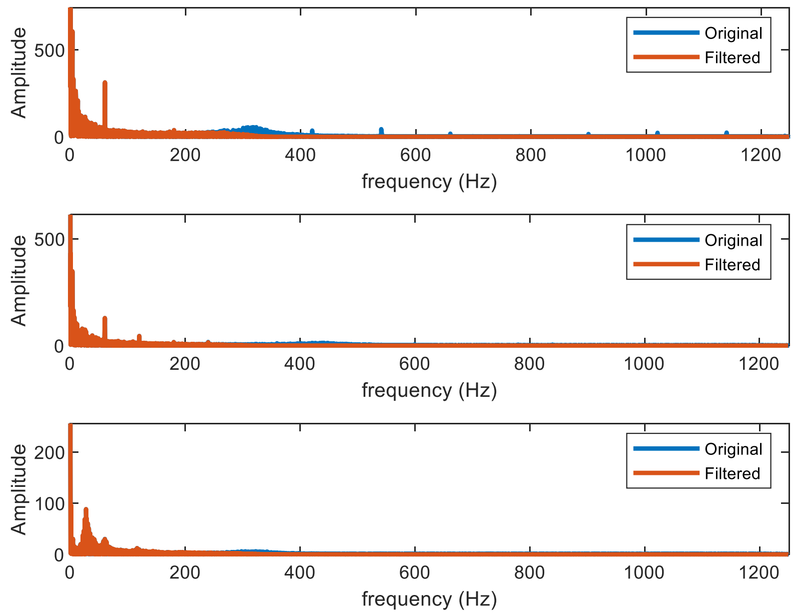

Figure B.104. FFT plots for both the original and filtered signal at upstream floor (sensor 2), upstream baffle face (sensor 3) and downstream floor (sensor 5) at the discharge of 0.09 PMF- data set 1

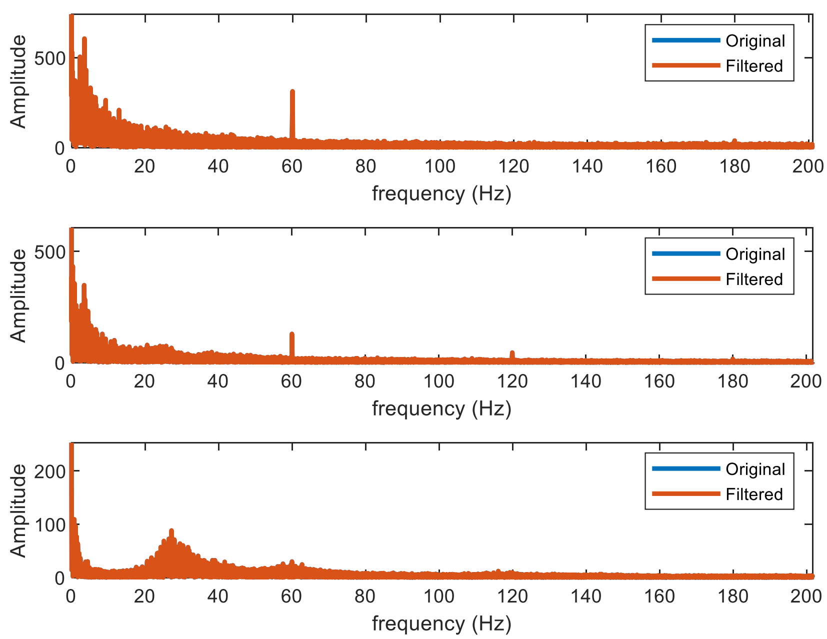

Figure B.105. Closer view to 200 Hz- FFT plots for both the original and filtered signal at upstream floor (sensor 2), upstream baffle face (sensor 3) and downstream floor (sensor 5) at the discharge of 0.09 PMF- data set 1

The low-frequency peaks are 0.04211, 0.3526, 0.02632 Hz at the upstream floor, upstream baffle face, and downstream floor, respectively.

DATA SET2

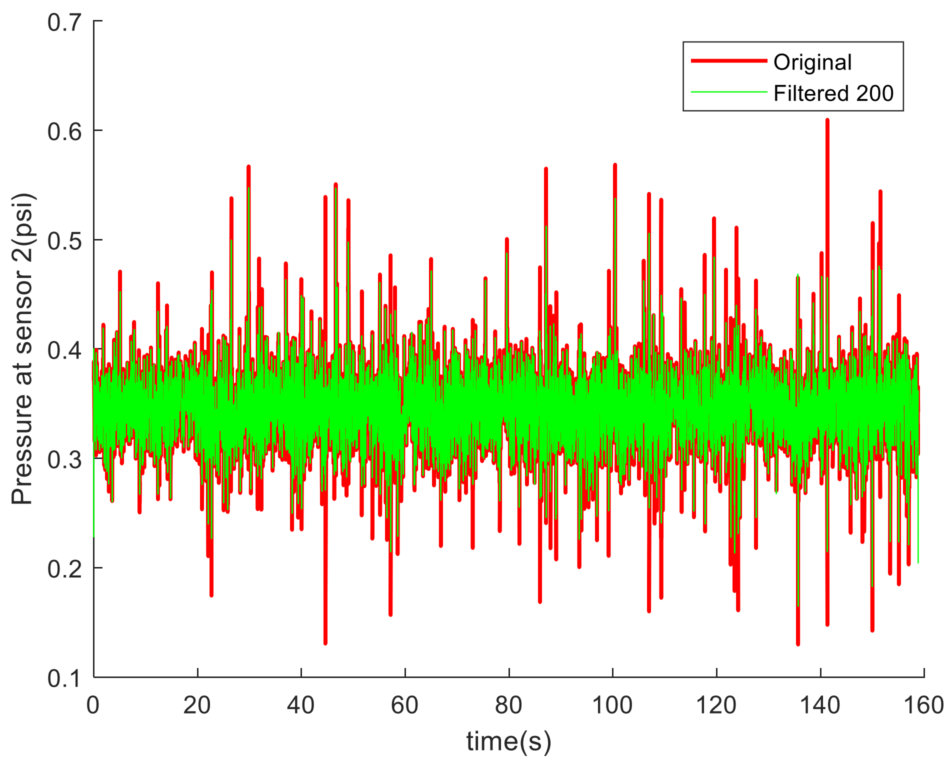

Figure B.106. Time versus pressure at sensor 2 (upstream floor) for the original and filtered signal at the discharge of 0.09 PMF- data set 2

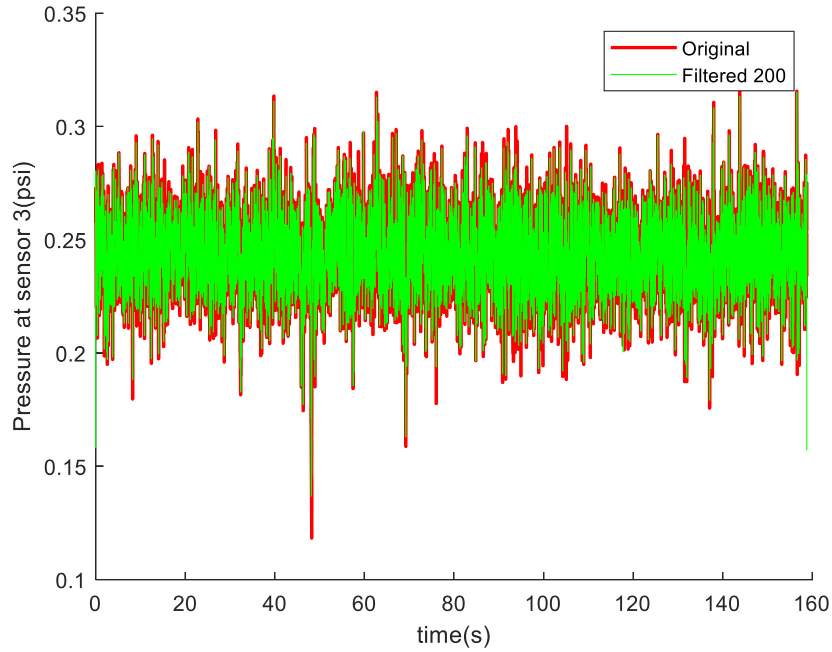

Figure B.107. Time versus pressure at sensor 3 (upstream baffle face) for the original and filtered signal at the discharge of 0.09 PMF- data set 2

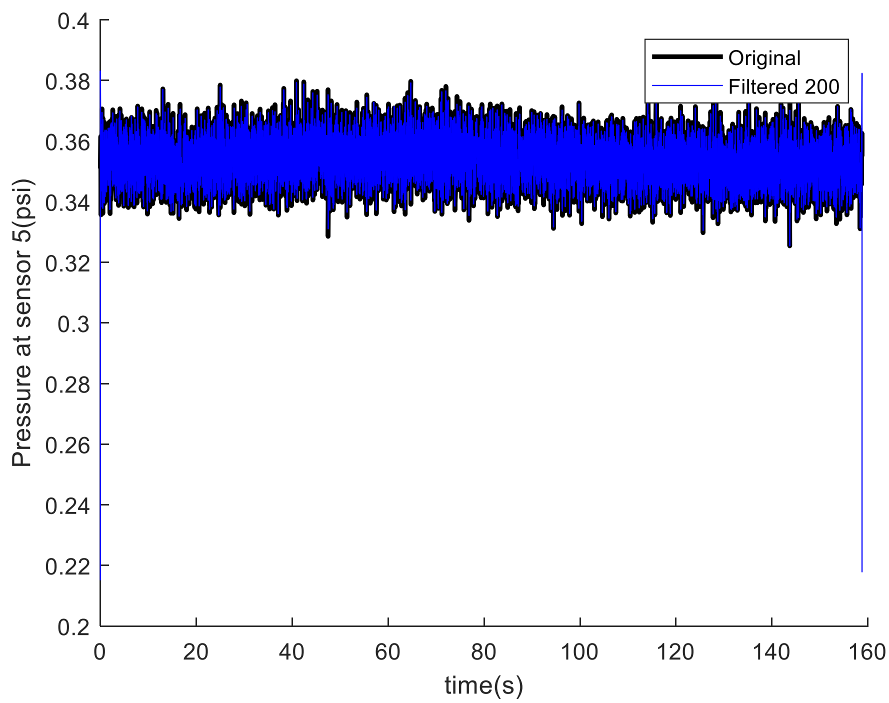

Figure B.108. Time versus pressure at sensor 5 (downstream floor) for the original and filtered signal at the discharge of 0.09 PMF- data set 2

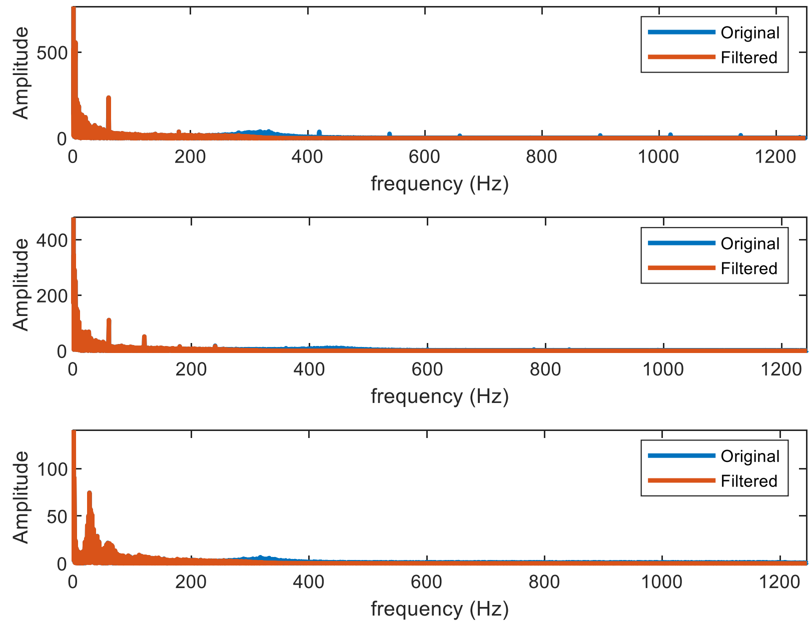

Figure B.109. FFT plots for both the original and filtered signal at upstream floor (sensor 2), upstream baffle face (sensor 3) and downstream floor (sensor 5) at the discharge of 0.09 PMF- data set 2

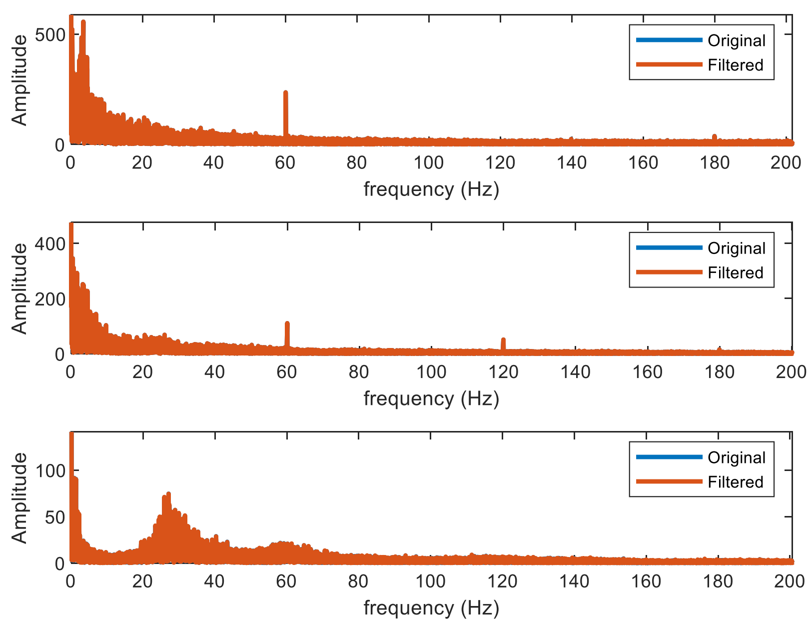

Figure B.110. Closer view to 200 Hz- FFT plots for both the original and filtered signal at upstream floor (sensor 2), upstream baffle face (sensor 3) and downstream floor (sensor 5) at the discharge of 0.09 PMF- data set 2

The low-frequency peaks are 3.394, 0.4282, 0.8565 Hz at the upstream floor, upstream baffle face, and downstream floor, respectively.

DATA SET3

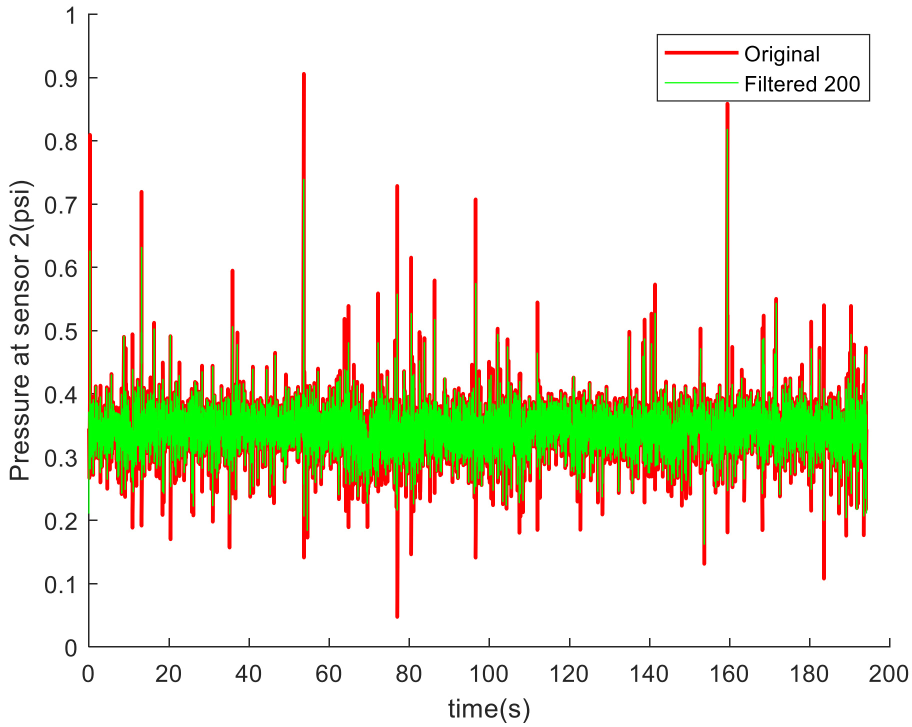

Figure B.111. Time versus pressure at sensor 2 (upstream floor) for the original and filtered signal at the discharge of 0.09 PMF- data set 3

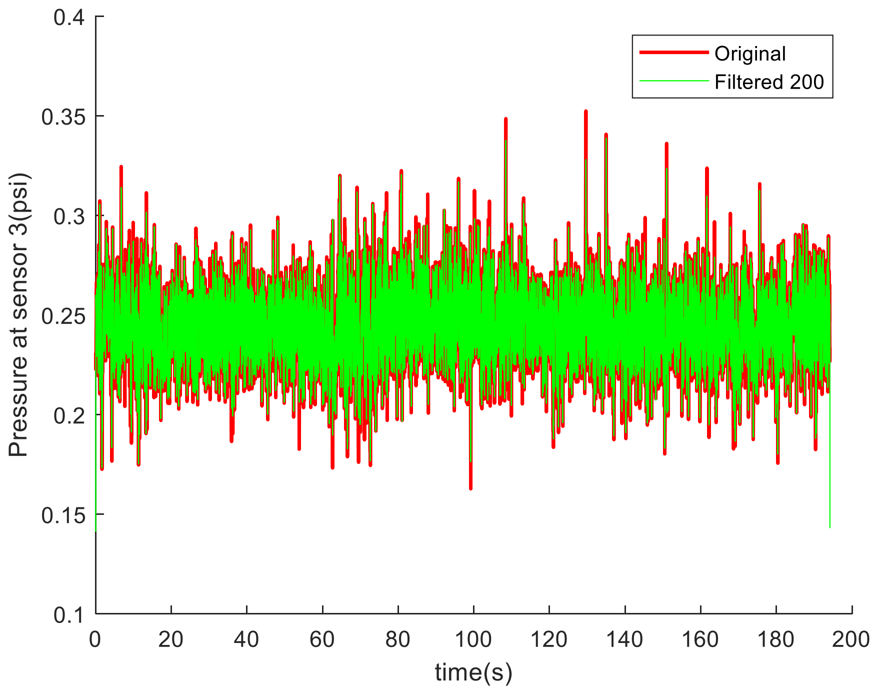

Figure B.112. Time versus pressure at sensor 3 (upstream baffle face) for the original and filtered signal at the discharge of 0.09 PMF- data set 3

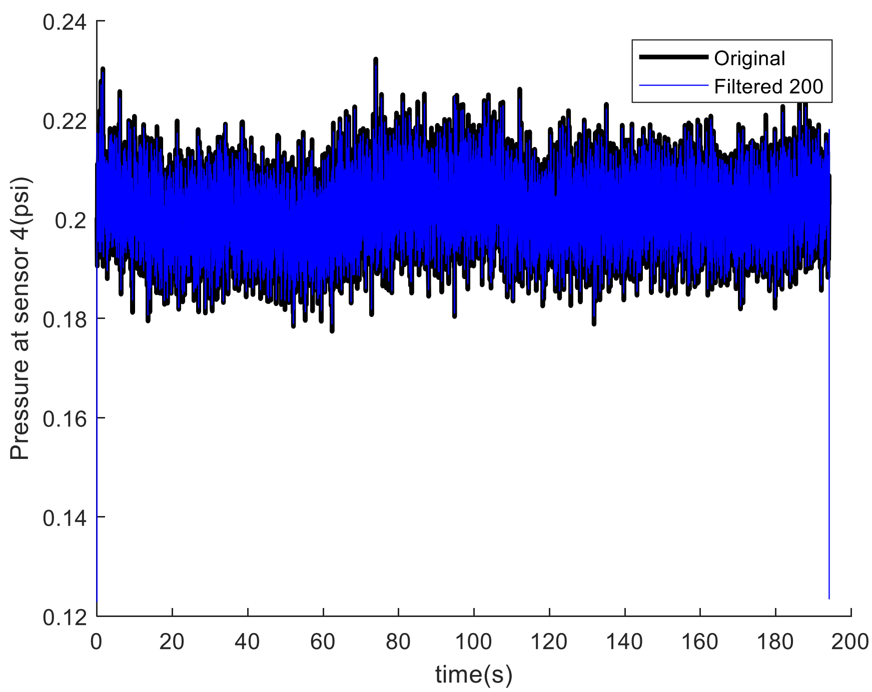

Figure B.113. Time versus pressure at sensor 4 (downstream baffle slope) for the original and filtered signal at the discharge of 0.09 PMF- data set 3

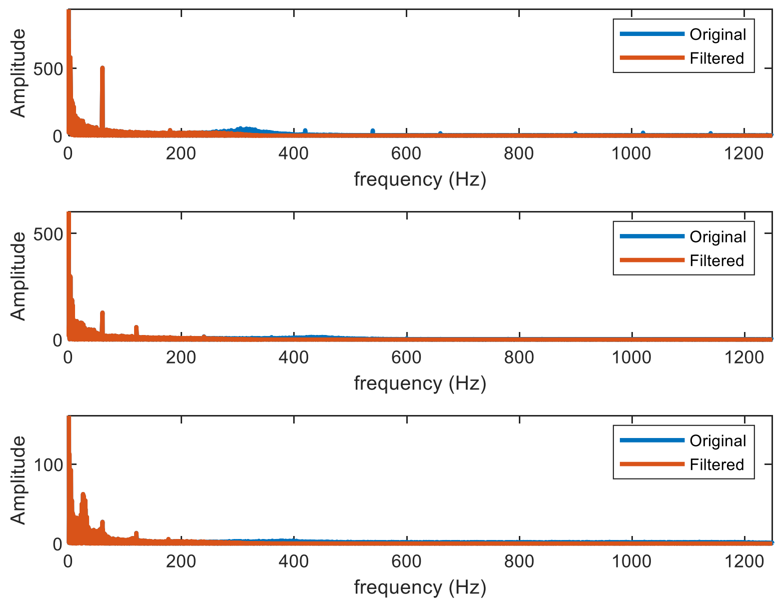

Figure B.114. FFT plots for both the original and filtered signal at upstream floor (sensor 2), upstream baffle face (sensor 3) and downstream baffle slope (sensor 4) at the discharge of 0.09 PMF for data set 3

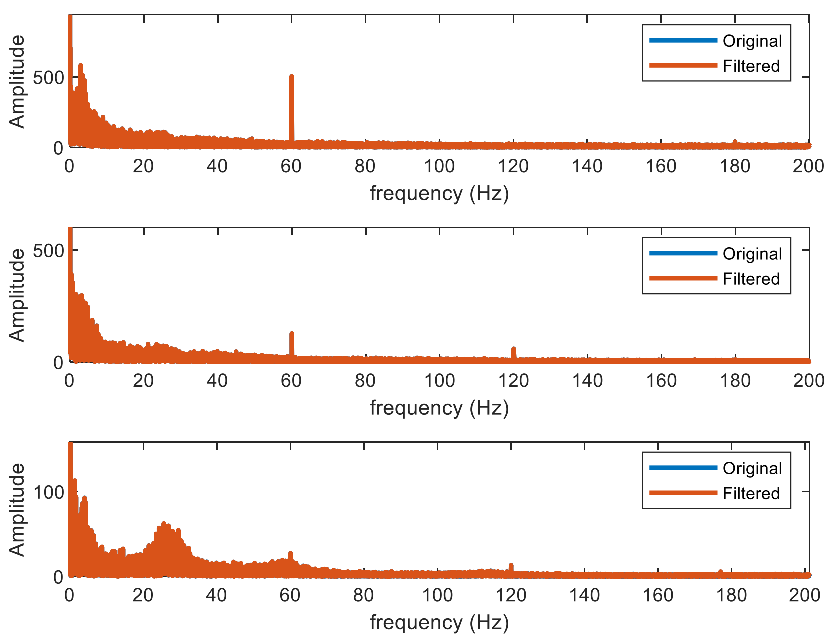

Figure B.115. Closer view to 200 Hz- FFT plots for both the original and filtered signal at upstream floor (sensor 2), upstream baffle face (sensor 3) and downstream baffle slope (sensor 4) at the discharge of 0.09 PMF for data set 3

The low-frequency peaks are 0.01545, 0.0103, 0.0309 Hz at the upstream floor, upstream baffle face, and downstream baffle slope, respectively.

DATA SET4

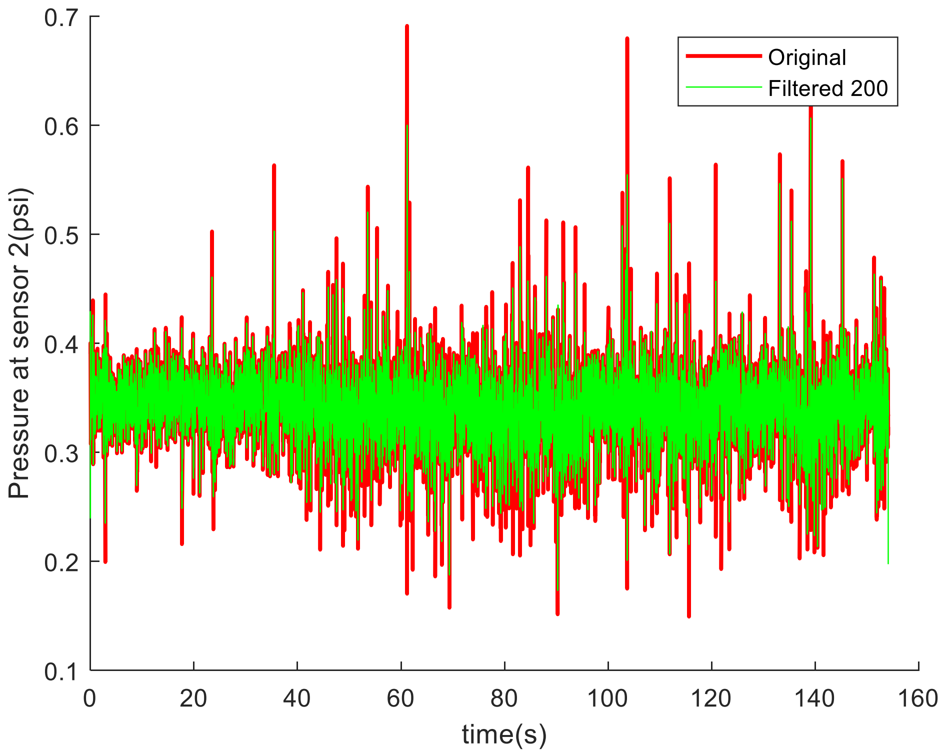

Figure B.116. Time versus pressure at sensor 2 (upstream floor) for the original and filtered signal at the discharge of 0.09 PMF- data set 4

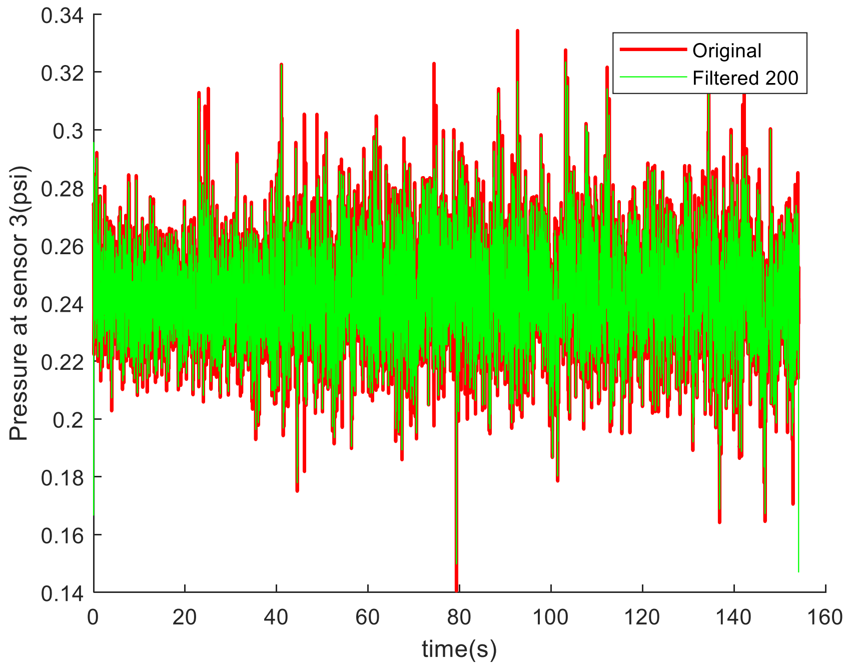

Figure B.117. Time versus pressure at sensor 3 (upstream baffle face) for the original and filtered signal at the discharge of 0.09 PMF- data set 4

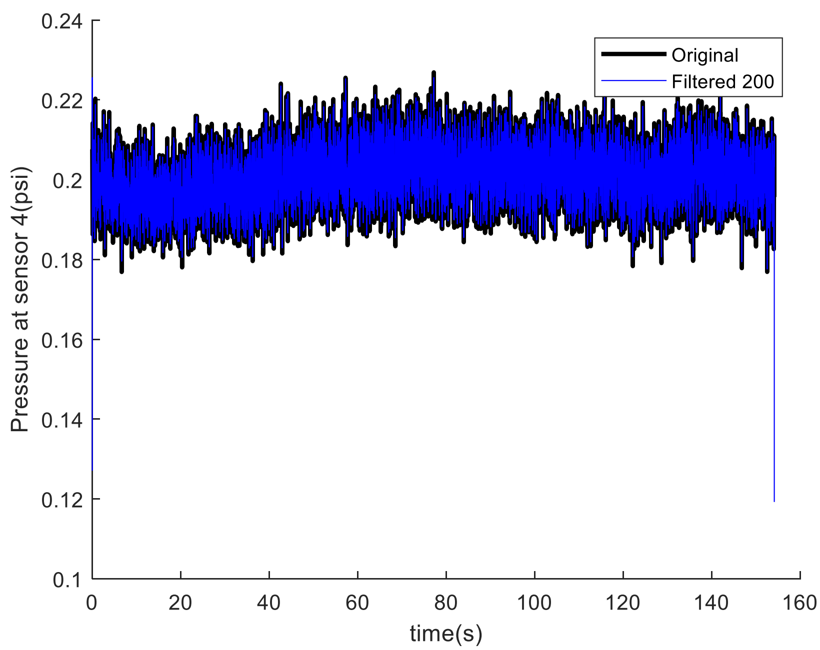

Figure B.118. Time versus pressure at sensor 4 (downstream baffle slope) for the original and filtered signal at the discharge of 0.09 PMF- data set 4

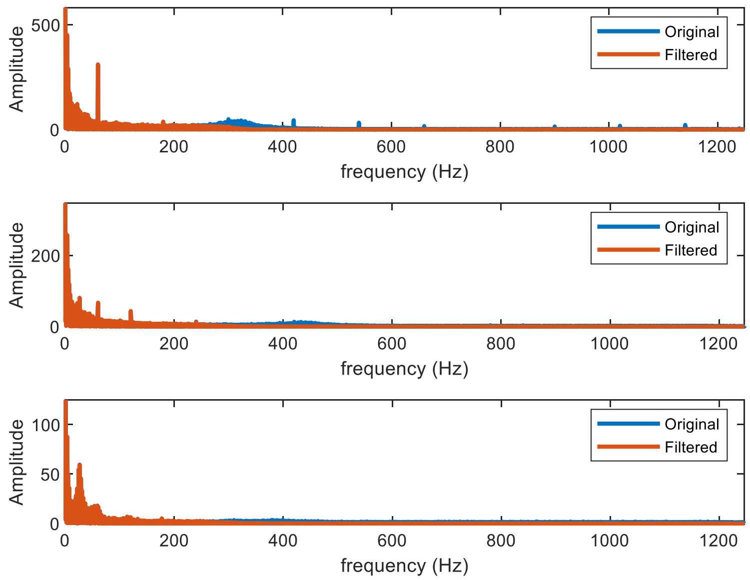

Figure B.119. FFT plots for both the original and filtered signal at upstream floor (sensor 2), upstream baffle face (sensor 3) and downstream baffle slope (sensor 4) at the discharge of 0.09 PMF- data set 4

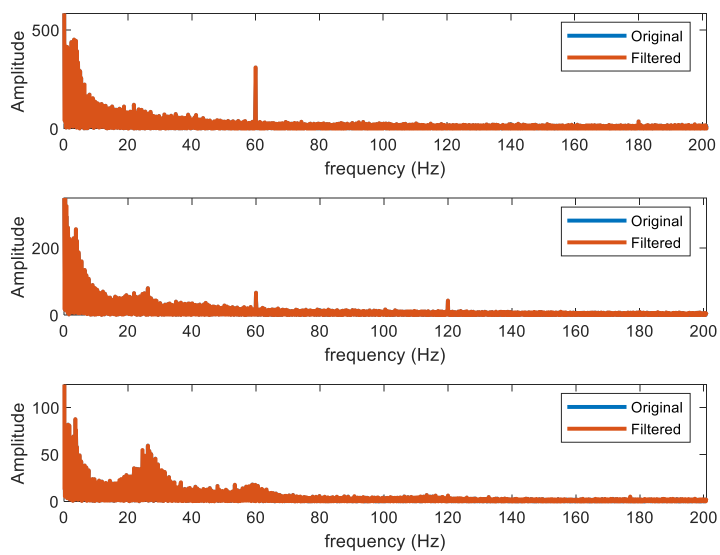

Figure B.120. Closer view to 200 Hz- FFT plots for both the original and filtered signal at upstream floor (sensor 2), upstream baffle face (sensor 3) and downstream baffle slope (sensor 4) at the discharge of 0.09 PMF- data set 4

The low-frequency peaks are 0.04542, 0.1363, 0.04542 Hz at the upstream floor, upstream baffle face, and downstream baffle slope, respectively.

APPENDIX C: MATLAB SCRIPT

```
%Low Pass Filter
clc
clear all
%% test signal
D = xlsread('1 PMF-DATA SET 1-psi2');
D1 = xlsread('1 PMF-DATA SET 1-psi3');
D2 = xlsread('1PMF-DATA SET 1-psi4');
%%
z = D(:,1); % psi2 is in kPa
x = D1(:,1); % psi3 is in kPa
y = D2(:,1); % psi4 is in kPa
%noise
n=0.2*randn(size(z));
% Signal + Noise
z_new=z+n;
t = D(:,2); % time is in seconds
Fs=2500; % sampling rate in Hz
Ts=1/Fs;
figure;
plot(t,z,'b'); %time domain original signal
hold on
plot(t, z_new,'r'); % plot time domain noised signal
xlabel('time (s)')
legend('Original Signal-psi2 (kPa)','Noised Signal-psi2 (kPa)')
ylabel('Signal')
box off; grid on;
%noise
n=0.2*randn(size(x));
% Signal + Noise
x_new=x+n;
t = D1(:,2); % time is in seconds
Fs=2500; % sampling rate in Hz
Ts=1/Fs;
figure;
plot(t,x,'b'); %time domain original signal
hold on
plot(t, x_new,'r'); % plot time domain noised signal
xlabel('time (s)')
legend('Original Signal-psi3(kPa)','Noised Signal-psi3 (kPa)')
ylabel('Signal')
box off; grid on;
%noise
n=0.2*randn(size(y));
% Signal + Noise
y_new=y+n;
t = D2(:,2); % time is in seconds
Fs=2500; % sampling rate in Hz
Ts=1/Fs;
figure;
plot(t,y,'b'); %time domain original signal
hold on
plot(t, y_new,'r'); % plot time domain noised signal
xlabel('time (s)')
```

```matlab
legend('Original Signal-psi4(kPa)','Noised Signal-psi4 (kPa)')
ylabel('Signal')
box off; grid on;
%%program to calculate the fourier spectrum of a signal
%plots mag. vs freq(Hz)
dt = 0.0004;
[A,f]=FAS(z,dt);
[A2,f2]=FAS(x,dt);
[A3,f3]=FAS(y,dt);
[A_new,f]=FAS(z_new,dt);
hold on
%plot(f,A_new,'r','lineWidth',2)
figure;
subplot(3,1,1)
plot(f,A,'b','lineWidth',2)
xlabel('frequency (Hz)')
ylabel('Amplitude')
[A2_new,f2]=FAS(x_new,dt);
hold on
%plot(f2,A2_new,'r','lineWidth',2)
subplot(3,1,2)
plot(f2,A2,'r','lineWidth',2)
xlabel('frequency (Hz)')
ylabel('Amplitude')
[A3_new,f3]=FAS(y_new,dt);
hold on
%plot(f3,A3_new,'r','lineWidth',2)
subplot(3,1,3)
plot(f3,A3,'m','lineWidth',2)
xlabel('frequency (Hz)')
ylabel('Amplitude')
%%
figure;
%plot(t,z_new,'r'); %time domain noisy signal
hold on
plot(t,z,'r','linewidth',1.5); %time domain original signal
%z_filted_1 = lowpass(z,0.1,Fs);
%plot(t,z_filted_1,'m'); %time domain filtered signal
z_filted_2 = lowpass(z,200,Fs);
plot(t,z_filted_2,'g'); %time domain filtered signal
%z_filted_3 = lowpass(z,400,Fs);
%plot(t,z_filted_3,'k'); %time domain filtered signal
xlabel('time(s)')
ylabel('Pressure at sensor 2(kPa)')
legend('Original','Filtered 200')
%legend('Original','Filtered 0.1','Filtered 200','Filtered 400')
%%
figure;
%plot(t,x_new,'r'); %time domain noisy signal
hold on
plot(t,x,'r','linewidth',1.5); %time domain original signal
%x_filted_1 = lowpass(x,0.1,Fs);
%plot(t,x_filted_1,'m'); %time domain filtered signal
x_filted_2 = lowpass(x,200,Fs);
plot(t,x_filted_2,'g'); %time domain filtered signal
%x_filted_3 = lowpass(x,400,Fs);
%plot(t,x_filted_3,'k'); %time domain filtered signal
```

```
xlabel('time(s)')
ylabel('Pressure at sensor 3(kPa)')
legend('Original','Filtered 200')
%legend('Original','Filtered 0.1','Filtered 200','Filtered 400')
%%
figure;
%plot(t,y_new,'r'); %time domain noisy signal
hold on
plot(t,y,'k','linewidth',2); %%time domain original signal
%y_filted_1 = lowpass(y,0.1,Fs);
%plot(t,y_filted_1,'r'); %time domain filtered signal
y_filted_2 = lowpass(y,200,Fs);
plot(t,y_filted_2,'b'); %time domain filtered signal
%y_filted_3 = lowpass(y,400,Fs);
%plot(t,y_filted_3,'b'); %time domain filtered signal
xlabel('time(s)')
ylabel('Pressure at sensor 4(kPa)')
legend('Original','Filtered 200')
%legend('Original','Filtered 0.1','Filtered 200', ''Filtered 400')
%%
dt = 0.0004;
[A_filt,f]=FAS(z_filted_2,dt);
[A2_filt,f2]=FAS(x_filted_2,dt);
[A3_filt,f3]=FAS(y_filted_2,dt);
%[A_new,f]=FAS(z_new,dt);
hold on
%plot(f,A_new,'r','lineWidth',2)
figure;
subplot(3,1,1)
%plot(f,A_filt,'b','lineWidth',2)
plot(f,A,f,A_filt,'lineWidth',2)
xlabel('frequency (Hz)')
ylabel('Amplitude')
legend('Original','Filtered')
%[A2_new,f2]=FAS(x_new,dt);
hold on
%plot(f2,A2_new,'r','lineWidth',2)
subplot(3,1,2)
%plot(f2,A2_filt,'r','lineWidth',2)
plot(f2,A2,f2,A2_filt,'lineWidth',2)
xlabel('frequency (Hz)')
ylabel('Amplitude')
legend('Original','Filtered')
%[A3_new,f3]=FAS(y_new,dt);
hold on
%plot(f3,A3_new,'r','lineWidth',2)
subplot(3,1,3)
%plot(f3,A3_filt,'m','lineWidth',2)
plot(f3,A3,f3,A3_filt,'lineWidth',2)
xlabel('frequency (Hz)')
ylabel('Amplitude')
legend('Original','Filtered')
```

FAS is a function of taking Fourier transform. dt is the time step. It also represents the time domain and converts to frequency domain, df. Low pass filter keeps the low part of the frequency and filters out the high frequency. Even though it filters out the high frequency, it stil includes some of content from the original signal. Once the cut off frequency is chosen, the new signal is obtained which is the signal after the filtered.

APPENDIX D: PRESSURE MEASUREMENTS IN THE STILLING BASIN

(PROTOTYPE SCALE)

Sensor Position	Sensor #	Ratio of PMF	Discharge (m^3/s)	Pressure mean (kPa)	Pressure STD (kPa)	Pressure min. (kPa)	Pressure max. (kPa)
upstream floor	2	1	981.99	241.68	97.68	-173.76	1188.00
upstream floor	2	1	979.16	241.68	96.00	-205.20	1128.48
upstream floor	2	1	981.99	246.48	99.36	-220.08	1188.00
upstream floor	2	1	979.16	241.68	97.68	-226.80	1027.68
upstream floor	2	1	979.16	241.68	97.68	-234.96	1189.68
upstream floor	2	1	981.99	243.36	99.36	-211.92	1242.72
upstream baffle face	3	1	981.99	307.68	120.72	-130.80	1307.28
upstream baffle face	3	1	979.16	307.68	120.72	-162.24	1297.20
upstream baffle face	3	1	981.99	302.88	120.72	-186.96	1050.72
upstream baffle face	3	1	979.16	306.24	120.72	-112.56	1434.72
upstream baffle face	3	1	979.16	306.24	119.04	-137.28	1204.56
upstream baffle face	3	1	981.99	307.68	120.72	-133.92	1298.88
downstream baffle slope	4	1	981.99	-1.68	11.52	-56.16	79.44
downstream baffle slope	4	1	979.16	-1.68	11.52	-77.76	104.16
downstream baffle slope	4	1	981.99	82.80	26.40	-122.40	281.28
downstream floor	5	1	981.99	69.60	18.24	-67.92	208.56
downstream floor	5	1	979.16	69.60	18.24	-89.28	218.40
downstream floor	5	1	979.16	69.60	18.24	-72.72	243.36
upstream floor	2	0.98	959.41	244.80	101.04	-210.24	1605.60
upstream floor	2	0.98	959.41	243.36	97.68	-153.84	1125.12
upstream floor	2	0.98	962.23	244.80	97.68	-160.56	1227.84
upstream floor	2	0.98	959.41	244.80	99.36	-195.36	1067.28
upstream baffle face	3	0.98	959.41	286.32	119.04	-463.44	1360.08
upstream baffle face	3	0.981	959.41	288.00	117.60	-349.20	1254.24
upstream baffle face	3	0.98	962.23	291.12	119.04	-395.52	1313.76
upstream baffle face	3	0.98	959.41	291.12	117.60	-412.08	1532.40
downstream baffle slope	4	0.98	959.41	0.00	11.52	-49.68	97.68
downstream baffle slope	4	0.98	959.41	0.00	11.52	-271.44	140.64
downstream floor	5	0.98	962.23	69.60	18.24	-61.20	264.72
downstream floor	5	0.98	959.41	69.60	18.24	-61.20	249.84

upstream floor	2	0.75	733.67	203.52	79.44	-144.00	984.48
upstream floor	2	0.75	736.49	205.20	81.12	-138.96	1075.68
upstream floor	2	0.75	733.67	203.52	79.44	-193.68	933.36
upstream floor	2	0.75	730.85	205.20	79.44	-140.64	972.96
upstream baffle face	3	0.75	733.67	178.80	69.60	-413.76	933.36
upstream baffle face	3	0.75	736.49	178.80	69.60	-307.68	883.68
upstream baffle face	3	0.75	733.67	177.12	69.60	-289.68	936.48
upstream baffle face	3	0.75	730.85	178.80	69.60	-330.96	948.24
downstream baffle slope	4	0.75	733.67	26.40	13.20	-33.12	107.52
downstream baffle slope	4	0.75	730.85	23.28	11.52	-36.48	99.36
downstream floor	5	0.75	733.67	77.76	13.20	-28.08	173.76
downstream floor	5	0.75	736.49	77.76	13.20	-49.68	210.24
upstream floor	2	0.5	488.17	135.60	48.00	-190.32	786.00
upstream floor	2	0.5	488.17	135.60	49.68	-109.20	734.64
upstream floor	2	0.5	488.17	135.60	49.68	-153.84	658.56
upstream floor	2	0.5	490.99	137.28	49.68	-157.20	731.28
upstream baffle face	3	0.5	488.17	104.16	33.12	-218.40	397.20
upstream baffle face	3	0.5	488.17	105.84	33.12	-226.80	599.04
upstream baffle face	3	0.5	488.17	105.84	33.12	-281.28	666.96
upstream baffle face	3	0.5	490.99	105.84	34.80	-183.60	393.84
downstream baffle slope	4	0.5	488.17	51.36	5.04	23.28	74.40
downstream baffle slope	4	0.5	488.17	51.36	5.04	21.60	79.44
downstream floor	5	0.5	488.17	74.40	6.72	23.28	114.24
downstream floor	5	0.5	490.99	74.40	6.72	8.16	132.48
upstream floor	2	0.25	245.50	71.04	18.24	-56.16	327.60
upstream floor	2	0.25	245.50	71.04	18.24	-33.12	350.88
upstream floor	2	0.25	245.50	71.04	16.56	-54.72	288.00
upstream floor	2	0.25	251.14	71.04	18.24	-86.16	327.60
upstream baffle face	3	0.25	245.50	59.52	11.52	-38.16	215.04
upstream baffle face	3	0.25	245.50	59.52	11.52	-21.60	162.24
upstream baffle face	3	0.25	245.50	59.52	11.52	-16.56	177.12
upstream baffle face	3	0.25	251.14	59.52	11.52	-21.60	192.00
downstream baffle slope	4	0.25	245.50	42.96	1.68	31.44	53.04
downstream baffle slope	4	0.25	251.14	38.16	5.04	14.88	54.72

downstream floor	5	0.25	245.50	67.92	1.68	56.16	76.08
downstream floor	5	0.25	245.50	67.92	1.68	56.16	77.76
upstream floor	2	0.19	183.42	61.20	9.84	-23.28	238.32
upstream floor	2	0.19	183.42	59.52	9.84	-19.92	206.88
upstream floor	2	0.19	183.42	61.20	9.84	-38.16	264.72
upstream floor	2	0.19	183.42	61.20	9.84	-51.36	253.20
upstream baffle face	3	0.19	183.42	51.36	6.72	11.52	120.72
upstream baffle face	3	0.19	183.42	51.36	6.72	1.68	115.92
upstream baffle face	3	0.19	183.42	51.36	6.72	1.68	114.24
upstream baffle face	3	0.19	183.42	51.36	6.72	1.68	127.44
downstream baffle slope	4	0.19	183.42	39.60	1.68	28.08	46.32
downstream baffle slope	4	0.19	183.42	38.16	1.68	23.28	46.32
downstream floor	5	0.19	183.42	64.56	1.68	56.16	71.04
downstream floor	5	0.19	183.42	64.56	1.68	56.16	71.04
upstream floor	2	0.09	90.30	56.16	3.36	8.16	129.12
upstream floor	2	0.09	90.30	56.16	3.36	21.60	101.04
upstream floor	2	0.09	90.30	56.16	3.36	8.16	150.48
upstream floor	2	0.09	90.30	56.16	3.36	24.72	114.24
upstream baffle face	3	0.09	90.30	39.60	1.68	28.08	61.20
upstream baffle face	3	0.09	90.30	39.60	1.68	19.92	53.04
upstream baffle face	3	0.09	90.30	39.60	1.68	26.40	57.84
upstream baffle face	3	0.09	90.30	39.60	1.68	23.28	54.72
downstream baffle slope	4	0.09	90.30	33.12	1.68	29.76	38.16
downstream baffle slope	4	0.09	90.30	33.12	1.68	29.76	38.16
downstream floor	5	0.09	90.30	57.84	1.68	54.72	62.88
downstream floor	5	0.09	90.30	57.84	1.68	54.72	62.88

APPENDIX E: FREQUENCY RANGES (PROTOTYPE VALUES)

Sensor Position	**Frequency Range in prototype** (Hz)
upstream floor	0.048 - 0.496
upstream baffle face	0.009 - 1.15
downstream baffle slope	0.006 - 1.396
downstream floor	1.406 - 1.544